The Design and Development of a Recirculating Water Channel: A Critical Assessment

Thesis

The Design and Development of a Recirculating Water Channel - A Critical Assessment

Adrian Millward

B.Sc.(Eng.), M.Sc.(Eng.), Ph.D.

A thesis submitted for the degree of Master of Philosophy at the Open University in the Faculty of Technology.

The work included in this thesis has not been submitted for the award of a higher degree at the Open University or any other awarding body. This thesis is the work of the author except where indicated by the appropriate references.

April 2002

DATE OF SUBMISSION: 26 NOVEMBER 2001
DATE OF AWARD: 9 APRIL 2002

ProQuest LLC.
789 East Eisenhower Parkway
P.O. Box 1346
Ann Arbor, MI 48106 – 1346

The Design and Development of a Recirculating Water Channel

- A Critical Assessment

Adrian Millward

Abstract

The thesis critically assesses the design, development and equipment of a recirculating water channel: the channel in the Department of Engineering at the University of Liverpool. It is intended to provide a valuable reference manual for such facilities.

The channel is a versatile item of equipment which can be used in four different configurations:- as a free surface water channel, including the ability to simulate shallow water and also to generate regular head waves; as a water tunnel; as a free surface cavitation channel or as a cavitation tunnel, with a minimum pressure of 1/30 atmosphere. The working section is 3.66m long, 1.4m wide and 0.84m deep with a maximum water speed of 5.7 m/s.

The thesis includes:

1. A description of the water channel in its four configurations and earlier development of a jet injection system to overcome a velocity defect at the water surface.

   The flow velocity in the working section and methods of flow measurement are discussed together with new measurements of turbulence velocity and the time to reach equilibrium speed.

The wavemaker has been shown to produce waves which are good approximations to a sinusoidal shape at low water speeds and can be maintained over a long period of time. At higher speeds it was found that the wave shape progressively degenerated; methods for improving the wave-maker are suggested.

2. The force measuring equipment is reviewed including a dynamometer for ship models and a miniature version for much smaller forces obtained on sea shells at low water speeds.

3. The principles of model testing are discussed together with a technique for measuring the actual wetted surface area in the case of fast ships. A new experimental and theoretical investigation into the effect of model size relative to the size of the working section is reported.

4. A final chapter reviews the design of the flume and all its equipment. Suggestions are made for further improvements suitable for a future water channel.

CONTENTS

Notation

Symbol	Definition	Formula
A_m	maximum cross-sectional area of model to flow	
B	beam of hull at waterline	
Ca	Cauchy number	$\frac{\rho U^2}{K}$
C_D	drag coefficient of stud	$\frac{D_s}{\frac{1}{2}\rho U^2 dh}$
C_F	force coefficient	$\frac{F}{\frac{1}{2}\rho U^2 S}$
C_f	frictional resistance coefficient	$\frac{R_f}{\frac{1}{2}\rho U^2 S}$
C_r	residual resistance coefficient	$\frac{R_r}{\frac{1}{2}\rho U^2 S}$
C_t	total resistance coefficient	$\frac{R_t}{\frac{1}{2}\rho U^2 S}$
Cw	wave resistance coefficient	
C_ψ	yaw meter sensitivity coefficient (see Eq. 5.13)	
D	dial setting for flume speed control	
D	drag or resistance force on dynamometer	
D_s	drag of turbulence stud	
E	Young's modulus of elasticity	
E	Euler number	$\frac{p}{\frac{1}{2}\rho U^2}$
E	constant in King's law	
F	constant in King's law	
F	hydrodynamic force	

F_n	Froude number of ship or model based on hull length	$\frac{U}{\sqrt{gL}}$
F_{nh}	Froude number based on water depth	$\frac{U}{\sqrt{gH}}$
H	water depth	
I	second moment of area	
I	electrical current	
J	jet injection system fine tuning control setting	
K	constant in flow direction measurement	
K	bulk modulus of fluid	
K	width of channel	
L	representative length of ship or model (usually water-line length)	
M	Mach number	$\frac{U}{a}$
M	momentum loss in jet and free stream combination	
M_1	momentum flux in two-dimensional jet	
M_j	momentum flux of injection jet	
N	floor position counter reading	
R_a	resistance of hot wire at ambient temperature	
R_c	wave resistance in a channel	
R_d	stud Reynolds number	$\frac{Ud}{\nu}$
R_f	frictional resistance of ship or model	
R_L	laminar deficit correction resistance	
R_r	residuary resistance of ship or model	
R_t	total resistance of ship or model	
R_w	resistance of hot wire at operating temperature	
R_w	wave resistance	

Re	Reynolds number - ship or model	$\frac{UL}{\nu}$
Re_X	Reynolds number based on distance X	UX/ν
RWSA	Running wetted surface of ship model	
S	wetted surface area of ship or model	
S_L	wetted area of model forward of studs	
SWSA	static wetted surface area of ship model	
T	wave period	
T	temperature of water	
T	draught of hull	
U	free stream velocity in the working section	
U	speed of ship or model	
$\bar{U}$	root mean square velocity of flow approaching studs	
U_H	Water speed at 50 mm below the free surface with water depth H	
U_p	potential flow at stud position	
V	DVM reading with force applied to dynamometer or load block	
V_{cal}	DVM reading with calibration weight applied to dynamometer arm	
V_o	DVM reading with no weight applied to dynamometer arm	
V_o	output voltage of Wheatstone bridge	
V_s	supply voltage of Wheatstone bridge	
W	dynamometer calibration weight	
We	Weber number	$\frac{\rho U^2 L}{\gamma}$
X	distance along hull waterline to stud	

a speed of sound in fluid

c wave speed or celerity

d stud diameter

g acceleration due to gravity

h injection slot height

h stud height

h contraction manometer head

h, h_1, h_2 manometer heads corresponding to p, p_1 and p_2

k constant

k strain gauge factor

k form factor in ship model testing

n index of boundary layer power law

n total number of studs on model

n rotational speed of propeller flow meter (rev/s)

n number of flexures

p local static pressure

p_v vapour pressure of water

p_1 total or pitot pressure

p_2, p_3 outer tube pressures in flow direction measurements

u local velocity at any point in jet or boundary layer

u_i component of u due to initial boundary layer

u_j uniform jet velocity at slot

u_m maximum velocity on profile

$\overline{u}$ root mean square turbulence velocity

u%	turbulence intensity	$\frac{\sqrt{\overline{u^2}}}{U}$
v	local velocity normal to hull surface at height y	
w	local velocity in z direction at height y	
x	coordinate measured axially downstream from injection slot	
y	coordinate measured perpendicular to boundary with origin on x axis	
z	coordinate parallel to surface normal to x direction	
Δu	difference between u and u_i in the region affected by the injection jet	
γ	surface tension	
δ	boundary layer thickness from the contraction or bow of model	
δ	dynamometer flexure deflection	
δ_j	injection jet thickness at distance x downstream from injection slot	
$\delta_{1/2}$	distance from axis of two-dimensional jet at which $u = u_m/2$	
ϵ	strain in one arm of Wheatstone bridge	
ζ	wave height	
ζ	non-dimensional vertical distance in terms of draught of ship hull	$\frac{z}{T}$
η	non-dimensional hull width in terms of half beam	$\frac{f(x,z)}{B/2}$
θ	momentum thickness	$\int_0^{\delta} \frac{u}{U}\left(1 - \frac{u}{U}\right) dy$
θ_i	momentum thickness of initial boundary layer	
μ	viscosity of water	
ν	kinematic viscosity of water	
ξ	non-dimensional length along hull	$\frac{x}{L/2}$

ρ	density of water	
Λ	ship/model scale ratio	$\frac{L_s}{L_m}$
λ	wave length	
λ	flexure length	
σ	cavitation number	$\frac{p-p_v}{\frac{1}{2}\rho U^2}$
ψ	yaw angle in vertical plane	
ω	wave frequency	

Suffixes

a	in absolute co-ordinates
c	in a channel
d	in deep water with unrestricted width
d	downstream direction
m	model
r	relative to observer
s	full size ship
u	upstream direction

1. Introduction

The high speed water channel (or flume) in the Department of Engineering at the University of Liverpool is a very versatile facility which can be of value in a number of fields, including hydrodynamics, fluid flow instrumentation, civil engineering, oceanography and marine engineering, and has been used for teaching, undergraduate and postgraduate projects, postgraduate and staff research and also by industrial organisations and research establishments. The flume has a wide speed range (up to 5.7 m/s) and can be used in a number of different configurations viz.

an open channel

a closed water tunnel

a cavitation channel

a cavitation tunnel.

A general view of the open channel arrangement is shown in Fig. 1 and it can be seen that this allows easy access to the working section which minimises overall testing time. The water flow can be accurately controlled down to very low speeds (less than 0.1 m/s) permitting calibration and development of oceanographic and fluid flow instruments such as tidal current meters, current direction meters and plankton meters. Other applications of the open channel arrangement include research and development of high speed surface vessels such as catamarans, hovercraft, hydrofoils and planing hulls, using the high speed range (up to 5.7 m/s) and also the investigation of problems associated with oil tankers, sailing yachts and submersibles used in oceanographic surveys. The open channel is also suitable for testing surface piercing struts and other shapes such as those encountered in the design of off-shore drilling rigs or jetty piles. In addition the effects of shallow water can be studied by

raising a false floor to the required depth. A wave maker is installed which can be used to generate regular head waves in the working section.

Two covers are available, one cover converts the open channel into a closed water tunnel, this being equivalent to a wind tunnel of the same size operating at up to 75 m/s on a Reynolds number basis or 180 m/s on a dynamic pressure basis. The other cover can be fitted over the whole of the working section, allowing the air pressure above the water surface to be reduced to approximately 0.03 atmospheres so that propellers and hydrofoils can be tested over a range of cavitation numbers with the free surface present. In addition the two covers can be installed together to form a cavitation tunnel which can be used for tests on propellers and ship stabilisers for example. The flume working section dimensions are given in Table 1 while a more detailed description of the flume and its development is given in Section 3.

A range of force measuring equipment, which has been designed and developed for the flume, is described in Section 4, while other instrumentation, for measuring or visualising flow speed and direction, is described in Section 5. The problems associated with model testing are discussed in Section 6 while an overall summary of factors which could be considered in designing any future water channel are given in Section 7.

2. A history of recirculating water channels

In the search to understand and quantify the nature of the flow around ships and other structures naval architects and other engineers have developed a number of experimental techniques. The more conventional method of investigating a hydrodynamic problem, when the free water surface is involved, is to tow a model of the vessel through a long narrow tank and observe and measure the characteristics of the model, and the flow around it, as it moves through the water. This method may date back as far as Leonardo da Vinci although a more usual historical baseline is attributed to William Froude who developed a towing tank for the Admiralty at Torquay in 1872 (Bailey, 1995). Many people have however been attracted by the alternative technique of keeping the model stationary and moving the water past it, in a similar way to a moving river flowing around a moored craft or to the wind tunnel used in aerodynamic research.

Some of the advantages of testing a model held in a moving stream are:

1. In a towing tank the maximum time available for measurements is governed by the length of the tank, the required model speed and the acceleration and braking characteristics of the carriage to which the model is attached. This restriction does not apply if a moving stream of water is employed since the testing time is effectively unlimited.
2. If the model is tested in a moving stream of water then it is easier to study the flow around the body because it is stationary with respect to the observer and also to the instrumentation. As a consequence photography, flow visualisation and pressure measurements, for example, become simpler to perform.

3. Experience suggests that there may well be a decrease in the overall testing time compared with a towing tank since there is no time wasted in returning the carriage to the start nor in waiting for the waves and currents produced by the previous run to subside. On the debit side however there is time expended in waiting for the flow to settle at the new speed and in making any adjustments which are necessary to obtain a flat, horizontal water surface.

The design of high speed water channels is particularly difficult since the velocity distribution must be uniform throughout the working section, apart from the boundary layer near the walls, but also the free surface must be free from standing waves and be level. Air entrainment should also be avoided as must cavitation on the impeller and cascades, particularly if the channel is to be de-pressurised for cavitation experiments. In addition the structure has to be designed to withstand the large dynamic forces involved in running at high water speeds and it must also be built to avoid leakage of water out under normal conditions or alternatively allowing air to leak in when the working section is de-pressurised.

Two major types of water channel have been developed:

1. channels which have a continuous circuit, similar to a wind tunnel, with small losses in energy through the circuit with the result that the power required to operate the channel is low;
2. channels where the flow is from an upstream stilling tank through a contraction into the working section. At the end of the section the water is collected in another stilling tank and returned through an enclosed pipe to the upstream tank. Because all the energy of the flow is dissipated in the stilling tanks, this design requires more power for

the same flow speed and working section size. Indeed in the case of a large water channel of this design the power requirement can be very substantial and contribute considerably to the overall running cost.

A further important factor in the design of a water channel is the maximum speed when related to the depth of the working section. It has been found that considerable problems are likely to be encountered if the speed of the flow U in the working section is in the region of the critical wave speed c for the depth of water H where

$$c = \sqrt{g\,H} \tag{2.1}$$

such that the depth Froude number F_{nh} is close to unity where

$$F_{nh} = \frac{U}{\sqrt{g\,H}} \,. \tag{2.2}$$

The critical speed is the fastest speed that a free standing wave can travel for a given depth of water. Thus at or close to the critical speed it is normally difficult to obtain a horizontal wave free water surface. In addition, as explained in Section 6.4, the wave pattern and resistance of a ship model changes significantly at speeds close to the critical Froude depth number i.e. when $F_{nh} \simeq 1$. As a result many water channels are designed to avoid this speed range and are therefore separated into either sub-critical or super-critical channels. The Liverpool water channel is able to operate at both sub and super-critical speeds and indeed at the critical speed where, under suitable conditions, a standing wave can be obtained as described later in Section 3.8.

The first re-circulating water channel appears to have been a small one used by Prandtl (1927) in 1904 for the observation of vortices. The channel consisted of a tank with a false floor splitting it into an upper and lower section. At one end of

the tank a horizontal axis paddle wheel pushed water through the upper section, over cascades, through the lower section and returning again once more to the paddle wheel. This type of channel proved successful, and in the following years many similar channels were built, mostly for ship model testing. They had dimensions up to approximately 1.5 m wide and 0.75 m deep although with low maximum speeds and poor quality of the free surface. A small water channel with a working section 0.23 m wide, 0.08 m deep and 1.2 m long overall, similar to the one designed by Prandtl, is still in use in the Department of Engineering at the University of Liverpool.

In the 1930s a free surface water channel was developed and constructed at V.W.S. in Berlin, as reported by Schuster (1959). This facility can be considered as the first modern channel for ship model testing to be successfully implemented, and as such has set the design trend for many other water channels. This channel had a working section 7 m long, 1.8 m wide and 1.2 m deep with a maximum speed of 6 m/s, corresponding to a maximum Froude number F_{nh}, based on the depth of the water in the working section, of 1.75. The water entered the working section via a closed contraction nozzle with the free surface being kept level and free from major standing waves by using a tilting false floor. At the end of the working section the upper part of the flow was diverted over a flap into a separate chamber to reduce the entrainment of air into the main flow and to inhibit the reflection of waves up stream.

In 1940s a very large channel was designed and installed at the David Taylor Model Basin (DTMB) now the Naval Surface Warfare Center in the United States of America. The design of the DTMB channel was similar to the channel constructed at V.W.S.. It had an overall length of 48 m with a working section 18.3 m long,

6.7 m wide and 2.74 m deep with a maximum speed of 4.8 m/s, giving a depth Froude number F_{nh} of 0.94, and is described in Saunders and Hubbard (1944). The DTMB channel was found to have poor flow quality, especially at the free surface, and was not very much used.

A channel of similar design to the one at V.W.S. was installed at the Duisburg Technical College in Germany. This channel, built by Kempf and Remmers of Hamburg, has a working section 5 m long, 1.5 m wide and 1 m deep, and a maximum speed of 2.4 m/s, corresponding to a depth Froude number F_{nh} of 0.77. This channel also had a tilting false floor and a closed contraction, although the nozzle ratio was only 2:1. At the exit from the working section the upper part of the flow was diverted over a flap and into a separate section containing screens. The screens were used to remove the entrained air from the water before it was re-introduced into the main flow.

In the U.K. Binnie et al (1955) studied the flow emerging from an enclosed nozzle and discovered that at higher speeds the flow developed a significant surface roughness, which would be detrimental to any model tests undertaken at these speeds. In order to rectify this problem it was decided to employ a method of surface skimming, in which the upper surface of the water was removed from the main flow by a knife edged flap. This approach had limited success and Binnie's attention turned to utilising natural draw-down instead of the enclosed nozzle. By the development of a cascade type weir at the exit from the working section he was able to hold a level surface up to a depth Froude number F_{nh} of 0.6. This research led to the building of a 1/10 scale model of a larger design which proved to be satisfactory, resulting in a full scale version being built at N.P.L Ship Division, Feltham (Steele, 1962); this had a working section 15 m long, 3.6 m wide and 3.6m

deep. The maximum water speed was 3.6 m/s, corresponding to a sub-critical maximum depth Froude number F_{nh} = 0.6, while the overall length of the channel was 106 m. The water flowed from a stilling reservoir through a 9:1 contraction but with a natural draw-down into the working section leaving via a weir and falling under the force of gravity into a large sump. This sump allowed the escape of entrained air bubbles from the water before the water was pumped upstream by a 1.5 MW axial flow pump. The channel was provided with an adjustable floor although in practice this seems to have been kept in one position. This water channel is no longer in existence.

In the United States two other high speed water channels are known to exist - one at the California Institute of Technology (CIT) and the other at Hydronautics Inc. in Maryland. Both these channels have relatively small working sections and have been designed to operate at super-critical speeds; the working sections can be de-pressurised and they have large de-aeration chambers through which the whole flow can be passed. The channel at CIT has a working section 0.61 m wide, 0.53 to 0.76 m deep and 2.43 m long. The maximum speed is 9.1 m/s and the free surface can be de-pressurised to 1/15 atmosphere. The channel at Hydronautics is similar with a working section 0.61 m wide, 0.30 to 0.61 m deep and 3.4 m long. The maximum speed is a little faster at 12.2 m/s but the lowest pressure obtainable is slightly higher at 1/11 atmosphere. The CIT channel has a fixed floor and there is a limited range of Froude numbers over which a wave free surface can be obtained while the Hydronautics channel has a fixed but tilted floor, compensating for the boundary layer growth, which apparently gives a good free surface over a wide speed range.

At about the same time as the channel at the University of Liverpool was designed a smaller water channel was designed and built at the University of Leeds. This has a smaller working section and an early problem encountered with this channel was that the internal surfaces in contact with the water were made from mild steel. This caused rapid contamination of the water from rusting of the mild steel and various attempts were made to find a suitable coating to prevent this.

3. The high speed water channel in the Department of Engineering

3.1 General description

The water channel at the University of Liverpool was designed to replace a much older low speed channel which had originally been built in 1925 for the now defunct Department of Naval Architecture. This new water channel was originally intended to have a working section 1.52 m wide, 0.9 m deep and 4.5 m long with a maximum speed of around 5.5 m/s. The design of the channel, which was undertaken by Preston and Norbury in conjunction with the firm of Kempf and Remmers, followed the principles established with the German water channels and had a closed contraction, a false floor which can be raised and tilted and also a diverter system to remove entrained air. It was subsequently decided to make the channel more flexible in the type of investigations possible and provision was made to incorporate de-pressurisation. The extra cost of this modification was partially met by a reduction in overall dimensions so that the final working section dimensions were 1.4 m wide, 0.84 m deep and 3.66 m long. The decision was also made that all internal surfaces which would be in contact with the water should be constructed

from stainless steel with the exception of the honeycomb which is brass and the propeller which is bronze. The external structure is made of mild steel.

The water channel, which is shown schematically in Fig. 2, has a capacity of approximately 90,000 litres of water circulated by a 75 kW electric motor driving an axial flow impeller. On leaving the impeller the water passes initially through a long circular section diffuser after which the cross-section becomes rectangular. Two sets of vanes are provided to guide the flow around the corners and a honeycomb reduces the flow unevenness. The flow is then accelerated through a 4:1 ratio closed contraction into the working section which is 1.4 m wide, 0.84 m deep and 3.66 m long. At the end of the working section, the topmost layer of water is separated from the main flow by an adjustable flap or "splitter plate". This narrow layer contains the majority of air bubbles caused by the presence of a model in the working section. This water is slowed down after the splitter plate by flowing through a divergent section where any air bubbles have time to collect on the three gauzes which are installed across the section and so escape from the water. At the end of this section the diverted water is then re-introduced to the main flow at a second adjustable flap. Because of the shallowness of the water over the "splitter" plate the initial flow at this point is normally super-critical and therefore no waves should be transmitted upstream. A more detailed account of the design of the flume is given by Preston (1966).

The flow velocity in the working section is uniform to within $\pm 1\%$ except close to the walls and floor where normal boundary layer effects are encountered. The speed can be set to an accuracy of better than 0.1%, the maximum speed being about 5.75 m/s, corresponding to a depth Froude number F_{nh} of 2.00. There is an adjustable false floor in the working section which, in conjunction with adjustment

of the "splitter" plate and the flap downstream of the working section, allows almost any chosen speed to be maintained without the presence of standing waves. In practice small waves of about 1mm height occur at low speed and some difficulties can be experienced with obtaining a horizontal water surface in the region of 2.5 m/s, particularly with a ship model in the working section, because this is close to the critical wave speed, based on the water depth which is nominally 2.7 m/s.

A small vacuum pump is fitted in the basement and connected to the top of the contraction together with a control valve, non-return float valve and sight glass. The purpose of this is to enable the contraction to be filled when the flume itself is filled with water since the top of the contraction is approximately a metre above the normal water level in the working section. Without this system the contraction would remain only partly filled and the flow velocity in the working section would be affected. It is therefore part of the normal running procedure to check that the contraction is full before starting the flow in the working section.

At the end of the diffuser on the return part of the circuit there is a small chamber on the top of the diffuser which collects any air bubbles in the circuit which have floated up to the top of the diffuser as the water slows down. Any bubbles collected in this chamber then rise up through a copper pipe and are released into the air cavity above the water just behind the splitter plate at the end of the working section. There is a valve in this pipe near the upper end which should not be shut except for some specific purpose since it will stop the air collecting chamber working properly. Also near the upper end of the pipe there is a T-piece in the pipe with a valve allowing the pipe to be open to atmosphere outside the flume. This valve should always be closed when the flume is running since any changes in water level which occur when changing speed may cause water to spill out through this valve.

However when the flume is being used as a cavitation tunnel or channel the purpose of this valve is to release air back into the working section after it has been de-pressurised.

Early work on the flume (Nicholson, 1972) showed that the wake in the top layer of the free surface in the working section, caused by the boundary layer on the upper surface of the contraction, was larger than had been anticipated. The resultant velocity defect was sufficient to make the results of tests on surface vessels unreliable and to correct this a jet bleed system was introduced. Water is taken from the return section of the channel and pumped back into the main flow through a 1 mm wide slot running the whole breadth of the channel at the beginning of the working section. A more detailed description of the jet bleed system can be found in Section 3.2.3 which is based on Millward et al, (1980).

Access to the upper part of the flume would normally be from the working section when it is drained but is limited in the upstream direction by the honeycomb and in the downstream section by the first set of corner vanes. In addition inspection and cleaning of the gauzes downstream of the working section but above the splitter plate is achieved by lifting the lids over this section. The lower part of the circuit can be inspected when the flume is empty by removing a hatch on the side of the flume just at the end of the diffuser section. This gives access to the section where any debris is likely to come to rest, since the flow is slowest in this section, and also gives access to the propeller and bearings as indicated in Appendix 7 for maintenance and replacement. It has however been found that in one or two cases where debris, such as strands of seaweed, has become caught on the corner vanes of the flow straighteners upstream of the propeller that it would be an advantage to be able to get access to other parts of the circuit, particularly upstream of the propeller. It is

therefore recommended that in any future design consideration should be given to providing more access hatches particularly to the section upstream of the propeller.

3.1.1 Working section windows

As can be seen in Fig. 1 there are six windows along each side of the working section which allow the observer to see the flow both above and below the water surface. Since it is important that the presence of the windows should disturb the flow in the working section as little as possible, the inner surface of the windows must be flush with the inner surface of the working section. In addition under cavitation conditions, when the pressure inside the working section is reduced below atmospheric pressure, there is a considerable force attempting to push the window inwards. In the original design therefore the windows were made from a transparent acrylic plastic with a flange milled all the way around as shown in Fig. 3. This allowed the window to fit in the hole in the side of the working section with the inner face flush with the inner surface of the working section itself. The window was held in place by a metal strip along each side, which was bolted in place, while a seal was provided by an O-ring under the flange to prevent water seeping out under normal conditions or air seeping in under cavitation conditions.

It was found however that over a period of years the material of the window absorbed water on the inner surface causing the window to bow inwards to the extent that eventually the false floor could not be raised through its full travel without scraping the surface of the window. A further drawback was that the material also showed signs of crazing on the inner surface which made observation of the flow less clear. Several possibilities were explored to obviate these problems including the use of glass rather than acrylic plastic. Unfortunately several attempts by Pilkington Glass

to laminate two layers of glass together to make the required shape proved unsuccessful. Eventually therefore the decision was made to modify the original design by making the window reversible. The new design is therefore thicker, although this does not seem to interfere with the transparency, but with the advantage that the window can be reversed every few years so that the water absorption and the associated bowing can be evened out. The old windows have been kept as spares for experiments where it is necessary to make holes in a window for instrumentation. In addition it has also been found that when exposed to the air on both sides the water eventually evaporates back out again and the bow in the window slowly reduces.

It is therefore recommended that, in any future design of water channel, the windows should be designed to be reversible if made from acrylic plastic in order to avoid bowing through water absorption. It would however be an advantage for measurements with a laser doppler anemometer system in particular if the windows could be made from optically flat glass. In the present design this has only been achieved by putting panels of optically flat glass as flush inserts in a normal window which gives only a limited area over which the laser beam can be traversed.

3.1.2 Modifications to the Laboratory

As originally installed in the laboratory in 1965, the flume was just the bare open channel recirculating water channel as illustrated in Fig. 1. Shortly afterwards, the two covers were delivered which enabled the open channel to be converted as needed into either a water tunnel, or a cavitation channel or a cavitation tunnel as illustrated in Fig. 4. In addition a vacuum pump was fitted in the basement near the main drive motor so that the pressure in the working section could be reduced. A number of modifications were made to the laboratory over the next few years in

order to make the channel an effective system such as the construction of a mezzanine floor so that the two covers could be stored away from the working section, the installation of an electric crane and also instrumentation so that the reduced pressure in the working section could be automatically controlled.

3.2 Flow Velocity in the Working Section

3.2.1 Speed control and calibration

The speed control of the flume is obtained from a DC motor supplied through a Ward-Leonard set - a synchronous three phase AC motor driving a DC generator. This is a standard system widely used for wind tunnels and gives an accurate and repeatable speed control throughout the design speed range. The power is transmitted from the DC motor through a pulley wheel system with a toothed drive belt to the main propeller shaft. The use of the toothed drive belt has been shown to be an advantage since a copy of the flume, at the Defence Research Agency (Haslar), used a more conventional v-belt system and it has apparently been found to cause some risk of slip at high speeds with a consequent effect on the repeatability of speed control.

In addition to the initial experiments to determine the variation of velocity throughout the working section, described in the next section, the velocity in the centre of the working section was determined as a function of the speed setting on the main console. This speed setting is through a ten turn potentiometer with 100 divisions in each turn so that the speed can be set to better than one division representing 0.006 m/s approximately. Markings on the dial on the console correspond approximately to the speed in ft/sec, that is 0 to 20 ft/sec, since the

Department used the Imperial measurement system at the time the flume was built. An alternative smaller pulley, half the size of the normal pulley, is available and could be used to reduce the overall ratio between the motor and the final drive wheel. This should reduce the top speed to approximately 2.8 m/s and therefore give a finer control over the low end of the speed range. Up to the present it has not been found necessary to use this pulley.

In the initial experiments the speed in the centre of the working section was measured with the pitot-static probe described in Section 5.1 for the moderate and higher speeds where the manometer head was large enough, with a propeller velocity measuring device for lower speeds, as described in Section 5.2, and for the lowest speeds using a float and stopwatch. Subsequent measurements to check to see whether the calibration changes with time have been confined to the range appropriate to the pitot-static probe. The earlier results corresponded to the linear relationship

$$\text{Dial setting } D = 166\ U \tag{3.1}$$

This calibration remained constant from the initial measurements in 1967 when the flume was first calibrated until alterations were made to the seating of the jet injection box in 1993 as a result of the installation and calibration of the wave-maker described in Section 3.3. At this stage the calibration was found to have changed slightly, presumably as a result of the small changes in geometry at the inlet to the working section. In the last year or so the whole drive system has been overhauled and refurbished with replacement of motor bearings, propeller shaft bearings and a new drive belt. Subsequently the channel was again recalibrated and the new calibration graph is shown in Fig. 5. The corresponding equation is still linear and only marginally changed to

$$\text{Dial setting } D = 165.14\ U \tag{3.2}$$

In addition, for cases where it is not possible to check the calibration of the working section, such as if it is suspected that the model is causing a significant amount of blockage, a separate calibration curve has been produced of the pressure drop across the contraction as shown in Fig. 6. The graph gives two curves - the first curve shows the measurements of pressure head h cm across the contraction against water speed U in the centre of the working section while the second curve shows the square root of the head $\sqrt{h}$ which is a straight line through the origin as might perhaps be expected. The equation of the line, which has been deduced using a least squares curve fit routine, gives an equation for the relationship between contraction head and working section velocity as

$$U = 0.4493\ \sqrt{h} \tag{3.3}$$

where h is given in centimetres for convenience because the manometer on which the measurements are made is calibrated in these units.

A separate calibration curve has been obtained for the case when the flume is being used at a water tunnel. In this configuration the calibration has been made with the floor in its normal position to give the full height of the working section and also with the normal slope on the floor of 260 units. In order to reduce the introduction of bubbles into the water and to reduce flow noise in the laboratory the splitter plate flap is also wound up until it seals with the end of the tunnel lid. Under these conditions the flow speed is slightly altered and the relationship between the dial setting and the working section velocity is

$$D = 163.1\ U\ . \tag{3.4}$$

3.2.2 Maximum Velocity

As stated in the previous section the maximum velocity in the working section is approximately 5.75 m/s although earlier documents, such as Preston (1966), quote the maximum speed as high as 6.4 m/s. Recently however it was found that attempts to achieve this speed caused the overload cut-out to operate which shut the Ward-Leonard generator set down. Measurements were made therefore to find the actual maximum speed permitted by the electrical current capacity of the Ward-Leonard generator set which is rated at 175 amps. As can be seen from Fig. 7, which shows measurements of the generator current against working section flow velocity U, the maximum velocity for continuous running is 5.7 m/s - a slightly higher speed can be achieved but there is always the risk that the overload cut-out will operate. If this occurs when the flume is being operated as a tunnel the water speed will slowly reduce to zero without any damage being likely to occur. However, if the flume is being operated as a free surface channel, then an emergency stop such as this will cause large waves to run upstream in the working section which may cause damage to any model in the working section - these waves will almost certainly swamp any floating ship model.

3.2.3 Jet injection at the free surface

For bodies such as high speed planing craft, hovercraft and other vessels which are immersed in the water at the free surface the variation of velocity with depth near the free surface must be zero and also should not vary along the length of the working section. It was appreciated in the original design that there would be a wake on the free surface caused by the growth of the boundary layer on the upper

surface of the contraction at the upstream end of the working section. This could produce variations of velocity over a small depth near the free surface but initially it was thought that this effect would be negligible. Measurements of the velocity distribution near the water surface as the flume was originally built are shown in Fig. 8, taken from Nicholson (1972), from which it can be seen that a significant velocity defect existed. This defect was particularly noticeable at the upstream end of the working section and decreased in intensity while increasing in depth along the working section as a result of mixing. For the flume to be of use for quantitative measurements which could be compared with a towing tank it was clearly important that this velocity defect should be removed.

Various methods of dealing with this velocity defect or wake were considered, such as skimming, suction, a paddle wheel and a continuous belt, and were rejected for reasons detailed in Nicholson (1972) before the eventual solution of injection was adopted. The method chosen, which is a technique used in aeronautics, involved injection of fluid through a nozzle to re-energise the boundary layer at the end of the contraction. If the injection velocity was high then the jet could be small so that the volume flow rate would also be small with the result that the required pumping power would therefore be low. The system was designed so that a plate extended downstream until the excess velocity was equal to the velocity defect with further mixing downstream to give a uniform velocity with the minimum of surface disturbance.

The injection system was designed by obtaining a general expression for the momentum deficit at the free surface, given in Nicholson (1972) and also in Millward et al (1980) and summarised in Appendix 1. This general expression included terms for the initial boundary layer profile at the end of the contraction

which was measured and found to be represented satisfactorily by the normal one-seventh power law. Solution of the equations indicated that the appropriate slot width would be 1.27 mm and the plate length would be 152 mm. In order to confirm the concept model tests were carried out in a smaller channel with a 150 mm wide working section as described by Nicholson (1972). Since these tests showed that the concept of the proposed injection system was viable the full scale injection system was designed and subsequently installed in the working section.

A schematic diagram of the jet injection system for the full scale injection system is shown in Fig. 9 as it currently exists. In common with the remainder of the working parts of the flume in contact with the water, the injection plenum chamber was constructed of stainless steel and brass and fitted across the whole width of the working section. The pump speed control was coupled into the main speed control of the flume so that the jet velocity would automatically be set correctly at all water speeds although a fine adjustment control was also provided to allow for manual tuning should any small differences occur. A bleed valve was also installed on the top of the plenum chamber of the injection system, as shown in Fig. 9, so that air could be bled out of the plenum chamber after the working section of the flume has been re-filled with water or maintenance carried out on the injection system. Although a by-pass filter system was subsequently installed to filter dirt and other debris out of the water in the whole of the flume, as described in Section 3.2.4, it was found that this did not entirely prevent particles getting into the plenum chamber and hence blocking the injection slot. Two hatches were therefore cut into the top of the plenum chamber to allow access to the chamber and in addition mesh filter baskets have been fitted to the end of the supply pipes inside the plenum chamber.

The jet injection system was then calibrated to determine the optimum setting of the pump speed at all water velocities using a small pitot tube with particular interest being on the region midway along the working section where it can be expected that any model would be placed. The most recent equation for this calibration curve is

$$J = 615 - 0.115D \tag{3.5}$$

where J is the jet injection system control potentiometer and D is the main control potentiometer.

The velocity distribution near the water surface before the injection system was installed has been shown in Fig. 8 from which it can be seen that a significant velocity defect existed. This defect was particularly noticeable close to the upstream end of the working section but decreased in intensity while increasing in depth with distance downstream as a result of the mixing process. The velocity profiles measured in the working section after the injection system had been installed are shown for comparison in Fig. 10 at the same free stream velocity of 1.48 m/s. It can be seen that by the midpoint of the working section, 1.83 m from the nozzle, the excess momentum in the upper layer of the water caused by the injection system has been evenly dispersed and just counter-balances the momentum defect caused by the growth of the boundary layer on the contraction. Similar results were obtained at other speeds.

A beneficial side effect of the injection system, which had been discovered in the tests on a model of the flume, was that the jet also made the free surface considerably smoother in appearance. This same effect was found in the flume itself and, although a quantitative measure of the roughness is difficult to specify, the effect can easily be appreciated from Fig. 11. This shows photographs taken of two

crosses painted onto a black background which had been laid on the floor of the working section 0.84 m below the water surface. The difference in the clarity of the crosses as a result of the smoothness of the water is very evident when the injection system is operating.

3.2.4 Time to reach equilibrium water speed

Recently a laser doppler anemometer system (LDA), described in more detail in Section 5.4, has been used to measure the water speed at suitable time intervals after the water speed had been changed, since this would affect the time taken to reach equilibrium conditions for the new forces and moments such as would exist on a ship model. An experiment was carried out therefore where the flume speed was increased in increments of approximately 0.5 m/s at the normal rate, usually around 20 to 30 seconds, and measurements were made using the LDA system for a period of 60 seconds with a further gap of 60 seconds between each data set until equilibrium conditions had been reached. In each case the floor and flap settings for the new speed were set before the speed was changed.

Sample graphs of the measurements of both mean and turbulence velocities against elapsed time are shown in Figs. 12a through to 12d. It can be seen that for the initial setting, where the speed was being increased from 0 to 0.5 m/s (Fig. 12a), the time to reach a steady state for both mean speed and turbulence is surprisingly long at about 9 minutes while for the other speeds illustrated it is rather shorter at about 7 minutes. An overall plot of the time to reach equilibrium conditions across the whole speed range was deduced and is shown in Fig. 13 where it can be seen that above about 2.5 m/s the settling time has been reduced still further to about 3 minutes. A curve showing the envelope of the time taken to reach equilibrium

conditions has been inserted in Fig. 13 and it is recommended that this should be used as guidance for the settling time. The experiment was subsequently repeated while reducing the speed in 0.5 m/s increments approximately from 5.5 m/s downwards and the deduced result for the time to reach the equilibrium speed in each case is shown in Fig. 14. It can be seen that in general the time to reach the equilibrium speed is more uniform although a little longer than for the ascending speeds, averaging approximately 4 minutes for each 0.5 m/s decrease. This suggests that it would be marginally more economic in total elapsed time to make measurements on the ascending speeds if at all possible. It is recommended that the curves shown in Figs. 13 and 14 should be used as a guide to the amount of time allowed for the water speed in the flume to settle where the increase in speed is of the order of 0.5 m/s noting particularly the long time required for the first 0.5 m/s. In cases where the increase in speed is larger than 0.5 m/s then it is suggested that the settling time should be estimated as the total time as though the increase were made in the standard 0.5 m/s increments.

3.2.5 Turbulence velocities

The laser doppler anemometer system (LDA) was also used to measure mean and turbulence velocities in the centre of the working section over the range of operation of the flume for both ascending water speeds and descending speeds in 0.5 m/s increments. The measurements of the turbulence at the equilibrium speed are shown in Fig. 15 for the ascending speeds and for the descending speeds in Fig. 16

in the form of the turbulence intensity where

$$u\% = \frac{\sqrt{\overline{u^2}}}{U} \times 100 \, . \qquad (3.6)$$

It is interesting to note that, while the average for the ascending speed was approximately 3%, for the descending speeds the general level was a little higher, averaging about 4% even though the flume was allowed to settle for over 20 minutes in some cases to be certain that a steady state had been achieved. In both cases the overall shape of the curve with speed is similar with a slightly higher level of turbulence measured at around 2.5 to 3 m/s which is close to the critical speed for the flume based on water depth.

The only other measurements of turbulence velocities in the working section were those made by Cheah (1982) in the course of experiments with modelling the formation of heavy gas plumes in air by the release of salt water in the fresh water of the flume. For these experiments he created an artificial thickened boundary layer on the false floor of the working section and measured both the mean and turbulence velocities through the boundary layer with a hot film anemometer. Cheah's results for the turbulence velocity outside this thickened boundary layer were almost identical with those obtained with the LDA system at 3% to 4% also as can be seen in Fig. 30.

3.2.6 Water quality

When the flume was first installed apparently no attempt was made to control the quality of the water which has since been found to be important since one side of the laboratory contains windows which face south. As a result the sun, particularly in summer, shines directly on the working section and there were evident signs of the

growth of algae which can have a significant effect on resistance. These algae, which can affect the boundary layer on a model in much the same way as long chain molecule polymers, have been shown to be the cause of the 'tank storms' referred to in Phillips-Birt (1970). In addition the water became visibly green and opaque which was not desirable for flow visualisation and photography. It was therefore deemed necessary by the author to develop some suitable method of controlling the quality of the water, particularly since it used to take some three days to fill the flume completely so that frequent changes of water were not practical even if the cost factor was ignored.

Initial experiments for keeping the water clean were made by dosing the water with sodium hypochlorite since this is a method which has been found acceptable in small towing tanks. However the results suggested that prolonged use might cause interaction of the chlorine released with the structure of parts of the flume. A complete water quality control system was therefore designed and installed which served the dual purpose of filtering out solid particles and also treating the water to remove bacteria and algae. The system has a capacity of 5,000 litres/hour and takes water from a junction in the pipe supplying the jet injection system at the bottom of the return circuit and returns it to the main circuit just downstream of the working section after the "splitter" plate. The pump for the system is time controlled and is normally left operating only overnight so that there is no possibility of this flow, even though it is small, affecting the flow through the injection system while the flume is in use for experiments. The first part of the system consists of two conventional mesh filters in parallel with a 400 micron mesh size. These are intended to remove major particles while leaving smaller particles which are an advantage to

have in the water as a seeding agent for LDA measurements. The filters are constructed from non-corroding materials including the mesh which is stainless steel.

The second part of the system is a commercially available unit by Tarnpure intended for use in swimming pools instead of chlorination. It works by releasing small amounts of copper and silver ions into the water from anodes. Experience in the flume has shown that the current consumption can be set as low as 0.5 amp because of the lack of contamination compared with a swimming pool, resulting in a long life on the electrodes.

This bypass water treatment system has been found to be extremely satisfactory and gives very clear water which can be kept in the flume indefinitely. The longest period without replacement so far has been about a year but even then the water was emptied in order to carry out maintenance of the flume rather than because it needed changing.

Up to the present the interest has been in keeping the water clean to enhance flow visualisation and free of algae to avoid any possible effects on viscosity. It is anticipated that in the future it may be necessary to introduce substances which may contaminate the water such as an investigation of the effect of drag reducing polymers on the boundary layer on a submerged body. In such a situation it may not be sufficient just to empty and refill the flume since quite minute quantities of the substance can affect the viscosity of the water. It is therefore important to be able to monitor the viscosity of the water in some way. Fortunately a miniature pipe flow device, described in Millward and Wade (1972), is available for this purpose.

3.3 The wave-maker

The wave-maker used in a recirculating water channel is different from the conventional wave-maker used in a towing tank and consists of a hinged paddle which lies on the surface of the water. It rests in contact with the plate of the jet injection system at the upstream end of the working section as shown in Fig. 17. The wave-maker is capable of producing regular head waves and is driven by an electric motor via a chain gearbox system. As the motor rotates, a Scotch yoke, which allows for adjustment of wave height, moves the paddle up and down on the surface of the water. The wave-maker has a minimum rotational frequency of 0.7 Hz and a maximum of 2.7 Hz. Since the use of a wave-maker in a recirculating water channel is unusual, some preliminary tests have been made to check that the waves produced were an acceptable representation of normal waves and to investigate any other problems such as the presence of standing waves and the reflection of waves back up the working section. These tests and the related theory of wave propagation are described below and are based on Sutcliffe (1995).

3.3.1 Wave-current interaction

The creation of waves in the water channel requires the imposition of a wave system on an underlying current. It has been shown that the effect of a current on a wave system can, in some cases, lead to changes in the wave height, length and form. In order to be able to superimpose the correct wave system on the vessel or structure to be tested, it is therefore necessary to investigate whether the current present in the flume will affect the wave system. In the experiments conducted so far the intention was to model regular head waves with a known wave length, frequency and wave height with the interest being in the shape of the waves produced by the

wave-maker and the problems of reflection back upstream from the end of the working section.

The speed of a wave is given by

$$c = \sqrt{\frac{g\lambda}{2\pi} \tanh\left(\frac{2\pi H}{\lambda}\right)} \qquad (3.7)$$

where λ is the wave length, H is the depth of water and g is the acceleration due to gravity. If the depth of the water is more than approximately half the wave length the equation above simplifies to

$$c = \sqrt{\frac{g\lambda}{2\pi}} \simeq 1.25\sqrt{\lambda} \qquad (3.8)$$

with the wave speed now being dependent on wave length only and is termed a deep water wave. If, however, the water depth is less than approximately 1/25 of the wave length ($H < \lambda/25$) then Eq. 3.7 simplifies to

$$c = \sqrt{g\,H} \simeq 3.1\sqrt{H} \qquad (3.9)$$

so the wave speed or celerity is no longer dependent on the wave length but just on the water depth. This type of wave is most frequently seen on beaches. Any wave which forms on water between these two limiting depths is considered to be a transitional wave and the full form of the wave speed equation (Eq. 3.7) should be used. Since the flume has a working section depth of 0.84 m, the limit of the wave length for which deep water waves will exist in the working section is approximately 1.7 m. This is likely to be satisfactory for most cases but there may be some instances, such as the case of a sailing yacht, where there may be some restrictions. For example it can be expected that the range of wave lengths likely to be of interest for a yacht model with a 1 m water-line length is 0.5 m to 2 m so that the waves

produced are likely to be deep water waves except near the upper limit of this range. As can be seen in the results given in Sutcliffe and Millward (1998), the main area of interest is in wave lengths near to the length of the yacht so that the results obtained are likely to be representative of those for deep water waves.

3.3.2 Wave scaling laws

In order to investigate the effect of waves on a full size vessel through experiments using a model in the flume or in a towing tank it is necessary that the waves should be correctly scaled relative to the size of model used. If Λ is the scaling factor between the model (subscript m) and the full size ship (subscript s) or structure then both the wave height ζ and the wave length λ should also be scaled in the same manner i.e.

$$\zeta_m = \frac{\zeta_s}{\Lambda} \tag{3.10}$$

and

$$\lambda_m = \frac{\lambda_s}{\Lambda} . \tag{3.11}$$

However if the full scale wave period is given by

$$T_s = \sqrt{\frac{2\pi\lambda_s}{g}} \tag{3.12}$$

and the model wave period is given by

$$T_m = \sqrt{\frac{2\pi\lambda_m}{g}} \tag{3.13}$$

then the wave period will instead be scaled by

$$T_m = \frac{T_s}{\sqrt{\Lambda}} \tag{3.14}$$

and the wave frequency is correspondingly scaled by

$$\omega_m = \omega_s \sqrt{\Lambda} \,. \tag{3.15}$$

This shows therefore that while the physical lengths are scaled directly as the scale ratio the wave periods must be decreased instead in proportion to the square root of the scale ratio. This has the result that the model with both the model and wave size correctly scaled and the wave period too, the model will have a higher encounter frequency at a given Froude number than the full size vessel. This has the effect that model tests in waves appear wrong to the observer because the encounter frequency appears high and a video film of a test, for example, must be slowed down by the appropriate factor to appear correct visually.

3.3.3 The effect of current on waves

With no current present in the flume the wave speed c is determined by Eq. 3.7 for deep water or transitional waves. If a current flows in the same direction as the waves then the absolute wave speed will exceed the wave speed without the current while the relative wave speed c_r will also exceed the no current wave speed because the current lengthens the waves. If the current is in the upstream direction

(an opposing current) then the relative wave speed will be lower than the no current wave speed because the water flow shortens the wave length.

If a train of regular waves (wave length λ, height ζ) is travelling on a steady, uniform current of speed U then to a stationary observer the wave appears to have a speed c_a with a current flow velocity U. If the observer were to move downstream at the same speed as the current, then no current would be seen, with the waves having a speed of c_r (the relative wave speed). Consequently for the case of head waves

$$c_r = c_a - U \ . \tag{3.16}$$

The waves will pass a stationary observer with period T_a so

$$c_a = \frac{\lambda}{T_a} \tag{3.17}$$

although they would pass the moving observer with period T_r where

$$c_r = \frac{\lambda}{T_r} \ . \tag{3.18}$$

In the moving frame of reference, the waves seem to be propagating on "still" water so consequently

$$c_r = \left[\frac{g\lambda}{2\pi} \tanh\left(\frac{2\pi H}{\lambda}\right)\right]^{0.5} \tag{3.19}$$

Thus, combining Eqs. 3.16, 3.17 and 3.19,

$$\lambda = \left(\left[\frac{g\lambda}{2\pi} \tanh \frac{2\pi H}{\lambda} \right]^{0.5} + U \right) T_a. \qquad (3.20)$$

In the tests Eq. 3.20 was used to set the required wave period on the wave-maker and so produce a wave of the desired length for any water speed.

3.3.4 Reflected waves

If the waves created by the wave-maker impinge on a surface at the downstream end of the working section, they will be subject to reflection and the reflected wave will travel upstream with the same period as the incident wave. If there is a current present, then the current will reduce the apparent speed of the reflected wave because of the interaction of the current and the wave train. Therefore, as the wave frequency is reduced, the likelihood of reflected waves being present in the working section is increased, because the reflected waves are of higher speed, and can therefore overcome the flow of water against them. The waves propagating downstream have a wave length given by

$$\lambda_d = \left(\left[\frac{g\lambda_d}{2\pi} \tanh \frac{2\pi H}{\lambda_d} \right]^{0.5} + U \right) T_a. \qquad (3.21)$$

The reflected wave will have the same period as the downstream wave and hence the reflected waves have a wave length given by

$$\lambda_u = \left(\left[\frac{g\lambda_u}{2\pi} \tanh \frac{2\pi H}{\lambda_u} \right]^{0.5} - U \right) T_a. \qquad (3.22)$$

A graph of wave period against wave length can therefore be plotted for various water speeds, as shown in Fig. 18, for the downstream and reflected waves

separately. When combined, as shown for one speed in the upper diagram of Fig. 19, the minimum wave period for reflected waves is given by following the arrowed line. All wave periods above this threshold are likely to be reflected whilst all periods below this should not be reflected.

3.3.5 The production of waves in a water channel

As mentioned earlier the method of producing waves in a recirculating water channel is different from that used in a towing tank so that tests had to be carried out to determine the shape of the waves produced in the working section, to investigate the possibility of standing waves and the conditions over which waves would be reflected from the downstream end of the working section.

3.3.5.1 Wave height measurement

A resistance wave probe was used to make measurements of wave height in the working section of the flume. This measures the change in resistance caused by the depth of immersion of the probe as the wave passes by and was connected to a commercially available package made by Cambridge Instruments. The wave probe itself however was designed specially for the application "in house" since a standard wave probe, which is circular in cross-section, would not give accurate readings because of the wave formation around the front of the section and the possibility of ventilation at the back at higher speeds. The probe used therefore consisted of two stainless steel symmetrical hydrofoil sections held in a Perspex holder (to provide electrical insulation) at the top and the bottom. Bi-convex foil sections were used rather than flat section in order to give adequate stiffness while still giving a streamlined shape to avoid ventilation. The probe holder was held in a mounting

which allowed the probe to be adjusted vertically against a scale for calibration purposes. The mounting was itself positioned on an existing beam across the working section which allowed the probe to be positioned anywhere across the width of the working section as for the initial calibration of the working section using the pitot-static probe.

The output from the signal conditioning box of the wave probe was connected into the analogue-digital converter (ADC) of a PC after first being passed through a low pass filter to remove any unwanted signal noise. The ADC board used was a 16 channel multiplexed board with a 12 bit resolution (1 part in 4096). In order to synchronise the wave probe with the wave-maker the drive shaft of the wave-maker was fitted with a toothed wheel which had 80 teeth milled in the edge. A light sensitive diode was fitted to the toothed wheel to act as a trigger and was also connected to the computer so that 80 samples of data from the probe or other sensors could be collected per complete wave. A schematic diagram of the data collection equipment is given in Figs. 20 and 21. The computer programs to operate the ADC board were written in QBasic.

3.3.5.2 Reflected waves

The nature of the design of a recirculating water channel means that there is a possibility that waves could be reflected back up the working section from the downstream structure, as explained in Section 3.3.4, and will therefore set the minimum speed at which the water channel can be run with waves present for each wave length. Tests were therefore carried out to determine the minimum wave period for reflected waves at each water speed and also to compare the experimental results with the theoretical values given for example in Fig. 19. Measurements were made

by visual observation of the waves in the working section with photographs taken to provide a permanent record if needed. Two regimes of reflection were observed in the experiments. The first regime was when a stationary wave was apparent just upstream of the splitter plate at the end of the working section; the second was when the waves could be seen to propagate upstream. The wave frequencies at which both regimes occurred are shown in the lower diagram of Fig. 19 together with the corresponding theoretical curve. It can be seen that the wave periods obtained in practice were slightly higher than predicted by the theory. The stationary wave curve gives the minimum wave period at which experiments can safely be undertaken to ensure that no reflected waves are present since the second curve shows the frequencies at which the waves can just be seen travelling upstream. Some scatter in the data was obtained as a result of the difficulty in judging the occurrence of the waves and also because of the "slapping" effect from the splitter plate at the downstream end of the working section. It was also noted that the waves tended to find it easier to propagate upstream close to the sides of the working section, presumably because of the slower flow velocity there.

Two points were noted in this experiment - first, that if the reflected waves are allowed to propagate for any length of time, they eventually reach the wave-maker paddle and cause a confused sea in the working section. Secondly that once a train of reflected waves had formed in the working section it was difficult to remove except by increasing the water speed.

3.3.5.3 Wave propagation and shape

When the wave is formed at the wave-maker it propagates along the working section interacting with the current as it travels. Any change in the wave shape therefore would diminish the usefulness of the water channel as a facility for testing models in a water flow with regular head waves. In order to investigate this, measurements and photographs were taken of a range of waves to investigate the propagation of the wave along the working section at various water speeds.

The experiments related to reflected waves had shown that there was some effect at the walls of the working section. The first investigation therefore into wave shape was to determine how far from the wall this effect continued. Measurements were made of the wave shape and phase relative to the wave paddle for different distances from the wall of the working section. It was found that the wave probe needed to be 70 mm away from the wall for the wave to be in phase with the wave in the centre of the working section. This information was important since it defined the position of the probe for later experiments when there was a model in the working section in order to keep the probe as far away from the model as possible while still recording the true position and shape of the wave.

The sample sequence of profiles shown in Fig. 22 at a water speed of 0.56 m/s were constructed from individual samples taken at measuring points along the working section and in themselves demonstrate that the waves in the working section were steady over a long period of time - enough to obtain all the data points. The overall shape shows the progression of a wave along the working section and indicates that the wave does not change in length or height along the working section. The wave length is 1 m throughout showing no stretching of the wave as it travels downstream. It can also be seen that the wave height, which was slightly above 30

mm, showed no variation in wave amplitude through the cycle. A graph of the wave profile occurring along the centre-line of the water channel is shown in the upper diagram of Fig. 23 and it can be seen from this diagram that the wave shows little deviation from a sinusoidal curve fit applied to the raw data. Thus at this water speed and wave length the wave-maker was seen to be producing waves suitable for experiments on ship models.

The corresponding results for measurement of wave shape for a faster water speed of 0.88 m/s are shown in the next diagram, Fig. 24. Although the wave shape is still quite reasonable it can be seen that there is a small ripple on the overall wave shape. The corresponding graph of the wave profile along the centre-line of the working section is shown in the middle diagram of Fig. 23 together with a sinusoidal curve. This also shows that the underlying wave agrees quite well with the sinusoidal curve but the general agreement is less good than at 0.56 m/s because of the presence of the ripple wave.

Similar measurements were made for the same wave length and wave height but for a higher water speed of 1.2 m/s. The results, which are illustrated by the wave profiles shown in Fig. 25, show a marked deterioration of the surface shape of the wave. The ripple has now developed to a significant degree and there appear to be five ripples per cycle of the main wave. The actual wave height can be seen to vary as the ripple and the main wave interfere with each other although the underlying wave was still 1 m in length and 30 mm in height. A similar result is shown in the graph of the wave profile along the centre-line which is shown in the lower diagram of Fig. 23.

These measurements showed therefore that the wave-maker could produce a satisfactory wave profile at lower water speeds and that the both the wave length and

height could be set and maintained from the calibration settings of the wave-maker paddle and motor speed. However the presence of the ripple wave imposed on the main wave provided a limit on the effectiveness of the wave-maker in its present form.

3.3.5.4 Ripple waves

A preliminary investigation was made (Sutcliffe, 1995) to find the origin of the ripple waves and to see whether changes could be made to remove them. Observation of the water as it left the paddle of the wave-maker showed that these little waves could be seen leaving the edge of the paddle at the top and bottom of each stroke.

In order to produce a smooth regular wave in the flume it is necessary that the water should flow off the paddle in the correct direction; thus at the top and bottom of the wave the water should be flowing horizontally. However with the present design of the wave-maker paddle the water tends to be travelling at its maximum gradient at the top of the paddle stroke. A similar effect is found at the bottom of the paddle stroke. There is therefore a discontinuity of gradient at the top and bottom of the wave which appears to cause the ripple wave. Since the wave is small, it tends to have a short length and a correspondingly slower speed than the main wave so that, although created at the same frequency, a number of these ripples waves are superimposed on a single cycle of the main wave.

Some preliminary experiments were carried out with a flexible addition to the basic paddle with the idea that the flexible part would bend to follow the main wave shape as the paddle oscillated. This modification did seem to reduce the magnitude of the ripple wave suggesting that further work along this line might lead to further

improvements. A next step might be to provide a flexible or jointed paddle with the shape imposed by a series of cranks. An alternative would be to make the paddle out of "Smart" material with an electrical control system programmed to achieve the desired shape.

3.4 The water tunnel

As discussed earlier the flume can also be used as a water tunnel, in addition to its normal configuration as a water channel, through the use of one of the covers. This cover, which is normally stored on the mezzanine floor at one end of the laboratory, has to be lifted along and lowered into the working section. The cover rests on a number of arms which locate on the flat surface of the edge of the working section so that the lower surface of the cover is level with the normal water surface. The forward end of the cover is flush with the edge of the plate on the injection box. Two of the arms on the cover each contain two 16 mm diameter holes which coincide with similar holes on the edge of the working section. Stainless steel bolts are inserted into these holes and tightened down both to locate the cover and make sure that it does not move in the course of an experiment. There is a rubber seal around the edge of the cover which should be tightened up until it squeezes against the side of the working section so that water cannot escape from the working section. It is usually found to be an advantage to increase the water level by a further 50 mm to make sure that air bubbles do not get trapped on the under surface of the cover. Further advantage may also be gained by raising the splitter plate at the end of the working section so that it is flush with the end of the cover - this reduces noise and air entrainment. It should be noted that in this configuration the equation relating the

main dial setting on the console and the water speed in the working section is slightly altered and is given in Eq. 3.4.

The earliest use of the flume as a water tunnel was the work of Sachdeva (1973) in an investigation of the growth of the boundary layer on the underwater part of the hull of a tanker. The hull was attached to the cover which acted as a reflection plane to represent the free surface at the low Froude numbers at which the tanker would operate. The growth of the boundary layer was measured using the miniature Preston tubes developed by Cole (1973) and also reported in Cole and Millward (1978).

3.5 The cavitation tunnel

As stated earlier in Section 3.1, the flume is also capable of being used either as a cavitation channel or as a cavitation tunnel. In practice it has not been used as a cavitation channel, that is with the free water surface present but with the working section depressurised so that the cavitation number can be varied for tests on a model such as a hydrofoil. It has however been used as a cavitation tunnel on a number of occasions, notably in the research by Naylor (1981) on the formation of a tip vortex on ship stabilisers and the later work by Higgins (1993) on the oscillating forces on foils, again representing ship stabilisers.

The first stage of converting the flume into a cavitation tunnel is to install the cover which converts it into a water tunnel, with the model to be tested attached to the under surface of the cover if appropriate. Care needs to be taken at this stage in designing the model and measurement instrumentation since, once the cavitation lid is in place and the working section depressurised, there is no immediate access to the

model. Therefore any signal leads which are needed either to operate the model or to measure forces etc. have to come out through the cavitation lid. This is normally done by removing a small side window and replacing it with a board onto which plugs and sockets are installed so that leads are connected from the model to the inside of the board and from the outside of the board to the controls or signal conditioning equipment. It is essential that this connector board is well sealed to avoid leaks when the pressure in the working section is reduced. A detailed procedure for installing the cavitation cover is given in Appendix 6.

In earlier days the pressure in the working section was monitored with a simple U-tube manometer filled with mercury and was controlled by switching the pump on and off. This was, however, found to be awkward since it required an extra person to be present solely for this task. A modification therefore has been the addition of a pressure control valve in the pipe-line to the vacuum pump which switches the pump on and off at a chosen pre-set pressure.

It should be noted that, if the tests are to be undertaken at low pressures in the working section, the vacuum pump is sufficiently strong that the water will be pulled down out of the contraction unless the flume is run up to speed before the lower pressures are achieved. This should be taken into account when planning the sequence of the measurements to be taken.

In cavitation experiments it is important to be able to control the dissolved air content of the water. A de-aeration system has therefore been fitted to the water channel which draws water off from the flume, passes it through the de-aeration chamber and returns it to the main circuit. The manufacturer's specification shows that the air content of the water can be reduced to 5 parts per million in four hours. The air content of the water can be measured with a van Slyke apparatus if desired

and a method of correcting for the air content of the water has been developed and is described in Millward and Naylor (1984).

3.6 Shallow water

As described earlier in Section 3 the normal depth of the working section is 0.84 m and there is a false floor which can be adjusted in angle to avoid the presence of standing waves. However the screw jacks fitted to the false floor are sufficiently long so that, in addition to being used to adjust the angle of the floor, they can also be used to raise the false floor in the working section. This adjustment can be used in a number of ways such as to reduce the depth of the working section and so change a normal three dimensional aerofoil into a two dimensional foil. This was, for example, used in the tests by Higgins (1993) on ship stabilisers which are also described in Higgins and Millward (1996). A second possibility is to use the false floor to simulate the effect of shallow water on ship models. However it should be noted that adjusting the depth of the floor does reduce the water speed in the working section to a small extent as shown in Fig. 26 - this shows the water speed in the centre of the working section at 50 mm below the water surface as a proportion of the expected water speed as the depth of water above the false floor is reduced. A curve fit through the data points gives the equation

$$\frac{U_H}{U} = -0.1165\ H^2 + 0.1806\ H + 0.9305 \qquad (3.23)$$

where H is the depth of water in metres and U_H is the water speed measured at 50 mm below the water surface when the depth of water in the working section is H and U is the water speed at the same point with the normal depth of water in the working

section. It is however strongly recommended that an individual calibration should be obtained for any experiment where the depth of water is significantly less than the standard depth since the forces on a model are related to the speed squared and the results given above were obtained at one water speed only (2 m/s).

Originally the height and angle of the false floor had to be measured by inserting a special ruler into guides in the working section - each guide being in line with the position of the jacking point. This was however found to be impractical when working with ship models since the floor needed to be set and adjusted for each speed and, at higher speeds, it was possible that the ruler would be pulled out of the hand of the operator by the flow of water. A number of methods of recording the position of the floor remotely were investigated but the method finally chosen was to mount digital counters on the shaft of the electric jacking motors which adjusted the height of the floor. The counters have relatively large numerals and can be read by the operator from the operating platform although when the false floor is in a high position, i.e. for shallower water depths, the operator does have some difficulty because the counters rise with the jacking motors and are therefore hidden by the working section itself.

Steps have now been taken to be able to read the counters remotely at the operating console. A number of ways of achieving this were considered and the method chosen was to use an optical trigger mechanism mounted on the end of the shaft of the digital counters. Some problems were encountered in making sure that no count was lost when the motors were reversed in direction several times such as might well happen when making the last fine adjustments to get the floor to a particular setting. The floor settings can now be read conveniently from the console. It should be noted however that, as part of the normal operating procedure given in

Appendix 4, the readings of both the counters on the jacking motors and the electronic display at the console should be checked at the beginning of any run since it would be possible for the electronic display to become corrupted if there is any interruption of the electrical supply. On reflection, since a number of problems were encountered in making the trigger mechanism and associated circuits work properly without losing a count, it would probably have been cheaper, and just as suitable, to install small video cameras to read the existing digital counters with a display on a screen by the console. This method is recommended for any future water channel.

A calibration graph of the depth of water at the centre of the working section, midway between the two jacking points, is shown in Fig. 27 against the counter reading. The equation for setting the water depth H is

$$H = 100 + \frac{N}{11.95} \qquad (3.24)$$

where N is the average counter reading and H is found in millimetres. It can be seen that the shallowest water depth is 100 mm and, since the counters can be set to one digit in approximately 9,000 with care, the floor or water depth can be set to an accuracy of 1/12 mm. It should be noted that the depth of water given is the depth of water at the midpoint of the working section where it is assumed that any model is likely to be and is calculated from the average of the front and back counters. Eq. 3.24 has been expressed in this manner since it may be necessary, as in normal operation of the flume, to have a tilt on the floor (usually about 260 counts) to obtain a wave free water surface with the result that the actual water depth along the false floor will vary. In the case of the standard tilt this would be approximately 22 mm between the two jacking points although the effective water depth would be approximately constant since the tilt on the floor corresponds closely with the growth

in the displacement thickness of the boundary layer formed on the floor by the viscous effects of the water.

3.7 Generation of an artificial boundary layer

In the original design of the flume considerable trouble has been taken to make the flow in the working section as uniform as possible both across, along and through the depth of the working section. However in some cases it may be desirable to have a non-uniform flow distribution such as in the case of the work by Cheah (1984) which studied the spread and dispersion of a non-buoyant gas in air by modelling it with flow of a heavy salt solution in the fresh water of the flume. The advantages of this type of modelling, compared with working in a wind tunnel with gases which are usually either toxic or flammable, were that it was safe and, by using a conductivity probe, it would be possible to obtain measurements of the mean and fluctuating concentrations of the plume fluid - a measurement which is difficult in wind tunnel measurements using air. It was hoped that these concentration measurements together with the more usual measurements of mean and fluctuating fluid velocities would give a better insight into the dispersion mechanism.

In order to do these experiments however it was necessary to be able to create a boundary layer in the working section to represent a model of the atmospheric boundary layer into which the plume would be released in real life. Since the working section of the flume is only 3.66 m long the natural boundary layer on the floor would only be about 70 mm thick at the end of the working section and not therefore practicable for modelling purposes. A study was therefore made of the literature available on methods of creating artificially thickened boundary layers. This

review showed that there are basically three main methods of generating thickened boundary layers which are summarised below.

In the first category the rate of growth of a natural boundary layer is accelerated either by introducing a boundary layer trip, which produces an abrupt momentum deficit, or by using a roughened surface to increase surface friction. In both cases the net increase in the boundary layer thickness per unit length is small but the resulting flow has the desirable property that it closely resembles a naturally grown boundary layer. Although either method would be suitable for specially designed meteorological wind tunnels, which have a long working section, they would not be suitable by themselves for a normal wind tunnel or for the flume where there is a restricted length of working section.

The second category of techniques includes those based on "active" flow mixing devices such as wall jets which are used to augment the flow properties in both the inner and outer regions of the boundary layer. The turbulence field of the existing developing boundary layer is enlarged due to the intense turbulent mixing introduced by the jets because regions of influence of the large eddies are extended further away from the wall into a larger non-turbulent part of the flow. The enhanced mixing facilitates the diffusion of turbulent kinetic energy from the inner to the outer region and, since the mean flow field is retarded by increased Reynolds stress levels, the boundary layer thickness is increased. Such a system was used by Nagib et al (1974) using a counter-jet technique to create a neutral atmospheric boundary layer in a wind tunnel. Although the technique offered great flexibility in manipulating the turbulence level, fine control and adjustment of the counter-jet orientation were required. The major advantage claimed by this system is that the mean velocity and the turbulence are independently variable.

The third category includes methods that introduce shear and turbulence into a flow by causing a disturbance across the entire section including the potential flow region outside the existing boundary layer. This category includes any methods of producing shear layers with graded drag-producing mechanisms such as the use of gauzes, honeycomb or grids of rods or plates which are used to introduce a distributed blockage in the boundary layer as well as the free stream flow. For this method the formation of the mathematical model for the design of the grid of rods is generally based on some characteristic argument such as to neglect the production of shear stresses and to assume that no further change will occur in the profile once it has been produced.

A variety of methods has been used in the past and were reviewed by Cheah (1984). The most convenient technique for the experiments in the flume was considered to be a combination of boundary layer trip, rough surface and flow mixing devices. The technique generally uses some barriers, surface roughness and an array of protrusions or flow mixing devices which extend from the solid boundary into the free stream outside the approaching boundary layer. The turbulence field and the wake from the flow mixing devices convect downstream and merge with the existing wall boundary turbulence and an accelerated version of a naturally developed boundary layer is produced. A satisfactory configuration of the boundary layer simulation system was developed by Counihan (1969) and has since provided a technique for generating artificially a thickened boundary layer in a wind tunnel.

In the flume the same boundary layer simulation system developed by Counihan was used to generate a thickened turbulent boundary layer in the working section. A wooden false floor was installed in the working section 100 mm above the existing metal floor to make it easier to install the boundary layer generation devices

and also to incorporate the equipment necessary to be release the salt solution which created the heavy plume. The boundary layer simulation system consisted of a castellated barrier across the leading edge of the false floor followed by eleven quarter elliptical vorticity generators, with a constant semi-wedge angle of six degrees, and a rough surface. The arrangement of the boundary layer system is shown in Fig. 28. Initially three different barriers were tested - a 20 mm plane barrier, a 32.5 mm and a 20 mm castellated barrier. Investigation of the flow velocity and turbulence downstream of the barrier showed that the 20 mm castellated barrier was the best. The rough surface was originally provided by sticking sheets of expanded PVC mesh on the wooden false floor. However it soon became evident that the PVC mesh was unsuitable for studies involving the physical modelling of a dense plume because the porosity of the mesh allowed the fluid from plume to get below the mesh and therefore affect plume development. It was also found not feasible to measure the plume concentration within the mesh using the conductivity probe. The final model for the boundary layer simulation therefore used standard "Lego" boards to create the surface roughness.

Measurements were made of the velocity distribution and turbulence along the length of the working section and also across the width of the working section to determine the effectiveness of this method of creating an artificially thick boundary layer. Details of the investigation can be found in Cheah (1984) but are summarised in Figs. 29 and 30. It can be seen that the representation of the velocity distribution and turbulence of the atmospheric boundary is satisfactory.

3.8 The stationary wave

As discussed earlier, the main use of the flume has been related to tests on ship models and similar structures where the requirement of a water channel is that the water surface should be flat, horizontal and wave free throughout the operating range. In order to achieve this the method used in the flume was the tilting false floor which is adjusted in angle for each flow speed. In addition the screw jacks, used to adjust the floor, were sufficiently long that the false floor could be adjusted to give a chosen depth of water above the floor from 0.10 m to the maximum of 0.84 m without significantly changing the water speed in the working section as described in Section 3.6. A further attribute of the tilting false floor however is that, by tilting the floor the "wrong" way (with the downstream end slightly higher than the upstream end), a wave can be created in the working section which, at the appropriate combination of water speed and depth of water, travels upstream at the same speed as the water is travelling downstream so that the wave remains stationary in the working section. These waves are of a large scale, with a wave length comparable to the water depth, and have been used by McIver (1980) to make detailed measurements of the wave profile and particulary the velocities within the wave using the probe described in Section 5.5 as part of a study into waves. A typical wave which can be produced in the channel will have a wave length of 3 m and an amplitude of 0.15 m in 0.4 m depth of water and be generated by tilting the floor only about 0.1^{o} from the horizontal.

As shown in Section 3.3.1 the equation for the speed of a wave reduces in a finite depth of water to

$$c = \sqrt{g\,H} \tag{3.25}$$

where H is the depth of water. Thus for the full depth of the flume, which is 0.84 m, a solitary wave can be obtained at approximately 2.8 m/s and at lower speeds for shallower depths of water. At the full depth of 0.84 m McIver has shown that the wave obtained is distorted by the limited length of the flume working section but at shallower depths the wave obtained is a close approximation to the shape of a solitary wave. In practice it has been found that the amplitude of the wave can be varied by adjusting the tilt of the floor so that, for example, at full depth of 0.84 m the wave comes close to spilling over the sides of the working section. If the floor is tilted far enough the wave can be made to break. The onset of breaking appears to be aided by viscous effects at the sides of the working section since an oblique wave is formed at each side about half way up the front face of the wave. For a sufficiently steep wave these oblique waves are unable to surmount the crest and they meet. This appears to trigger breaking of the wave and a band of turbulent water spreads down the front face of the wave. By careful adjustment of the flow conditions it is possible to create a wave that will break periodically.

4. Force Measuring Equipment

A number of force measuring balance or dynamometer systems have been developed and can be used for tests, particularly in the open channel configuration. For most problems where quasi-static forces are being measured the standard signal conditioning equipment is suitable but a PC with analogue digital converter is available for recording and analysis of time dependent measurements.

4.1 Main dynamometer

In many cases with the open channel configuration the requirement is likely to be the measurement of the resistance of a surface vessel over a given speed range of the flume corresponding to the operating Froude number range of the vessel. In most cases it is also desirable to measure the trim of the vessel while for sailing yachts it is necessary to be able to set the leeway or yaw angle, to set or measure the heel angle, and to measure the side force in addition to the resistance. For a yacht sailing to windward a typical Froude number F_n could be in the region of 0.1 to 0.5, corresponding to flume speeds of between 0.3 and 1.5 m/s, whereas for a high speed displacement hull or catamaran a typical operating Froude number could be between 0.4 and 1.2 (corresponding to water speeds of 1.2 to 3.75 m/s) while for a planing hull, hovercraft or hydrofoil the speed range could be even higher. In designing a suitable dynamometer therefore, it was important to consider the wide speed range of hulls which might be tested and the corresponding wide range of resistance and other forces which needed to be measured with a good degree of accuracy. In addition consideration was given to the advantage of being able to do a check calibration of the dynamometer at frequent intervals to ensure the accuracy and repeatability of the measurements being made.

A schematic diagram of the dynamometer developed is shown in Fig. 31. The model hull, usually about 1 m in length, is normally attached through a gimbal to the centre post which is free to heave; this allows the model to adopt the attitude in the water dictated by the hydrodynamic forces and in addition is a safety device since the water level may change when the water in the flume is being speeded up or slowed down. Indeed, particularly when slowing down, quite large waves can be formed which advance up the working section against the water flow and care must be taken to make sure that the model is free to heave and that the wave does not force the bow of the model under the water. For slender models, with little bow buoyancy, it is often safer to lift the model partially or completely out of the water when slowing the water down.

As can be seen from the diagram in Fig. 31, the dynamometer consists of two cages which are each designed to measure a force; the upper cage measures side force while the lower cage measures resistance or drag. Each cage consists of four flexures, one at each corner, which are thin in the direction of the force to be measured but thick in the direction at right angles. The dimensions of the resistance and side force flexures are given in Table 3 and show that for the resistance balance the ratio of stiffness is approximately 60:1 while for the side force balance it is approximately 80:1. Thus the flexures will only deflect to the component of the total force which is in the required direction. In an earlier design of a similar dynamometer, at the University of Southampton, each flexure was made individually (Sainsbury, 1961). However this made the flexure difficult to hold for machining and also difficult to align and the design was later modified (Millward, 1967) so that the flexures were machined in pairs from a solid block of metal, as shown in Fig. 32.

This made them much easier to machine and also to align on installation or replacement so the same improvement was used in the present design.

The displacement of the flexures by the applied hydrodynamic force is measured with a linear variable differential transformer (LVDT) mounted on the centre-line of the floor of the cage but with the core, which moves in the LVDT, mounted on a rigid arm from the roof of the cage. The mounting includes a fine screw thread adjustment which allows the core of the LVDT to be positioned horizontally relative to the LVDT casing in order to get the physical zero as near coincident as practical with the electrical zero.

The principle of the LVDT is that the body of the device contains two coils; the first is energised with an A.C. signal (3 volts at 2.5 kHz). The position of the iron core in the coil generates a voltage in the secondary coil corresponding to that position which is then rectified in the signal conditioning unit, giving a maximum output of approximately 2.0 volts, and can, for example, be displayed on a digital voltmeter. The great advantage with this particular type of LVDT is that there is no physical contact between the body and the core so that there can be no friction in the system and therefore no viscous force preventing the dynamometer returning to zero after being deflected. The only restraining force could possibly come from the electrical wires feeding the LVDT but these are very thin and flexible. Provided care is taken to make sure that there is sufficient slack in these wires and that they are not disturbed during a test, any small restraint caused by the wires becomes part of the calibration of the dynamometer.

The thickness of the flexures was chosen so that the deflection under the design load matched as far as possible the displacement of the LVDT. The transducers chosen were the most sensitive of those available from Lucas-Schaevitz

Ltd and were Model 050 HR with a maximum displacement of ± 1.27 mm (± 0.050 in) for a linear calibration. If the resistance cage is considered as consisting of four springs or flexures, encastré at both ends, then the stiffness is given by

$$\frac{D}{\delta} = \frac{12\,E\,I\,n}{\lambda^3} \qquad (4.1)$$

where D = drag or resistance force, δ = cage deflection, E = modulus of elasticity of the metal of the flexure, I = second moment of area of one flexure, n = number of flexures and λ = length of a flexure. The design maximum resistance was chosen to be 9.81 N[1] which gave a value for I of 4.754 mm^4 with the flexures machined from an available aluminium alloy resulting in a flexure thickness of 1.65 mm. A similar calculation for the side force cage for the design side force of 29.4 N resulted in a thickness of 2.16 mm. In practice it has been found that the corresponding displacements under the design forces are 0.86 mm and 0.73 mm for the resistance and side force flexures respectively. This suggests that the equation used to design the flexures is not entirely satisfactory for the purpose and needs to be modified. A significant contribution to the discrepancy is that the flexures were designed with a radius each end as can be seen in Fig. 32. This was done in order to reduce the stress concentration in this area and also to ease the problems of machining. If the measured displacement is used in the equation then the effective length is found to be 130 mm for the resistance cage and 126 mm for the side force cage. In practice, in designing such flexures in the future it was first thought to be appropriate to incorporate a constant into the equation based on these results so that

[1] Note that at the time the SI system was not properly implemented so that the resistance calibration weight of 9.81N corresponds to a weight (not mass) of 1kg and the side force weight of 29.4N corresponds to 3kg.

$$\frac{D}{\delta} = \frac{12\,E\,I\,n}{(k\,\lambda)^3} \,. \qquad (4.2)$$

The results of these measurements showed that a value for k = 0.85 was appropriate. It was noted however that the length of the flexure which has a uniform cross-section between the end of the corner radii at each end of the flexure was 0.875 of the total length. Since this is very close to the value of k deduced from the measurements of the deflection of the flexures, this result would indicate that Eq. 4.1 can be used provided the length of the flexure is taken as the length over which the flexure is uniform and therefore excluding any corner radii.

As can be seen from the diagram (Fig. 31) a triangular arm is suspended on pivots from the roof of each cage of the dynamometer but also connected to the floor of the cage. Since each arm of the triangle is equal in length, a weight applied to the inner side of the arm will apply an equal force in the direction of the force that the cage is intended to measure. This can therefore be used for calibration and could also be used for check calibrations at intervals throughout an experiment. The outer arm will apply a force in the opposite direction when a weight is put on it and is therefore used to apply a unit force in the opposite direction to the force being measured when the magnitude of the measured force exceeds the design maximum load of the dynamometer. For example the resistance cage is intended to measure a force of 9.81 N with the full deflection of the LVDT giving a digital voltmeter (DVM) reading of approximately 2.000 volts. A larger reading of say 15 N would be read by placing a 9.81 N weight on the outer arm allowing the remaining 5.19 N to be read on the DVM giving a dynamometer with a wide range yet good sensitivity. It should be noted that the second arm coming down from the roof of each cage is part of a system which limits the horizontal motion of the cage. The adjustment screws of this

limiting system should be set to allow a deflection of not more than 1.3 mm in either direction for each cage of the dynamometer.

In normal use the check calibration weights, which correspond to the maximum force which each cage is intended to measure, are placed on the outer arm for ease of access. At intervals, usually as part of the familiarisation for a person using the flume, the dynamometer is calibrated by applying resistance and side force calibrations using weights on the lever arms to demonstrate that the calibration is linear as shown in Fig. 33. Secondly the dynamometer is calibrated by applying weights to represent the resistance or side force using a piece of light string over a pulley onto the centre post when the flume working section is empty but with the force applied at the height where the water surface would normally be. An additional calibration is sometimes carried out but with the calibration loads applied at a different height to demonstrate that the dynamometer responds only to the force applied and that, within reasonable limits, the line of action of the force is not significant. A typical calibration curve showing the results for two different heights of application is given in Fig. 34.

An off-load device is provided, attached to the centre post, so that the total weight of a model can be reduced if needed or alternatively the off-load weight can be adjusted so that the centre post and associated pieces are exactly counterbalanced - this is a useful procedure when the centre of gravity of the model under test is required to be in a given position which can be determined before attachment to the balance. A separate item of equipment is available to enable both the fore and aft position and the vertical position of the centre of gravity of a model to be determined.

A number of gimbals are available to provide the attachment between the model and the centre post. Each gimbal slots onto a keyway on the bottom of the centre post, which prevents the model rotating in yaw, and is secured by tightening a grub-screw. Each gimbal is attached at the other end to the model with four bolts which protrude from a baseplate fastened to the model. The baseplate is normally fastened permanently to the model and is made to a standard pattern. It is therefore relatively easy to detach the model from the dynamometer and also to remove the gimbal from the model for use in another model. The various gimbals have been designed for different applications so that most allow freedom to trim while some allow the heel angle to be fixed or free. The pivot point of the trim axis is 34.93 mm (1⅜ inches) above the base of the gimbal: this is an important measurement since in many ship resistance experiments the trim axis is set at the intersection of the vertical axis through the longitudinal centre of buoyancy (LCB) and the propeller shaft line. A separate device is available for determining both the longitudinal and vertical position of the centre of gravity of a model hull as mentioned above. A list of the various gimbals is given in Table 4.

The parameters which may be set or measured on the dynamometer are

Parameter		Increment
Side force	measured	29.4 N
Drag	measured	9.81 N
Yawing moment	measured	not in use
Yaw Angle	set $\pm 15^{o}$	vernier reading with remote adjustment
Heave	free	

The yaw angle, which is primarily used for tests on sailing yachts, can be set within the range $\pm 15^{\circ}$ to an accuracy of 0.1° using the vernier scale. Although the yaw angle can be set manually using the knurled knob on the dynamometer this is not encouraged since it needs to be done delicately. A more recent addition therefore is a modification which has added a small d.c. motor and screw thread system which allows the yaw angle to be set remotely by pressing the appropriate button on a control box, which is on a wandering lead, at the side of the water channel. In addition to its use in tests on sailing yachts, the yaw adjustment is used in tests on conventional boats in order to make sure that the model is aligned with the flow direction; it is assumed that the model is correctly aligned when there is no side force.

The signal conditioning box associated with the LVDTs is capable of supplying four channels of LVDTs or RVDTs (rotary variable differential transformer) - in normal practice the first two channels are reserved for the LVDTs which measure resistance and side force while the other two are used for the RVDTs on gimbal D which can be used to measure both trim and heel electronically. On occasion however, during tests on a yacht model in waves, for example, one channel has been used to measure heave (with a long displacement LVDT) instead of heel angle. The signal conditioning box therefore contains the power source for each of the four channels. Each channel supplies a separate 3 volt a.c. signal at 2.5 kHz to the primary coil of an LVDT or RVDT. The signal from the secondary coil of the LVDT or RVDT is rectified in the signal conditioning box and presented at an outlet terminal as a d.c. signal.

The output signal from the LVDT or RVDT signal conditioning equipment is normally of the order of 2 volts and, for the simplest situation, can be displayed

directly on a digital volt meter (DVM) to 1 mvolt accuracy. Although for calibration purposes direct display on a DVM is quite adequate, it was rapidly found that it was difficult to obtain a satisfactory measurement when the flume was running because of slight fluctuations in the forces being measured. A three channel integrator was designed by Fylde Ltd which averages the incoming signal over a chosen time period and it is then displayed on a DVM at the end of the timed period. The time periods available are 10, 20, 50 and 100 seconds and the integrator can also be switched out of the circuit if desired. In practice it has been found that a small shift of up to 5 mvolts may occur with the integrator switched in or out of the circuit so that the standard procedure is keep the integrator set on the same time period while measurements are being taken, including the check zero and full scale calibrations.

The standard operating procedure therefore, having set up the model in the working section, is to set the time period on the integrators (usually 50 seconds is found to be satisfactory), take the DVM reading with no weight on the dynamometer (V_0) and then take the reading with the calibration weight W on the off-load arm (V_{cal}). The flume is run up to the required speed and the appropriate force measured (V). The force in newtons can therefore be obtained from

$$F = -\left[\frac{V - V_0}{V_{cal} - V_0}\right] W \qquad (4.3)$$

where W is the calibration weight in newtons. It should be noted that the negative sign arises since the calibration weight is actually applying a force in the upstream (negative) direction so care needs to be taken to record the sign displayed on the DVM as well as the numerical value. A computer program has been written as part of the present work and is given in Appendix 3 which can be used to analyse data obtained on the main dynamometer. The program is written to allow measurements

of the DVM voltages corresponding to resistance, side force and trim to be recorded, together with the zero and calibration values. These are then processed, using Eq. 4.3, to give the forces and force coefficients on the model while the results can also be scaled to the full size vessel if required using the method shown in Section 6.1.3.

4.1.1 Dynamometer positioning

As originally designed the dynamometer was intended for measuring the forces and other parameters on a ship model positioned in the centre of the working section of the flume so that there would be minimum interference from the walls of the working section giving the nearest representation available to a model in open water. However, recently an investigation has been made into the motion axes of a sailing yacht (Sutcliffe and Millward, 1998) which required some modifications to the dynamometer. The proposition behind this work was that a sailing yacht does not move in the conventional earth axes as other vessels do when in waves but is constrained to move in body axes, by virtue of its shape and because the propulsive power comes from the sails. Experiments were therefore carried out on a yacht model to investigate this proposition and to measure the motion and resistance of a sailing yacht in both earth and body axes as shown schematically in Fig. 35. This involved modifying the lower part of the main dynamometer to allow motion in body axes when the yacht model was heeled over. It also resulted in the necessity of being able to move the dynamometer sideways across the working section in order to position the yacht back in the centre of the working section when heeled in body axes. A special sliding rail assembly was therefore designed so that this could be achieved.

It can be seen from Fig. 36 that the basis of the sliding assembly consists of two long angular steel sections which stretch the full width of the working section and are bolted to the main A-frame supporting the dynamometer parallel to the water surface. Two preformed rails with assemblies of linear ball races were attached to these supports - two sets of linear races at the back and one at the front with the top plate of the dynamometer attached to them. This allowed the top plate of the dynamometer to slide sideways across the working section while still remaining square to the flow direction and parallel to the water surface. A lead screw and slider mechanism were incorporated so that, by turning a hand wheel, the whole dynamometer could be positioned anywhere across the width of the working section. A scale and pointer were added so that the position could be set and recorded to an accuracy of better than ± 1 mm.

One of the advantages of this modification is the increased flexibility in the use of the flume since, with the position of the dynamometer a further variable, models can be positioned close to the walls of the flume in order to investigate the effect of a boundary on the resistance of a hull for example.

4.2 Force and Moment Blocks

As explained in the previous section the main dynamometer was required to be capable of measuring the forces and other parameters with suitable accuracy on ship models for a wide variety of problems ranging from measuring the forces on a sailing yacht at lower speeds to the forces on a planing craft at much higher speeds. It was anticipated that there was also a requirement for a versatile type of dynamometer capable of being adapted rapidly into different configurations to cope with a range of problems, particularly non-ship problems. An analysis of some of the

known tests suggested that the forces to be measured might range from 10 to 500 N in a variety of configurations. This indicated that a single dynamometer capable of this task would be very complicated, costly to manufacture and maintain and, if designed to cope with the largest forces and moments envisaged, would be insufficiently sensitive to measure the smallest loads with any acceptable level of accuracy. The idea adopted therefore was to design a dynamometer consisting of a series of unit blocks of different maximum capacities which could be assembled together into a variety of different configurations in order to cope with the most likely problems (Millward and Rossiter, 1983). In the majority of cases it was thought to be sufficient to measure one or two forces at right angles to each other together possibly with a moment to form a three component dynamometer e.g. lift, drag and pitching moment or side force, drag and yawing moment. In essence however there is no reason why a larger number of components cannot be measured although the greater the number of blocks assembled together the greater is the possibility that manufacturing tolerances will accumulate to give significant interaction effects between components.

The decision was made to use strain gauge blocks since force and moment measurements for the different load ranges could be obtained with small absolute deflections of each block in the dynamometer. This was thought to be an important factor in some cases, such as a rigidly held planing surface or a hydrofoil, where a significant deflection of the block could lead to a change in the overall geometry of the planing surface or hydrofoil with a consequent change in the hydrodynamic forces. An additional advantage of such a near rigid system, compared with the main dynamometer, is that fluctuating loads could be measured such as might occur on a hydrofoil or rudder near stall or even on a simple vertical strut.

Experience from other dynamometers (Millward, 1963) suggested that each block should be machined from solid to avoid any subsequent misalignment of the flexures. It was accepted that the initial cost of using solid blocks would be high in terms of machining time but it was felt that this was warranted in view of the higher level of reliability over a long period of time. A review of experience with possible materials for the blocks suggested the use of stainless steel, despite its higher initial cost and longer machining time, because it was inevitable that the blocks would be used close to the water with the associated problems of corrosion if either aluminium alloy or mild steel were used. This decision to use stainless steel has been vindicated since the blocks show no sign of corrosion and continue to be used regularly.

4.2.1 Load blocks

Two basic designs of load block were required - one to measure force and the other to measure moment. The dimensions of each type of block needed to be identical in overall dimensions but with the dimensions of the flexure adjusted to suit the designed maximum capacity. The choice for the overall size of the block, 101.6 mm (4 in), was necessarily a compromise solution taking into account such factors as the size of the flume itself, the height of the edge of the working section above the water surface, the number of blocks likely to be required at any one time and the flexure dimensions required to avoid measurable reaction to loads other than those intended to be measured.

The general appearance of a force block and a moment block is shown in Fig. 37. In each case the dimensions A and B depend on the design capacity of the block. The base plate at the end of each block contains four holes which have been located accurately on fixed pitch circle diameter while the holes have been drilled and

reamed to 7 mm diameter. This enables the blocks to be fastened together either in line or at right angles to each other using special stainless steel bolts which have a ground shank. There are also two L-shaped angle base plates with an identical pattern of holes in each arm of the angle so that blocks can be fastened at right angles or to a base plate. Finally there is also a beam which fits across the working section of the flume which has a plate mounted on it with the face of the plate on the centre line of the flume and normal to the water surface. The face plate again has the same pattern of holes and also a vertical adjustment of 10 mm. This system allows the blocks to be fastened together in a variety of ways but in an accurate and repeatable configuration. A diagram of the arrangement used to make measurements of lift and drag on a hydrofoil, for example, (Charlton et al, 1987) is shown in Fig. 38.

The design capacities of the force blocks in use are 10, 100 and 500 N with one moment block with a capacity of 50 Nm.

4.2.2 Strain gauges

Since the load blocks were intended to last for a considerable period of time - of the order of years - the decision was made to use strain gauges which were already mounted on a stainless steel mounting plate when obtained from the manufacturer and could therefore be simply welded in place. Although these gauges were considerably more expensive in capital cost it was felt worthwhile since they offered both the advantage of long term stability compared with ordinary glued gauges and also ease of installation by staff without previous experience in strain gauge techniques. Experience has shown that both these advantages have been borne out in practice.

Four 120 ohm gauges were mounted on each block and connected together in a full Wheatstone bridge configuration thus giving maximum sensitivity and also built-in temperature compensation. In the case of the force blocks the gauges were mounted on the inside faces of the flexures in order to protect them from mishandling as much as possible. On completion the gauges were also covered with a waterproof sealant to give further protection from water splashes.

Each load block can be connected to a standard strain gauge bridge unit with appropriate balancing controls. This is connected in turn to an amplifier unit and thence to a digital voltmeter. The laboratory has two bridge-amplifier units for this purpose - one three channel unit and one six channel unit; both are manufactured by Fylde Ltd and contain bridge sub-units and amplifier sub-units. This gives a flexible system since either unit can be used depending on the number of loads to be measured, particularly since the same units can be used with pressure transducers, and a rapid interchange can be made should a unit or sub-unit fail.

For steady conditions the output signal from the amplifier is displayed on a digital voltmeter (DVM). However for nominally steady conditions there is usually sufficient unsteadiness in the signal to make it difficult to read on a DVM directly so an integrator is placed in the circuit. This unit averages the signal over any of four fixed periods of time - 10, 20 50 and 100 seconds. For unsteady conditions or where it was required to know more than just the average of the signal the output of the amplifier could be connected to the analogue-digital interface of the PC in the laboratory.

4.2.3 Calibration

The calibration of a dynamometer consisting of a series of load blocks is considerably simpler than for a more complex multi-component dynamometer since each load block can be calibrated separately on the bench to determine the normal calibration curve. It is however necessary in the first instance at least to find out whether there are interactions between each component and also whether there are any reactions to loads other than those which it is intended to measure. Checks were also needed to measure the effects of hysteresis and creep.

A calibration frame was designed and constructed from ordinary mild steel but with a stainless steel faceplate where the load blocks were attached. The calibration frame is intended for periodic calibration checks but was also used initially with some temporary additions to make sure that the force blocks responded only to the applied force rather than a moment; this could be done by varying the point of application of the load. The calibration curve for each block was found to be linear within the design range as can be seen from the example shown in Fig. 39. This curve was obtained with the supply voltage set to 4 volts and with the gain on the amplifier set at 1000. The equation of the curve for this particular block was found to be

$$V = 1232.5\ W + 5 \qquad (4.4)$$

where V is the resultant voltage on the DVM in mv and W is the weight or applied force in newtons. It was found that this curve was repeatable to better than $\pm 0.5\%$ of the full scale reading even over a period of weeks although there was some drift of the zero reading. Initially it was thought that some care would need to be taken to make sure that a block was always connected to the same signal conditioning channel but subsequent experience has shown that this is unnecessary provided the

bridge supply voltage is set to the standard level of 4 volts. It is however recommended as good practice that a block should remain connected to the same channel throughout an experiment. It is also standard procedure that the strain gauge equipment should remain switched on for the whole period of an experiment, even at night.

In order to check that the force blocks responded only to force rather than moment the standard calibration apparatus was modified by clamping a piece of channel across the top of the block instead of the little load platform. The maximum design load was then applied at different distances from the base of the block and the voltage measured. The results showed that there was little effect from changing the distance thus demonstrating that the force blocks do indeed respond to force only rather than moment.

The output voltage V_o of the Wheatstone bridge in the system, and hence the sensitivity of the unbalanced bridge when a load is applied, is proportional to the bridge supply voltage V_s i.e.

$$V_O = V_S \, k \, \epsilon \qquad (4.5)$$

where k is the gauge factor and ϵ is the strain in one arm of a full bridge with four gauges and equal strains in each. In order to obtain the maximum sensitivity to the design load it is desirable to have the largest acceptable bridge supply voltage V_s. The major factors which determine the acceptable bridge supply voltage are the power dissipation properties of the gauge and the heat sink properties of the mounting surface. In this design the gauges were mounted directly on foil which was relatively large in area and was in turn welded to the metal block which provided a good heat sink. Several different supply voltages were tried leading to a choice of 4 volts d.c. as the standard bridge supply voltage to be used with these blocks.

4.2.4 Interaction

The origin of many interactions can be attributed to construction errors and also, in a conventional dynamometer, to incorrect positioning of the strain gauges. In the present design the block only responds to the load in the chosen direction because of the different stiffness of the flexures about each axis, as with the main dynamometer, so that poor positioning of the strain gauges has, within reasonable limits, a negligible effect except as a small difference in the sensitivity of blocks with nominally identical capacities. Correct positioning of the strain gauges was made easier because they were already mounted on the backing foil, when obtained from the maufacturer, and could be aligned easily with the edge of the block before welding into place.

The response of each force block to loads normal to those intended was checked and found to be very small. This check was particularly important since in some experiments, such as lift and drag on a hydrofoil, one force may be an order of magnitude greater than the force normal to it. It was therefore assumed that a likely worst case would be when the normal load was 10 times the maximum design load of the force block. The results of this test showed that errors of less than 0.5% were introduced.

Another possible source of interaction between components is due to lack of accuracy in manufacture resulting in misalignment of the various blocks when assembled together with joining pieces. In this design the critical dimensions and sources of error were the locating holes used to fasten the blocks together and also the squareness of both the blocks and the angle brackets used to fasten the blocks together in some of the anticipated configurations. Initially some problems were

encountered in the squareness of the angle brackets due to poor machining but these were subsequently resolved.

The purpose in designing the force and moment blocks was to give a versatile dynamometer system which could be tailored to suit a variety of measurement problems likely to be encountered in the water channel. The resulting load blocks have been shown to be successful in use with small interactions, good long term stability and ease of assembly into a chosen configuration. It should be noted however that, although very reliable, normal practice should be followed by calibrating each block before and after any experiment as a minimum.

4.3 The miniature dynamometer

This dynamometer was designed and built for some experiments where it was desired to investigate the swimming capabilities of various scallops (Millward and White, 1992) by measuring the lift and drag developed by these scallops over a range of water speeds which was thought to be appropriate for their swimming capability. Since the scallops were approximately 50 mm or so in diameter it was convenient to test plaster models of the actual scallops so that their shape and surface texture were accurately reproduced. The models were therefore full size representations of the real scallops so that no problems of scaling were involved. The models were tested at the real water speeds thought to be appropriate, in this case up to 0.6 m/s. Initial estimates of the lift and drag forces likely to be developed, using the work of Gruffydd (1976), Thorburn and Gruffydd (1979) and Hoerner (1967), indicated that the forces were too small to be measured sensibly on the main dynamometer. The shell models were therefore mounted on the specially designed dynamometer, shown

in Fig. 40, which was capable of measuring lift and drag. As can be seen from Fig. 40, the shells were mounted on a short arm from the dynamometer and held in the vertical plane so that the lift force was measured as a horizontal force. This method was adopted to make the setting of the angle of incidence simple and to avoid the problem of the lift force and the weight of the model acting in the same plane causing instability, as encountered by Gruffydd (1976). This design of dynamometer also avoided the other problem encountered by Thorburn and Gruffydd (1979) who measured the drag using a pulley upstream of the model and therefore had the likelihood that the wake from the pulley impinged on the model with unknown effects. The support arm between the shell and the dynamometer was made from thin aluminium alloy plate which was chamfered to reduce its drag. This support arm was glued into a slot machined into the model on what would be the undersurface in the swimming mode. This followed the normal practice in the aeronautical field so that the support strut would not interfere with the flow on the 'upper surface' of the model. A streamlined support shield was made for the vertical support from the model to the dynamometer so that the drag of the support itself was reduced and hence would not be a major proportion of the total measured drag force.

As can be seen from Fig. 40 the principle of this dynamometer is the same as for the main dynamometer described in Section 4.1, that is the dynamometer consists of two cages which are each designed to measure a force. Each cage has four flexures, one at each corner, which are thin in one direction but thick in the direction at right angles. Thus the cage only deflects to the component of a force which is in the direction normal to the plane in which the flexures are thin. In the case of the main dynamometer the flexures were machined in pairs from a solid billet of metal with a web joining the pair together in order to make the possibility of misalignment

as small as possible. For this shell dynamometer however this type of construction technique was not possible because the forces being measured were so much smaller and the corresponding thickness of the flexure was too small to be machined from solid. The flexures were therefore made from available spring steel. The flexures were clamped into blocks at each end with holes drilled through both the block and the flexure which were pinned to prevent the flexure coming out. This method of construction however had the disadvantage that care had to be taken to make sure that the clamps did not work loose which would affect the calibration.

The displacement of the flexures was measured in the same way as for the main dynamometer - using an identical LVDT for each cage. This resulted in the additional advantage that the same signal conditioning and processing equipment was suitable for this dynamometer as well. For the experiments reported in Millward and White (1992) the dynamometer was mounted over the working section of the flume using one of the angle brackets made for mounting the load blocks described in the previous section.

The dynamometer was calibrated in the working section at the beginning of the experiments by emptying the working section until the water was below the false floor which was partly raised; this was to economise on the amount of water released. A thin cord was attached to bottom of the support strut and stretched over a special low friction pulley system which was mounted on a board further down the working section. Care was taken to make sure that the cord was parallel to the centre line of the working section and weights were added in increments to give a calibration curve of the load against output voltage on the DVM. The dynamometer was turned by 90^{o} in order to calibrate the lift force cage.

Care had to be taken in use since, unlike the main dynamometer in its present form, the incidence of the shell had to be set manually on the incidence control on the drag cage. This needed a very delicate touch although calibration at the end of the experiments showed that no harmful effects had occurred. In retrospect, since the magnitudes of the lift and drag on the shell were of the same order of magnitude, unlike an aerofoil, it might have been better to arrange the incidence by rotating the whole dynamometer thus keeping the shell model fixed relative to the dynamometer. This would therefore have measured the normal and tangential forces of the model and the lift and drag forces could have been deduced from them.

4.4 T.E.M. dynamometer

This dynamometer, which was obtained from a commercial source, is shown schematically in Fig. 41. Attachment of the model is made directly to the balance so that unless any separate provision is made the model is held in a fixed position. This balance is therefore more suitable for fully submerged models such as submersibles, hydrofoils or aeroplane models. A more detailed description of the balance is given in Appendix 9 which is taken from the manual supplied with the equipment.

Measurements can be made of lift, drag and pitching moment with this balance. (Maxima - Lift 98 N; Drag 38 N, Pitching Moment 1.8 Nm). It should be noted that this balance is calibrated in Imperial units.

4.5 Time dependent measurements

The majority of the experiments carried out in the flume involve measurements of the steady or quasi-steady parameters such as the resistance and trim of a ship model at steady speed which will be obtained once the speed of the flume has settled to the pre-set condition. In these cases therefore the output signals from the LVDTs and RVDTs on the main dynamometer or from the strain gauges on the load blocks should be independent of time. In reality the signals are never totally independent of time since the water surface of the flume is not precisely steady - there are always tiny fluctuations in speed and water surface which lead to small variations in the parameters being measured. However it has been found sufficient in these quasi-steady conditions for the output signals to be passed through an integrator before being displayed on a DVM. As discussed in Section 4.1, the integrator averages the input signal over a fixed time period chosen by the operator from 10, 20, 50 or 100 seconds. This has been found to be satisfactory and, for example, with experiments on catamarans and other fast vessels a time average over 50 seconds gives very repeatable answers to within a few millivolts where the full scale signal is around 2 volts.

In some cases however, such as when using the wave-maker, the measured parameters will be time dependent and a more sophisticated data collection system is required. Early attempts to measure time dependent forces and other variables involved the use of equipment such as ultra-violet recorders with the analysis involving much manual labour but more recently the advent of the modern micro-processor and analogue-digital converter has made this task much easier. Thus for experiments such as those on the wave-maker by Sutcliffe, (1995), the laboratory has been equipped with a PC with an analogue-digital converter (ADC). The output

signal from the measuring equipment is first passed through a low pass filter before being input to the ADC which is a 16 channel multiplexed converter. This allows a number of channels to be sampled simultaneously and a schematic diagram for the measurements of forces etc. on a yacht in waves is shown in Fig. 42. As can be seen from the diagram, for this particular set of experiments channels 1 and 2 were used for the wave-maker position and wave probe respectively while the drag force, side force and heeling moment were input on channels 3, 4 and 7 with the pitch and heave on channels 5 and 6. The signal from each channel could be displayed on an oscilloscope or DVM so that it could be monitored for calibration and inspection purposes.

A number of programs were written for this data collection and are discussed briefly in Appendix 2 while a more detailed discussion is given in Sutcliffe (1995).

5. Measurement of water speed

5.1 Pitot static probe

The conventional method of measuring the flow speed in many applications is to use a standard pitot-static probe. Provided the probe is aligned with the flow within about 15°, then for a probe with an ellipsoidal head the recorded pressure difference is within 1% of the true value and hence the measured velocity within ½% which is adequate for most applications (Bryer and Pankhurst, 1971). When the flume was built a pitot-static probe assembly was supplied which was mounted on the end of a symmetrical bi-convex blade with a chord of 60 mm and a total length of 1.40 m. The blade had a scale engraved on it so that the distance of the probe below the water surface could be determined. The blade was mounted in a carrier which was in turn mounted on a beam across the working section. The carrier could be moved along the beam, which also had an engraved scale, and clamped in any chosen position on the beam. Finally the beam itself could be moved along the working section on brass rails and clamped in any position. This allowed the probe to be positioned at any depth, cross-stream or stream-wise position in the working section.

The pressure tubes from the pitot and static probes, which were concentric, were embedded in the support blade and projected out through the top of the blade so that they could be connected to a manometer which was also supplied. The manometer was mounted on the side of the contraction in such a way that it could be easily removed for cleaning the tubes and to allow air to be bled out of the tubes. In its normal position, the menisci in the manometer were approximately half way up the tubes and, of course, level with the static water in the working section when there was no flow in the flume. Since in normal running the static water level, and hence the static pressure in the manometer, does not change greatly this meant that

the largest pressure difference between static and pitot pressures was half the length of the tubes or about 1m. This is likely to be inadequate at the higher water speeds since, with a maximum speed of 5.7 m/s, the head difference would be expected to be 1.66m. The top of the manometer was therfore fitted with a manifold so that both tubes can be equally pressurised with air using a bicycle pump or other convenient means. In this way the static pressure level can be lowered to near the bottom of the manometer allowing the full length of the manometer to be used. In practice it has also been found that the heads in the manometer are not particularly steady so restrictors have been inserted in the tubes leading from the probe to the manometer.

Initial measurements, when the flume was being commissioned in about 1967, showed an unexpected problem with the pitot-static probe caused by the hydrodynamic forces on the support blade. Although the blade was nominally symmetrical and in line with the flow, if there was any small perturbation such as a variation in the incidence or flow direction, the blade would generate a sideways force, acting as an aerofoil section at an angle of incidence. The resulting side force could be expected to have a line of action at the quarter chord point approximately acting as a moment around the torsion axis at the centre of the section. This gave an unstable situation which was divergent and in practice resulted in a violent bending of the blade. A solution was found by holding the blade in a sub-mounting which is pivoted at a point forward of the leading edge of the blade section. This, together with the rubber torsion sleeve in the pivot to provide damping, gives a stable configuration such that any side force generated tends to return the blade to a zero angle of incidence in a similar manner to a weathercock. This modification has proved to be successful and should be incorporated in any future design. As a result the pitot-static probe has been in use ever since for speed measurements at medium

to high speeds where the head generated on the manometer is sufficient for satisfactory measurement.

5.2 Propeller flow meter

A portable propeller flow meter instrument is available in the laboratory which can be used to measure flow velocities in the working section of the flume such as downstream of an object. However the diameter of the larger of the two propellers is 50 mm so that the discrimination of changes in flow field would not be very fine. Even the smaller of the propellers has a 30 mm diameter. A more common use is to calibrate the flow meter in the flume and then to use the flow meter to measure the flow speed elsewhere such as in the small paddle wheel flume.

The instrument, which is made by Ott, consists of a propeller on a shaft which protrudes from a housing mounted at the end of a tubular support shaft. The head of the shaft is slotted and is a push fit into the propeller - this is sufficient to hold the propeller firmly in place while allowing the propeller to be changed to suit different flow ranges without the use of tools. The shaft is mounted in very smooth bearings which are oil lubricated. Rotation of the shaft operates a reed switch and the number of revolutions can be recorded on a counter which is part of the apparatus.

A new calibration of each of the two propellers is shown in Fig. 43 for the speed range up to 0.3 m/s. This calibration was obtained for each propeller by mounting the shaft in the centre of the working section of the flume and recording the time on a stopwatch for a suitable number of revolutions given by the counter for a range of water speeds. A least squares line has been drawn through the experimental points. It can be seen that the data from the larger propeller gives a line which almost passes through the origin whereas the data from the smaller propeller

results in a line which intercepts the axis at a flow speed of approximately 0.02 m/s. This suggests that the larger torque from the larger diameter blades of the larger propeller would give better results at the lower speeds. This was not verified but the tests on the smaller propeller showed that no reliable results could be obtained below about 0.075 m/s, presumably because of the bearing friction. In practice the choice of propeller is likely to be affected by the size of the propeller relative to the area of flow to be investigated but it should be noted that, since the rotational speed of the larger propeller is approximately one quarter of that of the smaller propeller, the time over which the count of revolutions should be made needs to be considerably longer in order to obtain satisfactory results.

The calibration curves obtained for the two propeller flow meters were, for the small propeller

$$U = 0.0571\, n + 0.0175 \tag{5.1}$$

and for the large propeller

$$U = 0.2538\, n - 0.008 \tag{5.2}$$

where n is the rotational speed in rev/s and U is the water speed in m/s. Also shown on Fig. 43 is the manufacturer's calibration curve for the large propeller which was

$$U = 0.2570\, n + 0.002\ . \tag{5.3}$$

It can be seen that the manufacturer's curve gives a slightly higher water speed for the same rotational speed (approximately 7%) and is probably due to some small deterioration in the bearings since the instrument was first calibrated in 1975. Although the change in calibration is small in this case, and may be related both to the care taken of it and the little use it has had, the present calibration (made in 1999) does show that instrument calibrations can change and that any flow meter,

particularly one used outside the laboratory, should be checked at suitable intervals. There was no manufacturer's calibration available for the smaller propeller so that Eq. 5.1 would have to be used unless a more recent calibration were available.

5.3 Hot film anemometer

While the pitot-static probe described in Section 4.1 has been found to be perfectly adequate for measuring mean velocities in the working section of the flume, there have been occasions where it has been necessary to make measurements of fluctuating velocities such as in the investigation of the spreading and dispersion of heavy gases which was modelled by Cheah (1984) by studying the spreading of a salt solution in the fresh water of the flume.

Hot wire and hot film sensors have been in use for some sixty years for the measurement of fluid flow velocities, particularly in air, and were one of the first methods of measuring fluctuating velocities. A review of their use in air can be found in Bradshaw (1963) and also Sandborn (1972) while a review of their use in a marine environment can be found in Dobson, Hasse and Davis (1980). Although in many cases it may be preferable to use a more modern technique, such as the laser doppler anemometer (LDA), this involves a large financial commitment to purchase and a similar time commitment in learning to use the equipment. The hot film anemometer is both cheaper to purchase and easier to use so that it still has a useful place in the range of equipment which may be considered for use in any investigation in a flume although there are special problems associated with making measurements in water.

The principle of the hot film or hot wire anemometer is that the cooling of a heated wire or film is dependent on the velocity and density of the flow past the wire so that, after calibration in a known flow field, the anemometer can be used to

determine velocities in another flow field. The probes are small (and delicate) with typical dimensions of the wire in air of 5 μm diameter and 3 mm long. It is normal these days to use commercially available probes since accurate production requires some skill and this is even truer for the hot film sensors which are used in water. Because of the larger dynamic pressures involved in measurements in water the probes need to be mechanically stronger than in air so the simplest form usually consists of a cylindrical quartz or glass core covered with a platinum film which is in turn electrically insulated with a very thin quartz or ceramic coating. Typical dimensions are a 50 to 70 μm diameter of the core with a coating 0.1 μm thick film and the insulating coating 2 μm thick with the length of the cylinder being again about 3 mm. Hot film sensors are available in other shapes as well and may be conical, wedge shaped, hemispherical and flush surfaced depending on the particular problem but are less easy to calibrate, particularly if it is necessary to be able to obtain reliable measurements of the actual magnitude of the fluctuating velocities.

There are two modes of operation for a hot film anemometer - constant current or constant temperature. Constant current operation is electronically less demanding but in this method the temperature of the element is very dependent on the flow speed perpendicular to the wire and at very low speeds overheating of the film may occur. The constant temperature method is electrically more demanding since a servo-loop is used to maintain the temperature constant so that the power consumption is a measure of the cooling of the element. The constant temperature method is the more common particularly in a marine environment.

An introduction to the theory of the hot film anemometer can be found in Hinze (1959) and is generally known as King's Law. The response of a single wire

or film for flow perpendicular to the film cylinder can be written as

$$\frac{I^2 R_w}{R_w - R_a} = A + BU^n \qquad (5.1)$$

where I is the electrical current, U is the flow velocity, R_w and R_a are the resistances of the film at the operating temperature of the film and at the ambient temperature of the fluid respectively and n is an unknown power index.

For constant temperature operation the resistances can be taken as constant so the expression can be simplified to

$$I^2 = E + F\sqrt{U} \qquad (5.2)$$

where the constants E and F need to be found experimentally. A sample calibration for a hot film anemometer (in air) is shown in Fig. 44 in the form of a graph of I^2 against $\sqrt{U}$ and it can be seen that the results conform quite closely with Eq. 5.2.

Equations 5.1 and 5.2 are for the case where the flow is perpendicular to the wire but in reality the cooling of the wire or film depends on the components of velocity perpendicular to the film and, to a lesser extent, the flow parallel to the wire. In general it is usual to assume that the component of velocity in the flow direction is much larger than the components in other directions so that any error caused by these components is small. However, in some cases such as the work of Cheah (1984) with the spreading of heavy plumes, it is desirable to measure the components in other directions which can be done using two wires together in an X or V configuration as follows. If the components of velocity in the x, y, z directions

are u, v and w then the velocity sensed by the wire or film is

$$V^2 = u^2 + k^2v^2 + k_1^2w^2 \ . \qquad (5.3)$$

For flow where the major component is perpendicular to the wire and the wire is sufficiently long so that the effects of the probe supports are small then $k_1 \rightarrow 0$ and $k \rightarrow 1$. Eq. 5.3 therefore reduces to

$$V^2 = u^2 + v^2 \ . \qquad (5.4)$$

If an X-sensor probe is mounted in the x, z plane such as in a boundary layer where it might be expected that, in addition to the mean flow velocity U, there may be fluctuating velocities u and v, then the cooling velocity for the wire perpendicular to the z axis measures

$$V_1 = (\overline{U}+u)^2 + v^2 \qquad (5.5)$$

while the wire parallel to the z axis measures

$$V_2 = (\overline{U}+u)^2 \qquad (5.6)$$

so that both the mean and fluctuating flow velocities can be deduced.

In the work undertaken in the flume by Cheah (1984) an X-sensor probe was used rather than the more robust conical or wedge shaped probes because the requirement was to investigate the mean and fluctuating velocities in the x and z directions resulting from the formation of an artificially thickened boundary layer on the false floor of the flume as described in Section 3.7. The X-array probe was connected to two constant temperature anemometer units, thence to two linearisers and into a true integrator with the turbulence signals being obtained from a turbulence processor.

Cheah found that care had to be taken to ensure that there were no excess voltages generated between the probe and the water which might damage the delicate film on the probe. A simple "grounding" method was therefore adopted by disconnecting all the earth connections in the instruments through the mains leads while leaving the probe and the water grounded through the framework of the flume which has its own foundations. A further point was that the probe had to be operated at a relatively modest overheat ratio (about 20°C) to avoid the formation of air bubbles around the probe which would have changed the heat transfer properties. It was also found that the calibration curve was sensitive to any changes in water temperature. As a result the standard procedure was to allow the instruments to warm up to operating temperature for about an hour with the flume running at low speed at the same time to ensure that the water was at normal running temperature and well mixed before any measurements were taken. Calibration of the probe was carried out normally each day but care had to be taken to check the water temperature at intervals through the day to ensure that no undue rise in temperature had taken place - the usual rise in temperature caused by the impeller was about 1°C through a day of 6-8 hours running.

The most serious problem encountered with using a hot film anemometer in the flume was the fouling of the probe by dirt present in the water. During the course of the experiments therefore, in addition to the normal filtering of the water at night with the by-pass filter system described in Section 4.5, the working section was covered at night to reduce the amount of dust and dirt getting into the water. In addition a clean soft-hair brush was kept available to clean the sensor throughout the experiments. It was also noted by Cheah (1984) that the calibration changed slowly through the experiments and inspection of the probe showed that the platinum film

was being slowly eroded, presumably through the impact of dirt particles. It was evident therefore that in such experiments in the flume the purchase of replacement probes must be taken into account as a consumable item.

An alternative to the hot wire anemometer is the thermistor flowmeter which is intended to measure low speed flows. This is potentially a more robust device than the hot wire anemometer because the sensing head is a glass bead thermistor but, depending on the size of the thermistor, would have a conveniently small spatial resolution. According to the work of La Barbera and Vogel (1976) it can measure flows in the region up to about 0.5 m/s with a response time of about 200 ms. Some experiments were made to develop a similar thermistor device but problems were encountered in obtaining a steady and repeatable zero reading. Further development of this device was therefore left in abeyance.

5.4 Laser doppler anemometer

As discussed in previous sections the standard methods for measuring local mean velocity include pitot-static probes and hot film or wire probes. However all these techniques require that an object be inserted into the flow in order to make the measurements. This object will in itself cause a disturbance in the flow and may therefore alter the flow from what it would be if the measurement instrument were not present. By contrast the laser doppler anemometer system (LDA) does not disturb the flow and, within limits, makes use of the particulates occurring in the flow. The system does however require that paths for the light beams on which the instrument depends are available into and out of the flow being studied. The LDA has the further advantage that, depending on the complexity of the system, it can measure

both mean and time dependent flows in one or more directions. The principles of the LDA instrument are described in detail in Durst et al (1976).

An LDA system has been installed in the flume, nominally a 2W system but operating at 500mW to avoid overloading the optic fibre cables. Measurements have been made of the time taken for the flume to settle at a new water speed and also to measure the level of turbulence in the working section. These experiments are described earlier in Sections 3.3.4 and 3.2.5.

Although the LDA is a very useful instrument its use in the flume caused a number of problems which may limit its general use :-

1. The working section of the flume is 1.4 m wide, so that a measurement point is likely to be in the middle of the working section. It is therefore 0.7m from the side of the flume, where the optical head of the LDA is located. In order to get a suitably small measurement volume for the beam crossover point the optical head has to separate laterally the incoming beams by some 100mm. This results in a large optical head (150 mm diameter) which has to get access to the working section through one of the side windows. In turn this means that, once the optical head has been mounted on the side of the working section, there is only a limited amount of movement available for traversing either normal to the flow or in the flow direction because of the size of the window. The current traverse system allows the measurement point to be moved 100 mm sideways in the streamwise direction (x direction), 150 mm vertically and 200 mm across the working section. Although the LDA head can be moved to any window in the working section this limitation needs to be taken into account when designing any experiment and at present only two windows have been modified for the LDA system as discussed below.

2. As described earlier in Section 3.1.1, the windows in the working section are made from acrylic plastic and are not sufficiently uniform in the optical sense for an LDA system. For the present therefore two of the windows have been modified and fitted with inserts of optically flat glass, which are flush with the inner surface of the window, so that the laser beams can shine through without distortion. Although this has been found to be satisfactory for the present experiments, it poses a limitation on the use of the LDA for wider measurement in the flume and raises the possibility of whether it would be possible to obtain glass windows for the working section rather than acrylic plastic as discussed in Section 3.1.1.

3. As mentioned earlier, most of the operation of the flume is carried out from the same side of the working section as the operating console. In view of the cost, delicacy and complexity of the LDA system, the decision was made to mount the LDA system on the opposite side of the working section from the operating console where it would be away from accidental contact. Implicit in this was that the detector head as well as optical head for the incoming beams would both be on the same side of the flume i.e. the LDA system would be operated in the back scatter mode. Since the laser used is fairly powerful care has to be taken that there are no safety hazards from the laser beams shining across the working section and, as a result, the windows on the other side of the working section must be blanked off on the outside.

5.5 Flow velocity and direction

In some cases it is necessary that the flow direction should be measured as well as the flow speed, notably in the work by McIver (1980), where it was required

to measure the flow speed and direction inside a solitary wave in order to correlate the results with theory. It was decided to use a three head tube probe, as described by Bryer and Pankhurst (1971), which consists of a central pitot tube and two chamfered side tubes. In this particular case the interest was in measuring the flow angle in the vertical plane with the result that the probe was made so that the probe head could be rotated in this plane. The probe head consisted of a central tube with an open end, which had been carefully cut so that the open end was at 90° to the axis of the tube, together with two tubes soldered alongside with their ends chamfered at 45° to give the maximum sensitivity to flow direction as indicated by Bryer and Pankhurst. The probe is aligned with the flow by the 'null reading technique' where the probe is adjusted until the two outer tubes give the same reading. The total pressure can then be obtained from the centre pitot tube while static pressure is deduced from the two outer tubes using a calibration curve in order to calculate the flow speed.

The probe and the mechanism to adjust the angle were attached to a streamlined blade similar to the one used for the pitot-static probe described in Section 5.1. This meant that the blade could be mounted in the same support frame and traversed across the working section of the flume on the same beam. The probe head was specially designed so that the nose of the probe stays in the same physical place even though the angle changes. The probe is mounted in a part with lugs which are machined so that they fit into a machined groove in the supports on either side. This groove is machined in an arc with the radius the same as the length of the probe. In this way the probe nose is the centre of a circle along the circumference of which the lugs move when any adjustment is made and the nose therefore stays in the same place. The control rod which operates the probe mounting comes down

through the support blade and at the top has a worm drive mechanism which allows the position of the probe to be recorded after calibration. The three pressure tubes on the probe are connected with plastic tubing to other tubes which are embedded in the support blade. These tubes can in turn be connected to a manometer or other pressure measuring device such as a pressure transducer. The whole probe mounting at the bottom of the blade was encased in a streamlined Perspex cover. A photograph of the probe when mounted in the flume is shown in Fig. 45.

Any asymmetry, caused by the angle of the chamfer on the outer tubes not being 45°, could lead to the pressure readings from these tubes not being equal when the axis of the probe was aligned with the flow. In order to assess any correction required to compensate for this the probe was tested in a horizontal flow in the working section with the inclination of the probe being noted when the outer tube pressures were balanced. The corrections were found to be small and within the measurement accuracy of the probe.

Although the deduction of the flow direction can be made directly, determining the flow speed requires prior calibration in a known flow field following the method of calibration outlined by Bryer and Pankhurst (1971). In the situation where the probe is aligned with the flow, the centre or pitot tube pressure is designated p_1 and the two outer tube pressures, which are equal, are designated p_2. The total or pitot pressure p_1 is related to the flow speed U and the static pressure p by Bernoulli's equation

$$p_1 = p + \tfrac{1}{2}\rho U^2 . \qquad (5.7)$$

The dynamic pressure $\frac{1}{2}\rho U^2$ is assumed to be proportional to the difference between

the inner and outer tube pressures so that

$$\frac{1}{2}\rho U^2 = K\,(p_1 - p_2) \tag{5.8}$$

where K may depend on the flow speed U. If measurements are taken in a normal horizontal flow of known speed, such as in the working section of the flume, and using a standard pitot-static tube for comparison, then the dependence of K on U can be found over a chosen range of flow speeds. The results of such a calibration are shown in Fig. 46 in the form of h_1-h against h_1-h_2 where h, h_1 and h_2 are the manometer heads corresponding to p, p_1 and p_2 respectively. It can be deduced from the results shown in Fig. 46 that K is a constant over the range of speeds used. A straight line was fitted through the data points using the method of least squares in order to determine the value of K which was found to be 1.84 in this case. The flow speed and the static pressure can be found subsequently in experiments using the relationships

$$U = \sqrt{2Kg\,(h_1 - h_2)} \tag{5.9}$$

and

$$p = \rho g h_1 - \frac{1}{2}\rho U^2 \,. \tag{5.10}$$

In order to assess the accuracy of a yaw-meter a non-dimensional sensitivity coefficient is often used as shown by Bryer and Pankhurst (1971). This is defined by

$$C_\psi = \frac{p_2 - p_3}{\frac{1}{2}\rho U^2 \psi} \tag{5.11}$$

where p_2 and p_3 are the pressures recorded by the two outer tubes when the probe is at an angle ψ to the direction of flow. The sensitivity coefficient is taken as a measure of the pressure difference between the two outer tubes caused by a unit angle of yaw to the flow. The smallest angular change which can be detected can be estimated as

$$\Delta\psi = \frac{\rho g \Delta h_{min}}{C_\psi \frac{1}{2}\rho U^2} \tag{5.12}$$

where Δh_{min} is the minimum change in pressure head that can be detected by the manometer system. However since the present pressure probe is normally operated using the 'null reading' technique the pressures p_2 and p_3 are equal. As a result the yaw angle ψ is zero and the coefficient C_ψ is therefore indeterminate. However for this situation Millward (1979) has proposed redefining the sensitivity coefficient as

$$C_\psi = \frac{1}{\frac{1}{2}\rho U^2}\left(\frac{\partial p'}{\partial \psi}\right)_{\psi=0} \tag{5.13}$$

where $p' = p_2 - p_3$ in order to overcome this difficulty. In general it has been found that the relationship between p' and ψ is linear for a small range of angles, usually about 15 ° (Bryer and Pankhurst, 1971), either side of the null position. The sensitivity coefficient was estimated at approximately 2 per radian so with a manometer which can be read to about $\pm$1mm the angle of flow is measurable to about 0.003 radians or 0.2°. The accuracy of the flow measurements can also be estimated. From Eq. 5.9

$$U^2 \simeq 2Kg\,(h_1 - h_2) \pm 4Kg\Delta h_{min} \tag{5.14}$$

so that the absolute error ϵ in U can be given approximately by

$$\epsilon \propto \frac{2Kg\Delta h_{min}}{U} . \qquad (5.15)$$

The calibration constant K is approximately 2 so that at a flow speed of about 2 m/s the error is about 0.02 or 1% of the flow speed U.

As mentioned earlier the probe was successfully used in the work by McIver (1982) investigating stationary waves in the flume.

6. Ship Model Testing

6.1 Model Size

There are several considerations to take into account when deciding on the size of the model to use for any particular series of tests primarily concerning the effects on the flow of placing the model in the working section. These effects are usually referred to as model blockage and can be separated into two parts, labelled for convenience as 'area blockage' and 'wave blockage'.

(a) Area blockage can itself be divided, as shown in Pankhurst and Holder (1952), into solid blockage, wake blockage and lift effect which may be present to a different extent in each case depending on the particular test being considered. The solid blockage causes a change in axial velocity past the model because it partially obstructs the flow in the working section. This in turn causes an effective reduction in local cross-sectional area of the working section and a corresponding increase in local velocity. It is the most common form of correction and would apply to the channel in all three configurations for all forms of test ranging from the calibration of oceanographic flow meters to resistance measurements on surface vessels. A general recommendation is that the immersed cross-sectional area of the model should not exceed 1% of the working section area i.e. $A_m < 0.012$ m^2 (18 in^2), but for any particular case, details should be checked from Pankhurst and Holder. A similar value is quoted by Phillips-Birt (1970).

(b) Wave blockage occurs only in the open channel configuration when testing a model at or near the free water surface. The wave pattern set up by the

model spreads sideways across the channel and will be reflected from the sides. This has two effects:

i. The reflected wave should not impinge on the model. This however would not normally occur for models less than about 1.8 m long as shown in Fig. 56.

ii. The condition that the wave must be reflected at the channel wall means that only certain wave lengths can exist in the channel, whereas in the sea all waves may exist. This means that the wave drag will be affected by the presence of the channel walls. At present the only direct evidence available (Cole, 1974) suggests that, for planing craft at least, provided the model width or beam is less than 250 mm, no change in wave drag is measurable.

The evidence quoted above however does not give very clear guidance nor a method of correcting any resistance of a ship model when measured in the water channel. Guidance from other facilities, mostly towing tanks, would suggest that the model length should be less than the width of the working section while work on shallow water of unrestricted width, such as Millward (1991), suggested that the hull length should be less than the depth of the water. i.e. less than 0.84 m in this case. However the correction would be only about 2% when the depth is half the hull length (L/H=2) and then only close to the critical speed. On the other hand practical experience from towing tanks has indicated that it is difficult to make models to the required degree of accuracy if the water-line length is less than about 1.0 m and it is also more difficult to keep the boundary layer turbulent on the model even with turbulence stimulators. An investigation was therefore made as part of the present

work to find the effect of model size on the resistance of a conventional fast hull by the use of existing theory and measurements of resistance on two different sized models in the flume.

6.1.1 Experimental measurements of resistance in the flume

A method of calculating the theoretical wave resistance of a Wigley hull in a water channel is given in Appendix 2. However this could only be used to correct measured resistance in the flume or to provide guidance on the maximum model length acceptable if the method had some form of verification in practice. Fortunately two models were available of a fast round bilge displacement hull (NPL 100A model) but with different water-line lengths - 1.0m and 1.376 m long. The smaller model therefore had a ratio of hull length to water depth ratio (L/H) of 1.19 and a hull length to channel width (L/K) of 0.714 while the larger model gave a ratio of hull length to water depth (L/H) of 1.638 and a hull length to channel width (L/K) of 0.983. Other details of the models can be found in Table 5 and in Bailey (1976) while an outline view of the hull and the hull cross-sections are given in Figs. 52 and 54.

Each model was ballasted to the datum water-line (DWL) and was tested in the working section of the flume over a speed range corresponding to Froude numbers F_n from 0.3 to 1.0. Care was taken to make sure that the attachment point for the gimbal was positioned such that the gimbal pivot, which is the point of application of the towing force, was at the same geometric position for each model, that is at the intersection of the longitudinal centre of buoyancy (LCB) and the datum water line (DWL). The balance was calibrated as described in Section 4.1 and alignment of the model with the water flow was checked by measuring the side force

at the upper end of the speed range. If the side force was not zero then the yaw angle was adjusted until it was zero. Measurements were then made of the resistance and trim for each model over the range of water speeds.

The experimental measurements of water speed and resistance voltage on the DVM were converted into resistance, resistance coefficient and Froude number using the computer program given in Appendix 5.

6.1.2 Discussion of results

The results of the theoretical calculations, using the method given in Appendix 2, are given in Fig. 57 in the form of curves of wave resistance coefficient C_w against Froude number F_n. The graph shows (as a solid line) the theoretical curve for the Wigley hull in deep water of unrestricted width together with curves representing the same hull in a channel with the depth and width of the flume working section (0.84 m and 1.4 m respectively) for the two different model lengths (Model 1=1.0 m and Model 2=1.376 m). In all calculations the length/beam ratio (L/B) and length /draught ratio (L/T) were identical with those for the NPL 100A models used in the experiments. It can be seen that the curve for the smaller model (Model 1) is almost identical to that for unrestricted water except for Froude numbers from about 0.9 to 1.0 which correspond to the critical speed range $F_{nh} \approx 1$ based on water depth. An alternative method of presenting the data is shown in Fig. 58 in the form of the ratio of wave resistance coefficient in the channel to wave resistance coefficient in deep water (C_{wc}/C_{wd}) against Froude number F_n. Over the speed range of interest, above a Froude number of 0.4, the ratio for the smaller model (Model 1) is very close to unity showing that any effect caused by the presence of either the walls or the bottom of the channel is small. The only major effect is above a Froude number F_n of 0.9.

As explained in other work, such as Millward (1996), the wave pattern and hence the resistance of a ship changes considerably in the region $F_{nh} = 1$ since this corresponds to the critical speed c given by the equation

$$c = \sqrt{g\,H} \tag{6.1}$$

where H is the depth of water. The simple linear wave theory involves a discontinuity in the calculated wave resistance at this speed although other work on the effects of restricted water depth only (e.g. Millward and Sproston, 1988) has shown that in practice there is not an abrupt change in resistance at the critical speed and the reduction in resistance predicted from theory is not normally achieved in practice until the speed is definitely super-critical; this would be at the end of the speed range of interest for this vessel. It was noted that larger differences occur at the lower speeds in Fig. 58 but reference back to Fig. 57 shows that these differences are near the bottom of the speed range of interest and occur as a result of expressing the results in the form of a ratio - the actual differences in resistance are so small that it is doubtful if they could be measured in an experiment.

The third curve in Fig. 57 shows the results obtained from the calculations for the larger Wigley hull (Model 2) and it can easily be seen that the effect of the restricted channel width and depth are significant over the whole speed range. This can also be seen in Fig. 58 where the difference amounts to as much as 10% close to the critical speed where $F_{nh} = 1$.

For comparison the experimental results for the two models of the NPL 100A hull are shown in Fig. 59 in the form of the residuary resistance coefficient C_r against Froude number F_n. As explained in Section 6.1.3 the residuary resistance is obtained by subtracting the estimated frictional resistance from the measured total resistance and for most vessels is considered to be substantially the same as the wave

resistance. In addition a curve is shown for the residuary resistance coefficient for the same hull taken from Bailey (1976). It can be seen that these latter results are very similar to the data for Model 1 except for the Froude number range F_n from 0.6 to 0.9 where the results obtained from the flume are a little higher. Otherwise the results are in close agreement particularly when it is considered that they were obtained on different models in different experimental facilities. The major difference in the results corresponds to the higher sub-critical speed range based on water depth and suggests that there may be a measurable channel blockage effect in this speed regime for the smaller model (Model 1) even though this is not indicated from the theoretical results. As might perhaps be expected, the measurements shown in Fig. 59 for the larger model (Model 2) indicate that there are significant effects from the presence of the channel boundaries throughout the speed range.

If the theoretical results for the Wigley hull, shown in Fig. 57, and the experimental results for the NPL 100A hull in Fig. 59 are compared it can be seen that the general shape of the curves is similar with the maximum value of the resistance coefficient occurring at approximately the same Froude number. However no reduction in resistance below the deep water value was obtained in the experiments at the speeds corresponding to the super-critical depth Froude numbers. An alternative method of comparing the theoretical and experimental results is given in Fig. 60. This graph shows the ratio of the theoretical wave resistances (C_w for Model2/C_w for Model 1) and the ratio of the experimental residuary resistances (C_r for Model2/C_r for Model 1) for the two models against Froude number F_n. It can be seen that the increase in resistance ratio caused by the effect of restricted channel width is similar for theory and experiment although considerably larger from the experiments. It is thought that this increase is at least partly due to the difference in

shape between the Wigley hull used for the theory and the NPL hull used in the experiments. The Wigley hull has parabolic water-lines while the NPL 100A hull, although slender, has a transom stern from which the flow will flow tangentially and could be expected to cause a larger disturbance to the water flow than a Wigley hull of the same water-line length. It might therefore be argued that the effect of a restricted channel would be larger for the NPL hull than for the more streamlined Wigley hull.

This aspect was investigated initially following the work of Couser et al (1998) where the flow behind the transom stern was simulated by the flow over a step using the work by Batchelor (1959) and Sinha (1981) where it was found that the flow over the step became re-attached after six times the step height. This was adapted by Couser et al to be six times the half-beam at the transom, presumably to allow for three dimensional effects, at lower Froude numbers when the transom is wetted. At higher Froude numbers, above about $F_n=0.4$, when the transom is dry the extra length was apparently taken to be the length of the air pocket behind the transom. Calculations were therefore made for a Wigley hull with the same beam and draft as the two NPL 100A hulls but with the water-line length increased by the estimated transom length and the results are shown in Fig. 61 - designated Models 1A and 2A. It was noted however that the curves of the variation of extra hull length given by Couser et al were based on only three points for the whole range of Froude numbers so an experiment was made to measure the extra length behind the transom on the smaller of the NPL 100A models (Model 1) in the water channel for the Froude number range from $0.3<F_n<1.0$. Although the extra length is not easy to estimate, even in the flume where the model is stationary, the results obtained were about half the magnitude of those given by Couser et al and were subsequently used

in a similar set of calculations shown as Models 1B and 2B in Fig. 62. The curves obtained in Figs. 61 and 62 show a similar pattern to those obtained for the unmodified Wigley hulls shown in Fig. 57 although with slightly higher values of the resistance coefficient as might perhaps be expected for hulls with a longer length in a fixed size of water channel. The various sets of calculated results were also plotted in terms of the resistance ratio in the channel to the resistance in deep water against Froude number and compared with the experimental results where it was found that the modified hull lengths (Models 1A and 2A and Models 1B and 2B) gave a better representation of the resistance increase that would be obtained in the flume caused by channel effects but neither were sufficiently in agreement with the experimental results that they could be used with any confidence. It was also noted that none of the models used in the calculations resulted in any increase in the resistance in the region $0.6 < F_n < 0.9$ for the smaller NPL 100A model (Model 1) such as was obtained in the experiments. This suggests that the present mathematical models are not able to represent channel effects adequately. The results of both the calculations and the experiments do however suggest that any correction for channel effects, if it could be made, would be small provided the model is approximately 1m long on the water-line as has been the practice in the flume. For greater water-line lengths the effect of the channel boundaries increases quite rapidly although it would not be appropriate as yet to apply a correction to any experimental data using the theory given in Section 6.4.1.

It is suggested that the problem merits further investigation and two possible methods could be considered:

1. a further set of experimental tests using two or more models of the Wigley hull of different sizes so that the hull shape used in both theory and experiment are the same. One disadvantage is that the Wigley hull does not resemble the normal shape of fast hull more usually tested in the flume so that any correction deduced might be not entirely applicable to a real hull shape. In addition the theory used so far is simple linear theory and this may not be adequate for such a complex problem. There is also the practical problem that it is not at present possible to produce the models needed.

2. An alternative approach would be to develop a more complex theory where the wave resistance of the real hull shape of the NPL 100 hull can be calculated. This is in progress using the panel method but is currently restricted to the deep water case. It is likely that the effect of shallow water will be introduced before long but the addition of side boundaries, which are needed to represent the working section of the flume properly, is some considerable distance into the future.

For the moment therefore, as discussed above, the current recommendation is that ship models to be used in the flume should be approximately 1.0 m on the water-line and that other models should follow the guidance on cross-sectional area to avoid significant blockage effects.

7. Summary and Recommendations for Future Designs and Operation

7.1 Water channel

As can be seen from Section 3 the basic design of the water channel has been found to be excellent and, with the addition of the free surface injection system, has given good results over a wide variety of experiments through the years. The basic design of the channel itself was sound and it is recommended that any future recirculating water channel should follow the same general principles:

1. a low resistance circuit on the same principle as a wind tunnel rather than the type mentioned in Section 2 where the flow is from an upstream stilling tank through a contraction and into a downstream stilling tank; this latter method requires much greater power since all the momentum of the water is lost again at the end of the working section.

2. A large contraction ratio, preferably at least 4:1 as in the present design. This, with the appropriate honeycomb grid and corner vanes, results in uniform flow in the working section with a low level of turbulence. Two suggestions for possible modifications to the design would be:

    a) a longer length of diffuser on the return part of the circuit coupled with a larger contraction ratio. This would result in lower flow speeds in the return part of the circuit and therefore allow a longer period of time for air bubbles, which get carried around in the stream, to settle out before re-entering the working section. Greater lengths on the vertical part of the circuit would also improve re-

absorption of the cavitation bubbles when the flume is being used as a cavitation tunnel or channel.

b) A contraction with a curved centre-line arranged so that the upper surface of the contraction is not higher than the free surface in the working section. As mentioned in Section 3.5, under cavitation conditions it is possible with the present design for the water to be sucked down from the top of the contraction thus disturbing the flow into the working section. An asymmetric contraction, if it can be made to work, would alleviate this problem.

3. A jet injection system to counteract the velocity defect produced at the free surface in the working section caused by the growth of the boundary layer in the contraction. It is recommended however, when this system is incorporated in the initial design, that the intake of water for the jet injection should not be placed at the bottom of the circuit at the end of the diffuser since this is a place where debris naturally gathers. On the other hand this is the place where the intake should be placed for the water filtration and treatment equipment which should also be included in the design.

4. A tilting floor which can be adjusted to help obtain a flat horizontal water surface in the working section. In the present design the floor can also be raised to about 10 cm below the normal water surface which has proven to be useful to simulate shallow water conditions. However it is suggested that in any future design it would be more useful if the false floor could be brought even closer to

the free surface. In the present design with a typical ship model size of 1 to 1.5 metre length the draught of the ship is likely to be about 5 cm so that the minimum depth of water represents twice the draught. This is larger than the draught to depth ratios (T/H) likely to be of interest in many cases. It would also be more practical to be able to bring the false floor right up to the water surface so that any equipment or instrumentation could be attached to the floor without having the operator having to get wet or alternatively having to empty the working section of water.

It has been found in practice that the floor position needs to be set and adjusted throughout the speed range so that a practical method of measuring the floor position must be included in the design. The method finally installed in the flume consists of digital counters attached to the jacking motors. This has been found to be entirely satisfactory in practice, being both reliable and accurate, but the counters are difficult to read in some circumstances such as when the floor is raised considerably. As discussed in Section 3.6 an electronic read-out system has recently been installed so that the position of the floor can be seen on the main console. However this proved to be considerably more difficult than originally anticipated and it is strongly recommended that a simpler system using small video cameras to read the digital counters would be as convenient and cheaper in real cost.

5. All internal surfaces of the water channel should be made from stainless steel as in the present design. This, together with the installation of a water filtration and treatment plant, has resulted in clean water which can be kept for long periods of time while retaining good clarity for flow visualisation and photography.

6. A larger working section. The size of the working section was reduced in the present design for budgetary reasons but has resulted in rather small ship models to avoid blockage effects. The small models in turn make it more difficult to ensure that a turbulent boundary layer is achieved on the model and also requires a high level of model making accuracy. It is suggested that a working section rather larger would alleviate some of these problems and make the water channel even more versatile without losing the low operating cost achieved because most models and equipment can be handled by one or two people - an important consideration in a university environment.

7. All normal controls should be able to be operated from one side of the working section, preferably from the main console. At present the two flaps at the downstream end of the working section have to be operated from the other side of the working section even though they need to be adjusted frequently. In some cases, such as the valve controls for the deaeration equipment, these are operated much less frequently so that the cost of installing remote operation would be less justifiable.

8. The windows in the working section should be designed so that they can be reversed at convenient intervals so that the absorption of water into the acrylic plastic can be equalised in order to prevent bowing of the window.

In view of the total cost of a flume it would be worth investigating whether it would be possible to manufacture glass windows instead. Although this would avoid the problem of water absorption, the main reason would be the advantage if it is intended to use LDA equipment for velocity measurements

since, with the present windows, an insert of optically flat glass had to made in two windows where it was required to make LDA measurements. The size of the insert resulted in some restriction of the distance over which the LDA beam could be traversed. The presence of the insert also means that these particular windows would have to be replaced with normal windows whenever the flume is to be depressurised for cavitation experiments.

9. Consideration should be given to providing more hatches in the side of the flume in order to give access to more of the flume circuit. At the moment, apart from access through the working section to the upper part of the circuit, there is only one access hatch on the return part of the circuit which gives access to the propeller and diffuser section. It would be particularly useful to have a hatch which allowed access to the section upstream of the propeller since there have been occasions when debris has become lodged on the flow straighteners.

7.1.1 The wave-maker

As discussed in Section 3.3 the wave-maker in a flume has to be different from the traditional wave-maker used in a towing tank or manoeuvring basin because it must not impede the flow into the working section. The present wave-maker, which is placed at the beginning of the working section, consists of a hinged plate driven by an electric motor through a Scotch yoke and gearbox. It is therefore intended to produce regular waves over a range of frequencies and amplitudes.

It is suggested that the flume is a suitable environment for experiments in waves, provided the required waves can be generated, because the model, the instrumentation

and the observer are stationary and the testing time is effectively unlimited so that the maximum benefit can be obtained from the tests. It is however likely that any tests would be limited to the production of regular head waves since the production of irregular waves or oblique waves would be problematic and therefore better carried out in a towing tank or manoeuvring basin dedicated to that type of test.

The ability of the wave-maker to produce regular waves has been investigated as described in Section 3 where it was used in a project concerned with the effect of waves on the performance of a sailing yacht (Sutcliffe, 1995). The measurements found that the wave-maker could produce a satisfactory wave at the lower water speeds ($U < 0.9$ m/s) and that both the wave length and height could be set and maintained over a long period of time from the initial calibration settings of the wave-maker paddle and motor speed. However, at higher speeds, a ripple wave was found to be present which limited the effectiveness of the wave-maker. It was deduced that the ripple wave was caused by the shape of the paddle since at the top and bottom of the wave the water surface needed to be horizontal whereas the paddle was at its maximum slope at these points. Some preliminary experiments showed that the use of a flexible paddle could reduce the magnitude of the ripple wave and it was suggested that the use of a flexible wave paddle warranted further investigation, possibly using a "Smart" material with electronic control so that the required shape could be achieved over a range of wave heights and frequencies.

7.1.2 The water tunnel

As discussed earlier in Section 3.4 the flume can be used as a water tunnel by lowering a special cover into the working section. This cover suppresses the free water surface so creating a water tunnel with the same size working section (1.4m by 0.84m)

and the same speed range (up to 5.7 m/s). The cover is normally stored on a gantry or mezzanine floor at the other end of the laboratory and is lifted into place using the overhead electric crane which was installed for this purpose. Since the cover is stored away from the working section models and instrumentation can be installed on it conveniently without interfering with other work on the flume. This arrangement has been shown to be extremely practical, allowing several projects to utilise the flume in rapid rotation.

Another possibility is that the height of the working section can be altered using the false floor since this can be changed from its normal position giving a depth of 0.84m to as little as 0.1 m. At present this flexibility has only been used in the work by Higgins (1994) on ship stabilisers where the floor was moved up so that it was almost touching the bottom of the stabiliser model and was therefore used to simulate two dimensional flow.

The change over from the open channel configuration to the water tunnel or vice versa can currently be achieved in less than an hour. The slowest part of the procedure used to be adjustment of the sealing strip around the edge of the tunnel cover after it had been lowered into the working section but this has recently been speeded up by the use of a standard rechargeable electric screwdriver.

7.1.3 The cavitation tunnel

Although the flume can also be used as either a cavitation channel or as a cavitation tunnel it has only been used as a cavitation tunnel so far, that is with the cover turning it into a water tunnel inserted first followed by the second cover which allows the working section to be depressurised. Since the flume was primarily designed

as a free surface water channel the process of changing over to be a cavitation tunnel is not particularly fast - it generally takes half a day to get both covers in place and sealed. Provided there are no problems with air leaks the pressure can then be reduced in the working section and the de-aeration equipment started; this takes a further half a day to reduce the air content of the water. As stated in Section 3.6 the air content of the water can be measured but only at present with a van Slyke apparatus. This entails extracting a sample of water from the flume, against the reduced pressure inside, and analysis of the sample can take an hour or so. In most experiments to date therefore, the de-aeration equipment has been run for some hours until little further change occurs and the experiments have been made with occasional running of the de-aeration system to keep the air content low. This is not however a very satisfactory method of operation and, if any substantial programme of work on cavitation were to be undertaken, a more convenient method of measuring air content would have to be sought.

A further practical improvement could be made by making up one or more windows in the cover with a number of sealed plugs and sockets, ranging from those suitable for signal measurements to transmission of electrical power, so that connections to the apparatus inside the flume can be made rapidly.

A more sophisticated improvement, which could only be incorporated at the design stage of a new flume, would be to use an asymmetric contraction, as discussed in Section 7.1, so that the upper surface of the contraction did not come above the static water level. This was originally proposed to avoid the complication and time delay, when emptying and filling the working section, of also having to fill the contraction. Such a change in design would also however avoid the problem in cavitation experiments that at the lowest pressures the water can be sucked out of the contraction unless the water is already running at speed. This would be particularly important if the

flume were to be operated as a cavitation channel since a partial emptying of the contraction would be almost certainly alter the flow distribution in the working section near the free surface where the model being tested would be likely to be.

7.1.4 Shallow water

The false floor was originally intended primarily to be able to be adjusted so that the water surface in the working section could be made horizontal and free from standing waves. However the jacks which move the floor were made sufficiently long so that the depth of water in the working section could be reduced down to 0.1 m. Two problems have been encountered with the design as it presently is - firstly that if any apparatus is to be installed on the floor it is necessary for the operators to work from the side of the flume or from a board placed across the working section but in either case they will get wet at least to the elbow. While this is not catastrophic it is inconvenient and would be avoided if the floor could be raised to just above the water surface so that the operators could actually stand on the floor; this would be particularly important if the working section were made larger as suggested in Section 7.1 when it would become difficult to reach to the centre of the working section from the side of the flume. The second problem arises when attempting to use the flume for tests on ship models in shallow water. Since the ship model is likely to be about 1 m long then the draught is likely to be approximately 50 mm so that, with the present design, the shallowest water depth is approximately twice the draught of the ship. While this is acceptable for high speed ships it is a much greater draught/depth ratio than is likely to be of interest for conventional ships which may well only have an underkeel clearance

of 1 m full scale or 10 mm model scale. Again the flume would be made more versatile for this type of application if the floor could be raised right up to the water surface.

As described in Section 3.6 the original method of determining the position of the false floor either for normal operation or for simulating shallow water was by measuring the water depth with a ruler inserted into the working section. This was rapidly found to be impractical and was superseded by digital counters attached to the shaft of the jacking motors. This method has been found to be very reliable and accurate over the years giving a position accuracy better than 0.1mm with care. The only minor disadvantage of the counter system was that it needed a clear sight-line to the counters which was not always easy, particularly when the floor was set high to simulate shallow water. More recently therefore a system has been developed using optical switches attached to the shaft of the counters so that the same reading as the counters is displayed at the operating console. This system has however been difficult to develop to the stage at which there is certainty that the count will not be lost when the floor is adjusted rapidly in opposite directions such as when making the final adjustments of floor position. It is therefore recommended that in any future design an alternative solution should be sought - the most practical at present seems to be the use of small video cameras viewing the digital counters with the video monitors mounted near the operating console.

7.2 Force measuring equipment

7.2.1 The main dynamometer

The main dynamometer has been described in Section 4.1 and was intended primarily for the measurement of the hydrodynamic forces on various types of marine craft including conventional low speed ships, fast craft including planing hulls and also

sailing yachts in calm water. In designing the dynamometer it was therefore important to consider the wide range of speeds of the various vessels and the correspondingly wide range of resistance and other forces which needed to be measured to an appropriate level of accuracy. It was also thought desirable as good experimental practice to incorporate a system so that the calibration of the dynamometer could be checked at frequent intervals if necessary. Although initially designed some years ago, the dynamometer has been improved by various modifications and has proved to be very reliable. The basic concept would be retained therefore if a new design were required provided the tests to be carried out were in calm water only. A limited amount of experience when investigating the performance of yachts in waves (Sutcliffe, 1995) has shown that the resonant frequency of the dynamometer is too close to the likely encounter frequency of the waves suitable for a sailing yacht and a modified form of the dynamometer would be needed and is discussed briefly later. At higher encounter frequencies, such as might be appropriate for a planing craft or high speed catamaran, the resonant frequency of the dynamometer should be sufficiently removed from the frequencies of interest such that measurements could be taken. This has not however yet been investigated.

Elements of the design which would be retained in any new design include:

1. the concept of measuring the resistance and side force using separate cages containing flexures which are thin in one direction only. In particular the idea of machining the flexures from solid material so that they are easy to align and replace has been proven to be sound and is a well established technique. It is accepted that this technique is more expensive in machining costs at the outset. In practice the flexures for the resistance cage only have had to be replaced just once in over twenty

years and then only because the model hull was swamped by a following wave when slowing the water down too fast.

2. Measurement of the deflection of the flexures using the linear variable differential transformers (LVDT) and the rotation of the gimbal using RVDTs has proved to be very stable and reliable over a long period of time.

3. The provision of the triangular arm system which allows the addition of extra weights when the force applied by the model hull exceeds the maximum incremental load of the dynamometer cage (usually the resistance). The same system enables the calibration of the dynamometer to be checked easily whenever desired.

4. The off-load system which can be used in a number of different ways - either to neutralise the weight of the heave post or to alter the weight of the model, particularly if the model is too heavy. The initial design used tubular pots to hang from the off-load hooks which can be filled with lead shot to the desired off-load weight. This system is still used although currently special lead weights have now been cast which are used for the more usual case where it is required to neutralise just the weight of the heave post.

5. The modification which enabled the yaw angle to be altered remotely has improved the reliability of the dynamometer by avoiding the chance of

the operator affecting the calibration. This again is a modification which should be incorporated in any new design while retaining the ability to adjust manually if needed as at present.

6. The recent addition of being able to move the dynamometer to any position across the working section has added to the flexibility of the flume and has permitted a wider range of experiments to be undertaken.

There are however some further changes which could be considered for incorporation in a new design:

7. At the moment the side force weight arm and the yaw angle vernier scale can only be read from the side of the working section opposite from the operating console. While this is not a major problem it makes it more difficult for the flume to be operated by a single person which is important in a university context where staffing levels are low. A revised design would therefore reverse the layout so that one operator could control the flume water speed and floor settings and at the same time make measurements using the dynamometer from one side of the working section. It would also be an advantage to reverse the resistance cage so that the arm used for calibration would be at the upstream end of the dynamometer. It would then also be the same arm as used for adding the incremental weights. The other arm would then almost be redundant but could be retained for unusual cases.

8. In the initial design the heave post was held in position with three roller bearings at the level of the resistance cage and a further three lower down as shown in the diagram in Fig. 31. These roller bearings allowed the centre post to rise and fall vertically while restraining it in the fore-and-aft and lateral directions (x and y axis) and also kept the post vertical. Restraint in yaw was provided by two arms projecting sideways from the heave post and clamped at a suitable height. These arms contained linear bearings which slid up and down machined and ground stainless bars therefore allowing the post to move vertically but preventing rotation. This proved not to be a very satisfactory system despite the care taken in manufacture with using ground bars, high quality linear bearings and careful alignment. Eventually it was realised that the system was over-constrained and needed to be simplified. The current configuration relies on only one arm to restrain yaw while the linear bearing has been replaced by two roller bearings which only resist yaw while not adding restraint against an x-z moment. Any new design would be similar to the current modification although with some simplification of the actual structure.

9. As commented earlier the existing dynamometer was designed primarily for testing ship models in calm water although a generous provision in the design for freedom to heave was included. This was included partly to allow for adjustment of the attachment position for different hull models, to allow for changes in water height as the water in the flume changes height with speed but in addition to allow for possible extension

of the work in the flume to include tests in waves. The only tests made to date in waves (Sutcliffe, 1995) were on sailing yachts where it was found that the relevant wave frequencies were close to the resonant frequency of the dynamometer (approximately 10 Hz) so that resistance measurements in particular were difficult to obtain. For these particular experiments new resistance flexures were manufactured which were much stiffer and therefore had a higher resonant frequency. Correspondingly the flexures also had a smaller deflection for the same resistance and so were unsuitable for use with the existing LVDTs which are the most sensitive available. The measurements were therefore made with using a strain gauge bridge system, as for the force blocks described in section 4.2, but, even though a full bridge system was used, these had to be specially temperature compensated by the strain gauge manufacturer in order to obtain satisfactory stability during a test run.

It is suggested that if tests in waves were to be envisaged a new dynamometer would be needed, probably using strain gauge measurement, although some increase in the resonant frequency of the present dynamometer design could be obtained by reducing the mass of the dynamometer below the resistance cage. It should be noted however that the major mass below the resistance cage is likely to be the model hull itself which cannot be changed.

7.2.2 Force and moment blocks

The purpose in designing the force and moment blocks was to give a versatile dynamometer system which could be tailored to suit a variety of measurement requirements likely to be encountered in the flume. The resulting load blocks have been shown to be successful in a number of different applications with small interactions, good long term reliability and stability with easy assembly into a chosen configuration. The design choice of using stainless steel for the basic material and the more expensive strain gauges which were already set on backing plates by the manufacturer has proven to be justified by their reliability and lack of corrosion. The only minor changes which might be incorporated in a new design would be:

1. a slightly enlarged size of block to reduce the level of interaction even more. Any increase in size however would increase both the size and weight of an assembly which would make it more difficult to install in the flume and it must also be borne in mind that the height between the top of the working section and the water surface is limited although it is unlikely to be a major constraint.

2. At present each block has a design maximum load which should not be exceeded by more than about 10 to 20% without risk of damage. No provision has been made to prevent overload and it is left to the skill of the experimenter to monitor the loads on the blocks to make sure that an overload does not occur. Particularly if such a system were to be used in a less controlled environment it would be wise to consider incorporating

some form of mechanical overload prevention, perhaps such as is currently used on the main dynamometer.

7.2.3 The miniature dynamometer

The miniature dynamometer was designed and built for some special experiments where it was desired to measure the hydrodynamic forces on full-scale scallop shells to determine their swimming capabilities (Millward and White, 1992). The principle of this dynamometer is basically the same as for the main dynamometer, as can be seen by comparing Figs. 40 and 31, but with compromises engendered by the small forces to be measured. The major compromise was that the flexures could not be made from solid material but from available strips of spring steel while the calibration arm system was omitted for simplicity in construction since it was envisaged that the dynamometer was primarily constructed for this one project.

One major disadvantage found with the dynamometer was that the control for varying the angle of the scallop shell to the water flow was below the force measuring cages. This needed a very delicate touch from the experimenter although calibration of the dynamometer both before and after the experiments showed that the calibration had not been affected. In retrospect however it was not appreciated until measurements were obtained that the lift and drag forces on the shell were of the same order of magnitude, unlike an aerofoil where the lift can be an order of magnitude greater than the drag. It would have been better to arrange for the incidence angle control to be made by rotation of the whole dynamometer thus keeping the shell model fixed relative to the dynamometer. The measurements would therefore have been of the normal and tangential forces relative to the axis of the shell and the corresponding lift and drag forces could easily have been deduced from them.

7.3 Measurement of water speed

A number of different methods of measuring water speed and also flow direction have been used in the flume for various purposes and are described in more detail in Section 5. Each method has its advantages and disadvantages depending on the particular problem being investigated. Since the methods operate on different principles the following comments have been separated into the advantages and disadvantages of the different methods rather than a discussion of each separate instrument in turn.

The primary techniques include:

1. Pitot-static probes used for measurement of steady state or mean flow speed and direction.
2. Hot film or thermistor probes which can be used for measurement of both mean and fluctuating flow speeds although with limitations discussed later.
3. Laser doppler anemometer (LDA) systems which can be used for measurement of both mean flow speed and fluctuating speeds.

Other devices such as propeller flow meters have been used in the flume for special applications although in many cases the purpose has been rather to calibrate the device in the known flow of the flume in order for it to be used elsewhere.

7.3.1 Pitot-static probes

The standard pitot-static probe supplied with the flume has been described in Section 5.1 with the mounting holder and beam placed across the working section and can be used to measure mean velocity at any point within the working section. Its most common use is for checking the calibration of the main dial against water speed,

particularly after any changes have been made to the machinery driving the flume. Since the bi-convex blade has been installed in the modified mounting the pitot-static probe has performed satisfactorily and would be recommended as a basic instrument for a flume. In addition the same mounting system has been used for the extra instrument which was designed for McIver (1980) so that flow direction in the vertical plane could be measured. A further bi-convex blade was made at the same time and is available for future instruments.

Some problems arise however if it is desired to measure the water speed using a different pitot probe such as in a more confined area since the standard probe is quite large both in diameter and in length. This has occurred on a number of occasions and, while it is relatively easy to manufacture or purchase other pitot or pitot-static probes, these are normally circular in cross-section so that two problems can be anticipated:

1. In comparison with the forces experienced in a low speed wind tunnel the fluid forces on a probe in the water flow in the flume are large because of the greater fluid density. Coupled with the height of the beam onto which any probe is likely to be fastened this often gives rise to oscillation of the probe stem with a consequent effect on the accuracy of the readings obtained. At lower water speeds this oscillation can usually be removed by the standard method of wrapping a wire around the stem in a spiral. At higher speeds the actual water forces may be sufficient to bend the probe out of line and the experimenter has the choice of designing a more sophisticated probe perhaps with sections of reducing concentric tubes so that the probe only becomes small in the region of the measurements to be taken. Another possibility is to mount the probe

on the available bi-convex blade system while a third possibility is to reduce the length of the probe as much as practicable by inserting it into the working section through one of the side windows instead of down through the free surface but this depends on the distance to the measurement point.

2. If the probe is mounted such that it enters the water through the free surface then the pressure distribution around the diameter of the probe at the surface is likely to cause ventilation - a pocket of air which is trapped behind the probe and whose depth depends on the water speed. The presence of the ventilation pocket can disturb the flow in the region of measurement and also causes air bubbles to be released into the water which may circulate completely around the circuit of the flume thus disturbing the incoming flow in the working section. The simplest solution to this is to provide the probe with a anti-ventilation fence or plate, rather less sophisticated than that used for hydrofoils (Du Cane, 1965), consisting of a circular plate fastened onto the probe and adjusted in height until it is just below the water surface. No detailed measurements have been carried out to determine the optimum diameter of the fence but it has been found during the course of several experiments that a value of three times the diameter of the probe is usually sufficient. A future project is planned to provide more informed guidance on the design of anti-ventilation plates.

7.3.2 Hot film techniques

As discussed in Section 5.3 the hot wire and hot film sensors were probably the first useful method of measuring turbulent velocities in fluids and, in the form of the hot wire probe, have been extensively used in air. Because of the greater dynamic forces obtained in water and other liquids the use of a hot wire probe is usually limited to lower fluid speeds and needs to be mechanically stronger than in air so the simplest form consists of a quartz fibre with the platinum film coated on the outside and in turn protected by a thin quartz or ceramic coating. Other shapes of sensor are also available and may be conical, wedge shaped or flush surfaced depending on the particular application but are less easy to calibrate and may not be suited to dependable turbulence velocity measurement. In the work undertaken by Cheah (1984), described in outline in Section 5.3, an X-sensor quartz probe was used rather than the more robust wedge or conical probes because the requirement was to measure the mean and fluctuating velocities in the x and z directions.

Although satisfactory results were obtained, a number of problems were encountered during the experiments some of which were general to the use of a hot film probe in a liquid and some were related to the special case of the flume. The main points which were noted were:

1. Care had to be taken that no hidden voltages were generated between the probe and the water which might damage the platinum film on the probe. The most common cause for this is through the formation of "earth loops" in the equipment and can be avoided by disconnecting all earth leads through the instruments themselves while leaving the probe and the

water grounded through the frame of the flume. This proved to work well in practice.

2. It was found that the calibration of the probe was sensitive to changes in water temperature despite the large volume of water contained in the flume (approximately 90,000 litres). A standard procedure was therefore adopted of running the flume at a low speed for about an hour to ensure that the water was well mixed and at normal running temperature before any measurements were taken. Although calibration of the probe was made each day the water temperature was monitored at intervals during the day to make sure that no undue change had taken place.

3. The most serious problem with using the hot film probe in the flume was caused by fouling on the probe by dirt present in the water. Most hot film experiments are carried out in a relatively small closed apparatus where it is easier to keep the fluid clean. As mentioned earlier the flume contains some 90,000 litres of water which is drawn from the mains. Although a filter system is installed the normal mesh size is 400 microns. Smaller mesh filters could be used and would undoubtedly reduce the size of the dirt particles in the water and an added precaution, which was taken by Cheah, was to cover the working section when it was not in use, particularly at night. It is evident however that erosion of the probes in any future experiments would need to be taken into account with frequent replacement of filters and also replacement of the probes themselves as a consumable item.

However, provided these problems are born in mind at the beginning of a project there is no reason why successful measurements should not be made in the flume using a hot film probe, particularly at low water speeds.

7.3.3 Laser doppler anemometer systems

Since any LDA system these days is likely to be a commercially obtained system there should be no major problems in making it work although a considerable amount of time may be needed in order to learn to use the instrument correctly. It is also worth using the instrument in a known flow, such as in the working section of the flume where it can be checked against the known flow speed calibration, before using it in an unknown flow.

The major problems encountered in using an LDA system in the flume were:

1. gaining access for the laser beams to the working section where it was desired to make the flow measurements. In the present case this was solved by putting inserts of optically flat glass in the normal acrylic windows. This did however result in a very restricted range of traverse of the optical head of the LDA system and also meant that the flume could only be run as an open channel or tunnel because of the fragility of the glass insert. This would therefore preclude any tests at reduced pressure where the interest might be in cavitation phenomenon. It is strongly recommended that the possibilities of using a glass window, capable of withstanding the reduced pressure, should be explored and, if

necessary, the design of the window and aperture modified to make this possible.

2. Although the water in the flume is normally filtered to remove major particles, it was thought that the dirt particles remaining in the water would be sufficient to provide adequate seeding for the LDA system to work. In practice this has not been found to be the case and some experimenters have opted to seed the water in order to obtain a good LDA signal. Unfortunately however it was found that the seeding particles settled out overnight onto the bottom surfaces and also clogged up the gauzes downstream of the splitter plate at the end of the working section and the main filters. Current practice therefore is to remove both the main filters and the gauzes when using the LDA system and to keep seeding to a minimum.

   It would be particularly suitable for the flume if seeding particles could be found which dissolved slowly in water. This would alleviate the problem of clogging of the gauzes and filters and remove the time delay in emptying and re-filling the flume after seeding has been used.

7.3.4 Particle image velocimetry

Particle image velocimetry (PIV) is another measurement system based on the use of lasers and can also be obtained commercially. As compared with conventional methods of velocity measurement, which normally can only measure at a single point in the flow, the PIV system has the advantage that it can measure the whole flow field instantaneously and, like the LDA method, is also non-intrusive.

The PIV method is based on the use of two lasers which are triggered in sequence with the light being projected into the flow through a cylindrical lens to form a thin plane of laser light in the chosen direction. Any small particles in the flow are illuminated by the light on two occasions a small time apart with the results being recorded by a camera which is positioned normal to the plane of illumination. From this picture both the flow speed and direction over the plane through the flow field can be calculated.

The PIV technique has been used successfully in the flume to measure the flow in a plane across the working section. However, like the LDA system, it sometimes requires seeding in the flow to get good results with the attendant problems of removing the seeding at the end of the experiments. In addition, again like the LDA system, the method requires the laser beams to be projected into the working section through optically flat glass. At present this limits its use to the areas where the laser beams can be projected through the existing windows with glass inserts as discussed in section 7.3.3. A further complication when using the PIV system is that the camera has to be at right angles to the plane of light. Thus if the flow field to be investigated is across the working section then the camera has to be positioned downstream of the flow field. In the measurements made to date this has been achieved by putting the camera in a water-proof container at the downstream end of the working section.

Despite these complications the PIV method does enable a complete picture of the flow field to be obtained at one instant complete with measurements of the flow speed and direction. The present system only allows measurements of two-dimensional flow but it is possible to make measurements in three dimensions with the addition of a further set of lasers and the appropriate computer software.

7.4 Model size

As described in Section 6.1 the available work on wind tunnels has given some guidance on the maximum cross-sectional area of a model (0.0012 m^2) that would be acceptable before a significant change occurred in velocity in the working section. Calculations have shown also that, as long as a model is less than about 1.8 m long, the waves created by the model will not reflect from the side of the working section back onto the model while early measurements with planing craft showed that a beam of less than 250 mm would be acceptable. However little information seemed to be available on the effect that the sides and bottom of the working section would have on the wave pattern and hence the resistance of a conventional ship model. As a result the theoretical and experimental investigation described in Section 6 was made to determine the effect of the channel on a model and so to deduce the most appropriate model size for use in the flume. The results indicated that the effects would be small when using a model 1 m long, as has been the practice in the flume, but significant effects were observed for the 1.376 m long model. However agreement between the theoretical approach and the experiments using two different sized models was not good. It is suggested that this could be due to a number of reasons which merit further investigation:

1. that the use of the Wigley hull to represent the NPL 100A hull, which is a round bilge displacement hull with a transom stern, is not sufficiently close. A first stage of improvement therefore would be repeat the experimental investigation but using Wigley hulls so that the hull shape used in the experiments and for the calculations is identical.

2. The theory used was linear wave theory based on the work of Michell and Srettensky. It should be possible to include higher order terms using modern computational techniques.

3. Modern computational techniques such as the panel method (Rigby et al, 2001) would allow the actual shape of the real hull to be used including the transom stern. At present however the work is limited to the deep water case although an extension to include shallow water effects is in hand. Further extension to include the effect of side boundaries is envisaged but is some time in the future. Such a method is also very extravagant in processing time with currently available computers.

8. Conclusions

8.1 The water channel

The basic design of the water channel has been found to be excellent and, with the addition of the jet injection system at the free water surface, has given good results in a range of experiments as a water channel, as a water tunnel and as a cavitation tunnel. A number of changes in design which could be incorporated into any future design include:

1. a longer length on the diffuser in the return circuit to reduce the possibility of bubbles being carried around the whole circuit.
2. An asymmetric contraction so that the upper surface of the contraction is not above the level of the free surface in the working section.
3. A longer length on the screw jacks of the tilting floor so that it can be raised up to the level of the free surface both for ease of access to models and instrumentation attached to the floor and also to maximise the range of shallow water that can be simulated.
4. Glass windows rather than acrylic plastic so that modern instrumentation such as a laser doppler anemometer (LDA) or a particle image velocimetry (PIV) system can be used.
5. An improved wave-maker so that regular head waves can be created over a wider range of water speeds than at present.

8.2 Force measuring equipment

The main dynamometer has been shown to be well suited to the variety of experiments on free surface craft although minor changes in configuration have been suggested in order to make it easier to operate by one person. If experiments in waves

are anticipated then a new dynamometer would be needed. The miniature version of the dynamometer, which was used for measurements of the hydrodynamic forces on scallops, worked well and the only modification suggested is that the incidence of the model to the flow could be better obtained by rotating the whole dynamometer.

The force and moment blocks were found to be very reliable because of their use of stainless steel as the material and the use of strain gauges which were integral with their mounting plate.

8.3 Model size

The results of experimental tests on two hulls of different sizes combined with calculations using existing linear theory for an unbounded liquid and also for a channel suggested that a model waterline length of approximately 1 metre was suitable for the size of the working section (1.4 m wide and 0.84 m deep).

These and other suggested modifications and improvements are discussed in greater detail in Section 7.

REFERENCES

Bailey D. (1995) "Ships in the Making" Lloyds of London Press Ltd.

Bailey (1976) "The NPL round bilge displacement hull series" Royal Institution of Naval Architects, Maritime Technology Monograph No. 4.

Batchelor K. (1959) "A proposal concerning wakes behind bluff bodies at large Reynolds numbers" Journal Fluid Mechanics, vol. 6, pp. 547-567.

Binnie A.M., Davies P.O.A.L. and Orkney J.C. (1955) "Experiments on the flow of water from a reservoir through an open channel - I. The production of a uniform stream. II. The formation of hydraulic jumps" Proc. Roy. Soc., vol. 230, pp. 225-236.

Bradshaw P. and Johnson R.F. (1963) "Turbulence measurements with hot wire anemometers" National Physical Laboratory, Notes on Applied Science No. 33.

Bryer D.W. and Pankhurst R.C. (1971) "Pressure probe methods for determining wind speed and flow direction" H.M.S.O., London.

Charlton G., Denman C.P.R. & Millward A. (1987) "An investigation into the feasibility of a human-powered rowing hydrofoil" International Shipbuilding Progress, vol. 34, no. 391, pp. 54-62.

Cheah S.C. (1984) "Dispersion of a heavy plume in a structured shear layer" University of Liverpool, Ph.D. thesis.

Clayton B.R., Bishop R.E.D. (1982) "Mechanics of Marine Vehicles" E & F.N. Spon.

Cole A.J. (1973) 'The Influence of Wedges on the Performance of Planing Hulls'. University of Liverpool, Ph.D. thesis.

Cole, A.J. and Millward, A. (1978) 'The measurement of skin friction a planing hull using miniature Preston tubes'. Trans. R.I.N.A., vol. 120, pp. 179-186, 1978.

Counihan J. (1969) "An improved method of simulating an atmospheric boundary layer" Atmospheric Environment, vol. 3, pp. 197-214.

Couser P.R.,Wellicome J.F. and Molland A.F. (1998) "An improved method for the theoretical prediction of the wave resistance of transom-stern hulls using a slender body approach" International Shipbuilding Progress, vol. 45, no. 444, pp. 331-349.

Dobson F., Hasse L. and Davis R. (1995) "Air-sea interaction instrumentation and methods" Plenum Press, pp. 47-64.

Du Cane P. (1974) "High Speed Small Craft" David & Charles.

Duncan, W.J., Thom, A.S., Young, A.D. (1960), 'Mechanics of Fluids', E. Arnold Ltd..

Durst F., Melling A. and Whitelaw J.H. (1976) "Principles and practice of laser doppler anemometry" Academic Press.

Higgins J. (1993) "Unsteady characteristics of a small aspect ratio oscillating hydrofoil" University of Liverpool, M.Sc.(Eng.) thesis.

Hughes, G., Allan, J.F., 'Turbulence stimulation on ship models'. Trans. S.N.A.M.E., vol. 59, pp. 281-314, 1951.

Insel M and Molland A.F. (1992) "An investigation into the resistance components of high speed displacement catamarans" Trans. Royal Institution of Naval Architects, vol. 134, pp. .

ITTC (1990) Proc. 19th International Towing Tank Conference, Madrid.

Kirsch M. (1966) "Shallow Water and Channel Effects on Resistance" Journal Ship Research, vol. 10, pp. 164-181.

La Barbera M. and Vogel S. (1976) "An inexpensive thermistor flowmeter for aquatic biology" Limnol Ocenaogr, vol. 21, pp. 750-756.

Lachman G.V. (Ed.) (1961) "Boundary Layer Control Flow: Its Principles and Application" vol. 1, Pergamon Press.

Lewis E.V. (Ed.) (1988) "Principles of Naval Architecture". S.N.A.M.E..

McIver P. (1980) "Stationary waves in open channels" University of Liverpool, Ph.D. thesis.

McIver P. (1982) "Stationary waves in a laboratory flume" J. Fluid Mech., vol. 119, pp. 283-296.

Michell J.H. (1898) "The Wave Resistance of a Ship" Philosophical Magazine, vol. 45, pp. 106-123.

Millward A. (1963) "Testing a wing-tail configuration in uniform and non-uniform subsonic flow" Von Karman Inst. Proj. Report.

Millward A. (1967) "The Induced Drag of a Vertical Hydrofoil" University of Southampton, Ph.D. thesis.

Millward A. (1979) "A definition of yaw meter sensitivity for the 'null reading' technique" Journal Hydronautics, vol. 13, no. 4, pp. 130-131.

Millward A. (1983) "Turbulence stimulator correction in ship model testing" University of Liverpool, Dept. Mechanical Engineering Report FM/85/83, March 1983.

Millward A. (1989) "The effect of water depth on hull form factor" International Shipbuilding Progress, vol. 36, no. 407, pp. 283-302.

Millward A. (1991) "A comparison of the effect of restricted water depth on a model and full size planing hull" Transactions R.I.N.A., vol. 133, pp. 237-250.

Millward A. (1996) "A review of the prediction of squat in shallow water" Journal of Navigation, vol. 49, pp. 77-88.

Millward A., Askew K.M. and Whattam P. (2001) "An investigation into the effect of running wetted surface area on the resistance components of a catamaran" International Shipbuilding Progress, vol. 48, no. 2, pp. 135-148.

Millward A., Nicholson K. & Preston J.H. (1980) "The use of jet injection to produce uniform velocity in a high speed water channel" Journal Ship Research, vol. 24, no. 2, pp. 128-134.

Millward A. and Rossiter J. (1983) "The design of a multi-purpose multi-component strain gauge dynamometer" Strain, vol. 19, no. 1, pp.27-30.

Millward A. & Sproston J.L. (1988) "The prediction of the resistance of a fast displacement hull in shallow water" Royal Institution of Naval Architects, Maritime Technology Monograph No. 9, 15 pp.

Millward A. & Wade J.H.T. "Drag reduction and degradation studies of high polymers using a simple rheometer" Transactions C.A.S.I., vol. 5, no. 2, pp. 71-76, 1972

Millward A. and White M.A. "The hydrodynamic characteristics of six scallops of the Super Family Pectinacea, Class Bivalvia" Journal Zoology, London, vol. 227, pp. 547-566, 1992

Nagib H.M., Morkovin M.V. and Tari-Atichat J. (1974) "On modelling of atmospheric surface layers by the counter-jet technique" AIAA 8th Atmospheric Testing Conference, Bethesda, Paper 74-638.

Naylor P. (1981) "Cavitation of the tip vortex shed from a small aspect ratio hydrofoil" University of Liverpool, Ph.D. thesis.

Naylor P. and Millward A. (1984) "A method of predicting the effect of the dissolved gas content of water on cavitation inception" Proc. Institution of Mech. Engrs. vol. 198C, no. 12, pp. 163-166, 1984.

Nicholson K. (1972) "Measurements of Hovercraft Wavemaking Drag on a Circulating Water Channel" University of Liverpool, Ph.D. thesis.

Pankhurst R.C. and Holder D.W. (1965) "Wind-tunnel technique: an account of experimental methods in low- and high-speed wind tunnels" Pitman and Sons.

Phillips-Birt D. (1970) "Ship Model Testing" International Textbook Co. Ltd.

Preston J.H. (1966) "The Design of High Speed, Free Surface Water Channels" NATO Advanced Study Institute on 'Surface Hydrodynamics'. Bressanone, Italy, pp. 1-82.

Prohaska C.W. (1966) "A Simple Method for the Evaluation of the Form Factor and Low Speed Wave Resistance" Proc. 11th International Towing Tank Conference.

Remmers K.,Schneider G. and Wendt A. "Results of test runs with a Model F12 of a circulating water channel" Kempf and Remmers (Hamburg) Report.

Rigby S.G., Nicolaou D., Sproston J.L. and Millward A. "Numerical modelling of the water flow around fast ship hulls", Journal of Ship Research, vol. 45, no. 2, pp. 85-94, 2001

Sachdeva (1973) "The development of three-dimensional incompressible turbulent boundary layers" University of Liverpool, Ph.D. thesis.

Sainsbury J.C. (1961) "The Southampton University Towing Tank and Its Use in Work with Yacht Hulls" University of Southampton, Advisory Committee for Yacht Research Report No. 7.

Sandborn V.A. (1972) "Resistance Temperature Transducers" Metrology Press, Colorado.

Saunders H.E. (1957) "Hydrodynamics in Ship Design" S.N.A.M.E.

Saunders H.E. and Hubbard C.W. (1944) "The circulating water channel of the David Taylor Model Basin" Trans. S.N.A.M.E., vol. 52, pp. 325-374.

Schuster (1959) "Der Umlauf kanal der V.W.S." Sonderbruck aus Schiffstechnik, B6, Heft 33, Seite 139-144.

Sinha S.N. (1981) "Backward facing flow experiments" AIAA Journal, vol. 19, pp. 1527-1530.

Spencer N. (1994) "An investigation into the resistance characteristics of high speed catamarans in calm water and in waves" University of Liverpool, M.Phil thesis.

Spencer N.J. and Millward A. (1993) "Guide to the Program for Calculation of a Ship Model Wetted Surface Area" University of Liverpool, Dept. of Mechanical Engineering Report TF/033/93.

Srettenski L.N. (1937) "Theory of wave resistance" Trudy Tsentraln. Aero-Gidrodynam. Inst. im Professor N.E. Zhukovskogo 458, Moscow (in Russian).

Steele B.N. (1962) "A design study of a circulating water channel" N.P.L. Report S.H.R. 26/62, March 1962.

Sutcliffe C.J. (1995) "The effect of waves on the performance of yachts" University of Liverpool, Ph.D. thesis.

Sutcliffe C.J. and Millward A. (1998) "The effect of motion axes on the performance of a yacht in waves" Transactions R.I.N.A., vol. 140, pp. 184-209.

Table 1 The major parameters of the flume

Working section size:

Width	1.40 m (4.5 ft)
Depth	0.84 m (1.75 ft)
Length	3.66 m (13 ft)

Variable depth:

The floor can be set to give any chosen depth of water from

0.10 m (0.33 ft) to 0.84 m (2.75 ft)

Flow velocity:

0 to 5.7 m/s

Table 2 Control settings for flat water in working section (no model)

Velocity m/s	Dial setting	Jet box setting	Front floor	Back floor	Floor diff-erence	Splitter flap	Main flap
0.5	82.5	600	8348	8607	259	100	82
0.75	123.8	600	8332	8593	261	100	82
1.0	165.0	600	8332	8593	261	100	82
1.25	206.3	600	8336	8593	257	103	60
1.5	247.5	600	8412	8546	134	93	80
1.75	288.8	600	8412	8546	134	115	60
2.0	330.0	550	8384	8591	207	125	60
2.25	371.8	550	8384	8591	207	125	60
2.5	412.5	550	8360	8573	213	110	60
2.75	453.8	550	8360	8573	213	110	60
3.0	495.0	550	8360	8620	260	110	60
3.25	536.3	550	8360	8620	260	110	60
3.5	577.5	550	8360	8620	260	100	60
3.75	618.8	550	8360	8620	260	100	60
4.0	660.0	550	8360	8620	260	100	60
4.25	701.3	550	8360	8620	260	100	60
4.5	742.5	550	8360	8620	260	100	60
4.75	783.8	550	8360	8620	260	100	60
5.0	825.0	550	8360	8620	260	100	60

Table 3 Dimensions of the dynamometer flexures

Force	Length (mm)	Width (mm)	Thickness (mm)	I_{max} (mm^4)	I_{min} (mm^4)	I_{max}/I_{min}
Resistance	152.4	12.7	1.65	281.65	4.754	59.2
Side force	152.4	19.05	2.16	1244.4	16.00	77.8

Table 4 Details of Gimbals

Identification	Trim	Heel
A	Free	Fixed - 0° only
B	Free - range -4° to +12° Fixed - ½° increments	Free - ±30° Fixed - 5° increments
C	Free - range -4° to +12° Fixed - ½° increments	Fixed - 0° only
D	Free - range -4° to +12° Fixed - ½° increments	Free - ±30° Fixed - 0° only
E	Free - range -4° to +12° Fixed - ½° increments RVDT measurement also	Free - ±30° Fixed - 5° increments RVDT measurement also
F	Free - range 0° to 12° Fixed - ½° increments	Fixed - 0° only

Table 5 Dimensions of the NPL 100A models

	Model 1	Model 2
Water-line length L m	1.000	1.376
Beam B m	0.160	0.220
Draught T m	0.055	0.076
Length/beam ratio L/B	6.25	6.25
Length/draught ratio L/T	18.2	18.2
Wetted surace area S m^2	0.165	0.313
Length/water depth ratio L/H	1.190	1.638
Length/channel width ratio L/K	0.714	0.983
Blockage ratio (%)	0.51	0.97

Appendix 1

Calculation of jet velocity for the jet injection system

The combination of the initial boundary layer on the contraction and the jet is shown schematically in Fig. A1 at some distance downstream of the injection slot. At some distance y from the surface the local velocity u is given by

$$u = u_i + \Delta u \tag{A1}$$

where u_i is the initial velocity due to the boundary layer on the contraction and Δu is the additional velocity from the jet injection system.

A general expression for the momentum deficit at this point is

$$M = \rho \int_0^{\delta} u\,(U - u)\,dy \tag{A2}$$

where ρ is the water density, δ is the boundary layer thickness and U is the free stream velocity. Substituting from Eq. A1 into Eq. A2 then

$$M = \rho \int_0^{\delta} u_i\,(U - u_i)\,dy - \rho \int_0^{\delta} \Delta u\,(2u_i - U + \Delta u)\,dy \tag{A3}$$

or

$$\begin{aligned} M = {} & \rho U^2 \theta_i - \rho u_m^2 \int_0^{\delta_j} \left(\frac{\Delta u}{u_m}\right)^2 dy \\ & - 2\rho u_m \int_0^{\delta_j} \frac{\Delta u}{u_m}\, u_i\, dy + \rho u_m U \int_0^{\delta_j} \frac{\Delta u}{u_m}\, dy \end{aligned} \tag{A4}$$

where θ_i is the momentum thickness of the initial boundary layer, u_m is the maximum velocity on the profile and δ_j is the limit of the jet at station x. In order to proceed

further it is necessary to find expressions for the variation of u_m and $\Delta u/u_m$ with distance x downstream. In order to do this the jet was considered to be half of a simple two dimensional free jet, as shown in Fig. A2, such that

$$\frac{\delta_{\frac{1}{2}}}{x} = k \tag{A5}$$

where k is a constant and

$$\frac{u}{u_m} = f\left(\frac{y}{\delta_{\frac{1}{2}}}\right) \tag{A6}$$

The momentum flux in the jet (M_1) is

$$M_1 = \int \rho u^2 dy \tag{A7}$$

and therefore be expressed as

$$M_1 = \rho u_m^2 \delta_{\frac{1}{2}} \int_0^{\delta_j} \left(\frac{u}{u_m}\right)^2 d\left(\frac{y}{\delta_{\frac{1}{2}}}\right) \tag{A8}$$

Substituting from Eq. A6 this becomes

$$M_1 = \rho u_m^2 \delta_{\frac{1}{2}} \int_0^{\delta_j} \left(f\left(\frac{y}{\delta_{\frac{1}{2}}}\right)\right)^2 d\left(\frac{y}{\delta_{\frac{1}{2}}}\right) \tag{A9}$$

which simplifies to

$$M_1 = \rho u_m^2 \delta_{\frac{1}{2}} A \tag{A10}$$

where A is some constant.

Substituting for the jet half width from Eq. A5 then

$$M_1 = \rho u_m^2 kAx. \tag{A11}$$

However since the momentum flux must be independent of x in order to preserve continuity then

$$M_1 = B \tag{A12}$$

where B is also constant so that the dependence of u_m with x can be obtained as

$$u_m = \frac{B}{(\rho kAx)^{\frac{1}{2}}} \tag{A13}$$

or in other words the maximum jet velocity decreases as $x^{1/2}$.

If the notation of Fig. A1 is substituted in Eq. A6 then for the surface jet

$$\frac{\Delta u}{u_m} = f\left(\frac{y}{\delta_j}\right) \tag{A14}$$

and it becomes necessary to assume a value for the function f. Some experimental data in Lachman (1961) suggested that a suitable function, which has to be asymmetric about the point (½, ½), was

$$\frac{\Delta u}{u_m} = \cos^2\frac{\pi}{2}\left(\frac{y}{\delta_j}\right). \tag{A15}$$

The increase of momentum flux in the jet can be expressed as

$$\rho u_j h(u_j - U) \tag{A16}$$

so that the total momentum loss between Stations 1 and 2 shown in Fig. A3 is

$$
\begin{aligned}
M &= \rho \int_0^{\delta} u\,(U - u)\,dy \\
&= \rho \int_0^{h} u_j\,(U - u_j)\,dy + \rho U^2 \int_h^{\delta} \frac{u}{U}\left(1 - \frac{u}{U}\right) dy \qquad (A17) \\
&= -\rho U^2 h \frac{u_j}{U}\left(\frac{u_j}{U} - 1\right) + \rho U^2 \theta_i \,.
\end{aligned}
$$

The design requirement is that at some distance downstream, which is unknown at this stage, the velocity profile will be uniform at velocity U. Thus at this distance M = 0 and Eq. A17 becomes

$$\rho U^2 \theta_i = \rho U^2 h \frac{u_j}{U}\left(\frac{u_j}{U} - 1\right). \qquad (A18)$$

Eq. A18 assumes that there is no boundary layer growth downstream of the jet. If Eq. A18 is substituted into Eq. A3 with M = 0 then after some re-arrangement

$$
\begin{aligned}
\left(\frac{u_j}{U} - 1\right) = \frac{u_j}{U}\left(\frac{u_m}{u_j}\right)^2 \frac{\delta_j}{h} \int_0^1 \left(\frac{\Delta u}{u_m}\right)^2 d\left(\frac{y}{\delta_j}\right) \\
-2\,\frac{u_m}{u_j}\left(\frac{\delta_j}{h}\right) \int_0^1 \frac{\Delta u}{u_m}\left(1 - \frac{u_j}{U}\right) d\left(\frac{y}{\delta_j}\right) \qquad (A19) \\
+\left(\frac{u_m}{u_j}\right)\left(\frac{\delta_j}{h}\right) \int_0^1 \left(\frac{\Delta u}{u_j}\right) d\left(\frac{y}{\delta_j}\right)
\end{aligned}
$$

which can be written as

$$= f_1(I_1) - f_2(I_2) + f_3(I_3). \qquad (A20)$$

It can be seen that I_1 and I_3 can be evaluated using Eq. A6 and are

$$I_1 = 0.375 \qquad I_3 = 0.500.$$

The second term of Eq. A20 can be treated in the following manner. From Eq.A4

$$\frac{\delta_j}{h} = \frac{kx}{h} \tag{A21}$$

and from Lachman (1961) k = 0.1. Measurements of the boundary layer on the contraction showed that the velocity profile could be adequately represented by the normal one-seventh power law so that

$$\begin{aligned}\left(1 - \frac{u_i}{U}\right) &= 1 - \left(\frac{y}{\delta_j}\right)^n \qquad \text{where } n = \frac{1}{7} \\ &= 1 - \left(\frac{y}{\delta_j}\right)^n \left(\frac{\delta_j}{h}\right)^n \left(\frac{\delta}{h}\right)^{-n}.\end{aligned} \tag{A22}$$

Substituting from Eq. A22 into the term $f_2(I_2)$ of Eq. A20 then

$$\begin{aligned}f_2(I_2) &= 2\left(\frac{u_m}{u_j}\right)\left(\frac{\delta_j}{h}\right)\int_0^1 \frac{\Delta u}{u_m}\, d\left(\frac{y}{\delta_j}\right) \\ &\quad -2\frac{u_m}{u_j}\left(\frac{\delta_j}{h}\right)^{n+1}\left(\frac{\delta}{h}\right)^{-n}\int_0^1 \frac{\Delta u}{u_m}\left(\frac{y}{\delta_j}\right)^n d\left(\frac{y}{\delta_j}\right) \\ &= f_4(I_4) - f_5(I_5)\ .\end{aligned} \tag{A23}$$

It can be seen that the integral I_4 is the same as I_3 and I_5 can be evaluated numerically to give:

$$I_4 = 0.5 \quad \text{and} \quad I_5 = 0.40275.$$

With the further substitution for δ_j from Eq. A21, Eq. A19 becomes

$$\left(\frac{u_j}{U} - 1\right) = 0.375 \left(\frac{u_m}{u_j}\right)^2 \frac{u_j}{U} \left(\frac{x}{10h}\right) + \left(\frac{u_m}{u_j}\right) \frac{x}{10h} \left(0.8055 \left(\frac{x}{10h}\right)^{\frac{1}{7}} \left(\frac{\delta}{h}\right)^{-\frac{1}{7}} - 0.5\right). \tag{A24}$$

A relationship between u, h and δ can be established from Eq. A18 for a given value of U since δ and θ_i were known from measurements of the initial boundary layer. Thus

$$\frac{u_j}{U}\left(\frac{u_j}{U} - 1\right) = \frac{7}{72}\,\delta \tag{A25}$$

The value of δ was found to be 23 mm from the initial measurements so that values of u_m/u_j could be determined from Eq. A24 for different values of x downstream of the injection slot for a given slot width h. Using this method the vertical velocity profiles of u/U against y/δ could be obtained for any slot width at different distances downstream with u_m/u_j determined from Eq. A24. Typical velocity profiles are shown in Fig. A4 for a slot width h = 1.27mm (0.05in).

Appendix 2

Model Scaling

Since the flume can be used for obtaining experimental measurements on a wide variety of models it is important to consider the appropriate model scaling techniques.

The motion of a vessel through a fluid causes a hydrodynamic force on the vessel or body. If the body were axi-symmetric and moving through a uniform stationary fluid with a velocity which is coincident with that axis then the total hydrodynamic force would be also along that axis i.e. it would be a drag or resistance force as illustrated in Fig. 47a; the nearest approach to this in marine transport is the deeply submerged submersible.

In the more usual case the vessel has a plane of symmetry in the direction of motion resulting in a fluid dynamic force which will be in that plane and which can be more conveniently resolved into lift and drag components as shown in Fig. 47b. In the case of the conventional ship the lift force is small but this will not be the case for planing vessels and hydrofoils which have been tested in the flume.

In a few special cases the plane of symmetry is not in the direction of motion and, as shown in Fig. 47c, the hydrodynamic force has a side force component - this is primarily found in hovercraft and sailing yachts which have each been tested in the flume.

It can be expected that the direction and magnitude of the hydrodynamic force will be dependent on a number of parameters such as:-

(a) the velocity of the body,

(b) the geometrical size and shape of the body,

(c) its position attitude relative to its velocity,

(d) the distance of the vessel from a fluid boundary (e.g. air-water, water-ground),

(e) properties of the fluid,

(f) gravity.

The last item affects not only the weight of the vehicle and therefore, for hovercraft etc., the lift force that must be produced but, because many vessels are normally moving close to or on the air-water boundary, they create waves which are gravity controlled. The wave system spreads behind the vessel thus consuming energy. This energy is provided by the body and is part of the drag of the vessel.

For most vessels, the aerodynamic and hydrodynamic forces on the vessel are considered separately and in many cases the hydrodynamic forces are predominant. The difference in densities between air and water (a factor of 800 or so) means that when moving through stationary air the air forces are normally small compared with water forces. This is however less true for high speed vessels whose major drag producing area (e.g. hovercraft) is in air and can become a dangerous simplification when the air is not stationary such as in strong winds. One of the advantages of the flume compared with the towing tank is that, because the model is stationary in the working section with the water moving past the model, there are no air forces generated. This contrasts with a model in a towing tank where a high speed run causes aerodynamic forces on the model which have to be taken into account in the measurement system.

If the concept of dimensional analysis is applied to determine the non-dimensional groups which may be relevant in a model test then the parameters

which may contribute are

Vessel speed	U (m/s)
Vessel size as represented by a characteristic length	L (m)
Gravity	g (m/s^2)
Fluid properties such as:	
density	ρ (kg/m^3)
dynamic viscosity	μ (kg/ms)
bulk modulus	K (kg/ms^2)
local absolute vapour pressure	p_v (N/m^2)
surface tension	γ (kg/s^2)

Thus the hydrodynamic force F can be shown to be a function of five main groups as explained in greater detail by Clayton and Bishop (1982), viz.

$$\frac{F}{\rho U^2 L^2} = f\left(\frac{\rho UL}{\mu}, \frac{U^2}{gL}, \frac{\rho U^2}{K}, \frac{p_v}{\rho U^2}, \frac{\rho U^2 L}{\gamma}\right) \qquad \text{(A2.1)}$$

or

$$C_F = f_1\,(Re, F_n, Ca, \sigma, We) \qquad \text{(A2.2)}$$

where

$$\text{force coefficient } C_F = \frac{F}{\frac{1}{2}\rho U^2 L^2}$$

$$\text{Reynolds number } Re = \frac{\rho UL}{\mu} = \frac{UL}{\nu}$$

$$\text{Froude number } F_n = \frac{U}{\sqrt{gL}}$$

$$\text{Cauchy number } Ca = \frac{\rho U^2}{K}$$

$$\text{cavitation number } \sigma = \frac{p - p_v}{\frac{1}{2}\rho U^2}$$

$$\text{Weber number } We = U\left(\frac{\rho L}{\gamma}\right)^{\frac{1}{2}}$$

noting that the term ρU^2 is normally replaced by $\frac{1}{2}\rho U^2$ since this latter term has the useful physical interpretation as the dynamic pressure in fluid flow. If K is the isentropic bulk modulus of the fluid then

$$Ca = \frac{\rho U^2}{K} = \frac{U^2}{a^2} = (M)^2 \qquad \text{(A2.3)}$$

where M is the Mach number and is more commonly used instead of the Cauchy number. Since the speed of sound a in water is large it can be considered an incompressible fluid and the Mach number ignored in terms of model scaling. In many cases the surface tension forces are small compared with inertia forces so that the Weber number is large and the effects of surface tension can also be ignored. This is normally the case when the models are large and move at moderate or high speeds. On the other hand surface tension can play an important part when models are small and moving at slow speeds which is one of the reasons why, for normal ship model testing, the smallest hulls used are not less than about a metre in length on the waterline.

It would follow therefore that the hydrodynamic force coefficient on two similar models would be identical numerically if the three remaining groups, i.e. Froude, Reynolds and cavitation numbers, had the same values. As will be seen later, this is not at present possible in model tests and steps have to be taken to account for the discrepancies that subsequently arise. The existence of the three separate non-dimensional groups would suggest that the hydrodynamic force can be separated into three identifiable parts, although they are not necessarily independent of each other.

The Reynolds number is related to viscous forces which show their effect in the presence of the boundary layer on the vessel. The viscous forces causing the boundary layer largely act tangentially to the body and, since the body in the case of a vessel is usually symmetrical about the x-axis and aligned with the axis of the flume, the viscous force contributes almost exclusively to the resistance of the vessel and a negligible amount to the lift or side force.

The cavitation number is a measure of the pressure forces on the vessel which act normal to its surface. In the case of a conventional ship or submarine therefore the pressure forces would mainly cause resistance whereas on a hydrofoil or a propeller where there is an inclined surface, the pressure forces contribute to both lift and drag - the exact proportion depending on the geometry of the lifting surface.

The Froude number is also related to the pressure forces on the vessel but exclusively to the case where it is close to the free surface, thus this would not apply to a deeply submerged submersible or submarine. However at or close to the free surface the presence of a moving pressure source creates waves on the water surface which require energy. In general the waves are symmetrical about the vessel and therefore contribute mainly to the resistance although it has been shown that the wave

pattern around a sailing yacht, which as mentioned earlier moves at a leeway angle, does have an asymmetric wave pattern which must therefore make some contribution to the side force.

If the Reynolds numbers are the same for both model and full size vessel then the viscous boundary layer, including points of separation and transition will be the same (geometrically); if the Froude numbers are the same then the wave pattern would be the same in the case of a vessel moving on or near the free water surface, and thirdly if the cavitation numbers are the same this would ensure cavitation inception would occur at the same place. Thus if all these conditions held then it would be possible to state that the hydrodynamic force coefficients would be identical i.e.

$$\left[\frac{F}{\frac{1}{2}\rho U^2 S}\right]_m = \left[\frac{F}{\frac{1}{2}\rho U^2 S}\right]_s \qquad \text{(A2.4)}$$

where the subscripts m = model and s = full scale ship and S is an appropriate area.

Unfortunately the complete fulfilment of all three requirements is not possible and it remains to the skill of the engineer to decide what approximations can reasonably be made for each particular case. The likely problems for ship model testing, which can all be tested in the flume, can usually be divided into three major categories which are discussed in increasing order of complexity:

A2.1.1 Non-free surface, non-cavitating vessels

A2.1.2 Cavitating, free surface vessels

A2.1.3 Non-cavitating, free surface vessels

A2.1.1 Non-free surface, non-cavitating vessels

The most likely vessel to fall into this category would be a submersible used for ocean exploration or rescue, a deeply submerged submarine or other underwater body such as a torpedo operating far from the free surface but not necessarily far from the ocean bottom or other solid boundary. In such cases the flume could be used in its water tunnel configuration; the same considerations would apply if the flume were used for tests on aeroplanes and similar vehicles provided that allowance is made for the difference in density and viscosity of the fluids. Because of the difference in kinematic viscosity of air and water the flume is equivalent in terms of Reynolds number to a wind tunnel with the same size working section with a speed of approximately 75 m/s.

For fully submerged vessels it is not necessary to fulfil all three similarity requirements - indeed the only relevant parameters are that the model should be geometrically similar to the full size vessel and that the Reynolds numbers should be equal. If it is assumed that the scaling factor from model to full scale is Λ, where usually $\Lambda > 1$, then the condition that the Reynolds numbers should be the same gives

$$Re_m = \frac{U_m L_m}{\nu_m} = Re_s = \frac{U_s L_s}{\nu_s} \qquad \text{(A2.5)}$$

or

$$\frac{U_m}{U_s} = \left(\frac{L_s}{L_m}\right)\left(\frac{\nu_m}{\nu_s}\right) = \Lambda\left(\frac{\nu_m}{\nu_s}\right) \qquad \text{(A2.6)}$$

with the simplification that, if the model tests are carried out in the same fluid as

for the full size vessel $\upsilon_m = \upsilon_s$, so

$$U_m = \Lambda U_s \qquad \text{(A2.7)}$$

i.e. the model has to be tested at Λ times the full scale speed. For example, if Λ=20 and the maximum full scale speed was 20 knots, then the required model speed would be 400 knots. In most cases however even this simplest requirement is almost impossible to fulfil unless very large test facilities are available where the model is almost the same size as the full scale vessel, in which case all the advantages of model testing such as lower cost and convenience are lost. However some cases do occur where it is possible for the model to be the same size or sometimes even bigger than the full size object although not usually with ships. One example, which has been investigated in the flume, was where it was required to measure the lift and drag forces on scallop shells as reported in Millward and White (1992). In this case the models used were plaster casts of the real shells (i.e. Λ=1) so that the tests were carried out at the actual speeds that the scallops were believed to swim at.

In practice, where it is not possible to carry out the tests at the correct Reynolds number, the measurements are made at the highest Reynolds number practicable and it is then assumed that the residual resistance coefficient C_r will apply to all speeds (not just the corresponding speed) with the friction resistance being allowed for in the normal way by use of a friction correlation line as explained in Section A2.1.3. Since the Reynolds number on the model will be lower than on the full size vessel care must be taken to make sure that the boundary layer on the model is turbulent using some form of turbulence trip as explained later in Section A2.2. There may also be some cases where the flow is less subject to the influence of Reynolds number, such as the flow over a non-streamlined object such as a ship's

superstructure or other bluff bodies, and the model speed can be varied to suit other parameters such as flow visualisation techniques.

A2.1.2 Cavitating, free surface vessels (high speed)

Model tests of some high speed vessels such as hydrofoils may also not need fulfilment of Froude number equality because their wave drag is negligible, leaving only the Reynolds number and cavitation index to be satisfied. If the tests are run at atmospheric pressure, with the flume being used as an open channel, then the relationship from model to full scale is, for cavitation,

$$\sigma_s = \frac{p_a + \rho_s g h_s - p_v}{\frac{1}{2}\rho_s U_s^2} = \sigma_m = \frac{p_a + \rho_m g h_m - p_v}{\frac{1}{2}\rho_m U_m^2} \qquad \text{(A2.8)}$$

or

$$\frac{U_s}{U_m} = \left[\frac{\rho_m}{\rho_s}\left(\frac{p_a + \rho_s g h_s - p_v}{p_a + \rho_m g h_m - p_v}\right)\right]^{\frac{1}{2}} . \qquad \text{(A2.9)}$$

The atmospheric pressure p_a is usually considerably greater than the terms ρgh or p_v so if $\rho_m = \rho_s$ then $U_s = U_m$ i.e. the model should be tested at the same speed as the full size vessel which is again unlikely to be possible bearing in mind that the maximum speed of the flume is 5.7 m/s. It also follows that Eq. A2.9 cannot be satisfied at the same time as Eq. A2.7 which was the condition for the Reynolds number to be the same for the model and the full size vessel since this requires the model to be tested at a higher speed than the full size vessel.

Some alleviation of this difficulty can be obtained with a facility such as the flume when used as a cavitation channel or tunnel since the pressure above the water in the working section can be reduced below atmospheric pressure. Even so, with the minimum pressure of approximately 1/30 atmospheric pressure, the simultaneous

satisfaction of Eq. A2.9 and A2.7 is still not possible. It is usual therefore to test as near to the correct cavitation number as possible so that any problems related to cavitation can be identified.

A2.1.3 Non-cavitating free surface vessels

Many vessels operate in sub-cavitating, free surface conditions and correspondingly their model tests should theoretically be carried out at the correct Froude and Reynolds numbers since their wave-making drag is significant e.g. conventional ships, the low to medium speed range hovercraft, hydrofoils and planing craft and submersibles when at or close to the water surface.

The Froude number equality requires the speed relationship

$$F_{nm} = \frac{U_m}{\sqrt{gL_m}} = F_{ns} = \frac{U_s}{\sqrt{gL_s}} \qquad \text{(A2.10)}$$

or

$$\frac{U_m}{U_s} = \sqrt{\frac{L_m}{L_s}} = \frac{1}{\sqrt{\Lambda}} \qquad \text{(A2.11)}$$

while the Reynolds number equality would be, as before,

$$Re_m = \frac{U_m L_m}{\nu_m} = Re_s = \frac{U_s L_s}{\nu_s}$$

or

$$\frac{U_m}{U_s} = \Lambda \ . \qquad \text{(A2.12)}$$

Thus in the case of a ship 250m long with a cruising speed of 25 knots, a model 5m long would be tested at 3.5 knots approximately or about 1.8 m/s on a Froude number basis, but at 1250 knots on a Reynolds number basis. Clearly therefore the Froude number and Reynolds number requirements cannot both be satisfied at the same time and indeed the Reynolds number requirement could never be met.

Even so tests on models of surface vessels are routinely carried out in towing tanks and water channels. The procedure followed is that developed by Froude, a contemporary of Reynolds and Kelvin. As described in Phillips-Birt (1970), Froude suggested that the model should be tested at the corresponding speed, now known as the Froude number, so that the correct wave pattern, and thus the correct wave resistance, around the vessel is obtained. The resistance was divided into two parts called the residuary (wave) resistance, dependent on Froude number, and the frictional resistance, dependent on Reynolds number, where the latter was calculated from tests on planks towed on edge i.e.

$$R_{tm} = R_{rm} + R_{fm} \qquad \text{(A2.14)}$$

with the assumption that there was no interaction between the two parts. This same technique is still used with some refinements such as the frictional resistance being calculated from a suitable friction correlation formula. It is assumed that if the model is run at the correct Froude number then the residuary resistance

coefficient will be the same for the model and the full scale vessel

$$C_{rm} = C_{rs}$$

$$\frac{R_{rm}}{\frac{1}{2}\rho_m U_m^2 S_m} = \frac{R_{rs}}{\frac{1}{2}\rho_s U_s^2 S_s} \qquad \text{(A2.15)}$$

noting that this assumption must be taken with some reservations since the residuary resistance includes form drag, spray drag etc as well as wave resistance.

Eq. A2.15 can be re-written as

$$R_{rs} = R_{rm} \left(\frac{U_s}{U_m}\right)^2 \left(\frac{S_s}{S_m}\right) \left(\frac{\rho_s}{\rho_m}\right) . \qquad \text{(A2.16)}$$

Now since from Eq. A2.11

$$U_s/U_m = \Lambda^{1/2}$$

and also

$$S_s/S_m = \Lambda^2$$

so <u>if</u> $\rho_m = \rho_s$ then

$$R_{rs} = \Lambda^3 R_{rm} . \qquad \text{(A2.17)}$$

It should be noted however that tests in a towing tank or water channel are usually carried out in fresh water while the vessel will normally operate in salt water. The more usual form of the equation is therefore

$$R_{rs} = R_{rm} \Lambda^3 \left(\frac{\rho_s}{\rho_m}\right) . \qquad \text{(A2.18)}$$

The basic technique developed by Froude therefore involved expanding the model results by the use of Eq. A2.18 and making an independent calculation of the frictional resistance using an appropriate formula such as the International Towing

Tank Correlation formula at both model and full scale sizes. The complete Froude procedure is, therefore,

$$R_{ts} = R_{fs} + (R_{tm} - R_{fm}) \left(\frac{\rho_s}{\rho_m}\right) \Lambda^3$$
$$= R_{fs} + R_{rm} \left(\frac{\rho_s}{\rho_m}\right) \Lambda^3 \qquad \text{(A2.19)}$$

or in coefficient form

$$C_{ts} = C_{fs} + (C_{tm} - C_{fm}) = C_{fs} + C_{rm} \qquad \text{(A2.20)}$$

where R_{tm} = model total resistance at the test Froude number

R_{ts} = ship total resistance at the test Froude number

R_{fs} = ship frictional resistance calculated from a specified frictional correlation formula

R_{fm} = model frictional resistance calculated from the same friction correlation formula

R_{rm} = model residuary resistance

with the corresponding coefficients obtained by non-dimensionalising by the factor $\frac{1}{2}\rho U^2 S$.

A more modern modification of the Froude scaling system makes an additional allowance for the form resistance by the introduction of a form factor k (Lewis, 1988) which attempts to introduce an allowance for the three-dimensional shape of the hull compared with the friction formulae which are esentially based on two-dimensional flat plate boundary layer formulae. This has the effect of reducing the residuary resistance

$$C_t = (1+k)\ C_f + C_r\ . \qquad \text{(A2.21)}$$

The form factor k can be found experimentally by the Prohaska method (Prohaska, 1966) which involves testing the model at low speeds, below the wave making resistance, and plotting the results in the form

$$\frac{C_t}{C_f} \quad \text{against} \quad \frac{F_n^4}{C_f}\ . \qquad \text{(A2.22)}$$

The value for the form factor is given by the value of the intercept at the y axis. In some cases it may be worth adjusting the value for the power of the Froude number to get a straight line on the data points. A sample of a curve is shown in Fig. 48 which is taken from Millward (1989). It should be noted however that many of the models tested in the flume are of high speed ships such as planing hulls, catamarans or round bilge displacement hulls where the flow pattern around the hull, particularly at the transom, and the trim of the hull vary quite markedly between the low speed necessary for determining the form factor using the Prohaska method and normal operating speeds. For these vessels therefore the form factor is difficult to measure with any degree of certainty and, following the recomendation of the ITTC (1990), the form factor is usually assumed to be unity so that any scaling of model results is obtained using the basic Froude method as given by Eq. A2.19.

It should also be noted that if Froude scaling is followed then the cavitation index on the model is Λ times full scale so it follows that absence of cavitation on the model is not a guarantee of its absence on the full scale vessel although this is most likely to be a problem on self-propelled models where the propeller is present.

This type of model test has not yet been carried out in the flume when cavitation is likely to occur.

When proposing the scaling procedure now named after him, Froude used data from tests made on flat planks of various lengths. Subsequently experiments such as those performed by Reynolds have shown that there are two distinct boundary layer flow regimes, each with an associated resistance law - laminar flow at low Reynolds numbers and turbulent flow at high Reynolds numbers. Curves representing the friction coefficients for laminar and turbulent boundary layers are shown in Fig. 49 against Reynolds number. Also marked on the graph are typical Reynolds numbers based on hull length for model and full size ships. It can be seen that while a real ship is likely to have a turbulent boundary layer over most of the hull, with about 1% or less being laminar, a model hull may have a large area of the hull covered by laminar boundary layer flow. In addition transition from laminar to turbulent flow does not always occur at a particular Reynolds number but appears to be dependent on a number of variables such as hull curvature, hull roughness, turbulence level, etc. The transition Reynolds number is therefore not known for any particular hull and a series of tests to discover which portions of the hull are covered by a laminar or a turbulent boundary layer would be complicated, and therefore expensive, and not necessarily satisfactory. The method adopted in most towing tanks and water channels therefore is to force the boundary layer to become turbulent and use an extrapolation of the turbulent boundary layer resistance formula to calculate the frictional resistance of the model at the model Reynolds number. In practice the normal turbulent boundary layer formula is not used since this has been derived from two-dimensional flat plate and axi-symmetric data. Instead a formula is used which is based on experience with correlation experiments and attempts to

take into account three dimensional effects and is more properly called a friction correlation formula. The most widely used of these formulae is the 1957 International Towing Tank Conference (ITTC) formula given below but others are discussed in Lewis (1988) and also in Phillips-Birt (1970).

ITTC (1957) friction correlation formula

$$C_f = \frac{0.075}{(\log_{10}Re - 2)^2} \qquad \text{(A2.23)}$$

An older friction correlation formula is the 1947 ITTC formula first proposed by Schoenherr and given below.

1947 ITTC (Schoenherr) formula

$$\frac{0.242}{\sqrt{C_f}} = \log_{10}(Re.C_f) \qquad \text{(A2.24)}$$

where Re is the Reynolds number based on the water-line length of the hull. As can be seen in the computer program given in Appendix 5, the ITTC formula is normally used to analyse data from tests in the flume.

A2.2 Turbulence stimulators

In order to cause transition from a laminar to a turbulent boundary layer flow it has been found that some form of turbulence stimulator is usually necessary, particularly for smaller models such as those used in the flume. It has however been found that in the flume a turbulent boundary layer can be obtained without turbulence stimulators at much lower speeds than might be expected in a towing tank (Cole, 1974), presumably because of the normal level of turbulence in the flow. In towing tanks some form of turbulence stimulator has been found to be necessary - various

types have been used ranging from a strut towed ahead of the models to sand-strips, trip wires or studs on the model. The strut has the advantage that, since it is not attached to the model, its own resistance is not measured as part of the model resistance whereas the other forms of stimulator are attached to the model and may therefore add to the measured model resistance. However experiments with struts and fine, high speed models which showed no signs of laminar flow without the strut have shown reduced resistance with the strut present, presumably due to some form of interaction with the strut wake (Lewis (1988)).

The use of studs 3 mm diameter and 2.5mm high was proposed by Hughes and Allan (1951) and has been widely adopted. Hughes estimated that for the models used in his experiments, about 5-6 metres in length, the added resistance due to the studs themselves was less than 1% of the model resistance and could therefore be neglected. For smaller ship models using the same size studs, such as those used in the flume, this assumption cannot necessarily be made and a procedure for estimating the stud drag has been derived by the author and is described in the next section. For conventional ships therefore it is normal practice to fit turbulence studs. However for high speed ships, particularly planing hulls where the length of hull in the water varies considerably with speed, it is not practical to fit turbulence stimulators and it is assumed that the turbulence in the water together with the broken water at the bow will be sufficient to trip the boundary layer. This assumption is supported by the experiments made by Cole (1974).

A second method of turbulence stimulation which has been used in the flume is by means of sand or carborundum strips which are 10mm wide with approximately 4 granules of carborundum per square centimetre. The recommended method of determining the additional resistance of the strip (ITTC, 1990) is empirical and is

obtained by measuring the resistance of the model with one strip in place and then with two strips in place. This technique has been used mostly with models of sailing yachts.

A2.2.1 Stud correction procedure

The procedure for calculating the drag of the turbulence studs is based on standard boundary layer flow theory. If the stud is placed on the surface of the model hull at some distance X from the leading edge, as shown in Fig. 50, then it may be wholly or partially immersed in the boundary layer which is assumed to be laminar up to that point. At the position of the stud the free stream velocity U_p outside the boundary layer is

$$U_p = k\,U \qquad (6.25)$$

where the value of k is to be determined. In general it can be assumed that for fine hulls k = 1 but this assumption is less likely to be valid for fuller forms and a value for k can be obtained from potential flow theory.

A graph showing the variation of the drag coefficient of a stud with Reynolds number based on stud diameter is given in Fig. 51 from which the drag for one stud can be calculated since

$$C_D = \frac{D_S}{\frac{1}{2}\rho \overline{U}^2 dh} \qquad (A2.26)$$

and

$$Re_d = \overline{U}d/\nu \qquad (A2.27)$$

where $\overline{U}$ is the mean velocity, d is the stud diameter and h is the stud height. For practical use in a computer program for analysis of model test data, such as shown

in Appendix 5, the curve given in Fig. 51 has been separated into three sections and a curve fit obtained for each section. For n studs therefore the resistance of the studs is

$$D_S = \tfrac{1}{2}\rho\overline{U^2} d\ h\ n\ C_D \qquad \text{(A2.28)}$$

assuming that all studs are equi-distant from the leading edge of the hull.

It is therefore necessary to be able to calculate the velocity $\bar{U}$ which is the root mean square velocity at the stud. If the stud is totally immersed in the laminar boundary layer then

$$\overline{U^2} = \frac{U^2}{h}\int_0^h \left(\frac{u}{U}\right)^2 dy\ . \qquad \text{(A2.29)}$$

From Duncan et al (1960) it can be shown that a reasonable approximation to the velocity distribution in a laminar boundary layer is

$$\frac{u}{U} = \frac{2y}{\delta} - 2\left(\frac{y}{\delta}\right)^3 + \left(\frac{y}{\delta}\right)^4 . \qquad \text{(A2.30)}$$

If Eq. A2.30 is substituted into Eq. A2.29 and the integration carried out then

$$\frac{\overline{U^2}}{U^2} = \left(\frac{h}{\delta}\right)^2\left[\frac{4}{3} - \frac{8}{5}\left(\frac{h}{\delta}\right)^2 + \frac{2}{3}\left(\frac{h}{\delta}\right)^3 + \frac{4}{7}\left(\frac{h}{\delta}\right)^4 - \frac{1}{2}\left(\frac{h}{\delta}\right)^5 + \frac{1}{9}\left(\frac{h}{\delta}\right)^6\right]. \qquad \text{(A2.31)}$$

The boundary layer thickness can be calculated from

$$\delta = 5.0\ X\ Re_X^{-\frac{1}{2}} \qquad \text{(A2.32)}$$

where

$$Re_x = \frac{UX}{\nu} \qquad \text{(A2.33)}$$

so

$$\delta = 5.0 \left(\frac{\nu X}{U}\right)^{\frac{1}{2}} . \qquad \text{(A2.34)}$$

Substitution of Eq. A2.34 in Eq. A2.31 enables $\bar{U}$ to be determined first and hence the total stud resistance from Eq. A2.28 using Fig. 51.

If however the stud is not completely immersed within the boundary layer but is projecting up into the free stream flow then a different expression is needed in place of Eq. A2.31

$$\frac{\overline{U^2}}{U^2} = \frac{K\delta + (h-\delta)}{h} . \qquad \text{(A2.35)}$$

The value of K is 367/630 which is obtained by substituting $h = \delta$ in Eq. A2.31. As a result Eq. A2.35 can be re-written as

$$\frac{\overline{U^2}}{U^2} = 1 - \frac{263}{630}\left(\frac{\delta}{h}\right) \qquad \text{(A2.36)}$$

and the procedure repeated as before.

One additional problem remains - on the model the boundary layer in front of the studs is assumed to be laminar whereas the model scaling procedure assumes that the boundary layer is turbulent over the complete model. In order to allow for this a small correction can be made for the difference between the ITTC and laminar boundary layer values for the frictional resistance over this area

$$R_{Lm} = \left[\frac{0.075}{\left[\log_{10}\left(\frac{U_m X}{\nu}\right) - 2\right]^2} - \frac{1.328}{\left(\frac{U_m X}{\nu}\right)^{\frac{1}{2}}}\right] \frac{1}{2}\rho U_m^2 S_L \qquad \text{(A2.37)}$$

noting that, since the resistance is normally greater for a turbulent boundary layer than for a laminar boundary layer, this correction actually adds to the model

resistance. The area S_L is the area forward of the studs so the assumption is therefore implied that transition occurs at the studs. In reality the wake spreads out from each stud until it meets the wake from another stud so a triangular area between the studs is likely to remain laminar. This error is however likely to be even smaller than the already small correction being made and at present no method for evaluating this area exists.

A computer listing, written in QBasic, is given in Appendix 5, using the information given in this section so that it can be added to any computer program used for analysing model test data and is already included as a sub-routine in the standard data reduction and scaling program which is also given in Appendix 5.

A2.3 Measurement of wetted surface area

As discussed earlier (Section A2.1) the standard Froude model scaling technique assumes that the total resistance can be considered as consisting of two components - the frictional resistance, due to viscous effects leading to the formation of a boundary layer along the hull surface, and the residual resistance which is primarily wave-making resistance but may also include spray resistance and induced resistance i.e.

$$R_t = R_f + R_r \,. \qquad \text{(A2.38)}$$

Typically for fast displacement hulls, such as those which are well suited to testing in the flume, the frictional resistance may account for approximately one third of the total resistance and is a function of a number of parameters including the wetted surface area (WSA). As stated earlier, in the standard method of scaling model data the frictional resistance is calculated using a friction correlation formula, usually the International Towing Tank Conference formula where

$$C_f = \frac{0.075}{(\log_{10}Re - 2)^2} \qquad \text{(A2.39)}$$

and the actual frictional resistance is calculated from

$$R_f = \tfrac{1}{2}\rho U^2 S\, C_f \,. \qquad \text{(A2.40)}$$

In order to use these equations the area S must be obtained. For many cases it is conventional to use the static wetted surface area, that is the area of the hull which is in the water when the ship or model is at rest and at the normal trim; this can be obtained from the drawing of the hull lines. However for higher speed hulls, it can be observed that, as the model's speed increases, the running water-line can be seen to change significantly from the static condition because of the effect of changes in trim, heave and the wave formation along the hull. These changes can be expected to result in a variation in the actual wetted surface area so that any calculation of the frictional resistance based on the static wetted surface could be in error. Indeed, in the discussion to the paper by Insel and Molland (1992), Dinham-Peren commented that in his experience at BMT Ltd. the change in wetted surface could be as high as 15% over the speed range of a conventional round bilge displacement hull so that the deduction of wave interference of catamaran hulls made by Insel and Molland could be significantly in error by not including this factor. A similar result was found by Spencer (1994) and Millward et al (2001). It is interesting to note that for planing craft, where the hull generates sizeable dynamic lift forces, it has long been deemed necessary to record the actual wetted surface area and use it in the data reduction procedure. Other cases can also occur where the wetted surface area may be altered such as for vessels moving in shallow or confined water where the effects of squat could be significant.

A well known method of obtaining the actual or running wetted surface area (RWSA) is to mark up additional water-lines on the model above and below the datum water-line as shown in Fig. 52. The position of the actual running water-line is then observed at each station during the test run. Subsequently it is possible to calculate the wetted girth at each station from this information and hence to calculate the total running wetted surface area. Since even a simple resistance test for one model may involve some twenty runs at different speeds, it can readily be seen that obtaining the running water-line information and then calculating the running wetted surface area for a complete resistance test is very time consuming. This is particularly so in a towing tank where, with the limited time available over the working portion of the tank length when the model is running at a steady speed, it is often necessary to photograph the model and deduce the running water-line after the photographs have been processed. This is less of a problem in the flume where the model is stationary and the running time unlimited but the calculation of the wetted area from the observations is still both tedious and time consuming. As a result of this experience a computer aided method of calculating the wetted surface area has been developed to make the calculations (Spencer and Millward, 1993) although the running water-line still has to be recorded manually. It is worth commenting that consistency in observation of the running water-line requires some practice and it is better for the same person to make all the measurements during an experiment.

The computer method uses the same basic principle as the manual method and therefore assumes that the model has been marked up with water-lines above and below the datum water-line at a number of stations along the hull. In practice it has been found that the normal 10 stations with a few extra half-stations near the bow

and stern are sufficient. The computer programs have been written to cater for either a fully symmetric hull, an asymmetric hull, such as might occur with a catamaran, or a heeled hull. Strictly speaking the program assumes that the model has a vertical transom and would need to be modified slightly if needed for other stern shapes but the error introduced is small.

It is assumed that an accurate set of hull lines exists for the model which is to be tested and is available in the form of a diagram of the transverse sections at each station and half-station along the hull. The first step in using the method therefore is to digitise the hull lines at each section - in the Department this is done using a Graphtec KD3300 digitising palette attached to a standard PC. Each transverse section is digitised in turn and the data stored in an individual file identified by a common name, representing the model, together with a number identifying the transverse section. In the case of a symmetric hull in symmetric flow only one side of the hull needs to be digitised while the program requires that all the hull lines are to the right of the hull centre-line. Since the normal layout of a diagram of hull sections gives the forward sections on one side of the centre-line and the aft sections on the other side the simplest method of obtaining all the sections on the right side is to copy the hull cross-sections on to transparent paper which can be turned over once half the sections have been digitised. The program has been written so that there is no need to ensure that the diagram containing the hull lines is placed squarely on the digitising palette since the program incorporates its own angle compensation procedure. Each transverse section has to be digitised using the following steps, as illustrated in Fig. 53:

Point 1 - the intersection of the datum water-line with the centre-line;

Point 2 - any point lying on the centre-line but below the lowest point of that section (usually the keel);

Point 3 - the point on the keel of the section at the centre-line;

Point 4 to N - a sequence of points describing the shape of the section with point N lying on the deck.

It should be noted that each transverse section must be described by the same number of points N, although there is no need for the points to be equally spaced, so that the result of the digitisation will be a list of files, one for each section, and all of the same length. The maximum number of transverse sections permitted by the program is 20 and each section can be described by up to 100 points. A convenient technique for making sure that each transverse section contains the same number of points which are evenly spaced is illustrated in Fig. 54: a series of lines are drawn on the diagram which radiate from the top of the centre-line and the hull is digitised at the intersection of the radiating line and the hull line. Care must be taken to include as a data point any discontinuity in the shape of the section.

The program, which is given in Appendix 5 and is written in QBasic, first calculates the static wetted surface area, assuming the running water-line to be the same as the datum water-line and then asks either for a file name in which the running water-line data is stored or asks for the running water-line data to be typed in from the keyboard. The running water-line can be displayed on the screen as a check that the data has been correctly entered before proceeding with the calculation of the wetted surface area. The running wetted surface area is given in absolute terms, both on the monitor screen and on the line printer and also as a ratio to the

static wetted surface area. A sample plot of the data obtained using the program is shown in Fig. 55 in the form of a graph of the ratio of running wetted surface area to static wetted surface area (RWSA/SWSA) against Froude number for an NPL round bilge hull (Bailey, 1976). This graph, which was taken from the data given in Millward et al (2001), shows that the wetted surface area ratio increases steadily with increasing Froude number reaching a maximum which is 10% greater than the static wetted surface area at a Froude number of one (F_n=1.0). This shows that the actual wetted surface area of a fast displacement hull does vary significantly with speed, agreeing with the comment by Dinham-Peren (Insel and Molland, 1992) quoted earlier and indicates that any calculation of frictional resistance based on static wetted surface area may be substantially in error for these fast hulls, particularly at the higher speeds, with the consequence that any subsequent calculation of residuary resistance and hence full-scale ship resistance will also be in error.

It was noted that in some cases, such as the NPL round bilge hull series, only the transverse sections of the parent hull are given rather than the specific hull being tested which may have a different length/beam ratio (L/B) and also a different draught/length ratio (T/L). Alternatively the drawing of the hull lines may not be of a suitable size for the digitiser palette. An additional program has therefore been written recently to allow the digitised section data to be scaled with the option that the scaling need not be the same in the vertical and horizontal directions. This program is also written in QBasic and given in Appendix 5.

Appendix 2

Channel effects on wave resistance

Earlier work by the author was based on that of Kirsch (1966) to investigate the effect of shallow water. This in turn was based on the work of Michell (1898) for the theoretical wave resistance of a ship in deep water and that of Srettenski (1937) in shallow water. In addition Srettenski extended his work to include the effect of a restricted width as well as restricted depth so that it should therefore be possible to use these pieces of theory to calculate the correction to the wave resistance measured in the flume in order to obtain the effective wave resistance in an unbounded fluid and hence the total resistance using the techniques discussed earlier.

A3.1 Theoretical wave resistance in an unbounded liquid

The wave resistance for a hull of length L, beam B and draught T in an unbounded liquid has been obtained by Michell (1898) and is

$$R_w = \frac{4\rho g^2}{\pi U^2} \int_1^\infty [J^2 + I^2] \frac{\lambda^2 d\lambda}{(\lambda^2 - 1)^{\frac{1}{2}}} \qquad \text{(A3.1)}$$

where

$$I = \int_{L/2}^{-L/2} \int_0^T e^{\frac{-\lambda^2 gz}{U^2}} \cos\left(\frac{gx}{U^2}\lambda\right) \frac{\partial f(x,z)}{\partial x} \, dx \, dz$$

and

$$J = \int_{L/2}^{-L/2} \int_{0}^{T} e^{\frac{-\lambda^2 gz}{U^2}} \sin\left(\frac{gx}{U^2}\lambda\right) \frac{\partial f(x,z)}{\partial x}\, dx\, dz \ .$$

In the present case it is assumed that the vessel is directly in line with the flow and in addition that the hull is symmetrical about the midships section so that the expression for I is equal to zero.

It is convenient to use the following dimensionless variables

$$\xi = \frac{x}{L/2} \qquad \eta = \frac{f(x,z)}{B/2} \qquad \zeta = \frac{z}{T}$$

and

$$\gamma_0 = \frac{1}{2F_n^2} \qquad \theta = \frac{2T}{L}\frac{\gamma^2}{\gamma_0} \qquad \gamma = \gamma_0\lambda \ .$$

In this case the wave resistance for a symmetrical ship becomes

$$R_w = \frac{8}{\pi}\rho g \frac{B^2T^2}{L} \int_{\gamma_0}^{\infty} \frac{\left(\frac{\gamma}{\gamma_0}\right)^2}{\left[\left(\frac{\gamma}{\gamma_0}\right)^2 - 1\right]^{1/2}} J^2\, d\gamma \qquad \text{(A3.2)}$$

where

$$J = \int_{0}^{1} \int_{0}^{1} \frac{\partial \eta}{\partial \xi} e^{-\theta\zeta} \sin(\gamma\xi)\, d\xi\, d\zeta \ .$$

If the ship hull is represented by a simplified shape where one factor is a function of length only while the other is a function of draft only then

$$f(x,z) = g(x) \cdot h(z) \tag{A3.3}$$

For the present work the most appropriate mathematically defined hull was thought to be the Wigley hull which is

$$f(x,z) = \frac{B}{2}\left[1 - \left(\frac{x}{L/2}\right)^2\right]\left[1 - \left(\frac{z}{T}\right)^2\right] \tag{A3.4}$$

This hull has parabolic water-lines and in this case also has parabolic cross-sections so that it resembles the round bilge NPL 100A hulls, used in the experiments, as much as possible.

In terms of the dimensionless variables the hull shape is therefore

$$\eta(\xi,\zeta) = (1 - \xi^2)(1 - \zeta^2) \tag{A3.5}$$

and hence

$$\frac{\partial \eta}{\partial \xi} = -2\xi (1 - \zeta^2) . \tag{A3.6}$$

Thus the expression for J becomes

$$J = -\int_0^1 2\xi \sin\gamma\xi \, d\xi \int_0^1 (1 - \zeta^2) e^{-\theta\zeta} \, d\zeta . \tag{A3.7}$$

This can be treated as two separate integrals, that is

$$J_\xi = -\int_0^1 2\xi \sin\gamma\xi \, d\xi$$

which, after integration, becomes

$$J_\xi = \frac{2}{\gamma}\left[\cos\gamma - \frac{\sin\gamma}{\gamma}\right]$$

while

$$J_\zeta = \int_0^1 (1 - \zeta^2)\, e^{-\theta\zeta}\, d\zeta$$

becomes

$$J_\zeta = \left[\left(\frac{1}{\theta} - \frac{2}{\theta^3}\right) + 2e^{-\theta}\left(\frac{1}{\theta^2} + \frac{1}{\theta^3}\right)\right]$$

so

$$J = \frac{2}{\gamma\theta}\left[\cos\gamma - \frac{\sin\gamma}{\gamma}\right]\left[\left(1 - \frac{2}{\theta^2}\right) + 2e^{-\theta}\left(\frac{1}{\theta} + \frac{1}{\theta^2}\right)\right] \qquad \text{(A3.8)}$$

noting that

$$\theta = \frac{2T}{L}\,\frac{\gamma}{\gamma_0}\,.$$

The expression for the wave resistance in deep water R_w given in Eq. A3.2 can therefore be integrated numerically with appropriate care being taken with the singularity when $\gamma = \gamma_0$.

A3.2 Theoretical wave resistance in a channel

The wave resistance for a ship in a channel of width K and water depth H is given by Srettenski as

$$R_c = \frac{4\rho g}{K}\left[I_0^2 + J_0^2 + 2\sum_{n=1}^{\infty}\left(I_n^2 + J_n^2\right)\right] \qquad \text{(A3.9)}$$

where

$$I_n = \frac{\int_S \int \cosh[\gamma_n(H - z)]}{\left[\left(1 + \frac{4\pi^2 n^2}{K^2\gamma_n^2}\right)\cosh^2(\gamma_n H) - \frac{gH}{U^2}\right]^{1/2}} \cdot \cos\left(x\left[\frac{g\gamma_n}{U^2}\tanh(\gamma_n H)\right]^{1/2}\right) \frac{\partial f(x,z)}{\partial x}\, dx$$

and

$$J_n = \frac{\int_S \int \cosh[\gamma_n(H - z)]}{\left[\left(1 + \frac{4\pi^2 n^2}{K^2\gamma_n^2}\right)\cosh^2(\gamma_n H) - \frac{gH}{U^2}\right]^{1/2}} \cdot \sin\left(x\left[\frac{g\gamma_n}{U^2}\tanh(\gamma_n H)\right]^{1/2}\right) \frac{\partial f(x,z)}{\partial x}\, dx$$

The value of γ_n is obtained from the solution of the equation

$$\frac{1}{F_{nh}^2}\tanh(\gamma_n H) = \gamma_n H - \frac{4\pi^2 n^2 H}{K^2\gamma_n} \qquad \text{(A3.10)}$$

where F_{nh} is the depth Froude number based on the depth of water and is defined by

$$F_{nh} = \frac{U}{(gH)^{1/2}} . \qquad \text{(A3.11)}$$

It should be noted at this stage that the parameters γ and γ_n both have dimensions of *length*$^{-1}$ in the case of flow in a channel which is different from the parameters γ and γ_0 for an unbounded fluid where they are dimensionless.

Using the same substitutions as before the wave resistance for a ship in a channel becomes

$$R_c = \frac{4\rho g}{K}\left[J_0^2 + 2\sum_{n=1}^{\infty} J_n^2 \right] \qquad \text{(A3.12)}$$

where, if the ship is symmetrical about the midships section, then $I_n=0$ as before and noting that Eq. A3.12 is not valid at $F_{nh}=1$ and for $F_{nh}>1$ then $J_0=0$. The expression for J can be re-written as

$$J_n = \frac{BT \int_0^1 \int_0^1 \frac{\partial \eta}{\partial \xi} \cosh[\gamma_n(H - T\zeta)]}{\left[\left(1 + \frac{4\pi^2 n^2}{K^2 \gamma_n^2}\right)\cosh^2(\gamma_n H) - \frac{1}{F_{nh}^2}\right]^{1/2}} \cdot \sin\left(\frac{L}{2}\xi\left[\frac{\gamma_n}{F_n^2 L}\tanh(\gamma_n H)\right]^{1/2}\right) d\xi\, d\zeta$$

or

$$J_n = \frac{BT}{Q}\int_0^1\int_0^1 \cosh[\gamma_n(H-T\zeta)]\, \sin\left(\frac{L\xi}{2}\left[\frac{\gamma_n}{F_n^2 L}\tanh\gamma_n H\right]^{1/2}\right) \frac{\partial \eta}{\partial \xi}\, d\xi\, d\zeta$$

where

$$Q = \left[\left(1 + \left[\frac{2\pi n}{K\gamma_n}\right]^2\right)\cosh^2\gamma_n H - \frac{1}{F_{nh}^2}\right]^{1/2}$$

Substituting from Eq. A3.6 the expression for J_n becomes

$$J_n = -\frac{2BT}{Q}\int_0^1\int_0^1 \xi\, \sin\left(\frac{L\xi}{2}\left[\frac{\gamma_n}{F_n^2 L}\tanh\gamma_n H\right]^{1/2}\right) \cosh[\gamma_n(H-T\zeta)\,(1-\zeta^2)\, d\xi\, d\zeta$$

which again can be separated into two expressions that can be integrated individually.

Thus

$$J_\xi = \int_0^1 \xi \sin a\xi \, d\xi$$

which integrates to

$$J_\xi = \frac{\sin a}{a^2} - \frac{\cos a}{a}$$

where

$$a = \frac{L}{2}\left[\frac{\gamma_n}{F_n^2 L} \tanh \gamma_n H\right]^{1/2}$$

while

$$J_\zeta = \int_0^1 (1 - \zeta^2) \cosh\gamma_n(H-T) \, d\zeta$$

which can be integrated to become

$$J_\zeta = \frac{1}{\gamma_n T}\left(\sinh\gamma_n H + \frac{2}{\gamma_n T}\cosh\gamma_n(H-T) - \frac{4}{(\gamma_n T)^2} \sinh\left(\frac{\gamma_n T}{2}\right) \cosh\left(\frac{\gamma_n(2H-T)}{2}\right)\right)$$

The expression for the wave resistance of a Wigley hull in a channel becomes

$$R_c = \frac{16\rho g B^2 T^2}{KQ^2}\left[J_0 + 2\sum_{n=1}^{\infty} J_n^2\right] \qquad \text{(A3.13)}$$

where

$$Q = \left[\left(1 + \left[\frac{2\pi n}{K\gamma_n}\right]^2\right)\cosh^2\gamma_n H - \frac{1}{F_{nh}^2}\right]^{1/2}$$

and

$$J = \frac{1}{\gamma_n T}\left(\frac{\sin a}{a^2} - \frac{\cos a}{a}\right)$$
$$\cdot\left(\sinh\gamma_n H + \frac{2}{\gamma_n T}\cosh\gamma_n(H-T) - \frac{4}{(\gamma_n T)^2}\sinh\left(\frac{\gamma_n T}{2}\right)\cosh\left(\frac{\gamma_n(2H-T)}{2}\right)\right)$$

with

$$a = \frac{L}{2}\left[\frac{\gamma_n}{F_n^2 L}\tanh\gamma_n H\right]^{1/2} .$$

This too can be summed numerically to give the wave resistance in a channel.

Appendix 4

Time dependent measurements

The subroutines which are available are:

F1	Flatest	this collects test data in flat water (i.e. without the wave-maker in operation) for resistance, side force, pitch, heave and heel moment.
F2	Calibrate	calibrates all the transducers for the flat water tests.
F3	Dragtest	collects flat water, drag and side force data.
F4	Dragcal	calibrates the transducers for the Dragtest.
F5	Speed	gives the flume main dial settings to achieve the required water speed. (This program has since been modified to incorporate the new main dial and jet injection settings without the wave-maker in place but a new calibration would be required for the injection system with the wave-maker in place).
F6	Frequency	measures the encounter frequency from the wave-maker to make setting the frequency easier.
F7	Scaletest	scales model forces to full size using Froude scaling method (also done by Shiptest).
F8	Flatest2	runs a modified flat water test program.
F9	Wavetest	collects data for tests in waves and includes wave height, resistance, side force, pitch, heave and heeling moment.
F10	Wavecal	calibrates the transducers for the full wave tests.

A brief description of each program or subroutine is given below but each program also contains suitable prompts and comments such that it should be possible to use it without detailed knowledge.

Speed

This program calculates the settings needed for a particular water speed for the main motor and the jet injection system which are controlled from the main console. The program incorporates the latest calibration of the flume and the jet injection system without the wave-maker present but as yet there is no corresponding calibration with the wave-maker in place.

Frequency

This calculates the rotational frequency for the wave-maker using the theory described in Section 3.3.1. The wave-maker frequency is then measured using the toothed disk on the wave-maker and the computer's internal clock. A loop in the program allows the measurement to be repeated so that, with care, the wave-maker frequency can be set to within about 2% of the desired value.

Wavecal

This is the subroutine which controls the calibration procedure for tests in waves. The operator is prompted to apply specific forces and movements to the model and dynamometer. This program is run before each individual speed run is started to ensure that no calibrations have changed. The following list gives the order in which forces and movements are applied:

Model condition	Measurement	Program variable
Zero heel	wave zero	WZERO
	pitch zero	PZERO
	heave zero	HZERO
	moment zero	MZERO
	5° bow down	PCAL
	5° bow up	PCALL
	0mm heave	HCAL
	10mm heave	HCALL
	moment calibration	MCAL
Required heel angle	0 N resistance	DZERO
	0 N side force	SZERO
	4.905 N resistance	DCAL
	9.81 N side force	SCAL

Once these stationary calibration values have been taken the flume is run up to the required speed for the test and the calm water values of the forces and movements are taken - this is to enable the added resistance, side force and motions due to the wave motion to be deduced and minimises the effect of any transducer drift. This was particulary true for the tests on a sailing yacht for which these programs were developed since a special resistance cage had to be used. This occurred because it was found that the natural frequency of the dynamometer in its normal configuration was too close to the frequency of the waves generated. Further details can be found in Sutcliffe (1995).

The readings taken with the flume running are:

	wave height	WZRUN
	resistance	DZRUN
	side force	SZRUN
	pitch	PZRUN
	heave	HZRUN
	heel moment	MZRUN

Wavetest

This program performs the data collection for the experiments in waves. Initially it calculates the wave-maker frequency, measures the actual frequency and permits the operator to adjust the setting. The calibration readings are then read in from a data file created by the calibration subroutine. The operator is then asked to enter whether earth or body motion axes are being used, the total number of wave cycles to be taken, the heel angle, leeway angle, wave height and wave length. Once this preliminary stage has been completed a set of data is taken for the calm water condition.

With flume running	wave height	WRUN
	resistance	DRUN
	side force	SRUN
	pitch	PRUN
	heave	HRUN
	heeling moment	MRUN

The number of cycles for each test is set by the operator with the average for one cycle being calculated.

With flume running	average wave height	AVEW
& wave-maker operating	average resistance	AVED
	average side force	AVES
	average pitch	AVEP
	average heave	AVEH
	average heeling moment	AVEM

The added quantity over and above the calm water value is calculated from the following formulae

$$\text{Added resistance} = 4.9034 \frac{(\text{AVED} - \text{DRUN})}{(\text{DCAL} - \text{DZERO})}$$

$$\text{Added side force} = 9.8067 \frac{(\text{AVES} - \text{SRUN})}{(\text{SCAL} - \text{SZERO})}$$

$$\text{Added pitch} = -10 \frac{(\text{AVEP} - \text{PRUN})}{(\text{PCAL} - \text{PZERO})}$$

$$\text{Added heave} = -10 \frac{\text{AVEH} - \text{HRUN})}{(\text{HCAL} - \text{HZERO})}$$

The phase relationships are calculated by comparing the peak of the measured readings to the peak in the measured wave data. Finally the non-dimensional quantities required by the operator are output to the screen, line printer and both hard and floppy discs.

Appendix 5

Computer Programs

A5.1 Stud correction program

Program name: STUD.BAS
Copyright: A. Millward, 1975

```
1000 REM model data stud correction program
1010 REM Studs assumed to be 3mm dia, 2.5mm high
1020 REM Required: Model speed Um(J)
1030 REM Required: No. of studs NS
1040 REM Required: Length to studs (m) LS
1050 REM Required: Area forward of studs (m^2) AFS
1052 REM Required: Water density RHO
1054 REM Required: Water kinematic viscosity NU
1060 REM RMC is correction
1070 HT = 2.5 / 1000: REM Height of stud
1080 DIA = 3 / 1000: REM Diameter of stud
1090 UM = UM(J)
1100 DELTA = 5! * SQR(NU * LS / UM)
1110 HD = HT / DELTA
1120 IF DELTA > HT THEN 1150
1130 U2 = UM * SQR(1 - 263 * DELTA / (630 * HT))
1140 GOTO 1160
1150 U2 = UM * HD * SQR(4 / 3 - 8 * HD ^ 2 / 5 + 2 * HD ^ 3 / 3 + 4 * HD ^
4 /7 - HD ^ 5 / 2 + HD ^ 6 / 9)
1160 RNS = U2 * DIA / NU
1170 IF RNS > 7000 GOTO 1250
1180 IF RNS > 4000 GOTO 1230
1190 CDS = 1.5241 - .0010245 * RNS + 8.06371E-07 - 7 * RNS ^ 2
1200 CDS = CDS - 3.32586E-10 * RNS ^ 3 + 6.83306E-14 * RNS ^ 4
1210 CDS = CDS - 5.48449E-18 * RNS ^ 5
1220 GOTO 1260
1230 CDS = 1.024231 - RNS * 5.0083E-05 + RNS ^ 2 * 6.002665E-09
1240 GOTO 1260
1250 CDS = 1.2239 - RNS * .0000469 + RNS ^ 2 * 1.5E-09
1260 RST = .5 * RHO * DIA * HT * NS * U2 * U2 * CDS
1270 REM LAMINAR DEFICIT CALCULATION
1280 RLD = .5 * RHO * UM * UM * AFS * ((.075 / (LOG(LS * UM / NU) - 2) ^
2) - (1.328 / SQR(LS * UM / NU)))
1290 RMC = (RST - RLD)
1300 RETURN
```

A5.2 Data reduction and scaling program

Program name: SHIP.BAS
Copyright: A.Millward, 1998

```
10 CLS : REM General data reduction and scaling program for ship models
15 REM Program name SHIP.BAS
20 REM working from dynamometer readings.
30 DEF FNDEC (X, N%) = INT(X * 10 ^ N% + .5) / 10 ^ N%
40 RHOS = 1026.8: NUS = 1.1907E-06: REM Standard values for sea water
41 REM for density and kinematic viscosity at 15 deg C.
50 INPUT "Give date ", A$: LPRINT "Date  "; A$: LPRINT
55 INPUT "Model name or number "; MODEL$: LPRINT "Model name  ";  MODEL$
60 REM Model information: LPRINT "Model parameters"
70 PRINT : INPUT "Waterline length "; WL
80 INPUT "Static wetted surface area "; WSA
90 INPUT "Number of studs "; NS%
100 INPUT "Distance of studs behind bow (mm) "; LS: LS = LS / 1000
110 INPUT "Area forward of studs (sq mm) "; AFS: AFS = AFS / 1000000!
120 INPUT "Ship/model scale "; SCALE
130 LPRINT "Waterline length "; WL; " m"; "    Static WSA "; WSA; " sq.m";
      "   Ship/model scale "; SCALE
135 LPRINT "No. studs "; NS%; "  Length to studs (mm) "; LS * 1000;
      "  Area fwd of studs (sq.mm) "; AFS * 1000000!
136 LPRINT
145 REM **********************
150 REM Experimental data
160 PRINT : INPUT "Water temperature "; T
170 RHO = 1001.1 + 6.044414E-04 * T - 5.163289E-03 * T * T
180 NU = 1.6914E-06 - 4.43E-08 * T + 5E-10 * T * T
181 NU = NU - 7E-13 * T * T * T
185 LPRINT "Water temperature "; T; "   density "; FNDEC(RHO, 1);
      "   kinematic viscosity "; NU
186 LPRINT
190 INPUT "Side force data required (Y or N)"; ANS1$
195 INPUT "Trim data required (Y or N)"; ANS2$
200 REM Calibration readings
210 PRINT : PRINT "Calibration weight readings required in volts "
220 REM Assumes 1 kg weight for Drag; 2 kg weight for Sideforce
230 INPUT "Drag load reading "; DCAL
240 INPUT "Drag zero "; D0
242 LPRINT "Drag (1kg) reading "; DCAL; "v"; "   zero "; D0; "v"
245 IF ANS1$ = "n" OR ANS1$ = "N" THEN 265
250 INPUT "Side force load reading "; SFCAL
260 INPUT "Side force zero "; SF0
262 LPRINT "Side force (2kg) reading "; SFCAL; "v"; "   zero "; SF0; "v"
265 IF ANS2$ = "N" OR ANS2$ = "n" THEN 300
270 INPUT "Trim reading "; TRIMCAL
280 INPUT "Trim zero "; TRIM0
290 INPUT "Trim angle "; ANGLE
```

```
292 LPRINT "Trim reading "; TRIMCAL; "v"; "   zero "; TRIM0; "v";
      "   angle "; ANGLE; "deg"
293 INPUT "Trim zero (gimbal free) "; TRIMF0
294 LPRINT "Trim angle (gimbal free) "; TRIMF0; "v"
300 REM Run experimental data
305 PRINT "Run number may include letters etc."
310 INPUT "Run number "; NO$
320 INPUT "Dial reading "; DIAL
330 VM = DIAL / 164.83
331 REM PRINT VM
340 INPUT "Drag reading "; DM
345 IF ANS1$ = "N" OR ANS1$ = "n" THEN 355
350 INPUT "Side force reading "; SFM
355 IF ANS2$ = "N" OR ANS2$ = "n" THEN 370
360 INPUT "Trim reading "; TRIMM
370 RES = -((DM - D0) / (DCAL - D0)) * 9.8065
375 IF ANS1$ = "N" OR ANS1$ = "n" GOTO 385
380 SF = -((SFM - SF0) / (SFCAL - SF0)) * 9.8065 * 2
385 IF ANS2$ = "N" OR ANS2$ = "n" GOTO 400
390 TRIM = ((TRIMM - TRIMF0) / (TRIMCAL - TRIM0)) * ANGLE
400 IF NS% > 0 GOTO 1000
410 RESCORR = RES - RMC
415 REM PRINT RES, RMC, RESCORR, SF, TRIM
420 PRINT "Resistance="; FNDEC(RESCORR, 3); "  Side force="; FNDEC(SF,3);
      "  Trim="; FNDEC(TRIM, 3)
430 REM RESCORR is model resistance corrected for stud drag
440 REM Model scaling section
450 RNM = VM * WL / NU: REM Model Reynolds number
451 REM PRINT RNM
460 CFM = .075 / (.43429 * LOG(RNM) - 2) ^ 2: REM ITTC model friction value
470 FFM = CFM * .5 * RHO * VM * VM * WSA: REM Model friction resistance
480 FRM = RESCORR - FFM: REM Model residual resistance
485 CTM = RESCORR / (.5 * VM * VM * WSA * RHO): REM Model total resistance
coefficient
490 CRM = FRM / (.5 * RHO * VM * VM * WSA): REM Residual resistance
      coefficient
495 IF SCALE < 1.1 GOTO 600
500 FRS = FRM * SCALE ^ 3 * RHOS / RHO: REM Ship residual resistance
510 VS = VM * SQR(SCALE): REM Ship speed m/s
520 RNS = VS * WL * SCALE / NUS: REM Ship Reynolds number
521 REM PRINT RNS, VS
530 WSAS = WSA * SCALE * SCALE: REM Ship wetted surface area
540 CFS = .075 / (.43429 * LOG(RNS) - 2) ^ 2: REM Ship ITTC friction
      coefficient
550 FFS = CFS * .5 * RHOS * VS * VS * WSAS: REM Ship friction resistance
560 CTS = CRM + CFS: REM Ship total resistance coefficient
570 FTS = CTS * .5 * RHOS * VS * VS * WSAS: REM Ship total resistance
600 LPRINT : LPRINT "Run number "; NO$: LPRINT "Model values",
      "model speed m/s = "; FNDEC(VM, 2)
```

```
605 LPRINT "Input data drag "; DM; "v"; "   side force "; SFM; "v"; "   trim ";
      TRIMM; "v"
610 LPRINT "Resistance="; FNDEC(RESCORR, 3); "N";
      "  Side force="; FNDEC(SF, 3); "N"; "  Trim="; FNDEC(TRIM, 3); "deg"
620 LPRINT "Ct="; FNDEC(CTM, 6), "Cr="; FNDEC(CRM, 6), "Cf=";
      FNDEC(CFM, 6)
625 IF SCALE < 1.1 GOTO 660
630 LPRINT : LPRINT "Ship values", "Ship speed m/s ="; FNDEC(VS, 2)
640 LPRINT "Resistance="; FNDEC(FTS, 1); "  Side force="; FNDEC(SFS, 1)
650 LPRINT "Ct="; FNDEC(CTS, 6), "Cf="; FNDEC(CFS, 6)
660 LPRINT : PRINT : INPUT "Another run "; ANS3$
670 IF ANS3$ = "Y" OR ANS3$ = "y" GOTO 300
680 END

1000 REM Model stud correction sub-routine
1010 REM Studs are 3mm dia, 2.5mm high
1020 REM RMC is model correction
1070 HT = 2.5 / 1000: REM Height of stud
1080 DIA = 3 / 1000: REM Diameter of stud
1100 DELTA = 5 * SQR(NU * LS / VM)
1110 HD = HT / DELTA
1120 IF DELTA > HT THEN 1150
1130 U2 = VM * SQR(1 - 263 * DELTA / (630 * HT))
1140 GOTO 1160
1150 U2 = VM * HD * SQR(4 / 3 - 8 * HD ^ 2 / 5 + 2 * HD ^ 3 / 3
      + 4 * HD ^ 4 / 7 - HD ^ 5 / 2 + HD ^ 6 / 9)
1160 RNS = U2 * DIA / NU
1170 IF RNS > 7000 GOTO 1250
1180 IF RNS > 4000 GOTO 1230
1190 CDS = 1.5241 - RNS * .0010245 + 8.06371E-07 * RNS ^ 2
1200 CDS = CDS - 3.32586E-10 * RNS ^ 3 + 6.83306E-14 * RNS ^ 4
1210 CDS = CDS - 5.48449E-18 * RNS ^ 5
1220 GOTO 1260
1230 CDS = 1.0124231# - RNS * 5.0083E-05 + RNS ^ 2 * 6.002665E-09
1240 GOTO 1260
1250 CDS = 1.2239 - RNS * .0000469 + RNS ^ 2.15E-08
1260 RST = .5 * RHO * DIA * HT * NS% * U2 * U2 * CDS
1270 REM LAMINAR DEFICIT
1275 RLSTD = LS * VM / NU
1280 RLD = .5 * RHO * VM * VM * AFS * ((.075 / (.43429 * LOG(RLSTD) - 2) ^
2) - (1.328 / SQR(RLSTD)))
1290 RMC = RST - RLD
1300 GOTO 410
```

A5.3 Wetted surface area calculation program

Program name WSACALC.BAS
Copyright: N. Spencer, A. Millward, 1992

```
10 REM WSA CALCULATION
12 'This is a program to calculate the Running Wetted Surface Area of "
   'model under test in the flume.
   'It requires files containing digitised data describing the sections
   'of the model and their relative position along the model. The
   'program corrects the digitised data for angle and re-writes it
   'in a separate file. This manipulation need only be performed once
   'per hull. The program initially assumes the Datum Waterline to
   'obtain the Static WSA. The program requires running waterline
   'DATA either from the keyboard or from a data file created using
   'the program RWL.BAS
20 DIM PX(100): DIM PY(100): DIM PXT(100): DIM PYT(100): DIM PXN(100)
30 DIM PYN(100): DIM HEIGHT(20): DIM GL(20): DIM Z(100): DIM X(100, 1)
40 DIM Y(100, 1): DIM a(100, 100): DIM B(100): DIM C(100): DIM DX(100, 1)
50 DIM DY(100, 1): DIM TXT(100, 1): DIM TYT(100, 1): DIM TX(100, 1)
60 DIM TY(100, 1)
70 CLS
80 DIM NUM$(20)
85 REM NUM$ IS THE NUMBER OF STATIONS (MAXIMUM 20)
90 NUM$(1) = "1": NUM$(2) = "2": NUM$(3) = "3": NUM$(4) = "4": NUM$(5)
      ="5"
100 NUM$(6) ="6": NUM$(7) ="7": NUM$(8) ="8": NUM$(9) ="9":
      NUM$(10)="10"
110 NUM$(11) = "11": NUM$(12) = "12": NUM$(13) = "13": NUM$(14) = "14"
120 NUM$(15) = "15": NUM$(16) = "16": NUM$(17) = "17": NUM$(18) = "18"
130 NUM$(19) = "19": NUM$(20) = "20"
140 REM setup
141 count% = 0
142 PRINT "If using any data files obtained through SCALING.BAS answer N"
145 PRINT "Is this a new hull with a"
150 INPUT "new set of data points (Y/N) ?", a$
160 IF a$ = "n" OR a$ = "N" GOTO 650
180 INPUT "Give file name of digitised data, ", DNAME$
190 INPUT "Give file name for corrected (angles) data, ", ONAME$
200 PRINT
210 INPUT "Give total number of stations, ", STATS%
220 INPUT "Give number of digitised  points per station, ", N%
230 REM  Open file to contain zdist,pyn(3) and pyn(n)
240 REM  for use in graphics subroutine.
250 OPEN "sec.dat" FOR OUTPUT AS #4
260 FOR J% = 1 TO STATS%
270 OPEN DNAME$ + NUM$(J%) + ".dat" FOR INPUT AS #2
280 OPEN ONAME$ + NUM$(J%) + ".dat" FOR OUTPUT AS #3
290 PRINT
300 PRINT "Give the distance of station "; J%
```

```
310 INPUT "from the aft perpendicular (mm) ", ZDIST
330 PRINT
340 WRITE #3, N% - 2
350 WRITE #3, ZDIST
360 REM  Write zdist to "sec.dat".
370 WRITE #4, ZDIST
380 REM rotation procedure
390 FOR K% = 1 TO N%
400 INPUT #2, PX(K%), PY(K%)
410 NEXT K%
420 FOR K% = 1 TO N%
430 PXT(K%) = PX(K%) - PX(2)
440 PYT(K%) = PY(K%) - PY(2)
450 NEXT K%
460 THETA = ATN(PXT(1) / PYT(1))
470 LENGTHDY = SQR(PXT(1) ^ 2 + PYT(1) ^ 2)
480 FOR K% = 3 TO N%
490 THI = ATN(PXT(K%) / PYT(K%))
500 THIN = THI - THETA
510 LENGTH = SQR(PXT(K%) ^ 2 + PYT(K%) ^ 2)
520 PXN(K%) = LENGTH * SIN(THIN)
530 PYN(K%) = LENGTH * COS(THIN) - LENGTHDY
540 NEXT K%
550 FOR K% = 3 TO N%
560 PRINT #3, PXN(K%); ","; PYN(K%)
570 REM  Write only PYN(3) and PYN(N%) to "sec.dat".
580 IF K% = 3 THEN WRITE #4, PYN(3)
590 IF K% = N% THEN WRITE #4, PYN(N%)
600 NEXT K%
610 CLOSE #2, #3
620 NEXT J%
630 CLS
640 GOTO 680
650 CLS
660 INPUT "Give corrected data file name ? ", ONAME$
670 INPUT "Give number of stations ? ", STATS%
671 REM Option to allow user to input from data file for running waterline
672 PRINT "Press ENTER to input waterline data from keyboard or"
673 INPUT "press F key to use an input file "; ANS$
674 IF ANS$ <> "F" THEN GOTO 680
675 INPUT "Give filename containing running waterline data ", RWL$
676 OPEN RWL$ FOR INPUT AS #1
677 FOR J% = 1 TO STATS%
678  INPUT #1, M%, HEIGHT(J%): PRINT "Station ", J%; "waterline height ",
       HEIGHT(J%)
679 NEXT J%: CLOSE : PRINT
680 IF count% > 0 GOTO 690
681 PRINT "Datum waterline assumed here to calculate Static WSA"
682 FOR J% = 1 TO STATS%
684 HEIGHT(J%) = 0
```

```
686 NEXT J%
688 GOTO 720
690 FOR J% = 1 TO STATS%
692 PRINT "Station "; J%;
700 INPUT " running waterline height data (mm)? ", HEIGHT(J%)
710 NEXT J%
720 CLOSE
725 PRINT
730 INPUT "Total wetted length (mm)? ", TOTLEN
740 REM  GIVE USER OPTION TO CHECK MODEL LINES
750 CLS
760 INPUT "Check lines of model? (Y/N)", D$
770 IF D$ = "Y" OR D$ = "y" THEN GOSUB 3840
790 REM  Give user option to view graphics.
800 LOCATE 21, 1
805 IF count% < 1 GOTO 850
810 INPUT "Show running water line? (y/n)", a$
820 IF a$ = "Y" OR a$ = "y" GOTO 850
840 GOTO 860
850 GOSUB 2830
855 IF count% < 1 GOTO 890
860 INPUT "Continue with calculation of WSA? (y/n)", B$
870 IF B$ = "N" OR B$ = "n" THEN GOTO 1650
890 REM girth length calculation
900 REM on entry STATS and height()
910 REM  After graphics option  the wsa is computed.
920 PRINT "computing..."
930 OPEN ONAME$ + "1.dat" FOR INPUT AS #2
940 INPUT #2, N%
950 INPUT #2, Z
960 CLOSE
970 GOSUB 1690
980 FOR OOP% = 1 TO STATS%
990 GL(OOP%) = 0
1000 FILENAME$ = ONAME$ + NUM$(OOP%) + ".dat"
1010 OPEN FILENAME$ FOR INPUT AS #2
1020 INPUT #2, N%
1030 INPUT #2, Z(OOP%)
1040 INPUT #2, XOLD, YOLD
1050 CLOSE
1060 GOSUB 2250
1070 FOR Z% = 1 TO N% - 1
1080 FOR K% = 1 TO 10
1090 U = K% / 10
1100 GOSUB 2720
1110 DELTX = ABS(XPOS - XOLD)
1120 DELTY = ABS(YPOS - YOLD)
1130 LENGTH = SQR(DELTX ^ 2 + DELTY ^ 2)
1140 IF YPOS >= HEIGHT(OOP%) THEN LENGTH = 0
1150 GL(OOP%) = GL(OOP%) + LENGTH
```

```
1160 XOLD = XPOS
1170 YOLD = YPOS
1180 NEXT K%
1190 NEXT Z%
1200 NEXT OOP%
1210 OPEN "gltemp.dat" FOR OUTPUT AS #2
1220 PRINT #2, STATS% + 1
1230 PRINT #2, "0"
1240 FOR J% = 1 TO STATS%
1250 PRINT #2, Z(J%); ","; GL(J%)
1260 NEXT J%
1270 PRINT #2, TOTLEN; ", 0"
1280 CLOSE
1290 FILENAME$ = "gltemp.dat"
1300 REM Calculation of WSA
1310 GOSUB 1690
1320 GOSUB 2250
1330 WSA = 0
1340 OPEN FILENAME$ FOR INPUT AS #2
1350 INPUT #2, N%
1360 INPUT #2, Z%
1370 INPUT #2, XOLD, YOLD
1380 FOR Z% = 1 TO N% - 1
1390 FOR K% = 1 TO 100
1400 U = K% / 100
1410 GOSUB 2720
1420 DIFFX = ABS(XPOS - XOLD)
1430 DIFFY = ABS(YPOS - YOLD)
1440 IF YPOS > YOLD THEN HEIGHT = YOLD
1450 IF YPOS <= YOLD THEN HEIGHT = YPOS
1460 AREA = DIFFX * HEIGHT + .5 * DIFFX * DIFFY
1470 WSA = WSA + AREA
1480 XOLD = XPOS
1490 YOLD = YPOS
1500 NEXT K%
1510 NEXT Z%
1520 CLOSE
1530 PRINT "The total wetted surface area= ", WSA * 2
1532 IF count% > 0 GOTO 1540
1534 SWSA = WSA * 2
1540 PRINT
1550 LPRINT
1560 LPRINT "Data file name "; ONAME$
1570 LPRINT
1580 FOR J% = 1 TO STATS%
1590 LPRINT "station "; J%; "    Water height "; HEIGHT(J%)
1600 NEXT J%
1610 LPRINT
1620 LPRINT "Wetted length= "; TOTLEN
1630 LPRINT
```

```
1640 LPRINT "Total wetted area "; WSA * 2
1645 LPRINT "W = RWSA/SWSA"; WSA * 2 / SWSA
1650 INPUT "Further waterline data (y/n) ?", C$
1660 count% = count% + 1
1670 IF C$ = "Y" OR C$ = "y" OR C$ = "" GOTO 670
1680 STOP
1690 REM set up interpolation data
1700 REM create matrix a
1710 FOR I% = 1 TO N%
1720 FOR J% = 1 TO N%
1730 a(I%, J%) = 0
1740 NEXT J%
1750 NEXT I%
1760 a(1, 1) = 2
1770 a(1, 2) = 1
1780 a(N%, N% - 1) = 1
1790 a(N%, N%) = 2
1800 FOR I% = 2 TO N% - 1
1810 a(I%, I% - 1) = 1
1820 a(I%, I%) = 4
1830 a(I%, I% + 1) = 1
1840 NEXT I%
1850 REM invert matrix a
1860 REM inverse of a put in a
1870 NN% = N% - 1
1880 a(1, 1) = 1 / a(1, 1)
1890 FOR M% = 1 TO NN%
1900 K% = M% + 1
1910 FOR I% = 1 TO M%
1920 SUM = 0
1930 FOR J% = 1 TO M%
1940 SUM = SUM + a(I%, J%) * a(J%, K%)
1950 NEXT J%
1960 B(I%) = SUM
1970 NEXT I%
1980 D = 0
1990 FOR I% = 1 TO M%
2000 D = D + a(K%, I%) * B(I%)
2010 NEXT I%
2020 D = -D + a(K%, K%)
2030 a(K%, K%) = 1 / D
2040 FOR I% = 1 TO M%
2050 a(I%, K%) = -B(I%) * a(K%, K%)
2060 NEXT I%
2070 FOR J% = 1 TO M%
2080 SUM = 0
2090 FOR I% = 1 TO M%
2100 SUM = SUM + a(K%, I%) * a(I%, J%)
2110 NEXT I%
2120 C(J%) = SUM
```

```
2130 NEXT J%
2140 FOR J% = 1 TO M%
2150 a(K%, J%) = -C(J%) * a(K%, K%)
2160 NEXT J%
2170 FOR I% = 1 TO M%
2180 FOR J% = 1 TO M%
2190 a(I%, J%) = a(I%, J%) - B(I%) * a(K%, J%)
2200 NEXT J%
2210 NEXT I%
2220 NEXT M%
2230 CLOSE
2240 RETURN
2250 REM Matrix creation for interpolation
2260 OPEN FILENAME$ FOR INPUT AS #2
2270 INPUT #2, N%
2280 INPUT #2, ZVALUE
2290 FOR J% = 1 TO N%
2300 INPUT #2, a, B
2310 X(J%, 1) = a
2320 Y(J%, 1) = B
2330 NEXT J%
2340 REM create matrix dx
2350 FOR J% = 2 TO N% - 1
2360 DX(J%, 1) = X(J% + 1, 1) - X(J% - 1, 1)
2370 NEXT J%
2380 DX(1, 1) = X(2, 1) - X(1, 1)
2390 DX(N%, 1) = X(N%, 1) - X(N% - 1, 1)
2400 REM create matrix dy
2410 FOR J% = 2 TO N% - 1
2420 DY(J%, 1) = Y(J% + 1, 1) - Y(J% - 1, 1)
2430 NEXT J%
2440 DY(1, 1) = Y(2, 1) - Y(1, 1)
2450 DY(N%, 1) = Y(N%, 1) - Y(N% - 1, 1)
2460 REM create temp tx matrix
2470 FOR I% = 1 TO N%
2480 SUM = 0
2490 FOR K% = 1 TO N%
2500 SUM = SUM + a(I%, K%) * DX(K%, 1)
2510 NEXT K%
2520 TXT(I%, 1) = SUM
2530 NEXT I%
2540 REM create temp ty matrix
2550 FOR I% = 1 TO N%
2560 SUM = 0
2570 FOR K% = 1 TO N%
2580 SUM = SUM + a(I%, K%) * DY(K%, 1)
2590 NEXT K%
2600 TYT(I%, 1) = SUM
2610 NEXT I%
2620 REM create tx matrix
```

```
2630 FOR J% = 1 TO N%
2640 TX(J%, 1) = TXT(J%, 1) * 3
2650 NEXT J%
2660 REM create ty matrix
2670 FOR J% = 1 TO N%
2680 TY(J%, 1) = TYT(J%, 1) * 3
2690 NEXT J%
2700 CLOSE
2710 RETURN
2720 REM Interpolation subroutine
2730 REM Assume mats X,Y,TX,TY and variables u,z are set.
2740 REM Output xpos,ypos.
2750 XPOS = U ^ 3 * (2 * (X(Z%, 1) - X(Z% + 1, 1)) + TX(Z%, 1) + TX(Z% +
1,      1))
2760 XPOS = XPOS + U ^ 2 * (3 * (X(Z% + 1, 1) - X(Z%, 1)) - 2 * TX(Z%, 1) -
TX(Z% + 1, 1))
2770 XPOS = XPOS + U * TX(Z%, 1) + X(Z%, 1)
2780 YPOS = U ^ 3 * (2 * (Y(Z%, 1) - Y(Z% + 1, 1)) + TY(Z%, 1) + TY(Z% +
1,      1))
2790 YPOS = YPOS + U ^ 2 * (3 * (Y(Z% + 1, 1) - Y(Z%, 1)) - 2 * TY(Z%, 1) -
TY(Z% + 1, 1))
2800 YPOS = YPOS + U * TY(Z%, 1) + Y(Z%, 1)
2810 RETURN
2820 REM N.J.Spencer March 1992, modified A.Millward 1997
2830 REM Graphics subroutine to show running water line.
2840 REM Open "sec.dat" for creation of graphics.
2850 OPEN "SEC.DAT" FOR INPUT AS #2
2860 REM Open 2 files to contain co-ords for keel and deck.
2870 OPEN "keel.dat" FOR OUTPUT AS #3
2880 OPEN "deck.dat" FOR OUTPUT AS #4
2890 REM Open file to contain only station distances.
2900 OPEN "zdist.dat" FOR OUTPUT AS #1
2910 REM Setup screen.
2920 SCREEN 9
2930 COLOR , 1
2940 CLS
2950 REM Draw static water line.
2960 LINE (1, 175)-(640, 175), 3
2970 REM Scale factor eg 2 => model dimensions/2.
2980 SCALE = 2!
2990 REM Setup start point (A,B).
3000 a = 15
3010 B = 175
3020 REM Enter first loop to draw model sections.
3030 REM Co-ords for keel and deck lines are written to files #3 and #4
3040 FOR J% = 1 TO STATS%
3050 PSET (a, B)
3060 INPUT #2, ZDIST, NY, PY
3070 ZDIST = ZDIST / SCALE
3080 WRITE #1, ZDIST
```

```
3090 X = a + ZDIST
3100 IF NY >= 0 THEN 3120
3110 GOTO 3220
3120 NY = NY / SCALE
3130 PY = PY / SCALE
3140 Y = B - NY
3150 Z = PY - NY
3160 PSET (X, Y)
3170 WRITE #3, X, Y
3180 DRAW "u=" + VARPTR$(Z)
3190 Y = Y - Z
3200 WRITE #4, X, Y
3210 GOTO 3310
3220 PSET (X, B)
3230 NY = NY / SCALE
3240 PY = PY / SCALE
3250 DRAW "NU=" + VARPTR$(PY)
3260 DRAW "NU=" + VARPTR$(NY)
3270 Y = B - NY
3280 WRITE #3, X, Y
3290 Y = B - PY
3300 WRITE #4, X, Y
3310 NEXT J%
3320 CLOSE
3330 REM Section to draw keel line.
3340 OPEN "keel.dat" FOR INPUT AS #3
3350 INPUT #3, XK, YK
3360 PSET (XK, YK)
3370 FOR J% = 2 TO STATS%
3380 INPUT #3, NXK, NYK
3390 LINE -(NXK, NYK)
3400 NEXT J%
3410 CLOSE
3420 REM Section to draw deck line.
3430 OPEN "deck.dat" FOR INPUT AS #4
3440 INPUT #4, XD, YD
3450 PSET (XD, YD)
3460 FOR J% = 2 TO STATS%
3470 INPUT #4, NXD, NYD
3480 LINE -(NXD, NYD)
3490 NEXT J%
3500 CLOSE
3510 REM Section to mark rwl points and draw rwl.
3520 OPEN "zdist.dat" FOR INPUT AS #1
3530 INPUT #1, ZDIST
3540 PSET (a, B)
3550 X = a + ZDIST
3560 Y = B - (HEIGHT(1) / SCALE)
3570 CIRCLE (X, Y), 3, 14
3580 PSET (X, Y)
```

```
3590 FOR J% = 2 TO STATS%
3600 INPUT #1, ZDIST
3610 NX = a + ZDIST
3620 NY = B - (HEIGHT(J%) / SCALE)
3630 LINE -(NX, NY), 4
3640 CIRCLE (NX, NY), 3, 14
3650 NEXT J%
3660 CLOSE
3670 REM Screen titles.
3680 PRINT "                REPRESENTATION OF MODEL RUNNING WATER
     LINE"
3690 PRINT
3700 PRINT
3710 REM Print key to colours.
3720 PRINT "static water line"
3730 LINE (180, 50)-(250, 50), 3
3740 PRINT "running water line"
3750 LINE (180, 65)-(250, 65), 4
3760 PRINT
3770 GOTO 3830
3780 H = TIMER
3790 T = TIMER - H
3800 IF T > 3 GOTO 3830
3810 LINE -(RND * 640, RND * 350), RND * 9
3820 GOTO 3790
3830 RETURN
3840 REM  SUBROUTINE TO DRAW MODEL LINES
3850 REM SCREEN SETUP
3860 SCREEN 9
3870 COLOR , 1
3880 CLS
3890 REM DRAW STATIC WATER LINE AND CENTRE LINE
3900 LINE (1, 175)-(640, 175), 3
3910 LINE (320, 20)-(320, 330), 3
3920 REM SCREEN TITLES
3940 PRINT "                    LINES OF MODEL DESCRIBED BY FILE '";
     ONAME$; "'"
3950 LOCATE 3, 39
3960 PRINT "Centre"
3970 LOCATE 4, 40
3980 PRINT "Line"
3990 LOCATE 12, 72
4000 PRINT "Static"
4010 LOCATE 13, 70
4020 PRINT "Water Line"
4030 REM MAIN LOOP TO COUNT THRU' SECTIONS
4040 FOR L% = 1 TO STATS%
4050 OPEN ONAME$ + NUM$(L%) + ".DAT" FOR INPUT AS #2
4060 a = 320
4070 B = 175
```

```
4080 SCALE = 2
4090 INPUT #2, NM2, ZDIST
4100 INPUT #2, X1, Y1
4110 X = a + (SCALE * X1)
4120 IF L% > (STATS% / 2) THEN X = a - (SCALE * X1)
4130 Y = B - (SCALE * .74 * Y1)
4140 PSET (X, Y)
4150 REM LOOP TO COUNT THRU EACH FILE
4160 FOR K% = 2 TO NM2
4170 INPUT #2, X1, Y1
4180 X = a + (SCALE * X1)
4190 IF L% > (STATS% / 2) THEN X = a - (SCALE * X1)
4200 Y = B - (SCALE * .74 * Y1)
4210 LINE -(X, Y), 14
4220 NEXT K%
4230 CLOSE #2
4240 NEXT L%
4250 RETURN 790
```

A5.4 Hull cross-section scaling program

Program name: SCALING.BAS
Copyright: A.Millward, 1998

```
10 DIM PX(100): DIM PY(100): DIM PXT(100): DIM PYT(100)
20 DIM NUM$(20): DIM RXT(100): DIM RYT(100), PXN(100), PYN(100)
30 NUM$(1) = "1": NUM$(2) = "2": NUM$(3) = "3": NUM$(4) = "4": NUM$(5)
       ="5"
40 NUM$(6) = "6":NUM$(7) = "7":NUM$(8) = "8":NUM$(9) = "9":NUM$(10) =
       "10"
50 NUM$(11) = "11": NUM$(12) = "12": NUM$(13) = "13": NUM$(14) = "14":
60 NUM$(15) = "15": NUM$(16) = "16": NUM$(17) = "17": NUM$(18) = "18":
70 NUM$(19) = "19": NUM$(20) = "20"
80 INPUT "Input hull data file name, ", DNAME$
90 INPUT "Input output file name for scaled data, ", ONAME$
100 PRINT
110 INPUT "Input total number of stations, ", STATS%
120 INPUT "Input number of digitised points, ", N%
125 INPUT "Input scale factors for X and Y directions X,Y ", SX, SY
126 REM Open file to contain ZDIST, PYT(3) and PYT(N%)
127 REM for use with graphics routine in WSACALC
128 OPEN "SEC.DAT" FOR OUTPUT AS #4
130 FOR J% = 1 TO STATS%
140 OPEN DNAME$ + NUM$(J%) + ".dat" FOR INPUT AS #2
150 OPEN ONAME$ + NUM$(J%) + ".dat" FOR OUTPUT AS #3
160 PRINT
162 PRINT "Give the distance of station "; J%
164 INPUT "from the aft perpendicular (mm) "; ZDIST
170 FOR K% = 1 TO N%
180 INPUT #2, PX(K%), PY(K%)
190 NEXT K%
194 PRINT : WRITE #3, N% - 2
195 WRITE #3, ZDIST
196 REM Write ZDIST to "SEC.DAT"
197 WRITE #4, ZDIST
198 GOSUB 500
200 FOR K% = 3 TO N%
210 PXT(K%) = PXN(K%) * SX
220 PYT(K%) = PYN(K%) * SY
230 NEXT K%
240 FOR K% = 3 TO N%
250 PRINT #3, PXT(K%); ","; PYT(K%)
252 REM Write only PYT(3) and PYT(N%) to "SEC.DAT"
254 IF K% = 3 THEN WRITE #4, PYT(3)
256 IF K% = N% THEN WRITE #4, PYT(N%)
260 NEXT K%
270 CLOSE #3, #2
280 NEXT J%
```

```
290 PRINT "Data scaling completed"
300 INPUT "End program (y/n)? ", A$
310 IF A$ = "Y" OR A$ = "y" GOTO 400
330 INPUT "Rerun with new data file (y/n)? ", B$
340 IF B$ = "Y" OR B$ = "y" GOTO 10
400 END

500 REM SUBROUTINE TO ROTATE DATA
520 FOR K% = 1 TO N%
530 PXT(K%) = PX(K%) - PX(2)
540 PYT(K%) = PY(K%) - PY(2)
550 NEXT K%
560 THETA = ATN(PXT(1) / PYT(1))
570 LENGTHDY = SQR(PXT(1) ^ 2 + PYT(1) ^ 2)
580 FOR K% = 3 TO N%
590 THI = ATN(PXT(K%) / PYT(K%))
600 THIN = THI - THETA
610 LENGTH = SQR(PXT(K%) ^ 2 + PYT(K%) ^ 2)
620 PXN(K%) = LENGTH * SIN(THIN)
630 PYN(K%) = LENGTH * COS(THIN) - LENGTHDY
640 NEXT K%
650 RETURN 200
```

Appendix 6

Flume running procedure

This procedure is the routine that is to be followed in order to start and stop the flume in its open channel configuration - a slightly modified procedure is necessary when the flume is used with either of the two covers in position, particularly with the cavitation cover.

Please remember that the flume is both expensive and potentially dangerous if misused - once the flume is running, there are approximately 100 tonnes of water in motion.

IMPORTANT:- THE FLUME MAY ONLY BE RUN UNDER THE SUPERVISION OF AN APPROVED FLUME OPERATOR AS INDICATED IN THE SAFETY PROCEDURE (see Appendix 7).

1. STARTING - (IF IN DOUBT : ASK!!)

    1. Check that all loose items (tools etc.) are removed from near the working section.
    2. Ensure that the test model and associated equipment are securely fastened in place.
    3. Make sure that the red 'STOP' switch (PB2) on control panel is pressed down.
    4. Switch on all four switches (S1 - S4) at Supply Cabinet (near laboratory door) starting with the Incoming Supply (S1).
    5. **Only to be attempted directly by an Approved Flume Operator**. Engage starter switch (S5) for the Ward-Leonard set; this is done by pressing the handle firmly and quickly up. If it does not stay in the 'ON' position let the handle go and allow the Ward-Leonard set to stop before trying again. It is, however, easy to damage the switch contact by misuse - it is not acceptable to start the Ward-Leonard set without prior instruction. The red light (SL1) on control panel labelled 'M.G. Set On' will now glow.
    6. Insert the appropriate keys in switches on the Main and Auxiliary Control Panels.

7. Check that contraction is full of water as shown on the sight glass. If not, the Vacuum Pump must be started. Turn on the cooling water (V1) for the vacuum pump in the flume basement. Turn the key switch on Auxiliary Control Panel - orange warning light SL3 will now glow to show that all controls are live. Switch on the Vacuum Pump on the panel and open valve (V2) in the vacuum pipe-line from the contraction. Note that, except under reduce pressure conditions in the working section, valve V6 should be left open since valve V2 is adequate. When the contraction is full, shut the pipe-line valve (V2), quickly switch off the Vacuum Pump and the key switch. Finally turn off the cooling water.
8. Check the level of water in the working section of the flume - the bottom of the meniscus should be level with the top of the tape on the working section windows. If water needs to be added, turn on supply valve (V3). To remove water, open valve V4.
9. Check the setting of the floor that it is in a sensible position and check that both the digital counters on the floor jacking motors and the electronic counters mounted on the console have the same reading (within one digit). For normal running there should be a slight slope on the floor with the upstream end higher than the downstream end to compensate for the growth of the boundary layer on the floor along the working section when the flume is running. Check and record the position of the floor - a difference of 260 units is normal between the front and back floor counter readings for most speeds, however the floor should be adjusted if necessary to suit each speed using the buttons on the Auxiliary Control Panel.
10. Release STOP switch and make sure that 'Speed Setting' control is zero.
11. Switch on main motor by turning 'Start' key (PB1) on Control Panel; red light (SL2) on panel labelled 'Flume Running' will glow. If the light SL2 does not come on then check all emergency stop switches to make sure that they have been reset; note that in addition to the switch on the console and the four near the working section there are a further two in the basement.

12. Slowly increase water speed to required setting by turning 'Speed Setting' control - see separate calibration curves.

13. Check that surface injection system is on - the green light will glow on the Injection System Panel and adjust jet setting on main control panel to give optimum velocity distribution using calibration curves.
Note that if the flume has not been used for some time or the working section has recently been emptied, it may be necessary to bleed the injection system by opening the tap on the injection box while the flume is running at about 1.5 m/s (4 ft/sec).

2. STOPPING: NORMAL RUNNING

1. Slowly decrease water speed to zero by turning 'Speed Setting' control - too rapid a decrease in speed will cause large waves in the working section which may damage or swamp the model.
2. Press 'Stop' button on Control Panel (PB2).
3. Remove keys from Main and Auxiliary Control Panels.
4. Press 'Stop' button on Ward-Leonard set switch gear.
5. Turn off switches (S1 - S4) on Supply Panel starting with Incoming Supply (S1).

3. STOPPING - EMERGENCY ONLY

1. Press 'Stop' button on Control Panel or any stop button adjacent to working section or in the basement.
2. Continue as for normal stopping from instruction 3.

N.B. Emergency Stop creates large waves in the working section which will almost certainly damage a model or equipment - this procedure must therefore only be used for genuine emergency situations.

Appendix 7

Flume - Standard Safety Procedures

General

The following set of standard safety rules apply to all use of the flume, and are in addition to the requirements laid down in the Departmental Code of Practice on Safety.

In addition to the above, for every specific project a risk assessment must be carried out, and a written record made, for all work where there is a significant hazard not covered by these standard procedures.

Procedures

1: At the entrance to the flume from the Hydraulics Laboratory, there are hazard lights. When these lights are flashing, do not pass beneath them, since they indicate that the overhead crane is in use.

2: The overhead crane may only be operated by someone trained and declared competent in its use.

3: Before commencing operation of the flume, all equipment and models in the vicinity of the working section must be made secure, and a check made that there are no loose items on the edges of the working section that may fall, or get knocked, into the flume.

4: The start up procedure for the flume must only be undertaken by an appointed Flume Operator.

The only appointed Flume Operators are Dr A. Millward and Mr W. Lanceley.

5: When the flume is running in the open channel configuration, a safety harness must be worn by anyone climbing on to the flume, or being in any other position from which they could fall into the flume.

Note that if the emergency stop button is pushed, the water continues to circulate for several minutes.

6: A Flume Operator must normally be present in the laboratory when the flume is running.

If it is necessary for the flume operator to leave the flume while it is running, no adjustments must be carried out to the flume nor to equipment on or in the flume until the flume operator returns.

If the flume operator has to leave the flume running while no one else is in the area, the flume must be left running at a safe speed, and in an otherwise safe condition, and the door to the flume laboratory closed and locked until the flume operator returns.

7: In the situation when more than one flume operator is in the area, they must establish a clear understanding of who is in control of the flume. The person in control must not subsequently leave the area with the flume running without first obtaining confirmation from the other operator that control of the flume has been taken over by the latter.

8: Entry to the working section when the flume is empty or part full must not be made unless another person is in constant attendance.

9: All instrumentation and other electrical equipment used in the area of the working section must be protected by an earth leakage circuit breaker.

AM/3 December 1996

Appendix 8

Cavitation cover installation

Before the cavitation cover can be moved into place on the working section, a rubber seal needs to be put in place around the top face of the working section. This provides the seal between the top face of the working section and the bottom face of the cavitation cover and is held in position by brass strips which are screwed on to the face of the flange around the working section. As a start therefore, any sections of brass strip which have been removed to allow the main dynamometer to be positioned on the working section, have to be put back in place. The next stage is to move the cavitation cover into place over the working section using the electric crane. This needs to be done cautiously since the cover weighs two tonnes and is suspended on the lifting chains. It is therefore wise to use the *slow* buttons on the crane control panel both for lifting and also for moving. The rubber seal needs to be held in position for the last stage of lowering the cover since it has a tendency to ride up over the brass restraining strip. It has been found necessary to have a number of people present for this last stage of lowering - usually one to operate the crane and four to keep the rubber seal in place, one at each corner. Four hooks, made from brass sheet, are used to hold the rubber seal in place against its tendency to ride up over the brass strip while allowing the people assisting to keep hands and fingers well away from the cover. The cover is then lowered gently down until it is just touching the rubber seal enough to hold the seal in place but still without its total weight on the seal, this allows the hooks to be withdrawn.

Before the vacuum pumps can be started to reduce the pressure in the working section, a number of minor checks and adjustments have to be made to reduce the possibility of air leaks into the flume. These are

1. the second valve V5 on the vacuum line from the top of the contraction must be closed. This valve is normally left open and the simpler gate valve V2 used to close off the pipe-line to the small vacuum pump in the basement. However it was found that, under vacuum conditions in the working section, the gate valve V2 was difficult to seal completely so the extra valve V5 was installed.
2. The pipe connecting the air chamber at the end of the diffuser on the return part of the circuit in the basement to the settling chamber at the end of the working

section has a T-junction and valve. This valve is used to release the air back into the working section after cavitation tests but must be closed before the vacuum pump can be started.

3. The lids on the top of the settling chamber at the downstream end of the working section are removable in order to be able to check on and clean the gauzes in the settling chamber. They also rest on rubber seals and are held in position by bolts inserted through their flanges. These bolts are normally left slack but must be tightened down in order to provide an initial seal. It is important to slacken these bolts off again at the end of testing otherwise the rubber seals will be kept under compression and will slowly deform.
4. Four bolts are inserted in the flanges around the cavitation cover on the working section and tightened down to provide an initial seal while the vacuum pump reduces the pressure inside the working section. Once the pressure is reduced these bolts can be slackened so that they do not come under too much tension at the end of the test when the pressure is released.

The vacuum pump can now be started with care being taken to make sure that the cooling water supply is adequate.

Appendix 9

Replacement of propeller shaft bearings

As described in Chapter 3 the water in the flume is circulated by a four bladed marine propeller, made of bronze, which is mounted in the lower part of the circuit as shown in Fig. 2. The cross-section at this point is circular and the clearance between the tips of the propeller blades and the wall of the flume is approximately 1mm. It is because of this small clearance that great emphasis is put in the Starting Procedure (Appendix 6) and the Safety Procedures (Appendix 7) on making sure that all loose items of equipment and tools are cleared from around the working section before starting the flume up. It is evident that if any object were to be carried down from the working section and become jammed between the propeller blade and the wall of the flume the damage to both the structure and the drive mechanism could be enormous.

As shown in Fig. 2 the propeller is driven from a 75 kW DC motor which is in turn driven from a Ward-Leonard motor generator set contained in a cell at the end of the laboratory. The DC motor drives the main propeller shaft through a "step-down" pulley system using a square toothed flexible belt. This drive system, coupled with the feed-back control mechanism, has been shown over the years to give a very reliable, steady and accurate speed control. The main shaft, which carries the large pulley wheel at one end and the propeller at the other end, protrudes through the end of the flume in the lower part of the circuit as shown in Fig. 2. The shaft, which is made of stainless steel, has two bearings - one at the end wall of the flume and the other just behind the propeller where it is supported by stream-lined struts from the outer skin at that point. The bearing behind the propeller is a simple journal bearing, made of Tufnol or similar material. The other bearing is more complex as can be deduced from the diagram in Fig. 2 since it has to absorb the thrust from the propeller. In addition, when the flume is operated as a free surface channel or water tunnel, with atmospheric pressure in the working section, there is a static head of water of approximately 3m at that point attempting to push water out past the shaft. However, if the flume is operated as a cavitation tunnel or cavitation channel where the pressure in the working section can be reduced to 0.03 atmospheres, then the static pressure at the bearing can be below atmospheric pressure and the air is likely to be attempting to leak into the flume past the

shaft. Thus this bearing consists of a stainless steel roller bearing with a double seal system.

Each of these two bearings on the propeller shaft may need replacement and a brief description of the method employed is given below.

1 **Thrust Bearing**

The main thrust bearing, consisting of a stainless steel roller bearing and four sealing rings is contained in a special sub-assembly which can be extracted from outside the flume without removing the propeller or the shaft using the following procedure:

1 Open the main drain valve at the bottom of the return circuit and allow all the water to drain away.

2 Turn off the main electricity supply (Switch S1) and remove the fuses so that the motor cannot be started accidentally.

3 Loosen the bolts holding down the DC motor and move it towards the shaft in order to slacken the drive belt.

4 Remove the safety cover over the pulley wheels and drive belt and slide the slackened drive belt sideways off the pulley wheels.

5 Support the large pulley wheel with a sling attached to the special bracket above it which is welded to the support flanges of the flume. Using the special two jawed hub-extractor carefully pull the large pulley wheel off the shaft and move it to one side.

6 Drain the oil out of the oil bath and remove the Perspex cover. Attach a different extractor tool which will pull the whole bearing assembly along the propeller shaft until it is free and can be slid off the shaft for dis-assembly.

7 The bearing assembly can now be taken apart and the seals or roller bearing replaced as appropriate. The appropriate identification numbers can be found on the official drawing.

8 The bearing assembly is then replaced back on the propeller shaft and carefully pushed back along the shaft into position using

9 The oil bath cover can be replaced and the oil bath filled.

10 The large pulley is moved back into place and pushed onto the shaft, the drive belt slid onto the two pulley wheels and the motor slid back along its guides and bolted down. Some minor adjustments may need to be made to the alignment of

the motor in order to get the drive belt tension correct and running true. Although no tension figure is known the drive belt should not be allowed to be slack when the motor is not running since at high speeds the belt may slacken further from centrifugal effects.

11 The safety cover should be replaced over the drive belt, the flume refilled with water and the fuses replaced in the electrical supply.

2 Propeller Bearing

The propeller bearing consists of a Tufnol (or similar material) journal bearing which is lubricated by the water in the flume. It is important therefore that the motor should never be used to rotate the propeller shaft when the flume is empty. Any checks on the propeller bearing should be made by rotating the shaft by hand from within the flume itself. In order to replace this bearing it is necessary to remove the propeller and the propeller shaft using the following procedure:

1 Open the main drain valve at the bottom of the return circuit and allow all the water to drain away.

2 Turn off the main electricity supply (Switch S1) and remove the fuses so that the motor cannot be started accidentally.

3 Loosen the bolts holding down the DC motor and move it towards the shaft in order to slacken the drive belt.

4 Remove the safety cover over the pulley wheels and drive belt and slide the slackened drive belt side ways off the pulley wheels.

5 Support the large pulley wheel with a sling attached to the special bracket above it which is welded to the support flanges of the flume. Using the special two jawed hub-extractor carefully pull the large pulley wheel off the shaft and move it to one side.

6 Drain the oil out of the oil bath and remove the Perspex cover. Attach a different extractor tool which will pull the whole bearing assembly along the propeller shaft until it is free and can be slid off the shaft for dis-assembly.

7 Remove the hatch on the side of the lower section of the flume in order to gain access to the propeller.

8 Take into the flume the special trolley which is needed to remove and support the propeller when it is off the shaft but assemble it inside the flume. The propeller trolley is normally kept in the basement around the back of the flume.

9 Remove the spinner from the propeller and attach the trolley making sure that the trolley is securely wedged so that it will not accidentally roll down the diffuser.

10 Use the extractor to pull the propeller off the shaft so that it is supported on the trolley and then move the trolley and propeller back down the diffuser so that access can be gained to the bearing and supports. This part requires two people at least to avoid the risk of the propeller and trolley running away on the slope.

11 Withdraw the propeller shaft out through the flume wall noting that it will pass out through the special hole made in the basement wall and into the main part of the laboratory.

12 Disassemble the journal bearing assembly and replace the bearing itself.

13 Re-assembly of the whole drive system is the reverse procedure, making sure that the drive belt is running centrally on the pulleys.

Appendix 10

MECHANICAL PROPERTIES OF WATER

The mechanical properties of fresh and salt water are given in the following tables in S.I. units. The tabulated values are taken from Saunders (1957).

1. KINEMATIC VISCOSITY IN S.I. UNITS

Temperature °C	Fresh Water x $10^{-6}m^2/s$	Salt Water x $10^{-6}m^2/s$	Temperature °C	Fresh Water x $10^{-6}m^2/s$	Salt Water x $10^{-6}m^2/s$
15.00	1.1413	1.1907	20.56	0.9933	1.0432
15.56	1.1250	1.1744	21.11	0.9803	1.0301
16.11	1.1090	1.1585	21.67	0.9675	1.0174
16.67	1.0934	1.1430	22.22	0.9549	1.0048
17.22	1.0781	1.1277	22.78	0.9427	0.9926
17.88	1.0632	1.1129	23.33	0.9307	0.9805
18.33	1.0486	1.0983	23.89	0.9190	0.9687
18.89	1.0343	1.0841	24.44	0.9075	0.9572
19.44	1.0204	1.0701	25.00	0.9862	0.9458
20.00	1.0067	1.0565			

The salinity of the salt water is 3.5%

A convenient interpolation formula for the kinematic viscosity of fresh water for use on a computer is:-

$$\nu = 1.6914 \times 10^{-6} - 0.0443 \times 10^{-6} \times T + 5.0 \times 10^{-10} \times T^2 - 7.0 \times 10^{-10} \times T^3$$

2. DENSITY IN S.I. UNITS

Temperature °C	Fresh Water Kg/m³	Salt Water Kg/m³	Temperature °C	Fresh Water Kg/m³	Salt Water Kg/m³
10.00	1000.6	1027.8	17.78	999.5	1026.2
11.11	1000.5	1027.6	18.89	999.2	1025.9
12.22	1000.3	1027.4	20.00	999.0	1025.6
13.33	1000.2	1027.2	21.11	998.8	1025.3
14.44	1000.0	1027.0	22.22	998.6	1025.0
15.00	999.9	1026.8	23.33	998.2	1024.7
15.56	999.9	1026.7	24.44	998.0	1024.3
16.67	999.7	1026.4	25.56	997.7	1024.0

The salinity of the salt water is 3.5%

A convenient interpolation formula for the density of fresh water for use on a computer is:-

$$\rho = 1001.1 + 6.044414 \times 10^{-4} \times T - 5.163289 \times 10^{-3} \times T^2$$

Note:

The need for adopting a single reference temperature for comparing the results of model tests and for predictions of ship performance has led to the adoption of an international or ITTC standard which is 59°F, 15°C. This is a reasonable engineering average for the waters of the world although somewhat low for water in the flume in general which averages about 68°F, 20°C.

Appendix 11

The T.E.M. "Technical College Balance"

The T.E.M. "Technical College Balance" is a parallel motion type of balance, designed to be used in wind tunnel tests to measure lift and drag forces and also the pitching moments acting on a model. The balance is supplied in either undertunnel or overhead form to suit any particular installation, the principles of either type are identical - the one bought for use with the flume is the overhead model.

This appendix, which is taken almost directly from the technical note supplied with the balance, outlines the basic principles of the balance which is shown in a schematic diagram in Fig. 41. The balance comprises a rigid earth frame to which a pair of horizontal cross beams are attached. The cross beams are normal to the flow direction and free to rotate through small angles by means of flexures; rotation is limited by the cross flexure hinges which link the earth frame and the beams. The cross beams move relative to each other as they are linked by the coupled arms which face inward from the cross beams, meeting at the centre line of the balance, linked by a single strip flexure. The force frame, carrying the mounting fixture for the model, is suspended from the cross beams by four vertical tie rods with strip flexures at each end. The lift weighbeam is mounted on one of the cross beams and linked to the earth frame by a lever. The drag weighbeam mounted on the earth frame, is linked to the force frame by a flexible horizontal tie. The pitching moment weighbeam is pivoted on the force frame and coupled to the model by a variable incidence linkage. Adjustable counterbalance weights are incorporated into each of the weighbeam mechanisms.

The Lift Measuring Mechanism

The lift measuring system consists of the force frame, the vertical ties, the cross beams, the coupled beams, the balance weights mounted on the coupled beams and the lift weighbeam.

The lift weighbeam is initially set at zero, that is in horizontal balance, by sliding the counterbalance weights on the coupled beams. An accurate spirit level mounted on the lift weighbeam indicates the point of horizontal balance. During testing the lift force acting on the model is transferred through the mounting fixture/bracket attached to the force frame, via the vertical ties to the coupled beams on each of the cross beams. The coupled beams will rotate out of balance in proportion to the force being exerted by the model and supports. By sliding the moveable balance weight along the weighbeam scale, until the coupled beams return to horizontal balance, the lift force acing on the model can be determined by reading the displacement of the weight on the weighbeam scale. Each division on the scale is calibrated to measure the lift force:

1 division on the lift scale = 2.45N lift

Total 40 units represents a maximum of 98N measurable lift.

The movement of the force frame by the lift force acting on the model causes a slight interference on the drag reading, calibrated by the manufacturer at 0.069N drag for 89N lift.

The moveable counterbalance weights on the coupled arms are initially used to balance the combined weight of the force frame, mounting fixture and the model. It is therefore practicable to balance the system so that the full range of the lift weighbeam can be used in tests.

The Drag Measuring System

The drag measuring system comprises the force frame, the vertical ties, the mounting fixture, the flexible link and the drag weighbeam.

The drag force acting on the model is transmitted through the mounting fixture to the force frame, which is free to move horizontally as it is linked by the strip flexures at each end of the vertical ties. The drag force acting on the model is translated into a horizontal movement of the force frame which acts on the weighbeam through the vertical link, moving the weighbeam out of balance. Equilibrium is restored by moving the balance weight along the drag weighbeam until the spirit level indicates that horizontal balance is restored. The drag force acting on the model can then be determined by reading the displacement of the moveable weight along the scale:

1 division of the drag weighbeam scale = 0.932N drag.

Total 40 divisions represent the maximum 38.26N measurable drag.

The displacement of the force frame, though substantially horizontal, will cause a degree of interference on the lift measuring system, calibrated by the manufacturer at 0.137N lift for 35N drag.

The drag linkage has an adjustable weight fitted to counterbalance the combined weight of the support fixture and the model acting on the force frame. It is practical to adjust this counterbalance weight so that the full range of the drag weighbeam can be utilised in tests.

The Pitching Moment Mechanism

The pitching moment system comprises the force frame, the support fixture, the tail support fixture, the variable incidence mechanism, the pitching moment weighbeam and the counterbalance weight.

The entire system is mounted on the force frame; the tail support fixture is attached to an arm projecting from the variable incidence mechanism, parallel to a line between the pivot of the mounting fixture and the tail support strut, forming a parallelogram of forces. Any alteration of the angle of incidence of the model will not affect the pitching moment mechanism, which will remain as a parallelogram at all angles of incidence. The moment acts through the support fixture at the model pivot and is measured as a load acting on the tail support fixture. The moment acting on the model is transferred through the moment weighbeam, rotating it from the horizontal balanced position. By adjusting the moveable weight along the weighbeam scale until balance is restored, it is possible to determine the pitching moment acting on the model. The balance is established using the sensitive spirit level mounted on the weighbeam.

1 division of the pitching moment scale = 0.048 N.m.

Total 40 divisions represent 1.86 N.m maximum measurable pitching moment.

Since the moment system is mounted on the force frame, the pitching moment acting on the model does not cause interference on the lift and drag systems. A counterbalance weight is fitted to the pitching moment system to compensate for any initial pitching moment acting on the system, this allows the full range of the weighbeam scale to be utilised during tests.

Setting Up The T.E.M. Balance

It is important to note that the balance must be set up correctly for maximum accuracy. The spring flexures will ensure repeatability, but care should be taken in initially setting the earth frame perfectly horizontal in the operating area. Horizontal balance is achieved by four adjustable screws and two spirit levels are fitted to indicate level. Excessive friction in the balance systems is detected through 'stickiness' of the moment system and poor repeatability of zero setting on the pitching moment weighbeam scale.

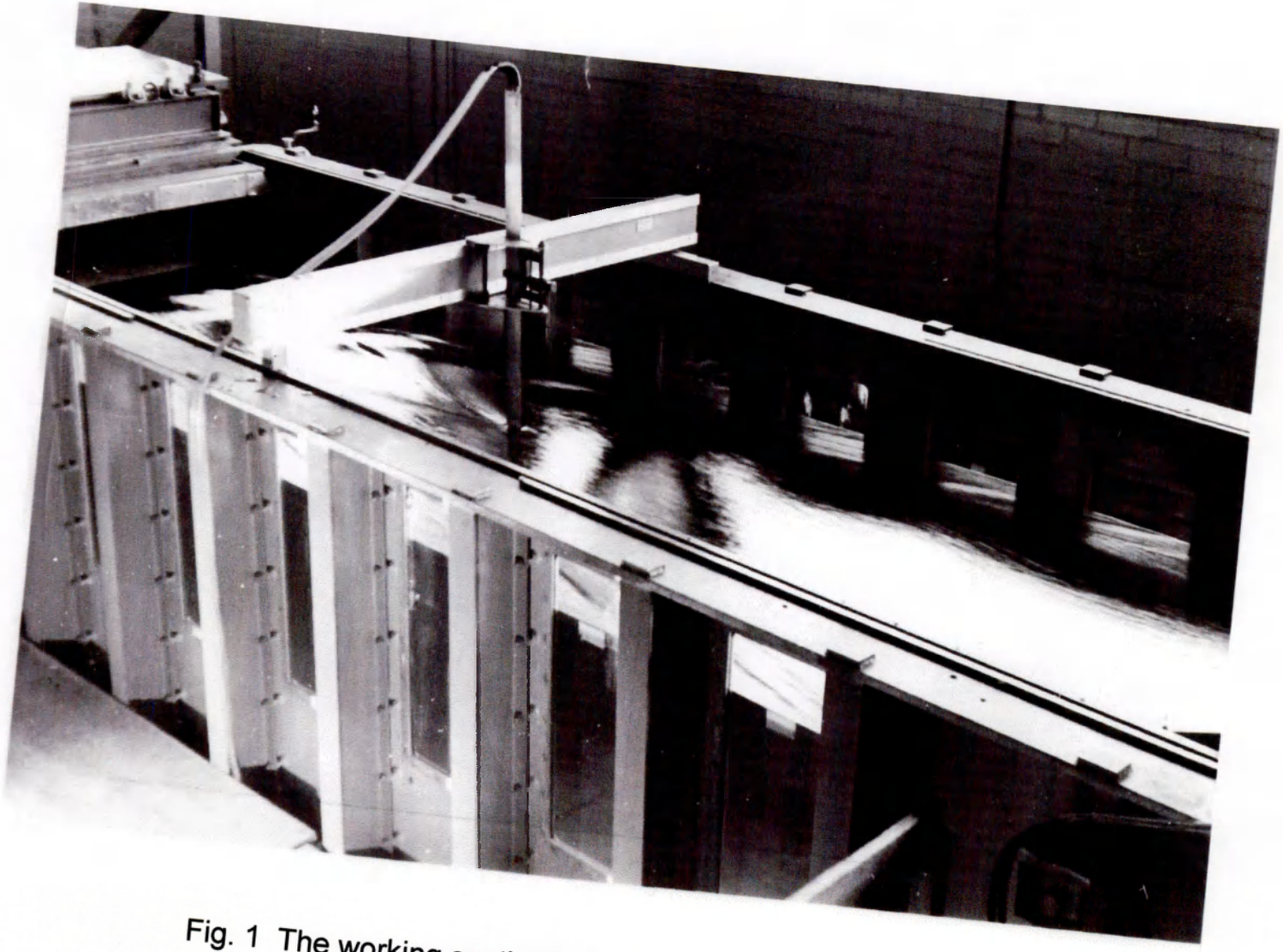

Fig. 1 The working section in the open channel configuration

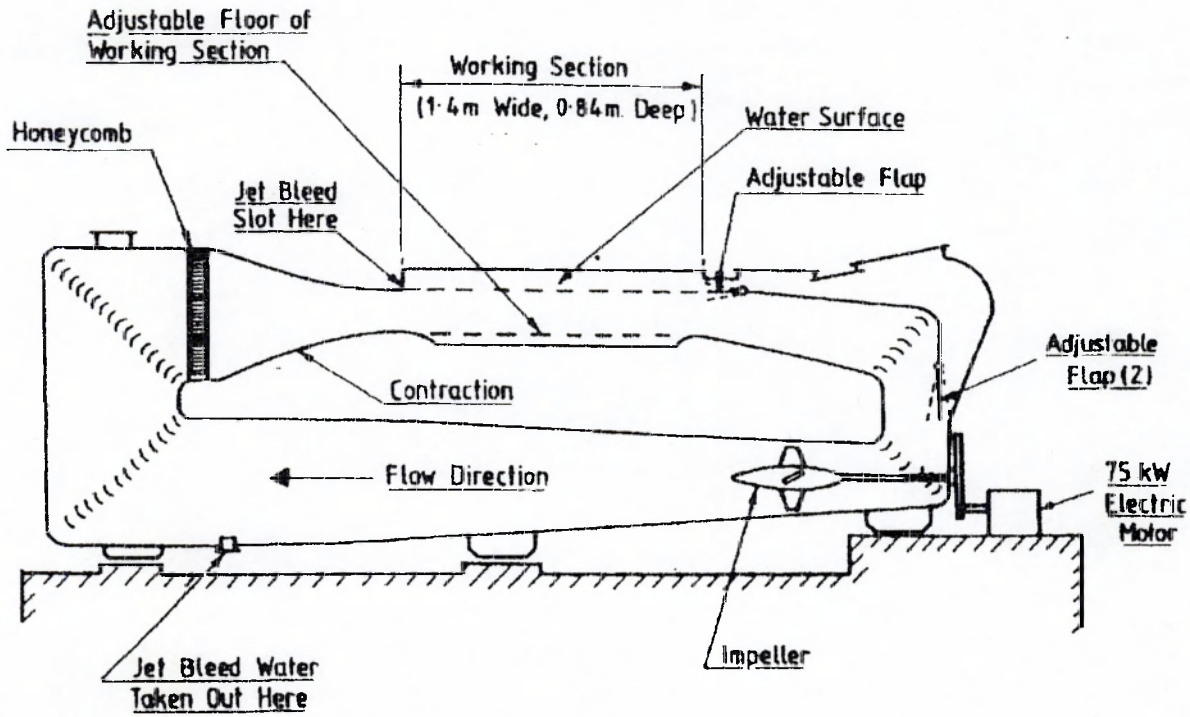

Fig. 2 A schematic diagram of the water channel

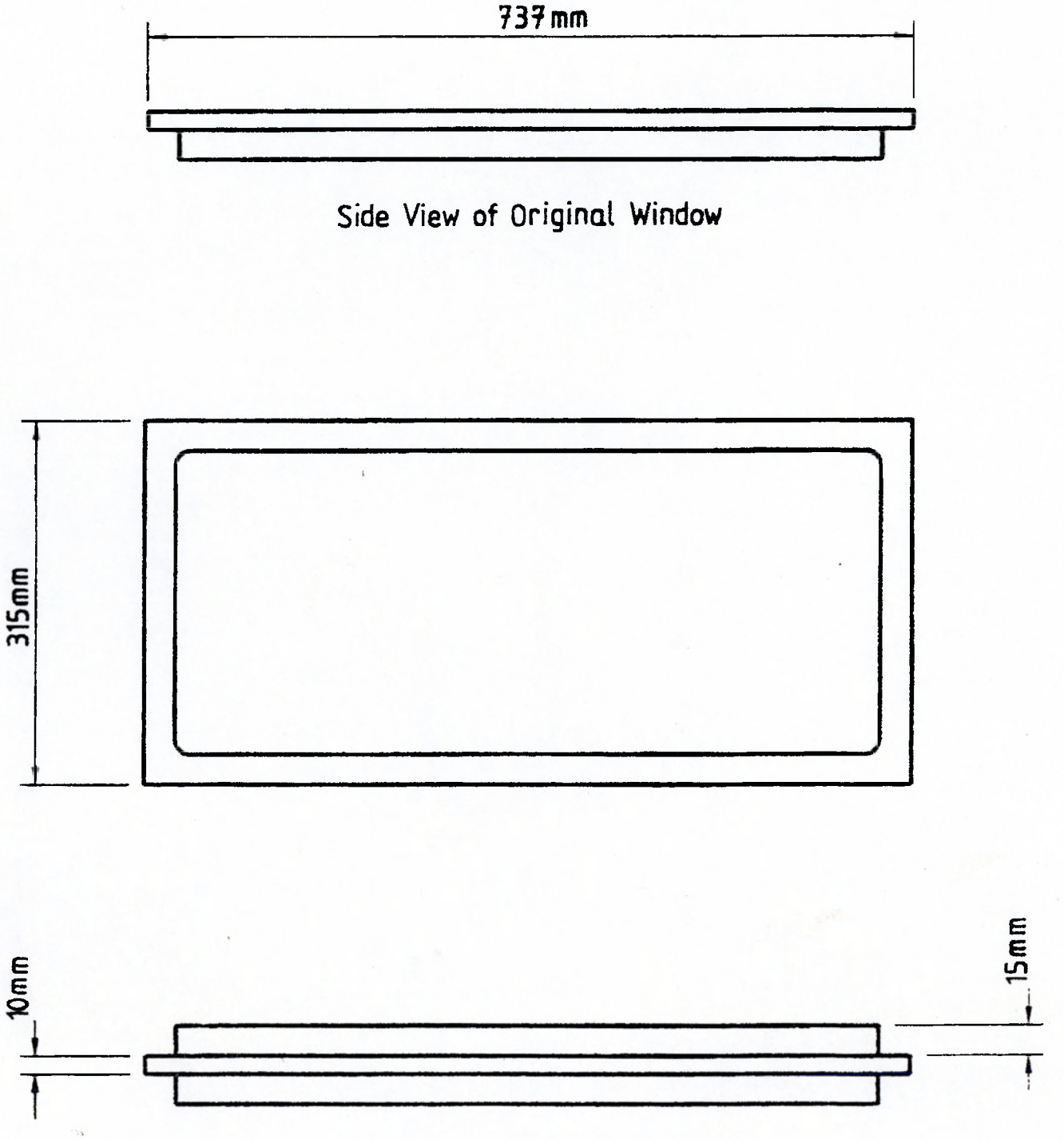

Fig. 3 Schematic diagram of the old and new working section windows

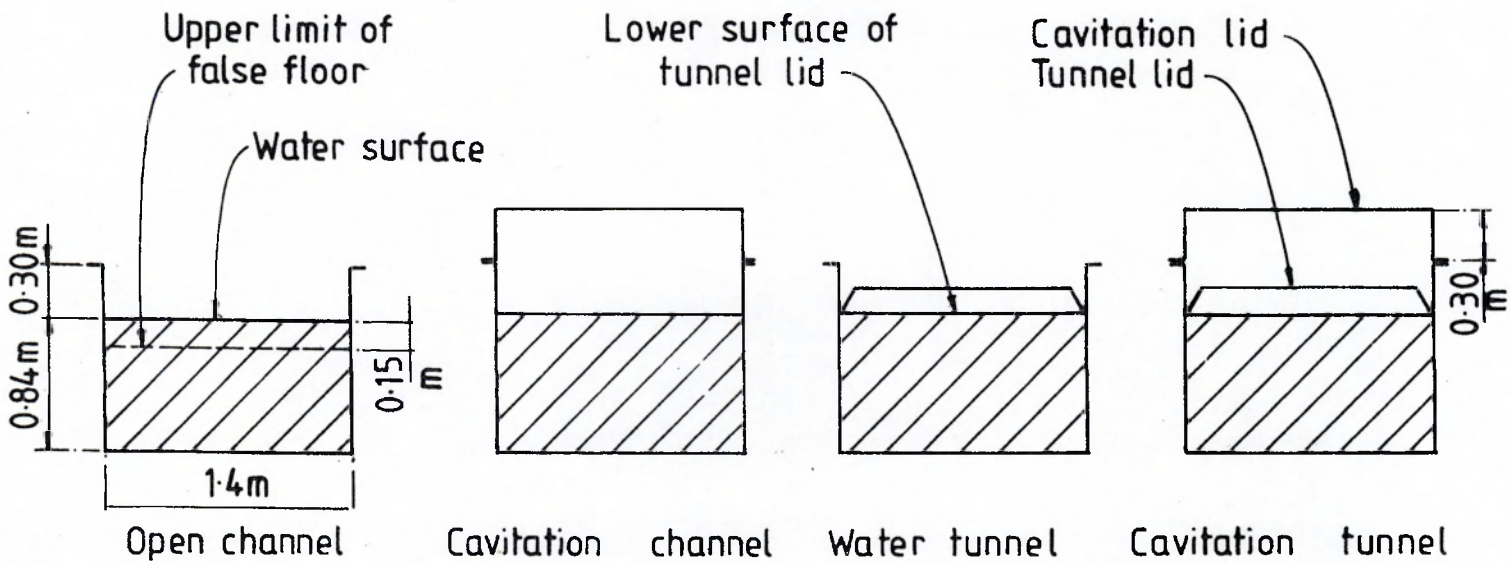

Fig. 4 The different configurations of the working section

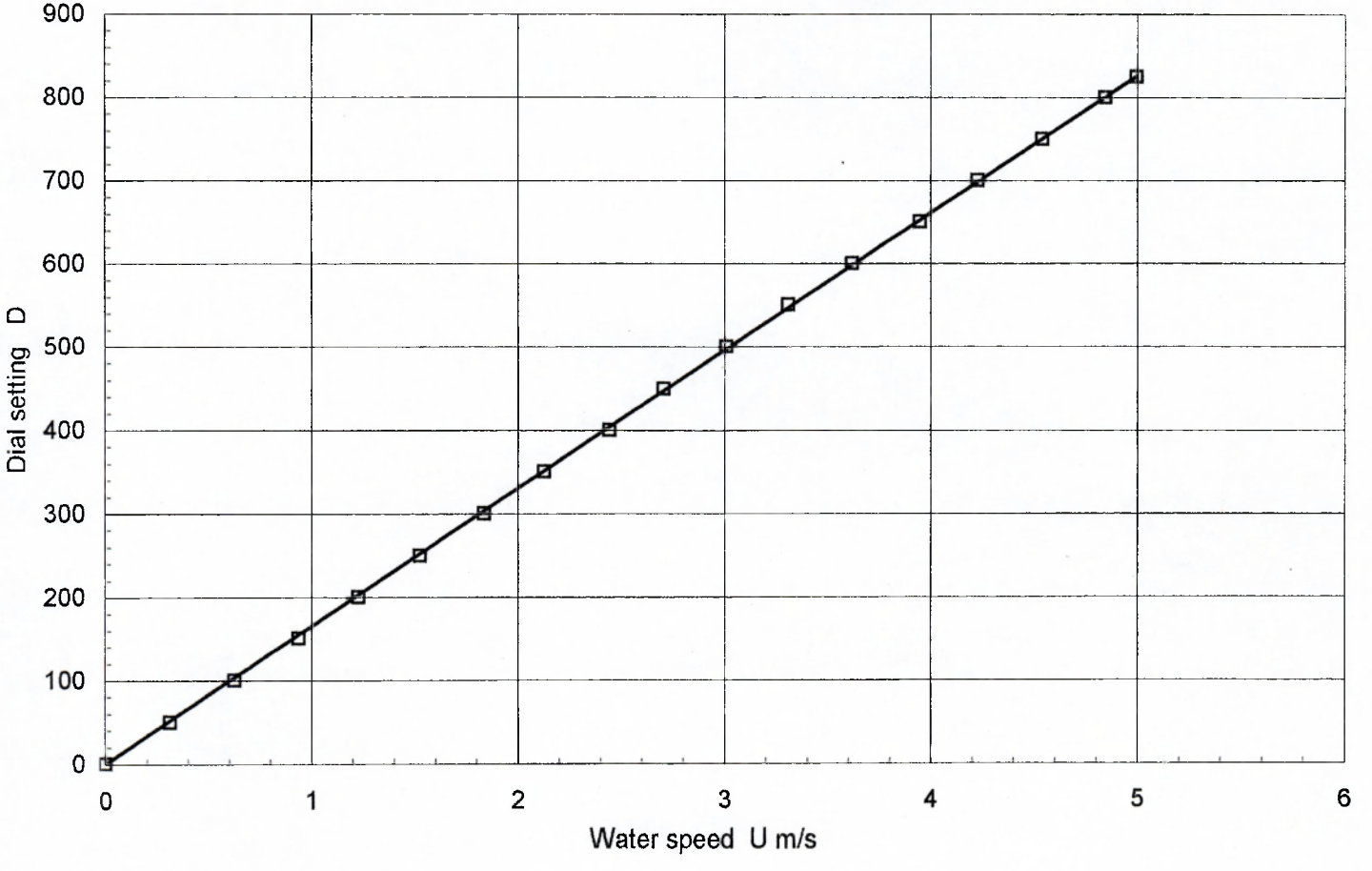

Fig. 5 Current calibration of the working section water speed

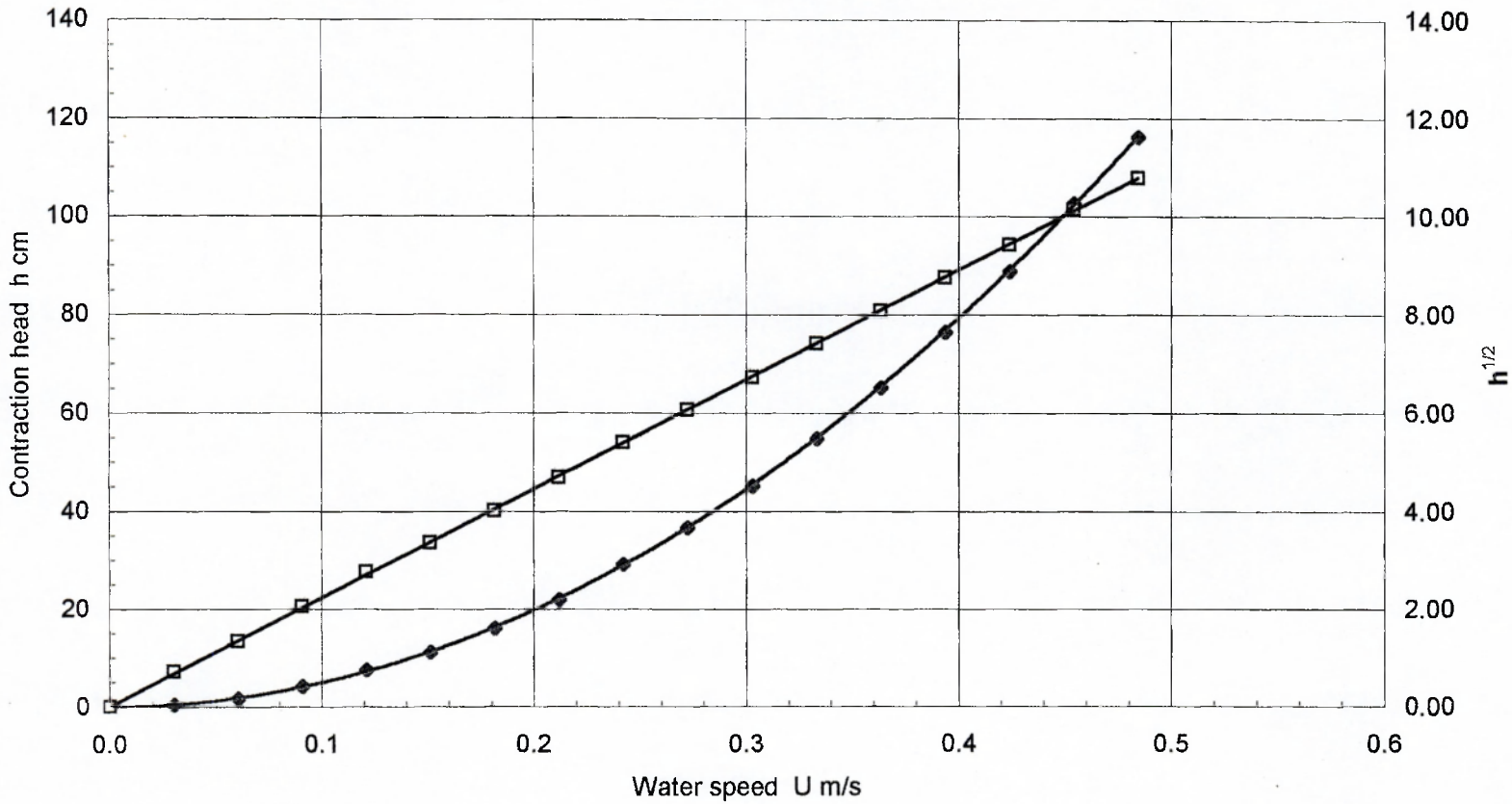

Fig. 6 Contraction calibration with flume water speed

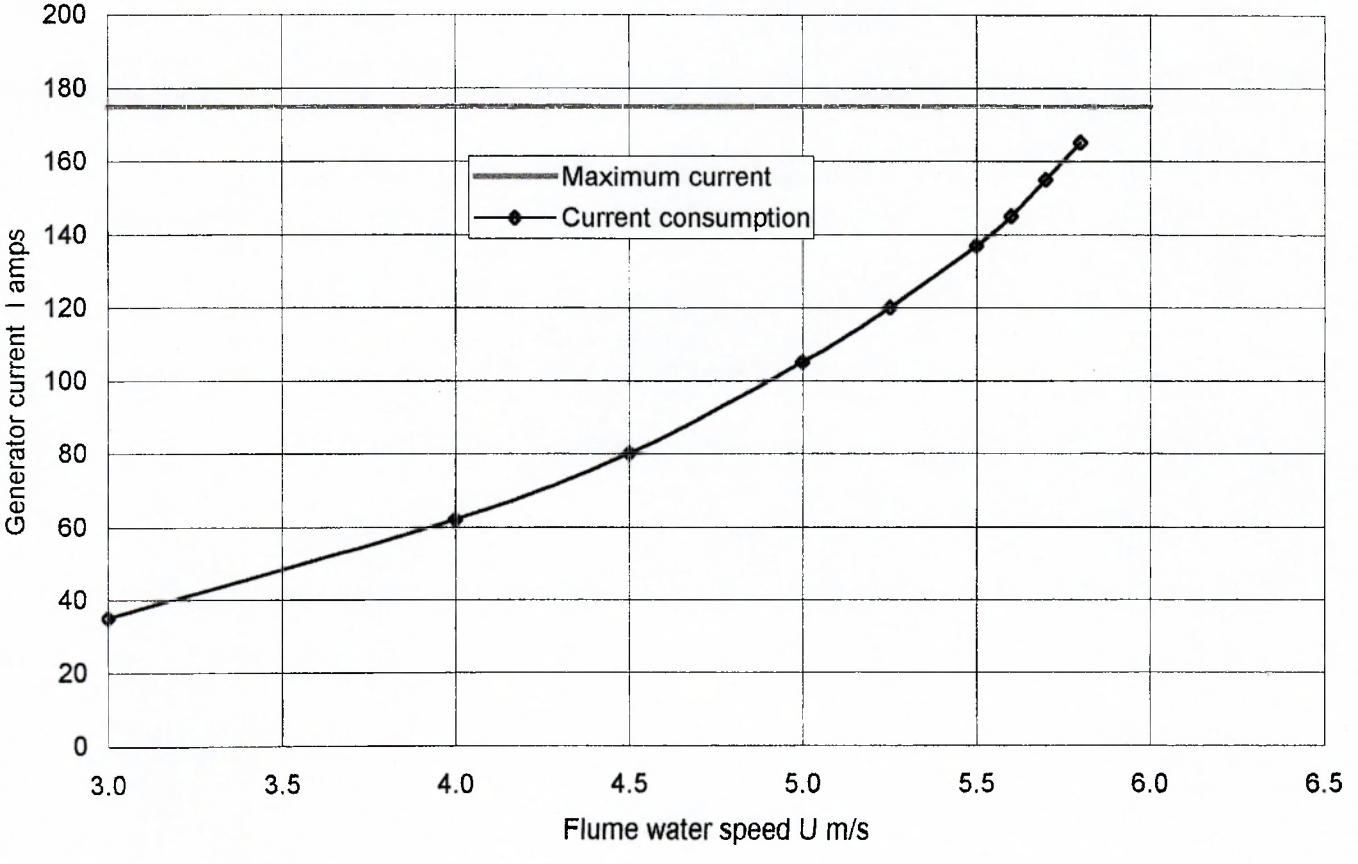

Fig. 7 The variation of generator current with flume water speed

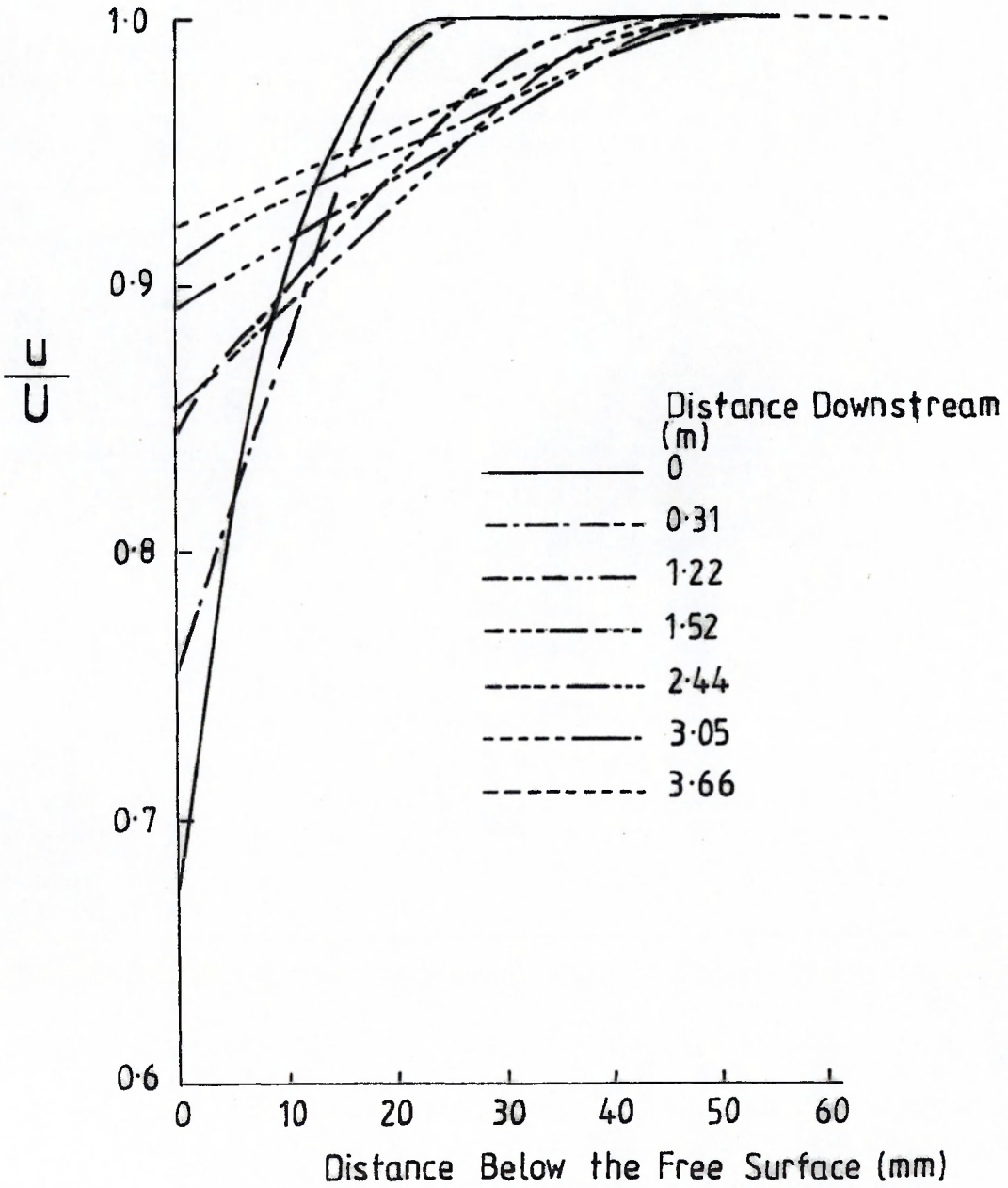

Fig. 8 The velocity distribution near the surface before installation of the injection system

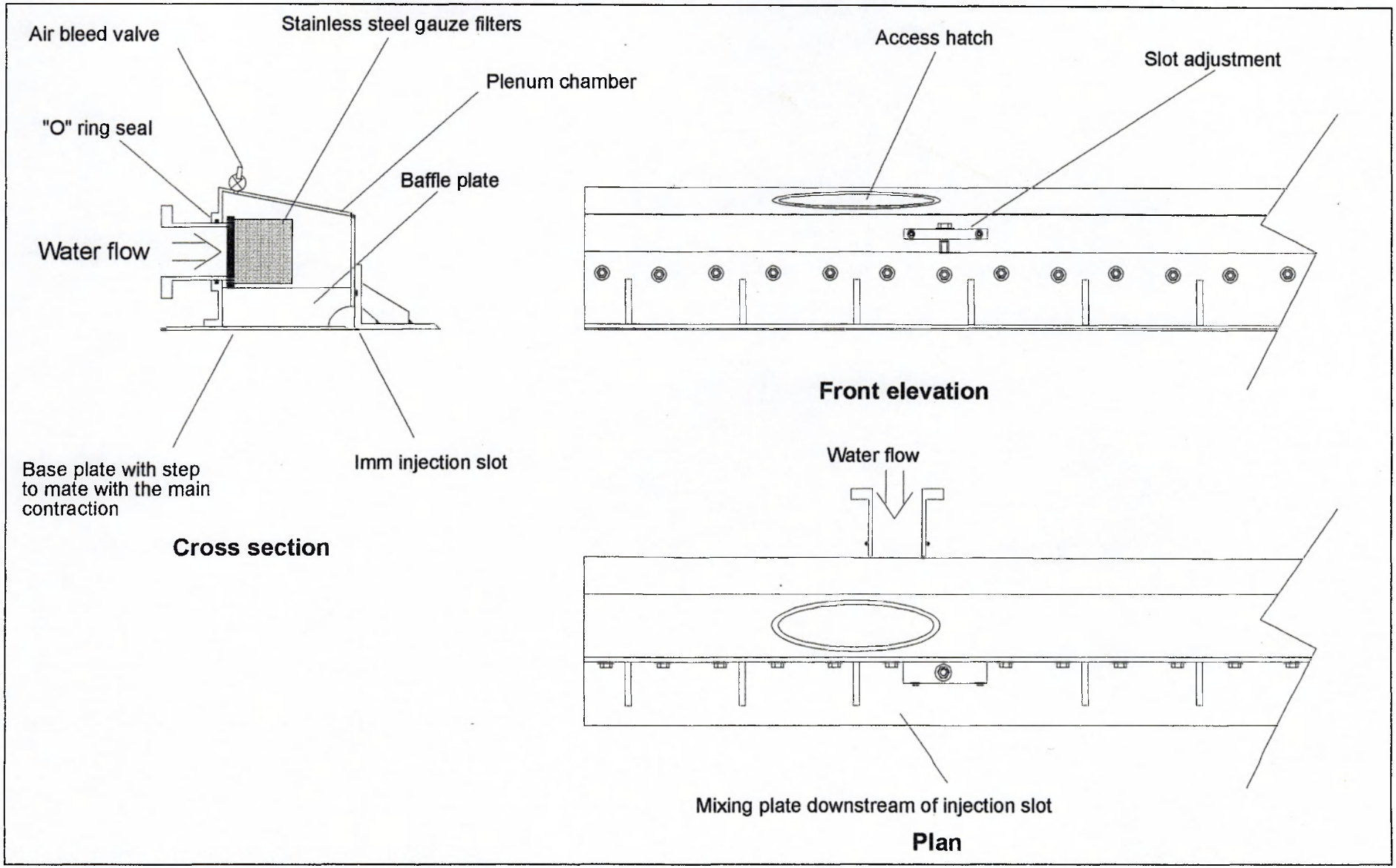

Fig. 9 Schematic drawing of the jet injection system

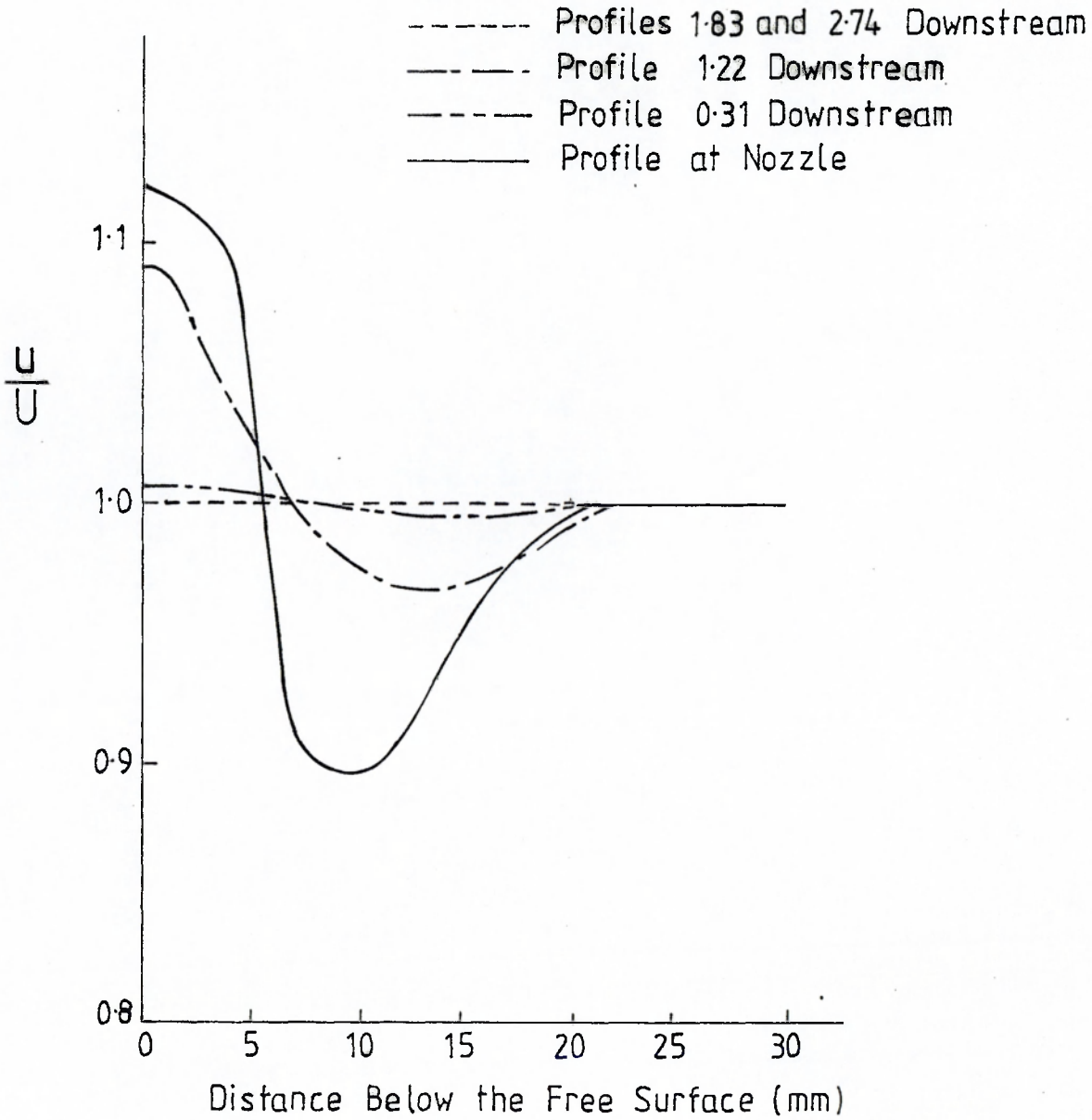

Fig. 10 The velocity distribution near the free surface with jet injection

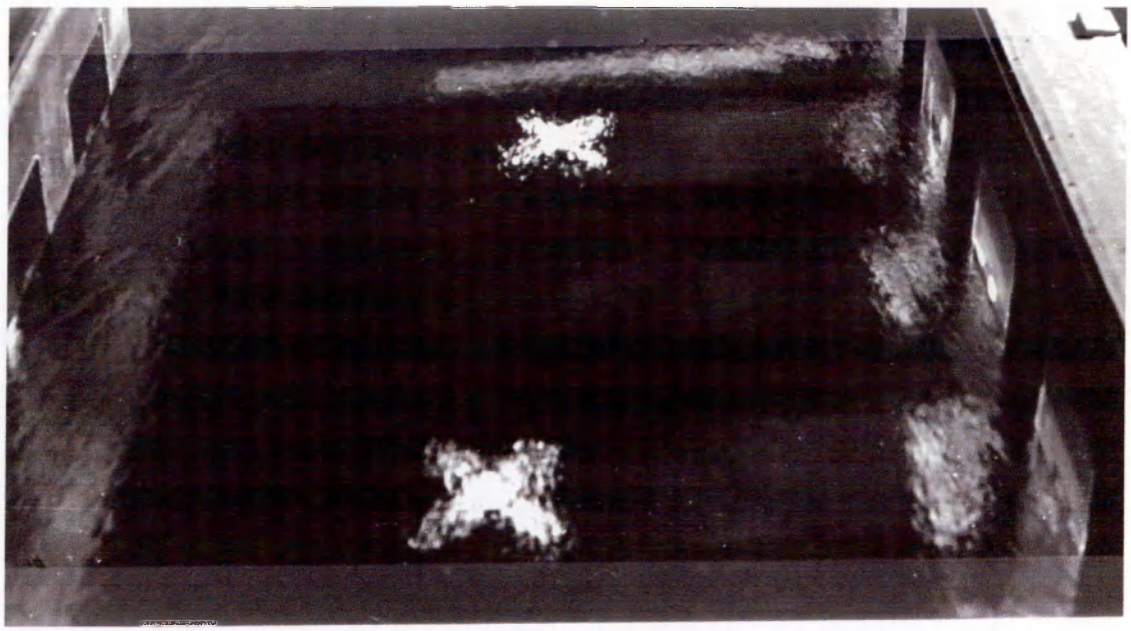

No surface injection

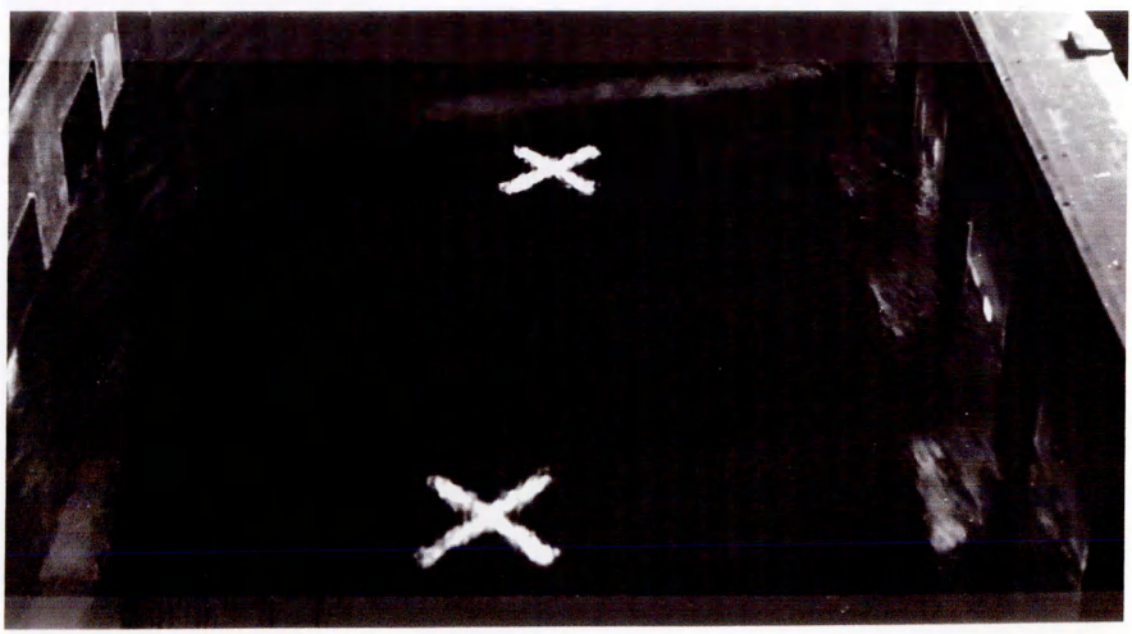

With surface injection

Fig. 11 The effect of jet injection on the free surface roughness

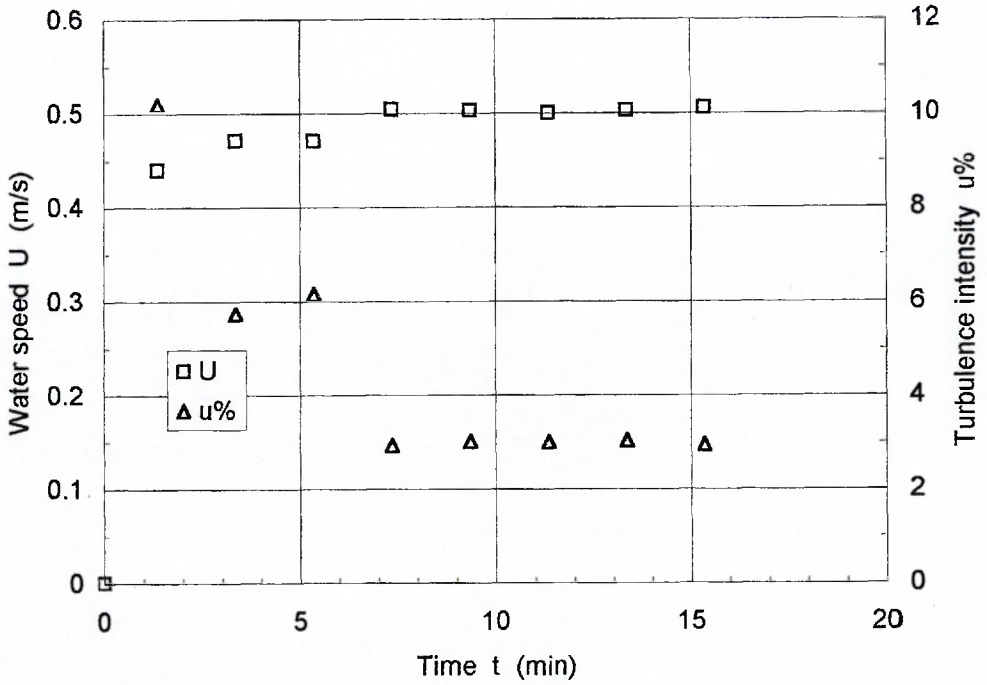

Fig. 12a Settling time on increasing flume speed (0 to 0.5 m/s)

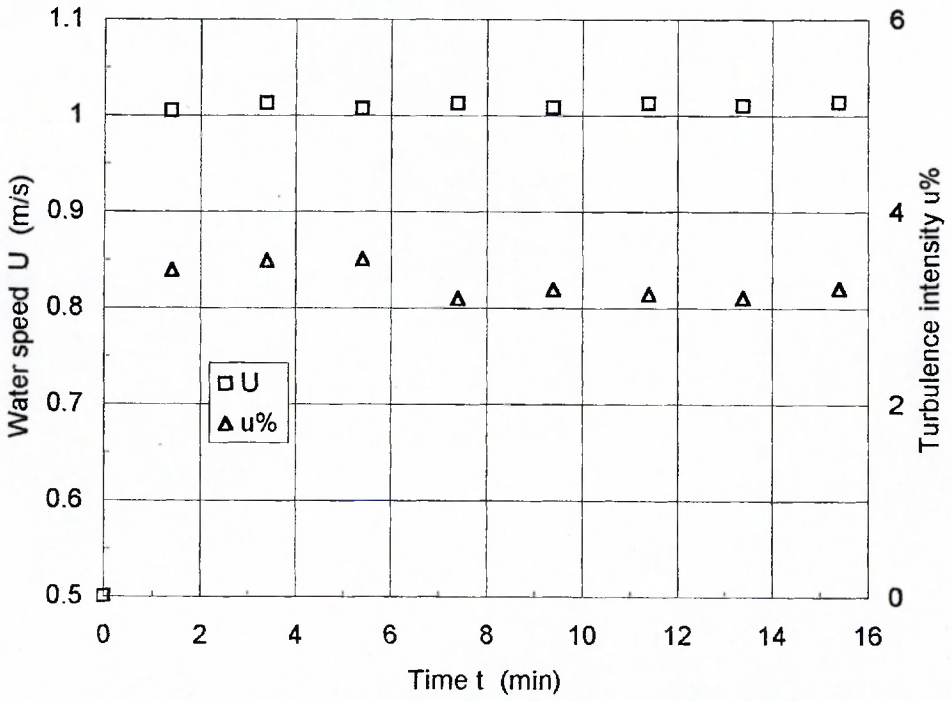

Fig. 12b Settling time on increasing flume speed (0.5 to 1.0 m/s)

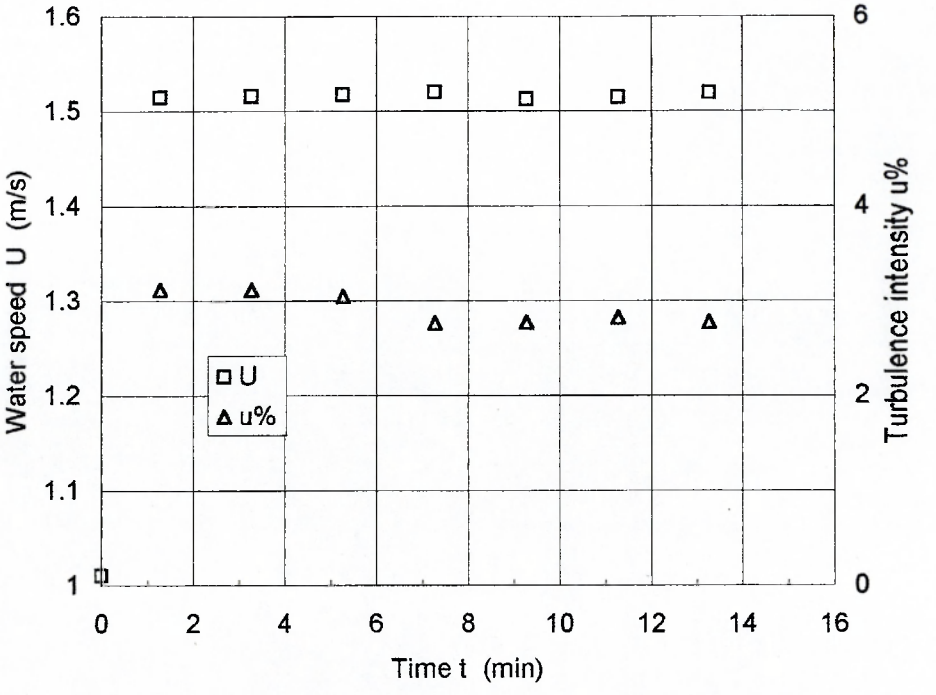

Fig. 12c Settling time on increasing flume speed (1.0 to 1.5 m/s)

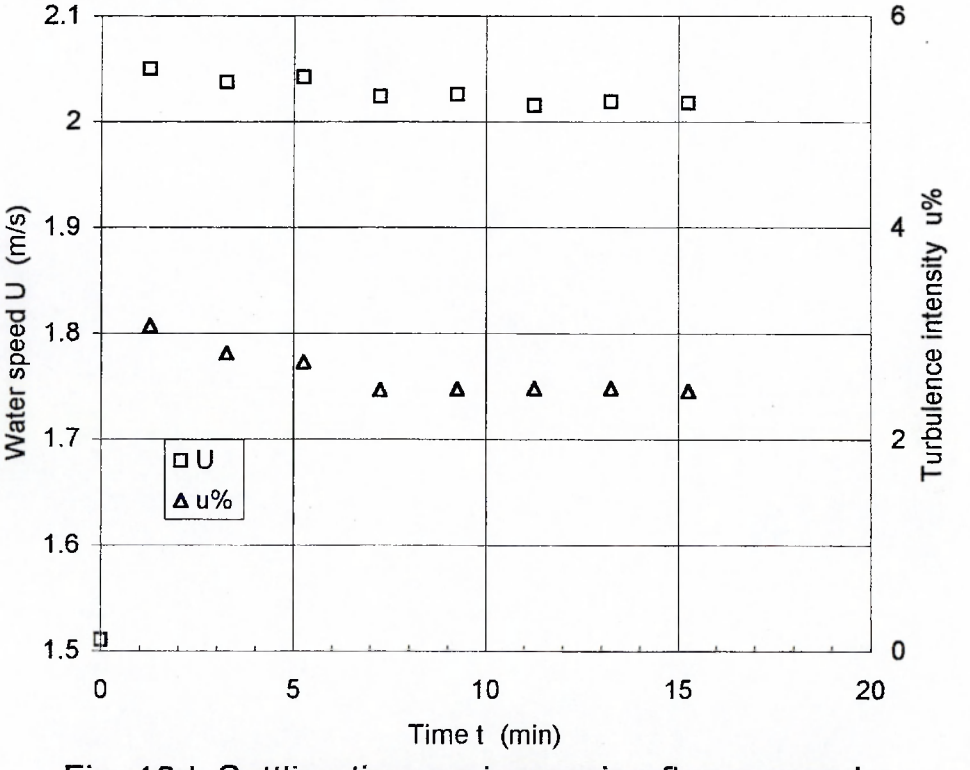

Fig. 12d Settling time on increasing flume speed (1.5 to 2.0 m/s)

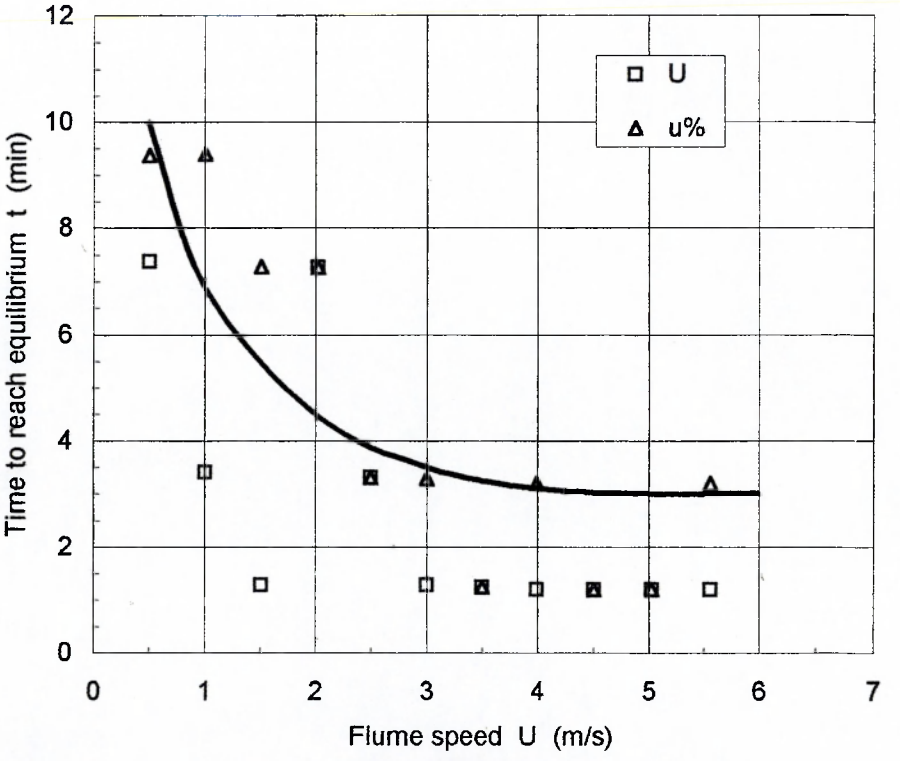

Fig. 13 The variation of settling time with flume speed - ascending speeds

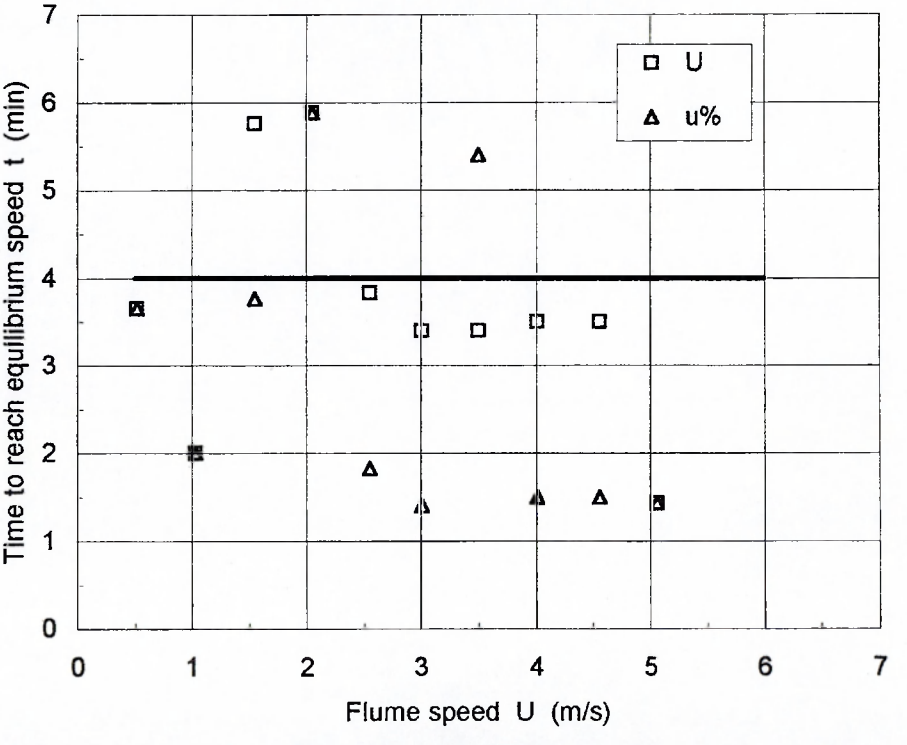

Fig. 14 The variation of settling time with flume speed - descending speeds

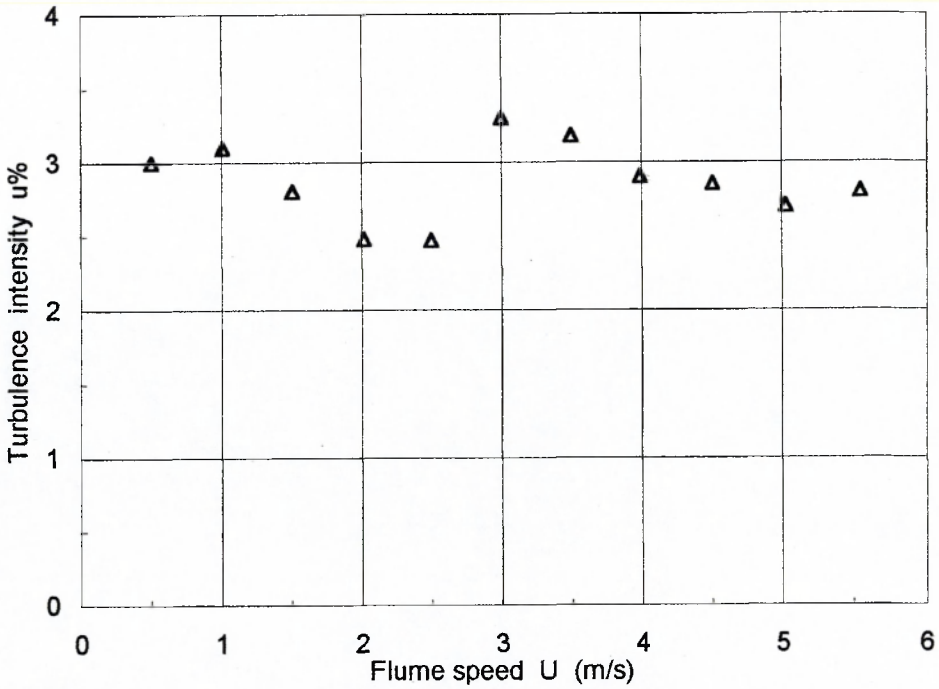

Fig. 15 The variation of turbulence with flume speed - ascending speeds

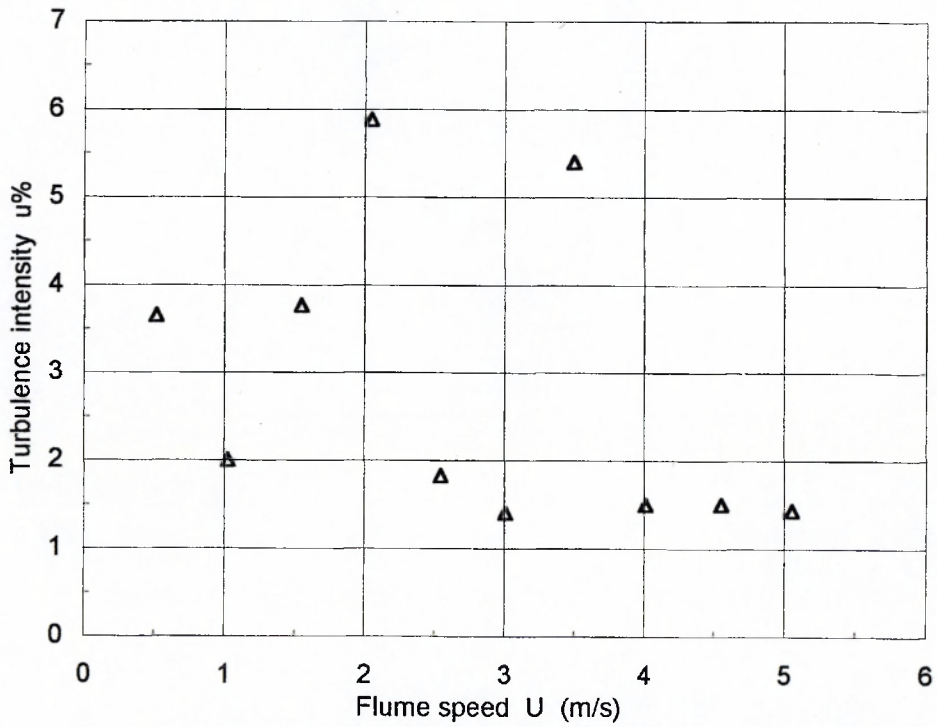

Fig.16 The variation of turbulence with flume speed - descending speeds

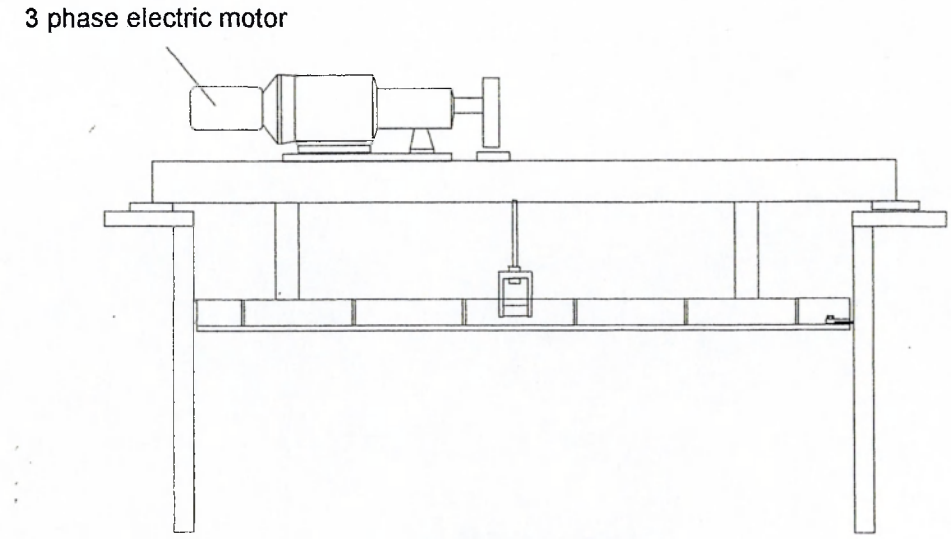

Front elevation
(looking upstream)

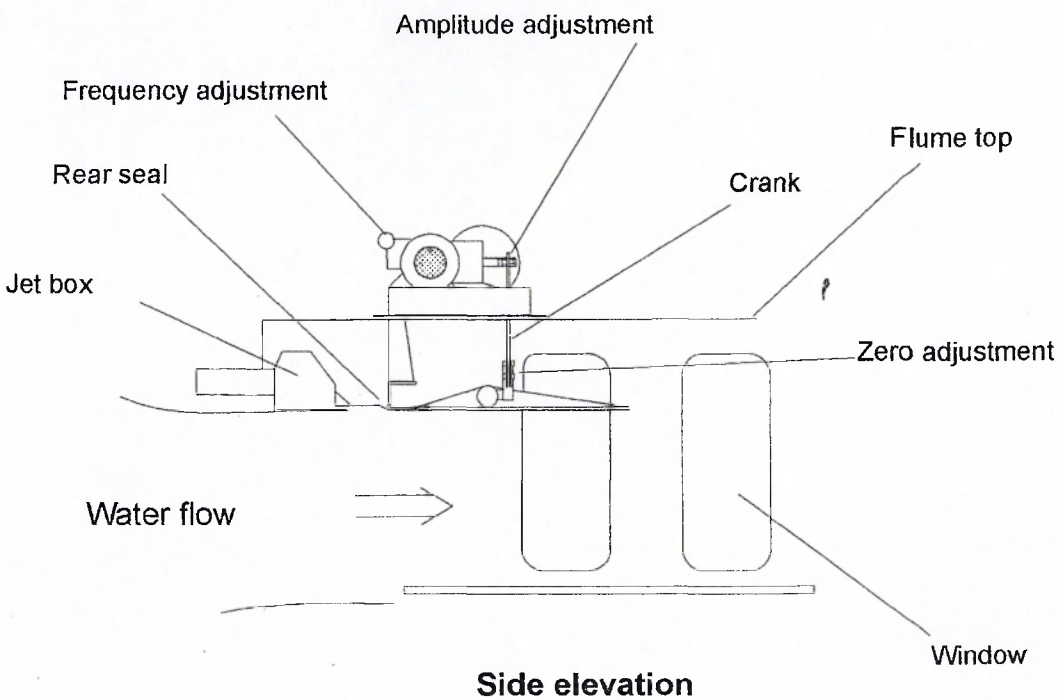

Side elevation

Fig. 17 Schematic diagram of the wave-maker

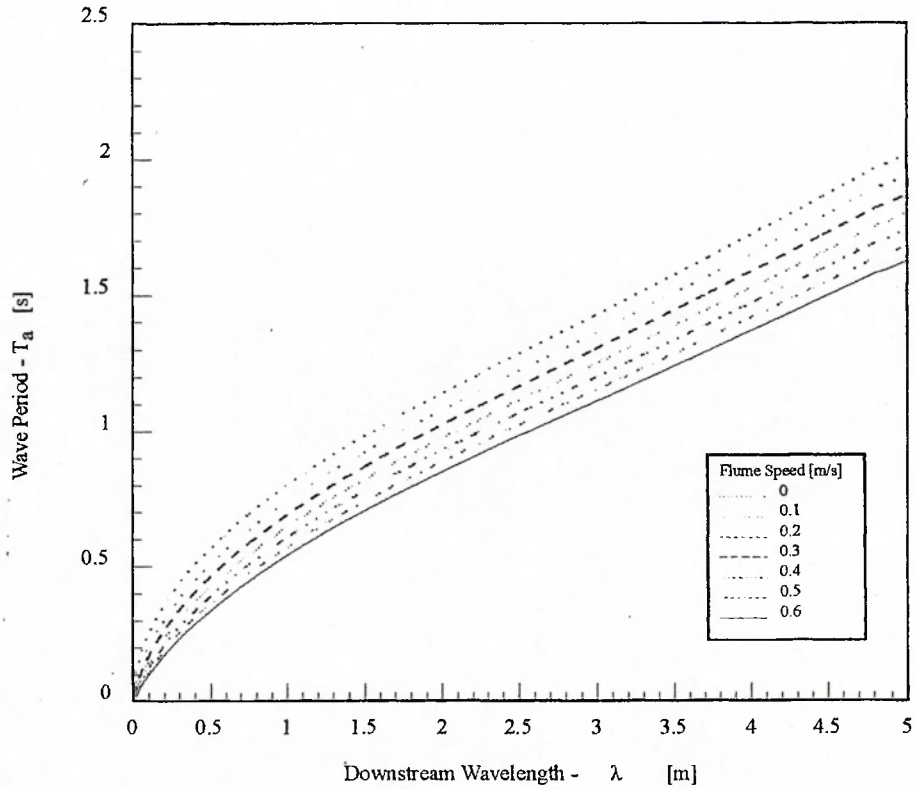

Downstream wave period charcteristics

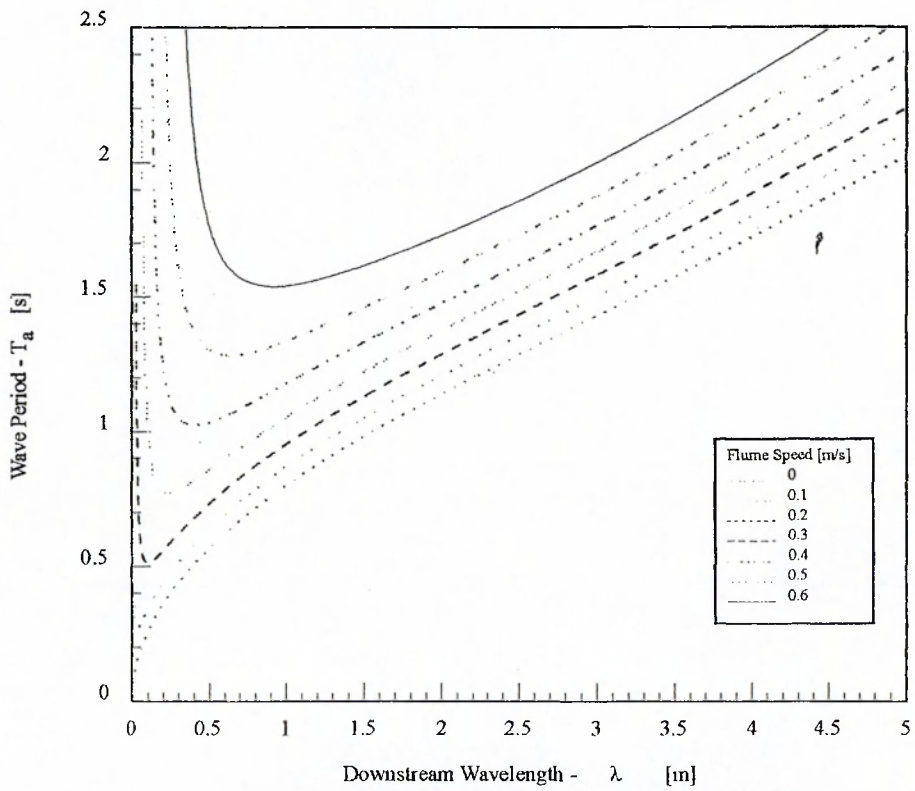

Reflected wave period characteristics

Fig. 18 Theoretical wave period characteristics for both upstream and downstream waves

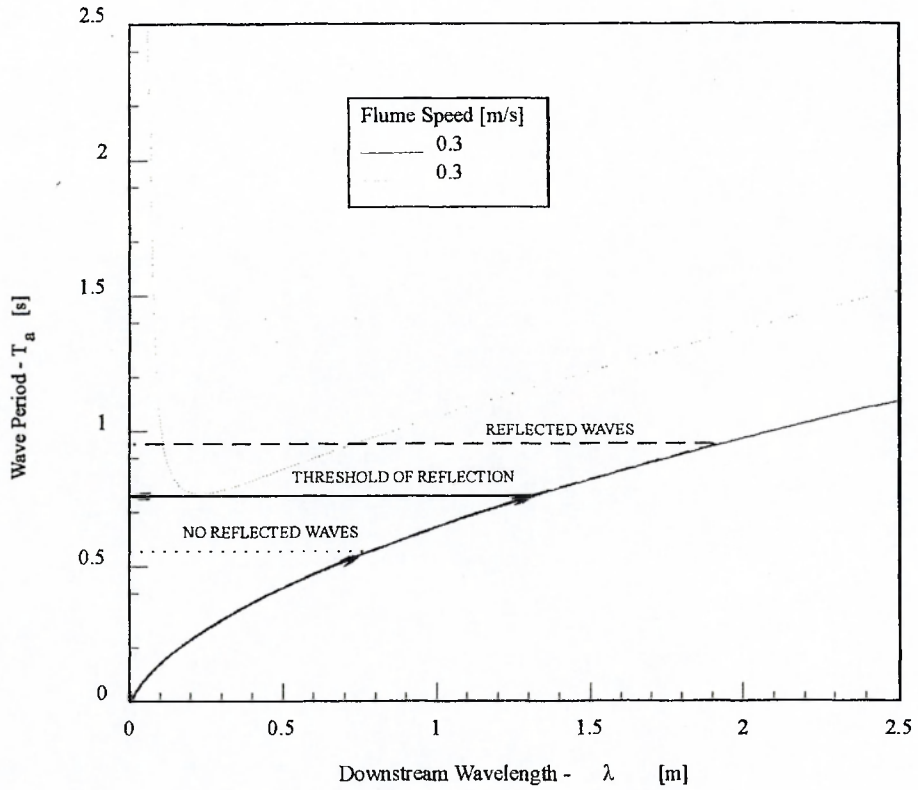

Calculation method for theoretical wave reflection

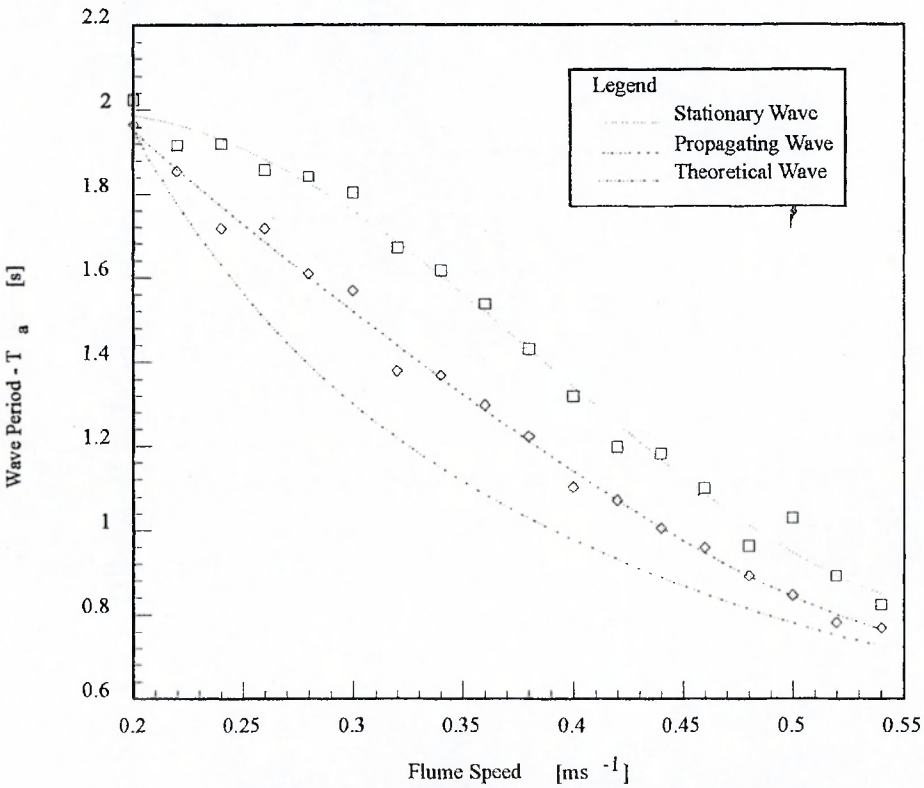

Comparison between theory and experiment

Fig. 19 Wave period characteristics for both upstream and downstream waves

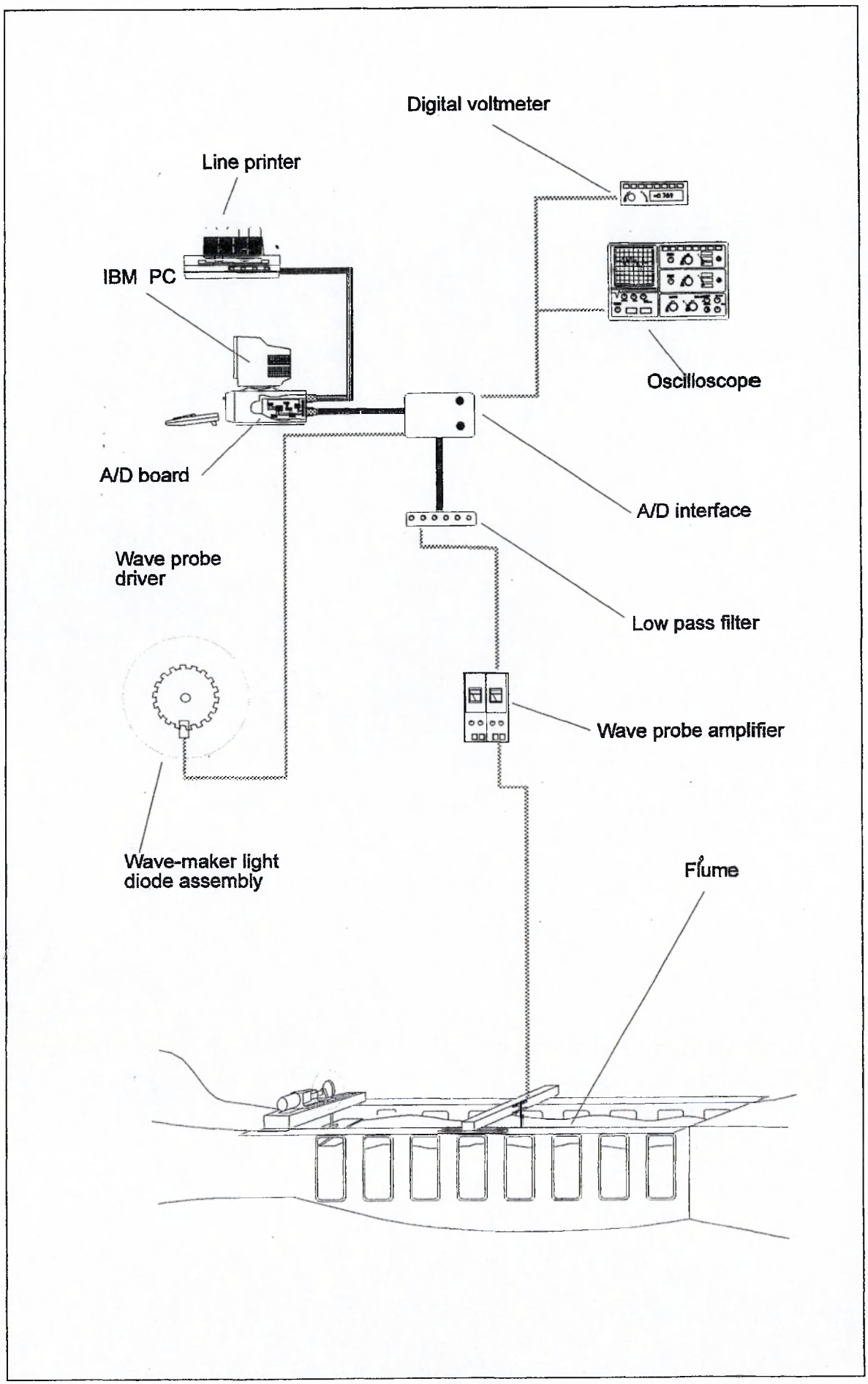

Fig. 20 Schematic diagram of the instrumentation for tests of the waves

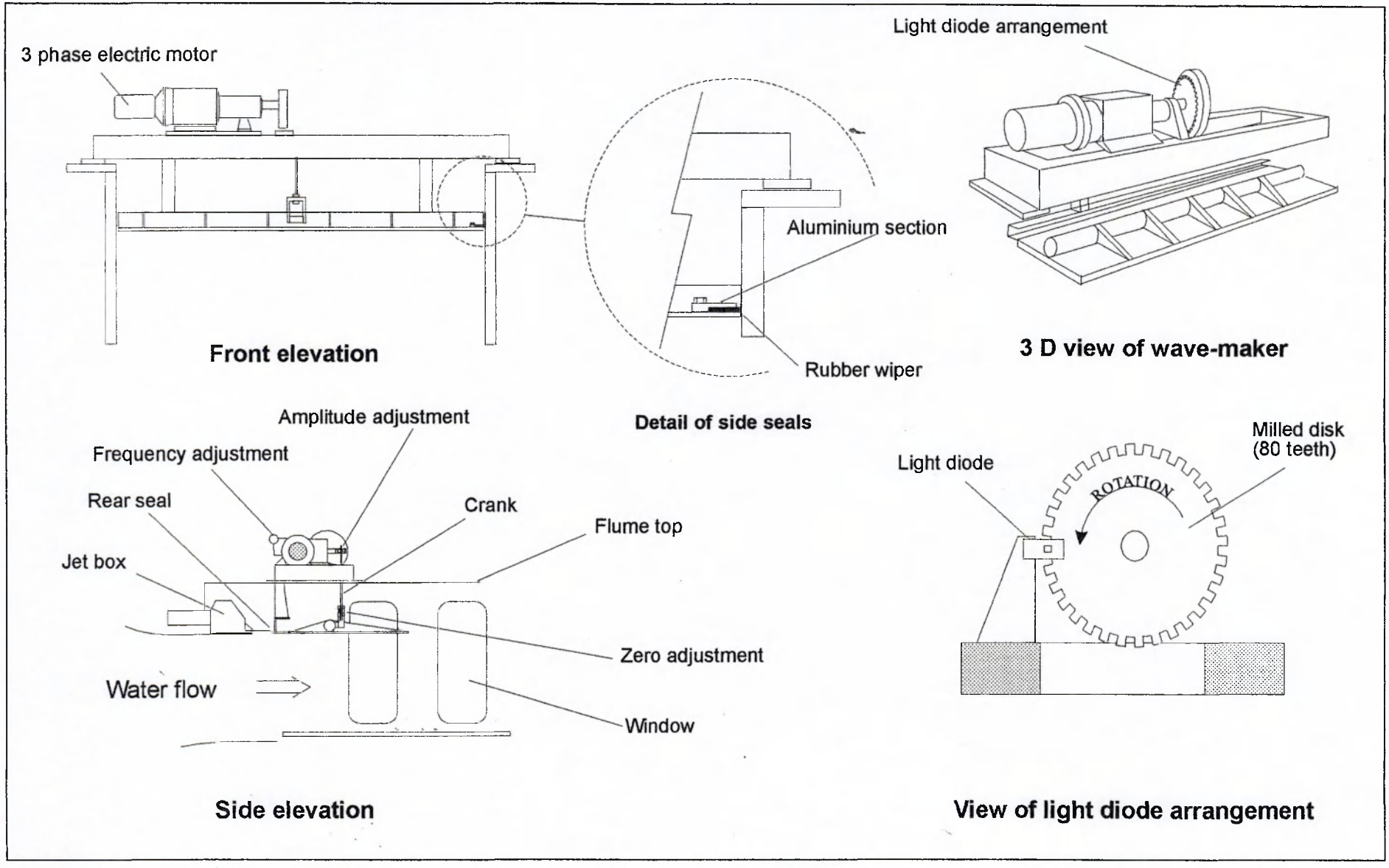

Fig. 21 Schematic diagram of the wave-maker with timing detector

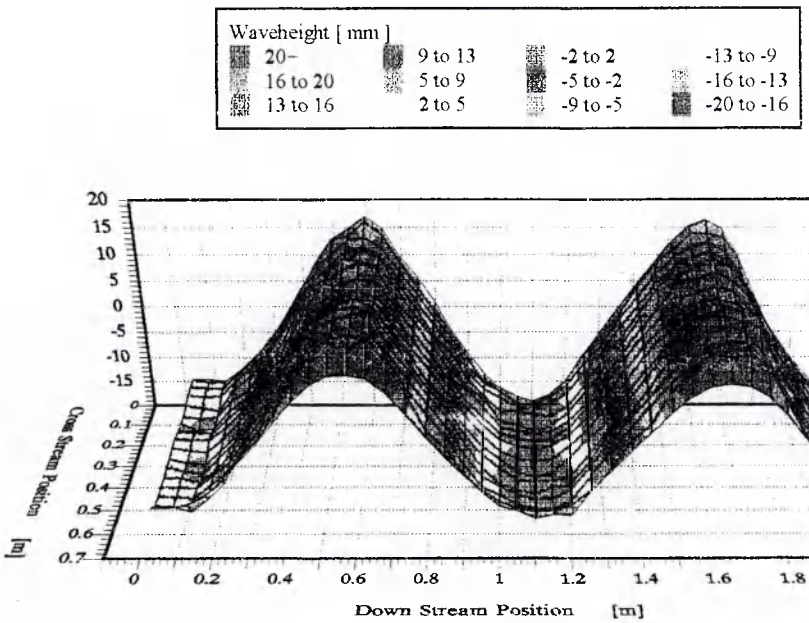

PROFILE 1

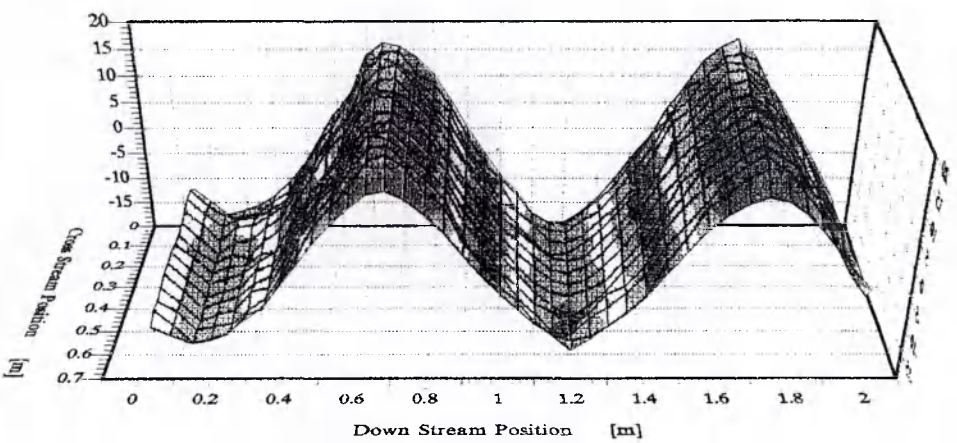

PROFILE 2

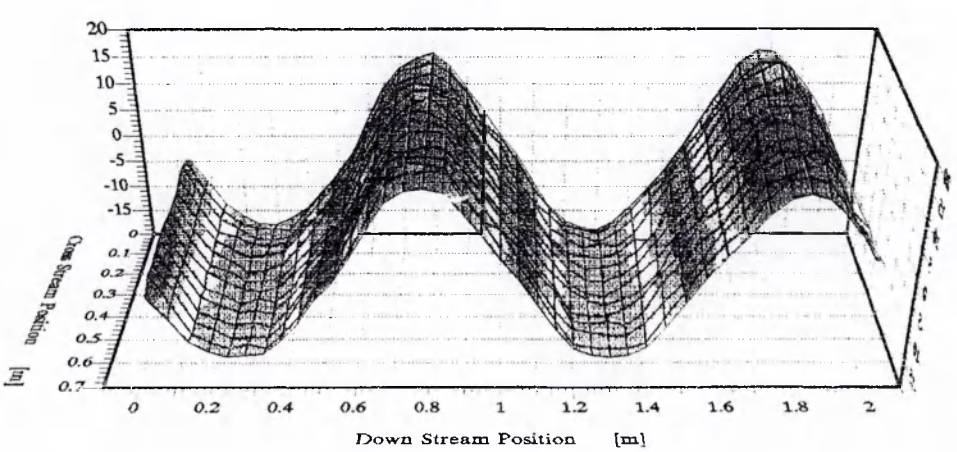

PROFILE 3

Fig. 22 Wave profiles along the working section for U=0.5 m/s

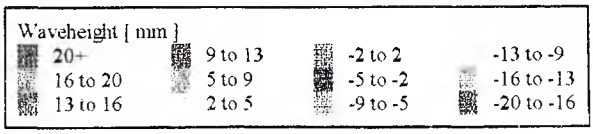

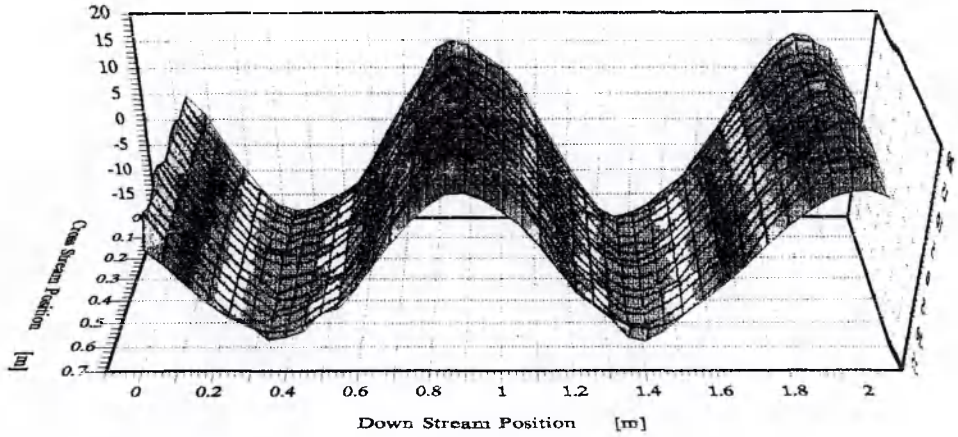

PROFILE 4

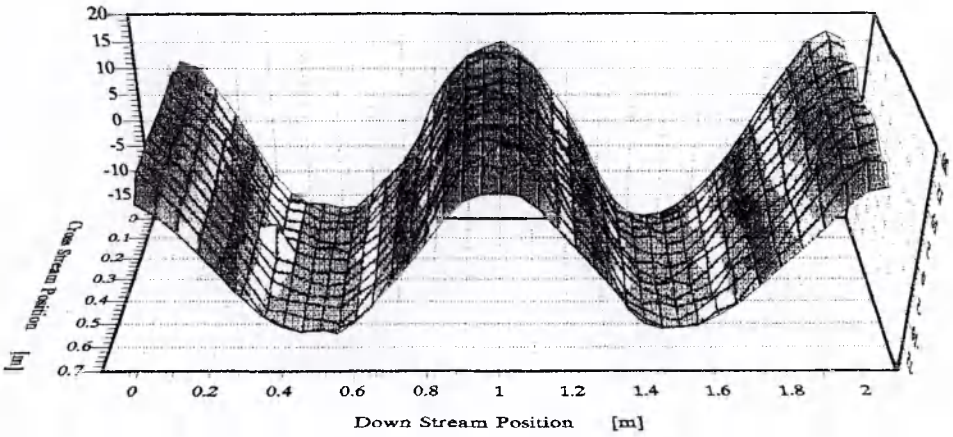

PROFILE 5

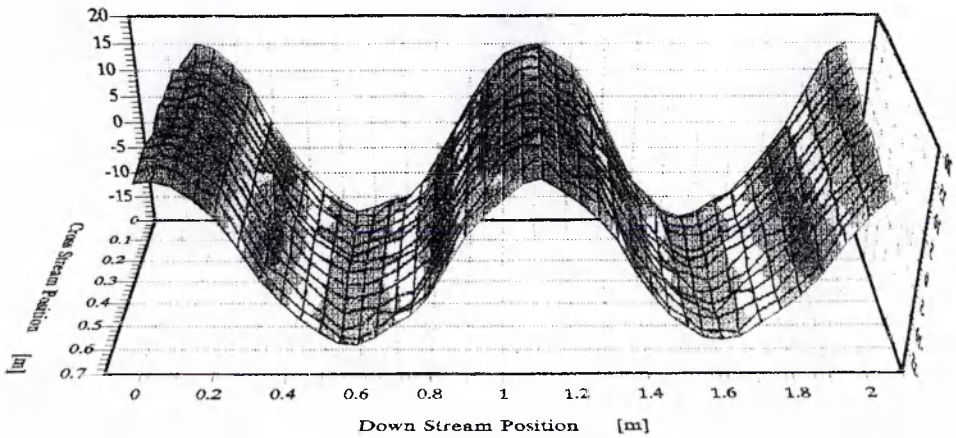

PROFILE 6

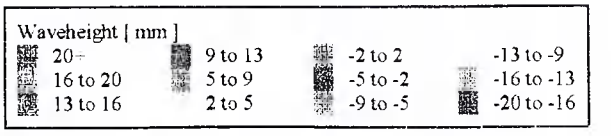

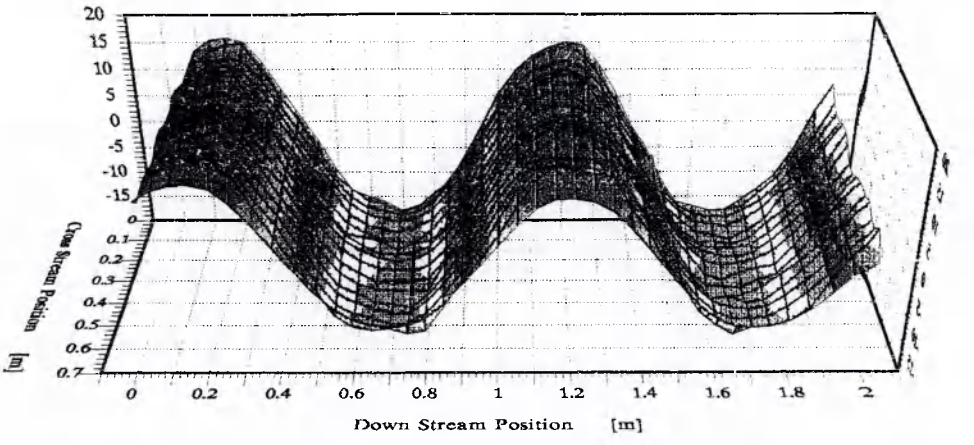

PROFILE 7

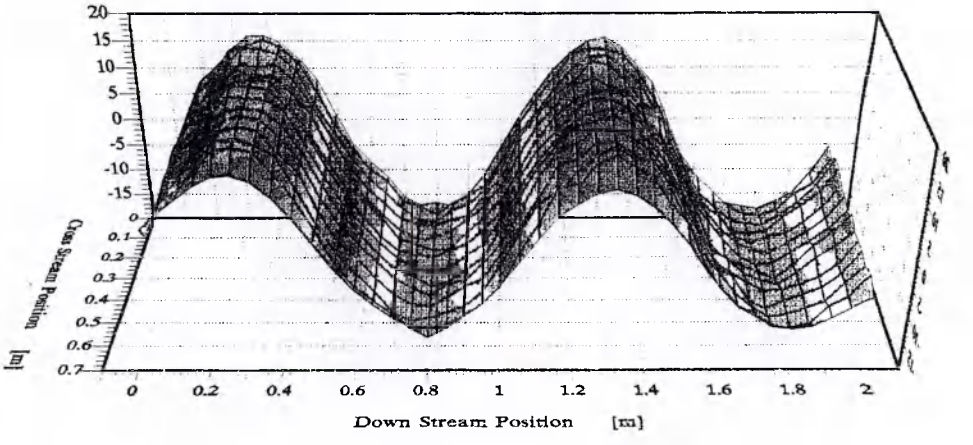

PROFILE 8

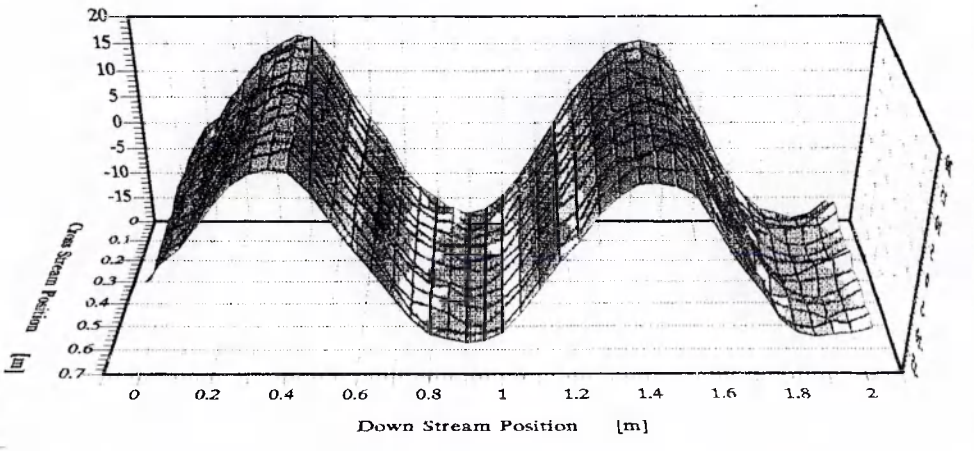

PROFILE 9

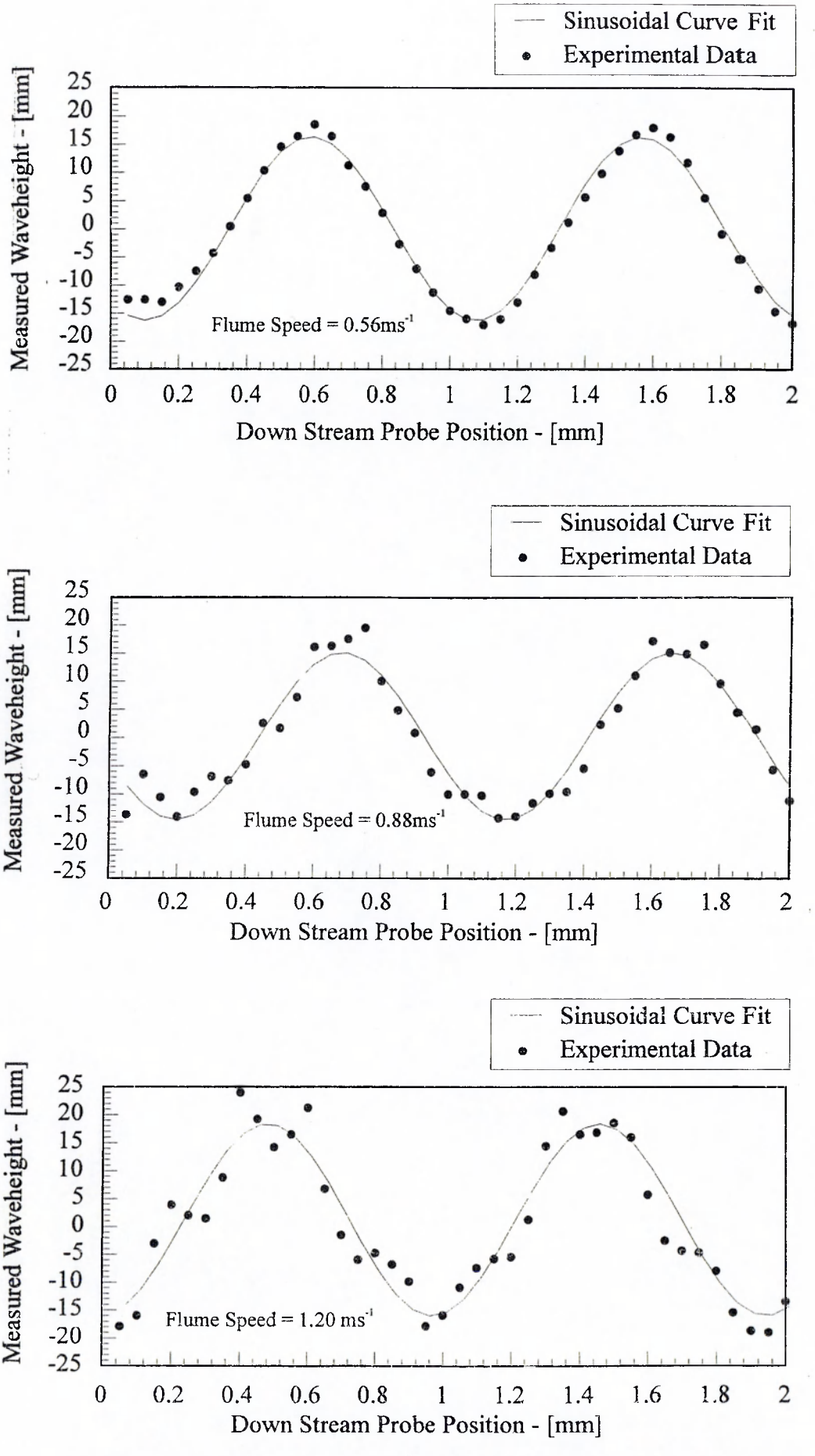

Fig. 23 Wave profiles along the centre-line of the working section

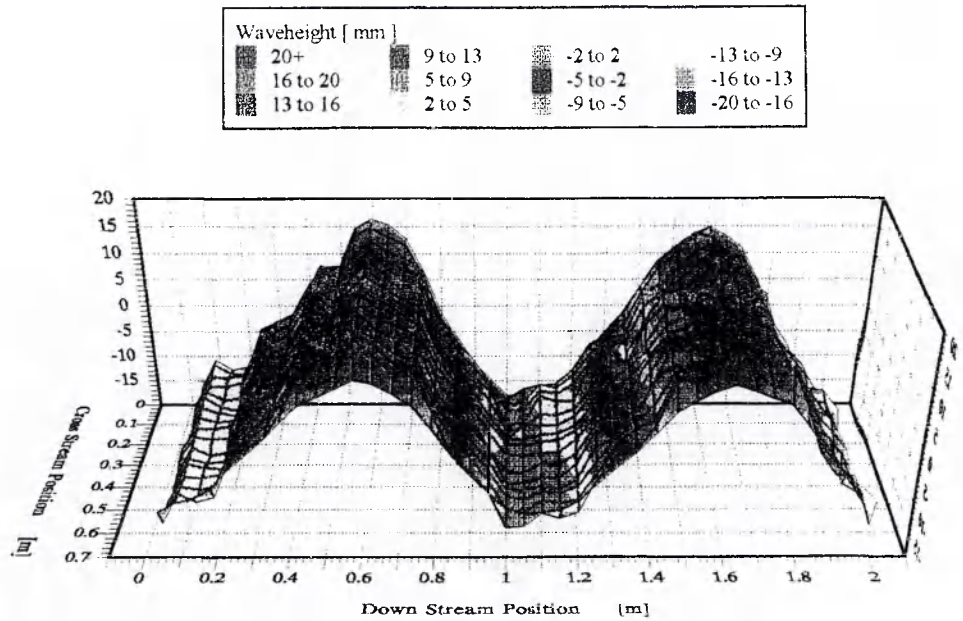

PROFILE 1

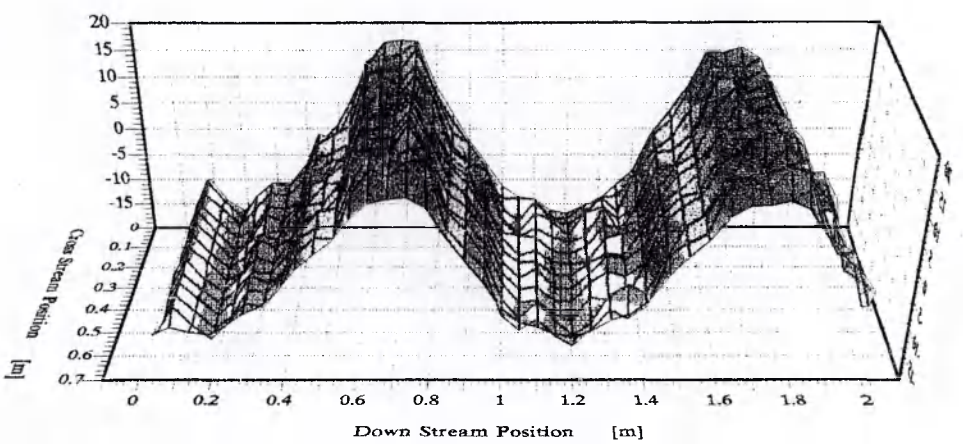

PROFILE 2

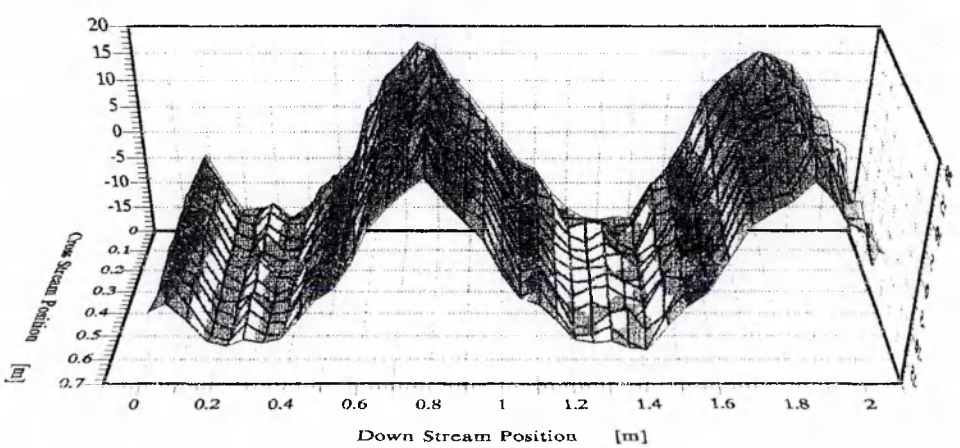

PROFILE 3

Fig. 24 Wave profiles along the working section for U=0.88 m/s

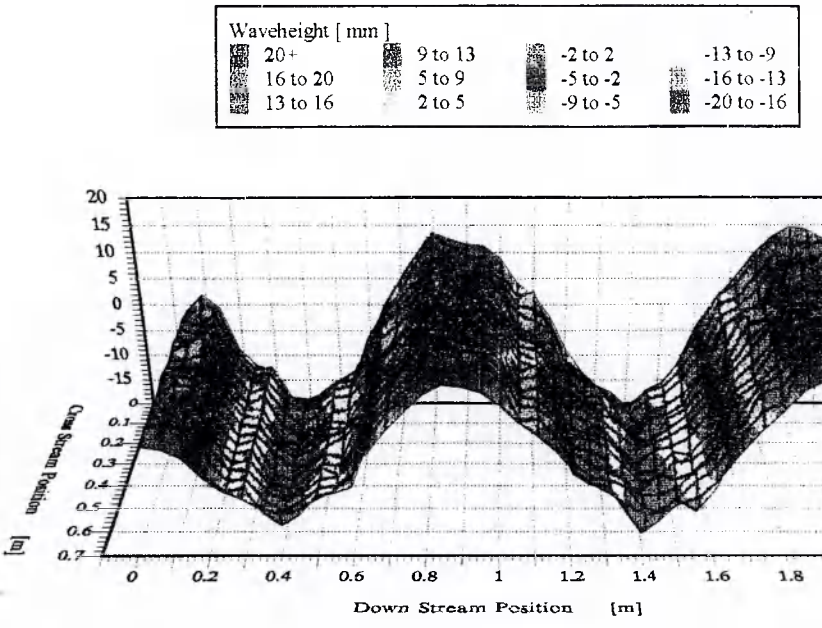

PROFILE 4

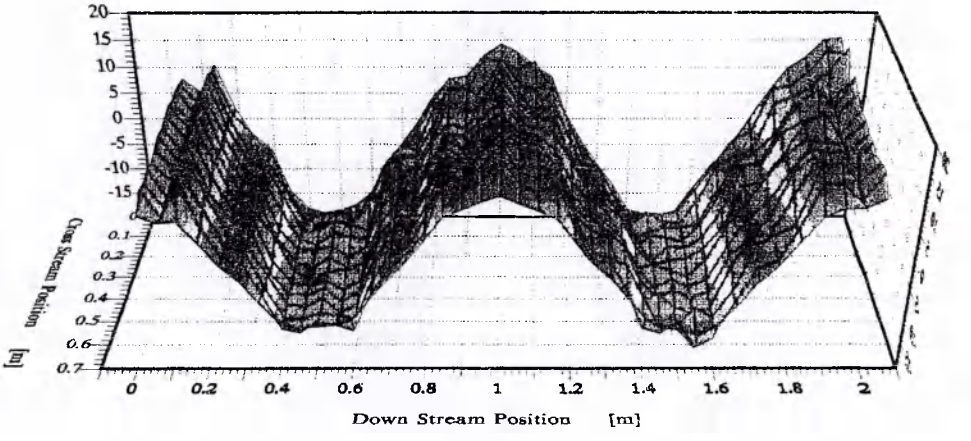

PROFILE 5

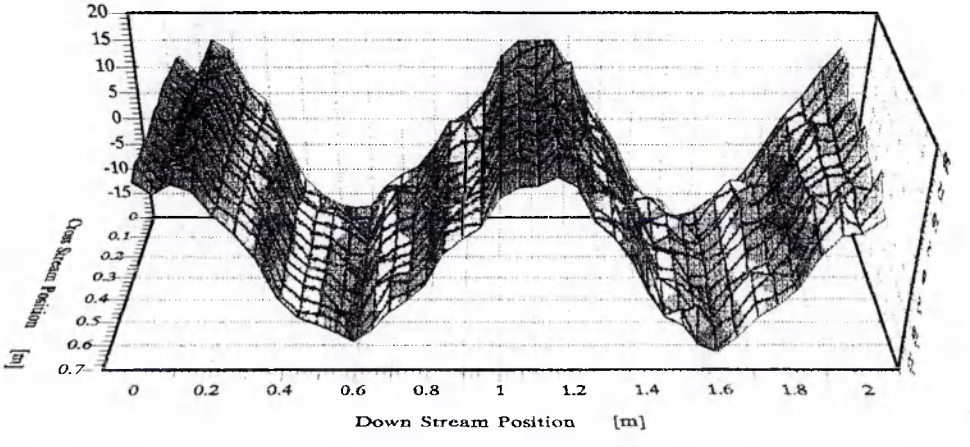

PROFILE 6

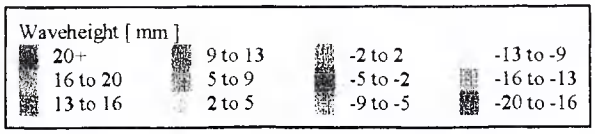

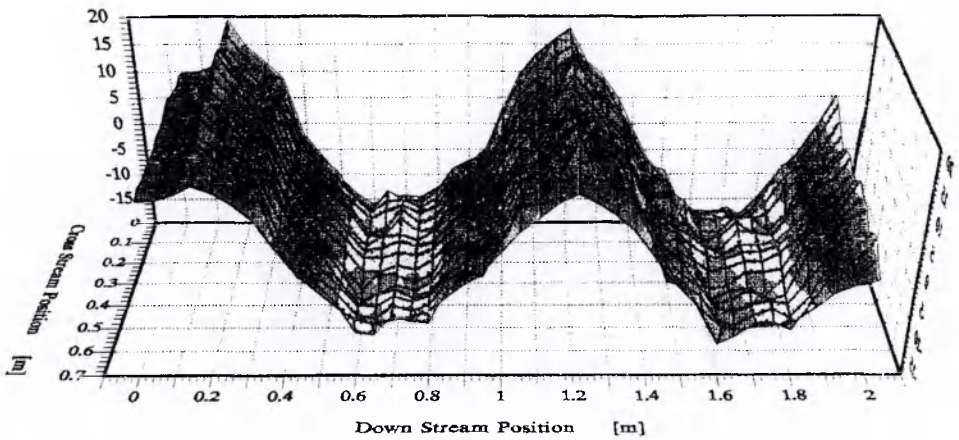

PROFILE 7

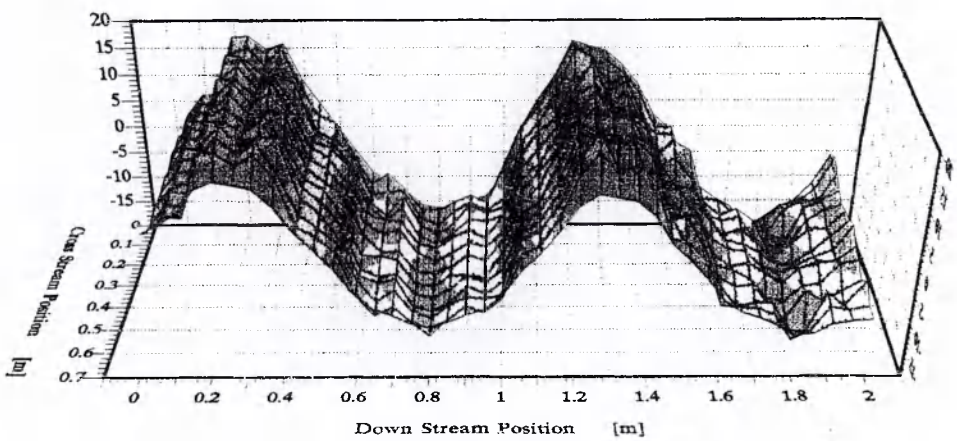

PROFILE 8

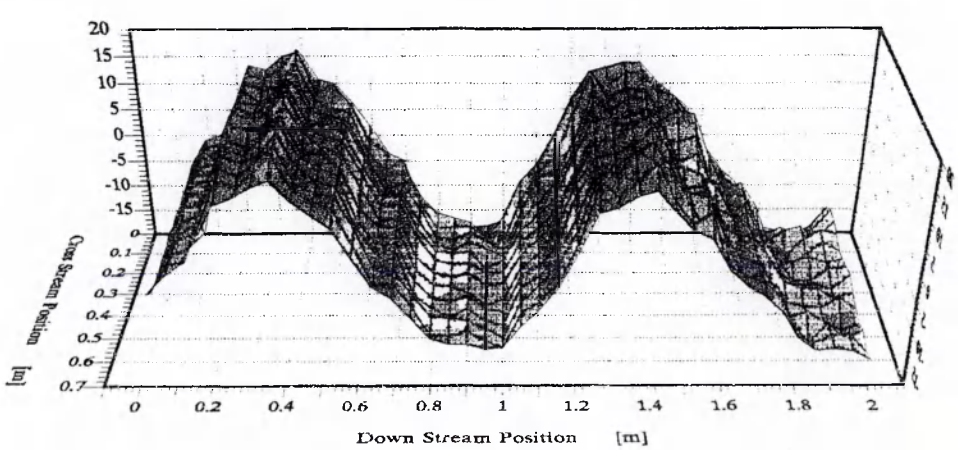

PROFILE 9

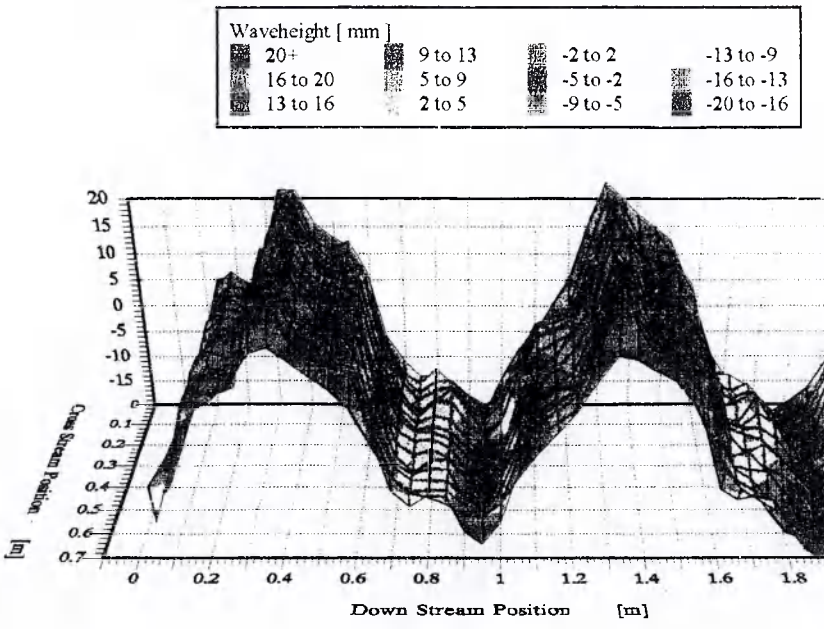

PROFILE 1

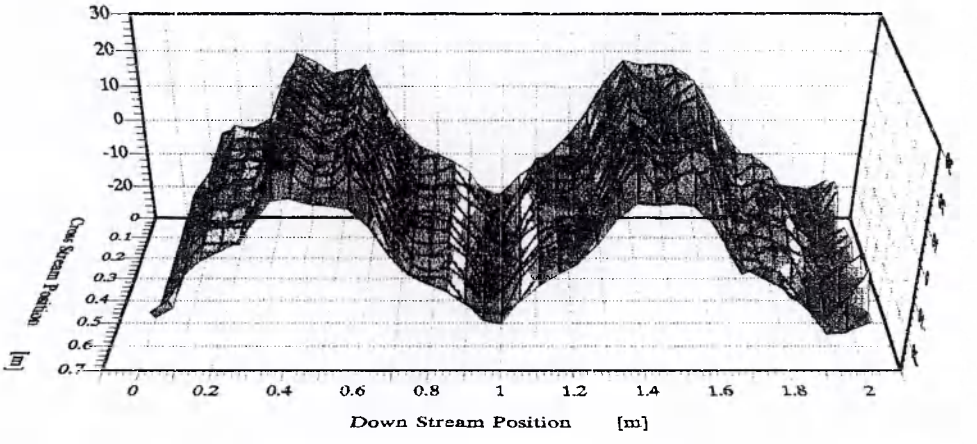

PROFILE 2

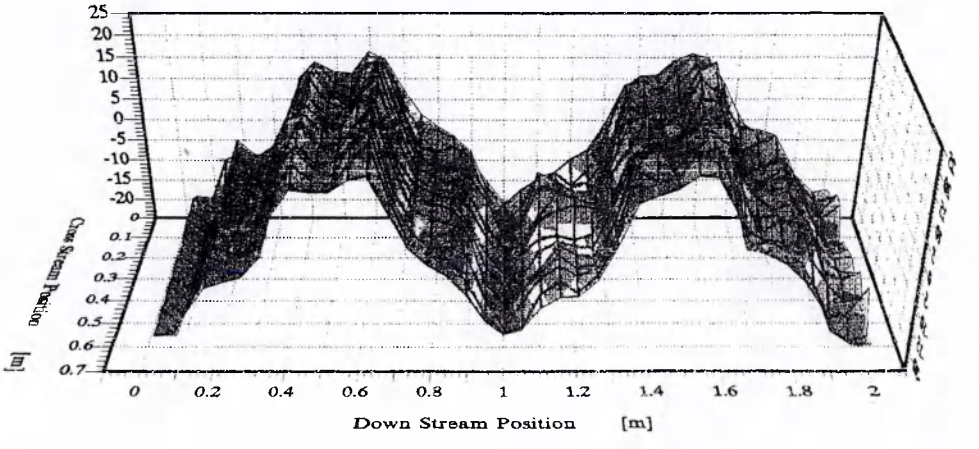

PROFILE 3

Fig. 25 Wave profiles along the working section for U=1.2 m/s

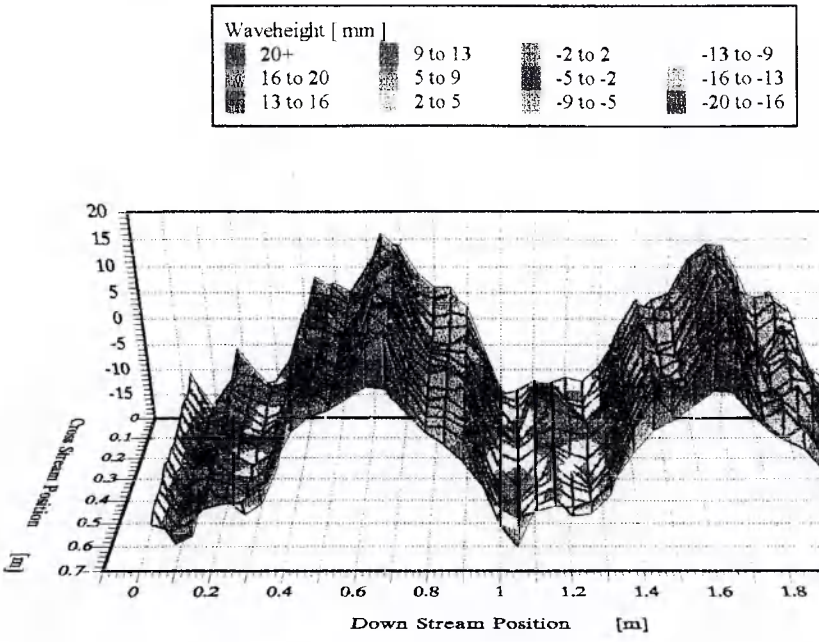

PROFILE 4

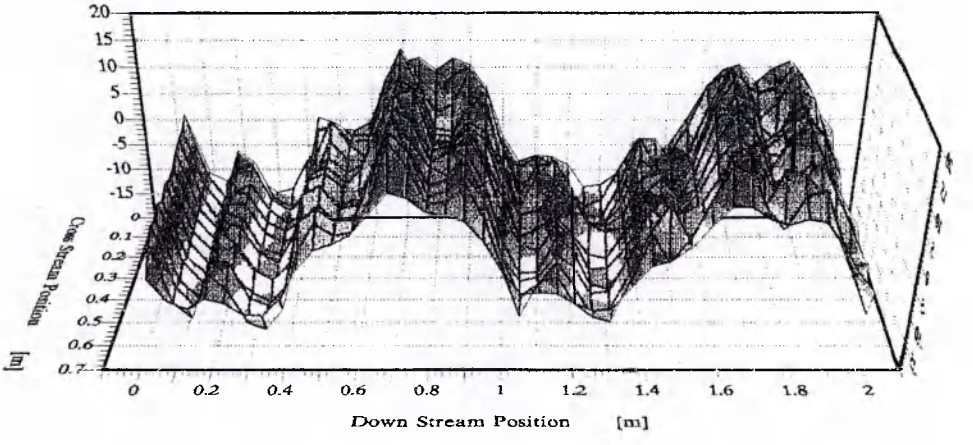

PROFILE 5

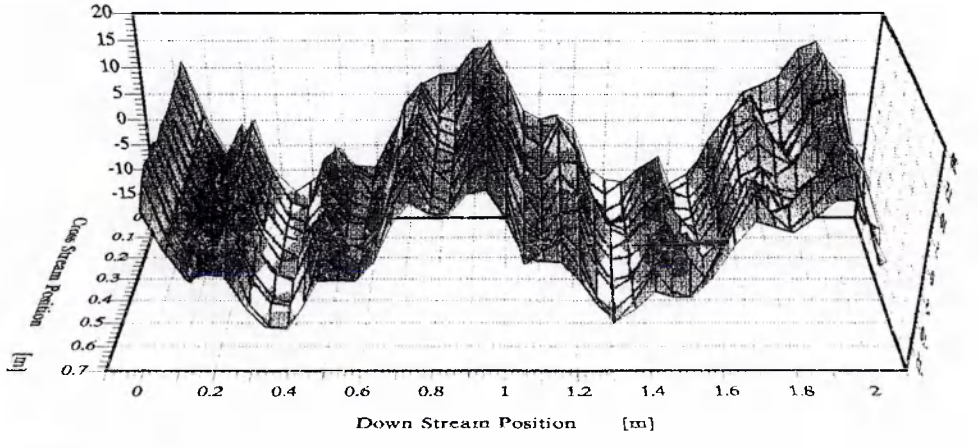

PROFILE 6

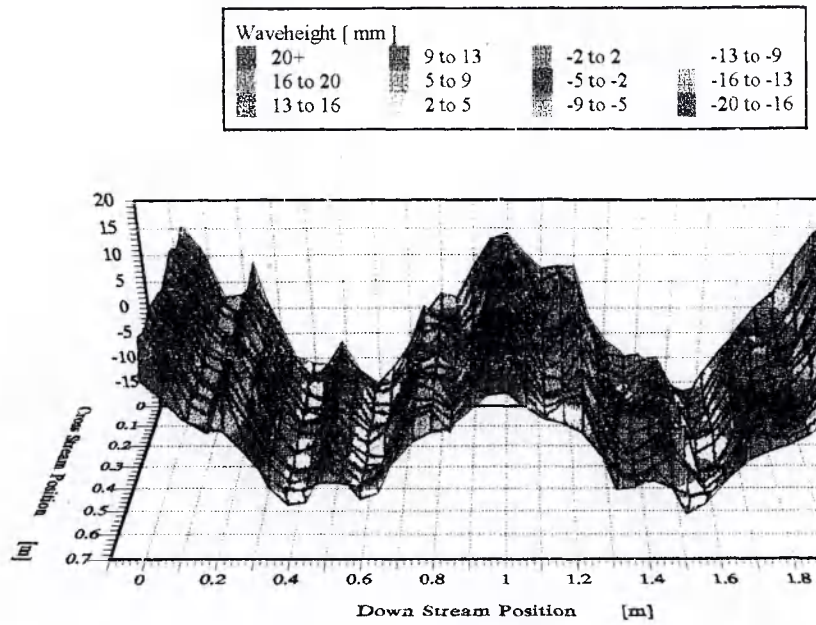

PROFILE 7

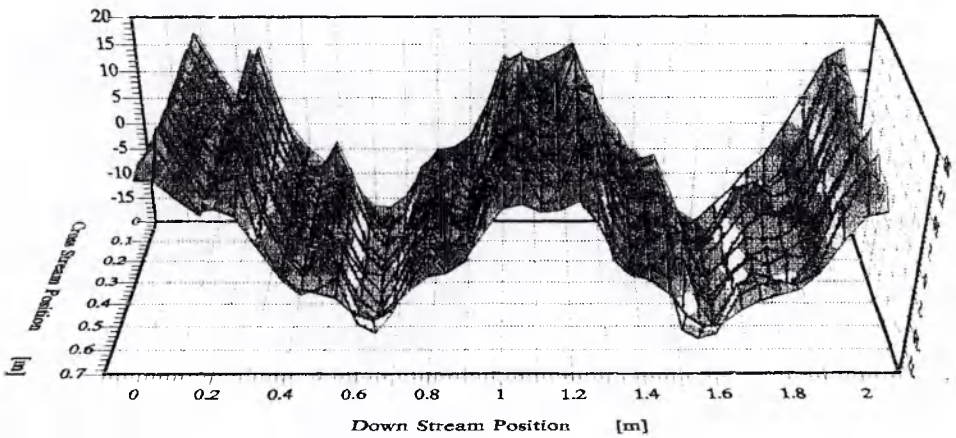

PROFILE 8

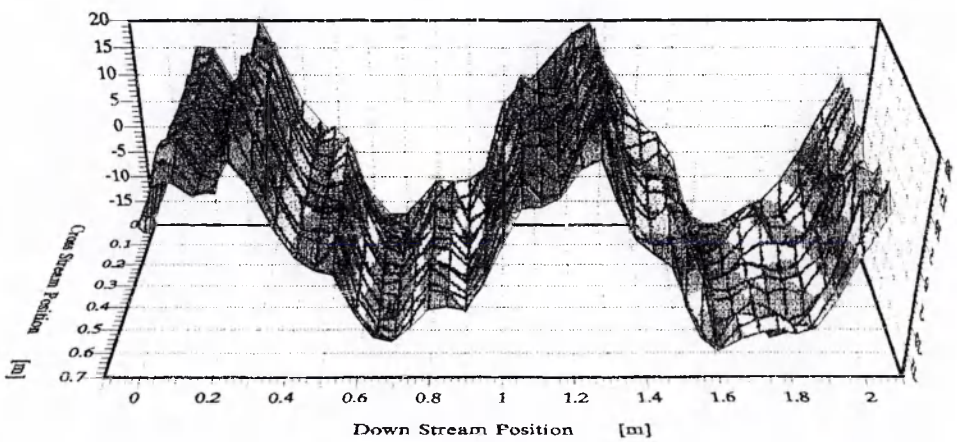

PROFILE 9

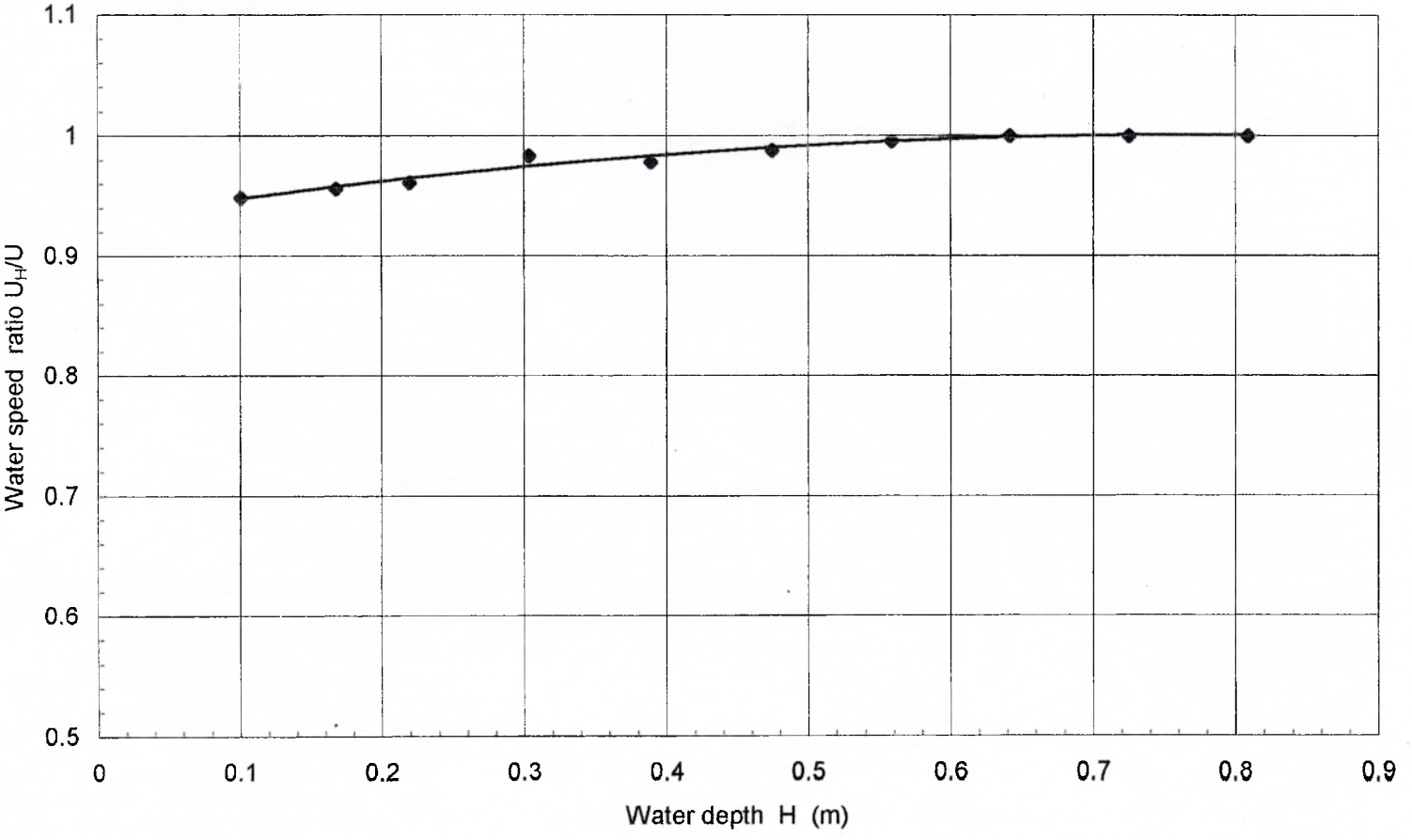

Fig. 26 The effect of reducing the water depth on the water speed

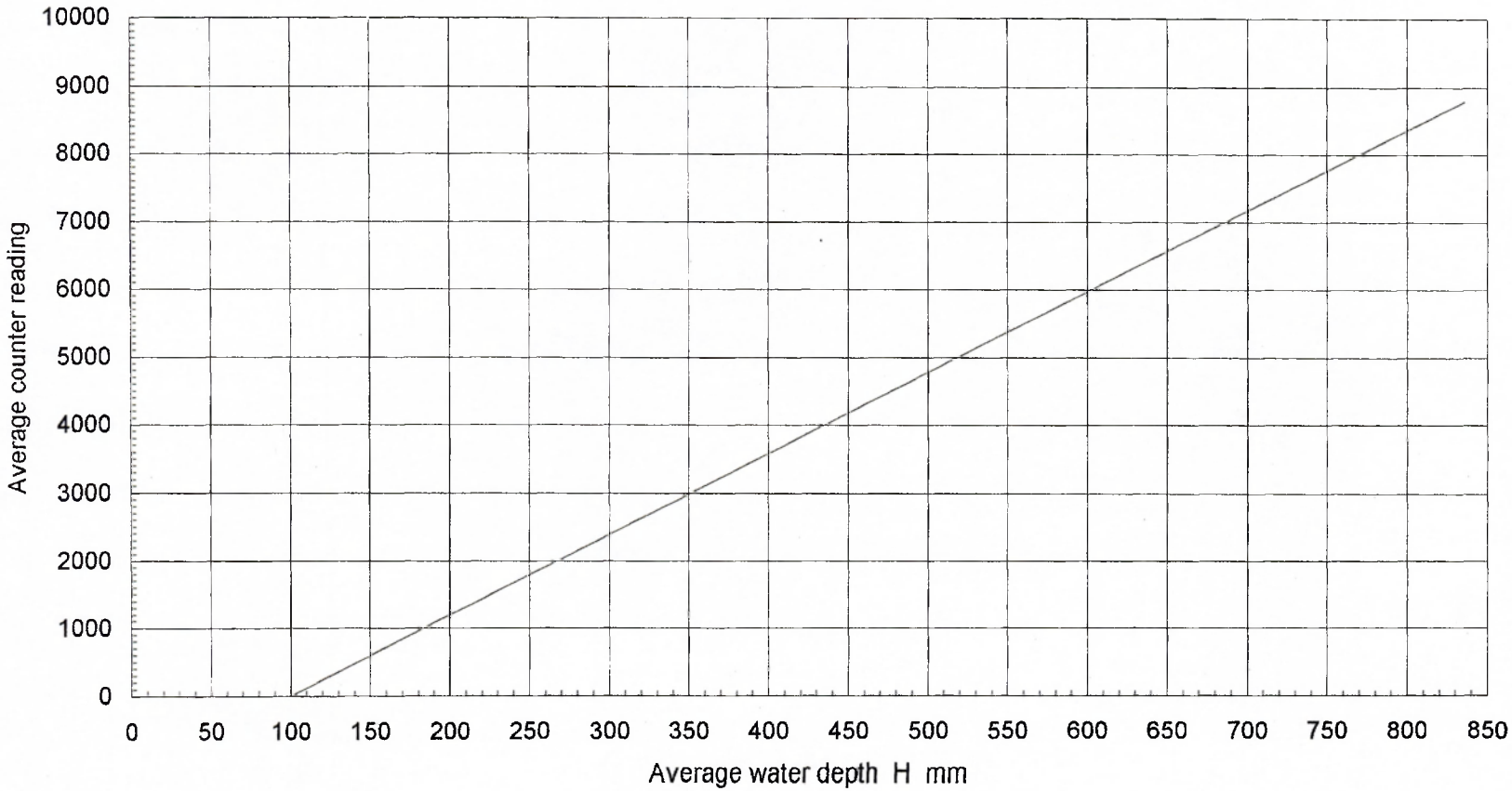

Fig. 27 Water depth calibration chart

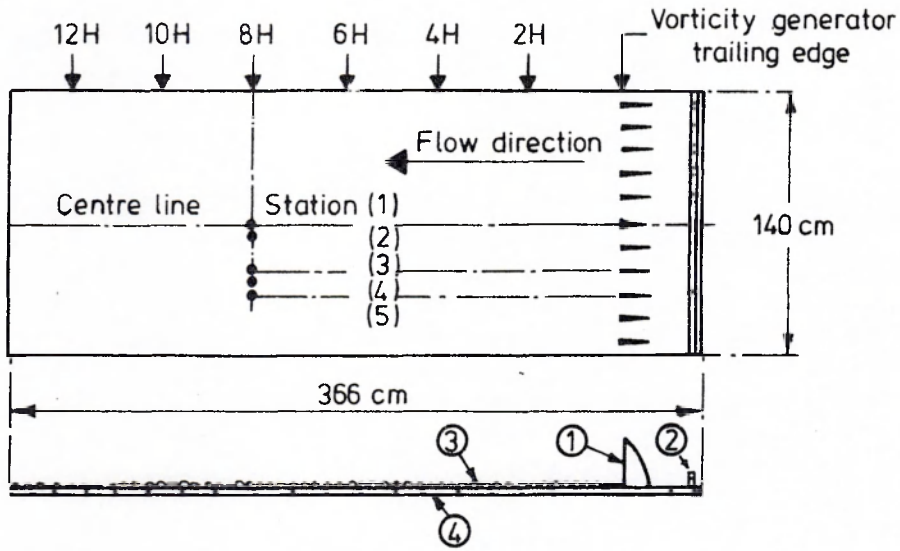

(a) Schematic layout

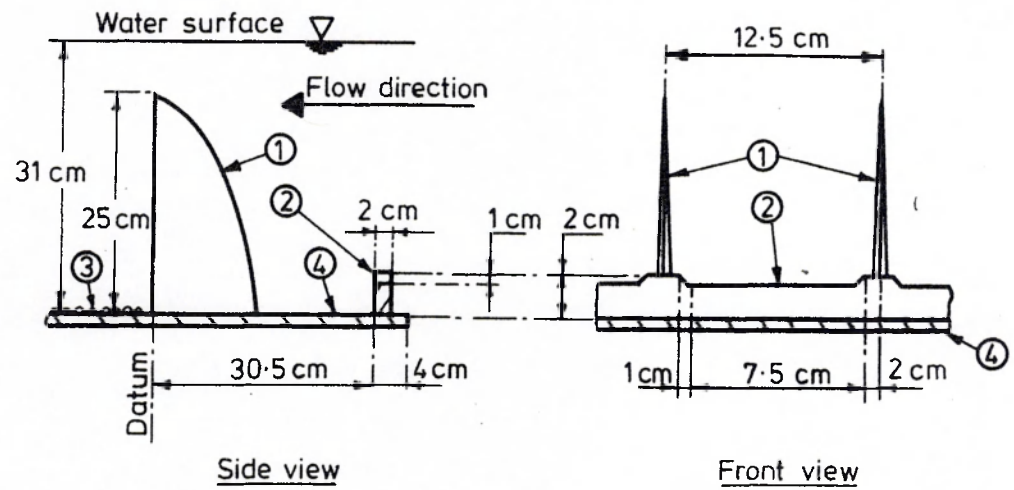

(b) Dimensions of hardware

Fig: 28 The artificial boundary layer system

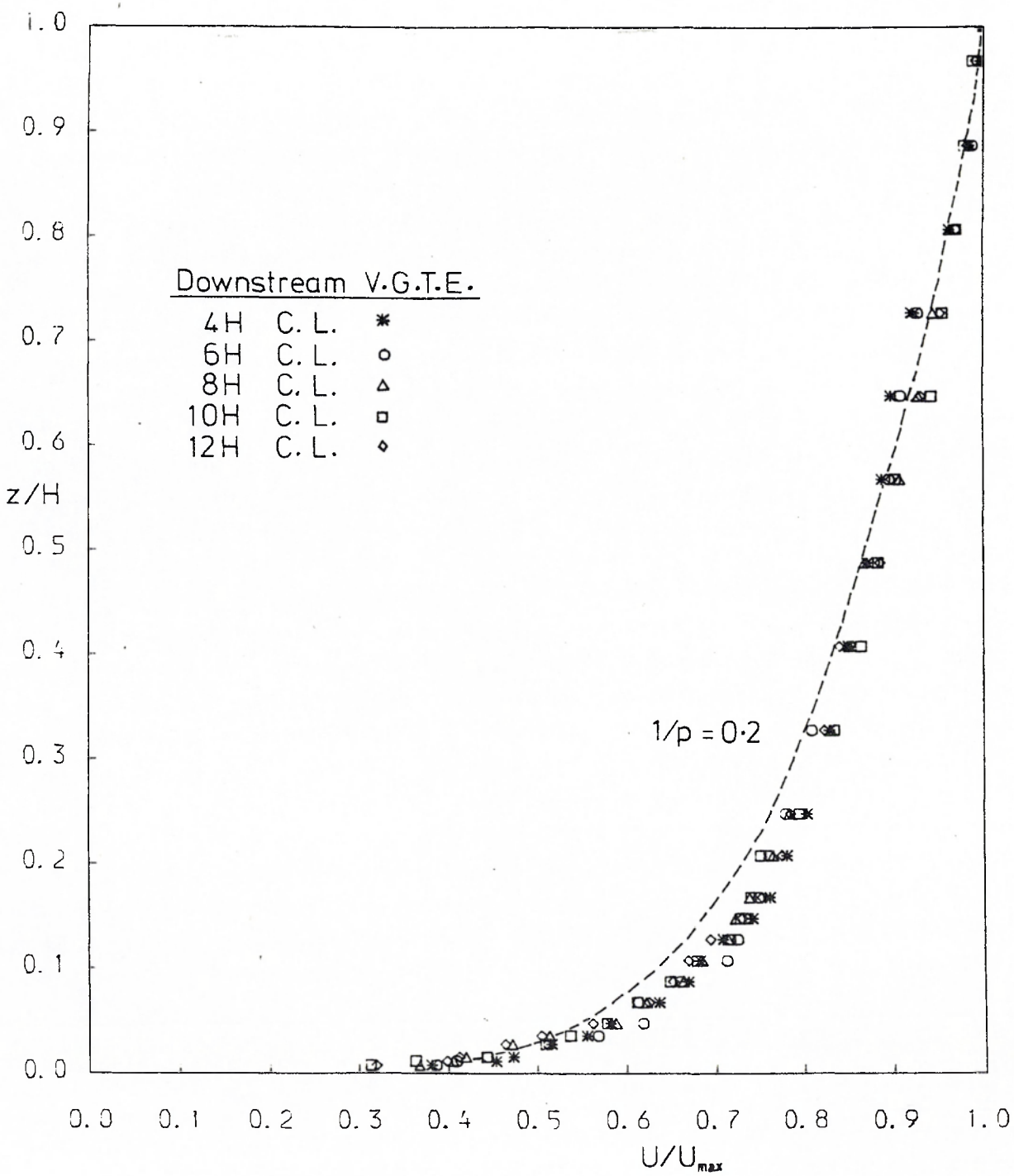

Fig. 29 The velocity distribution in the artificial boundary layer

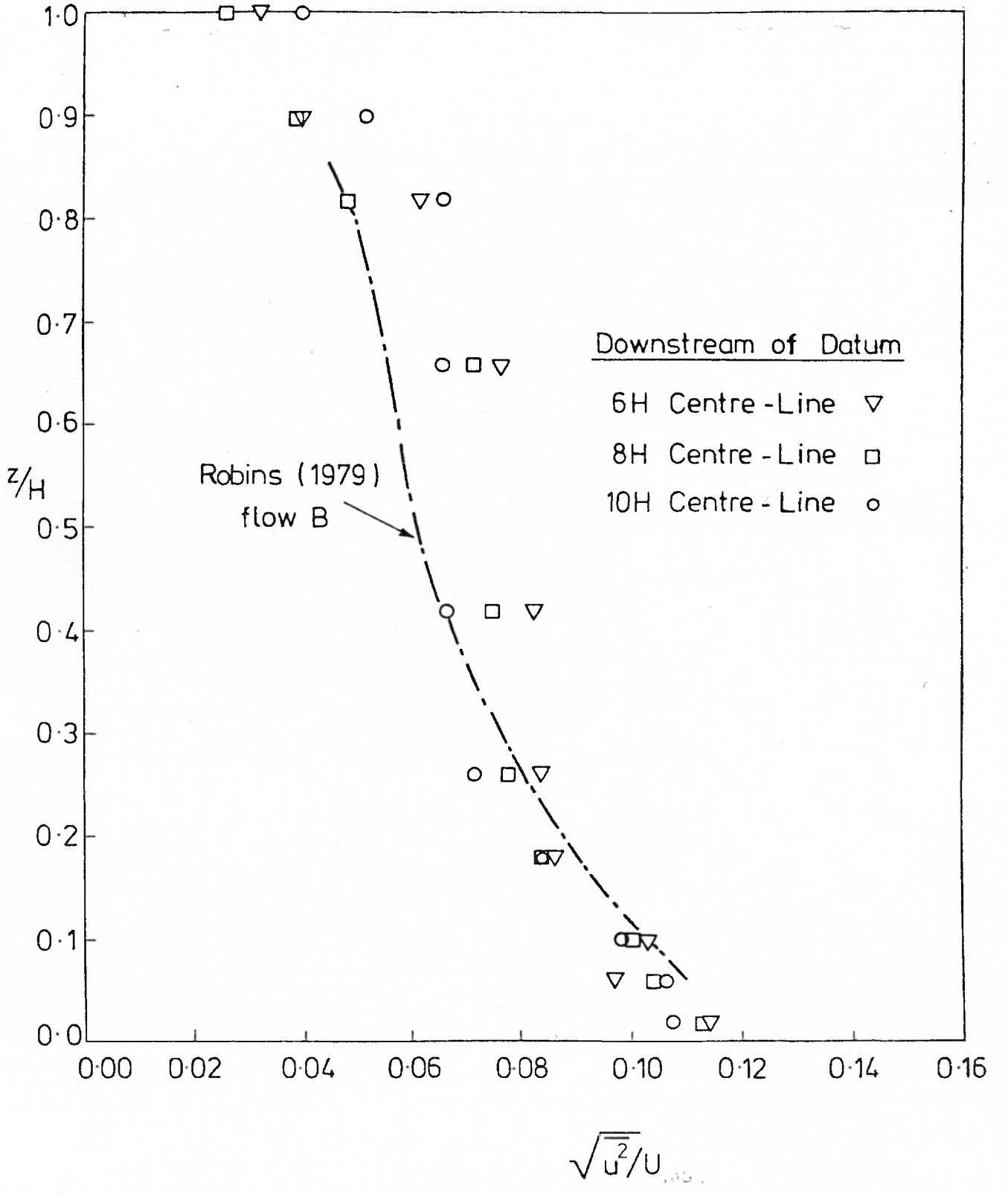

Fig. 30 The turbulent velocity distribution in the artificial boundary layer

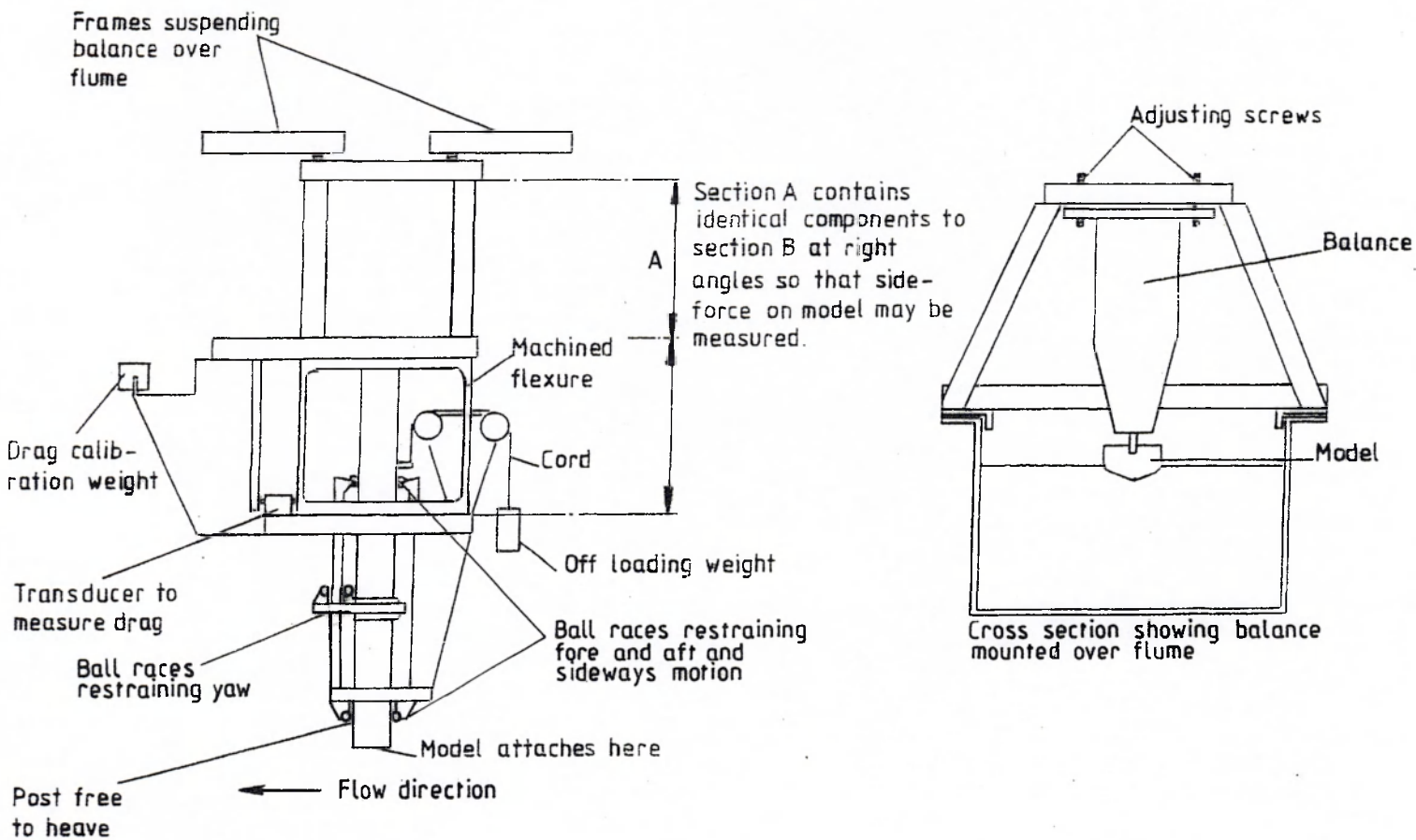

Fig. 31 Schematic diagram of the dynamometer

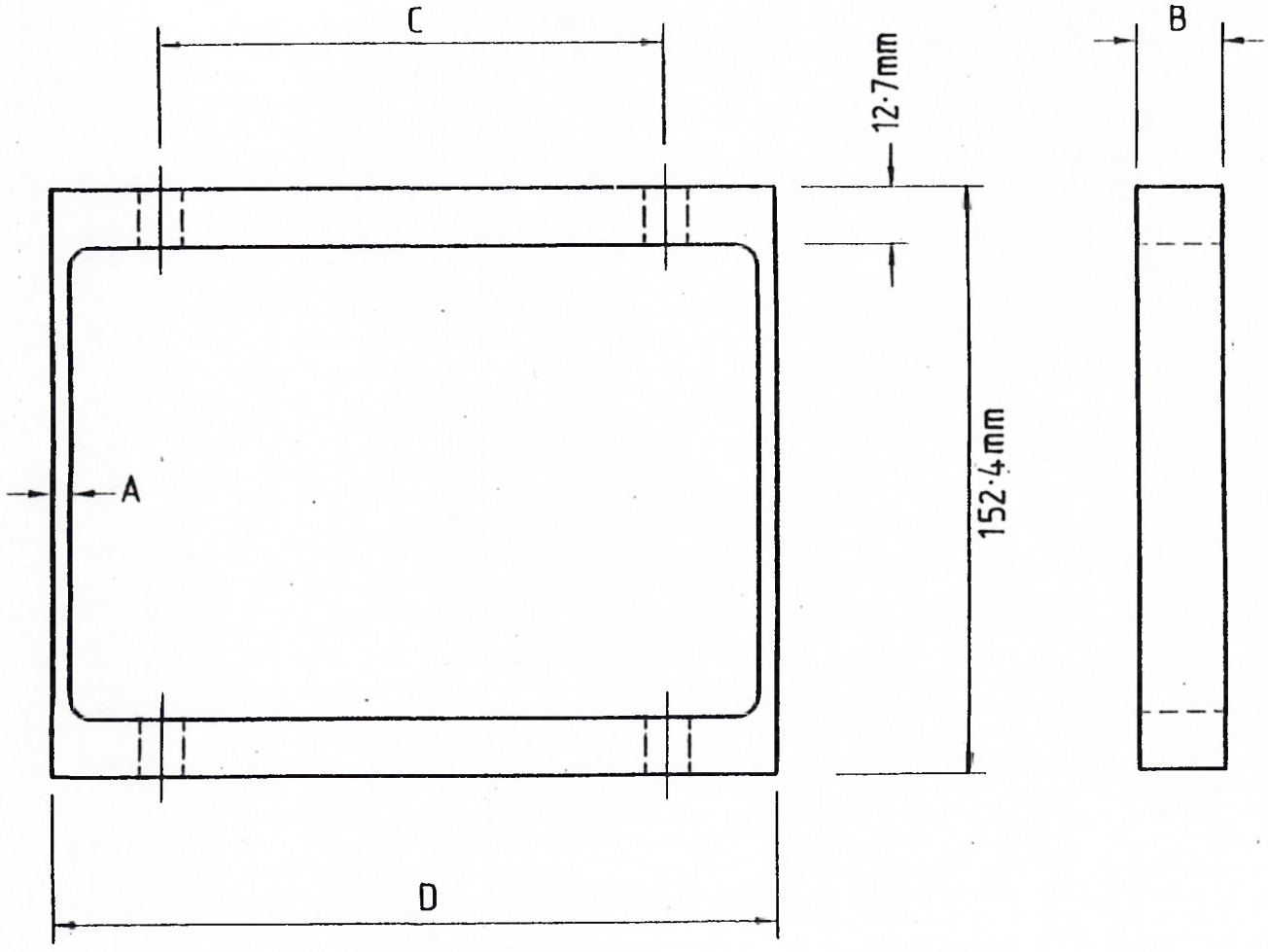

	Resistance	Side Force
A	1.65 mm	2.16 mm
B	12.7 mm	19.1 mm
C	914.4 mm	203.2 mm
D	190.5 mm	241.3 mm

Fig. 32 Diagram of the dynamometer flexures

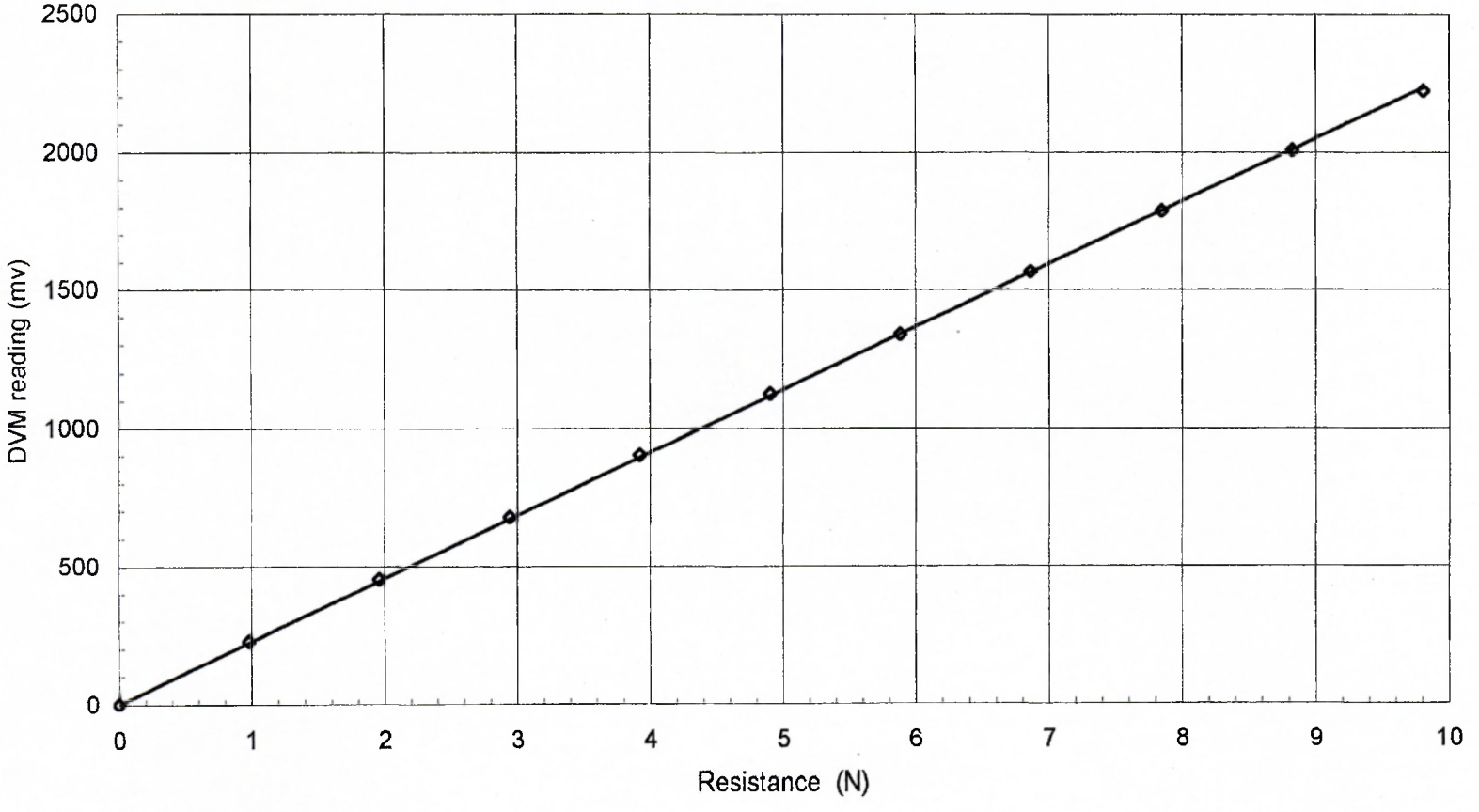

Fig. 33 A typical calibration of the resistance arm of the dynamometer

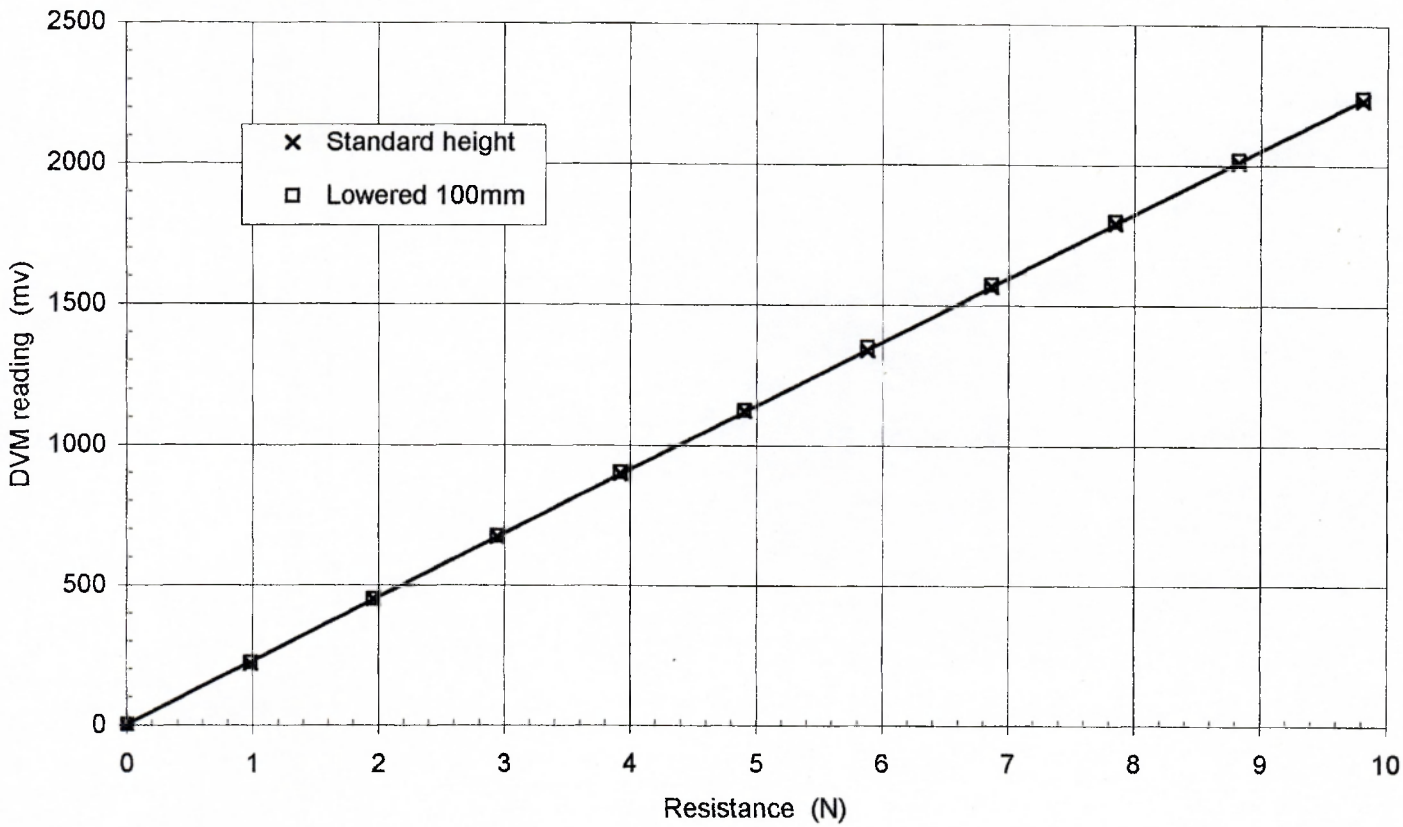

Fig. 34 Direct calibration of the resistance dynamometer

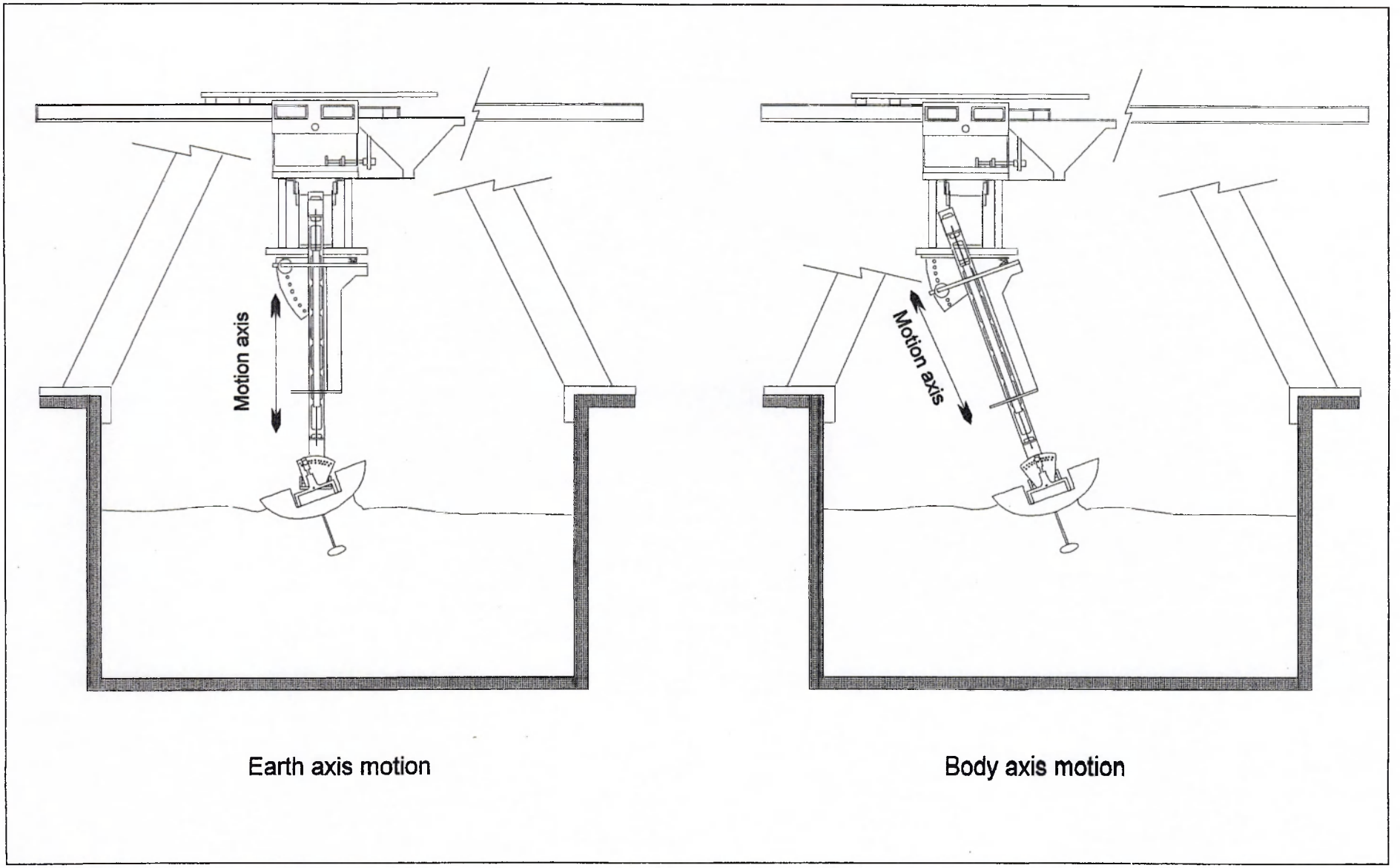

Fig. 35 General concept of the dynamometer modified for the motion axes tests

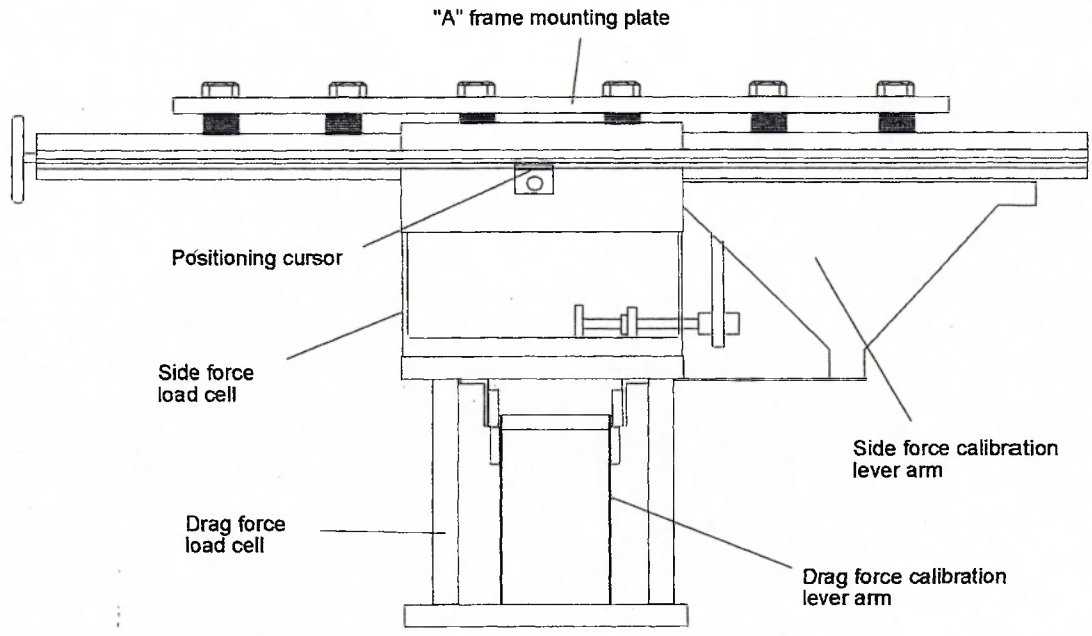

Front elevation

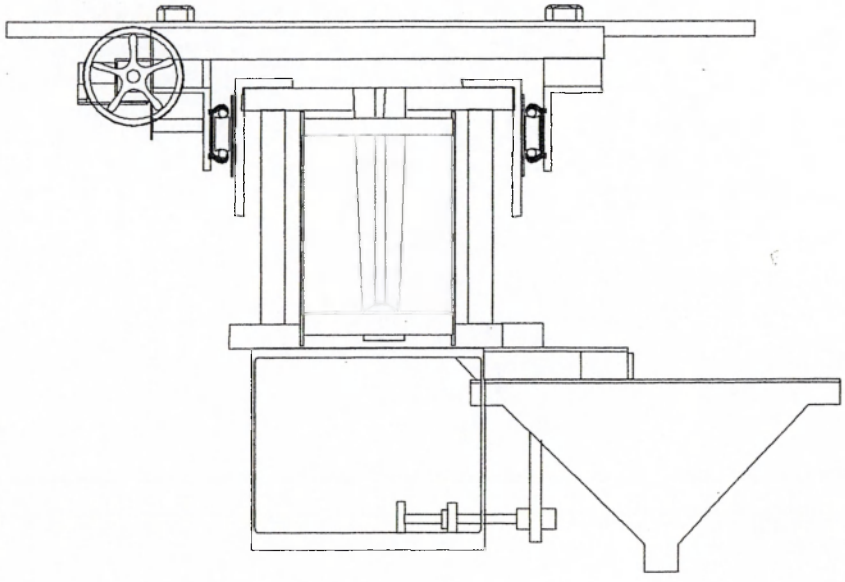

Side elevation

Fig. 36 Assembly drawing of the sliding rail system

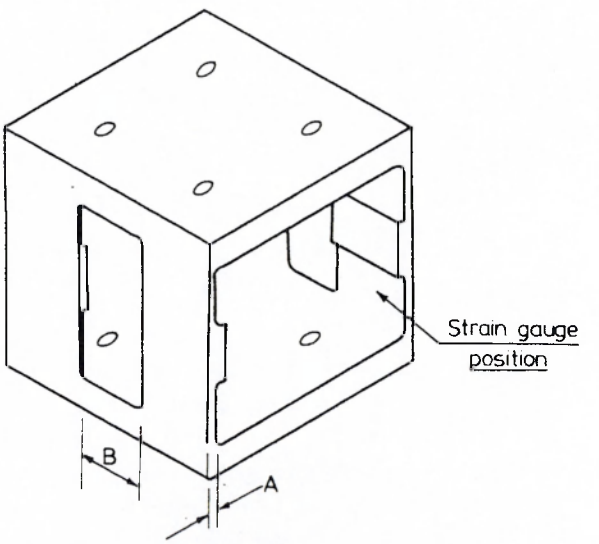

Diagram of force block

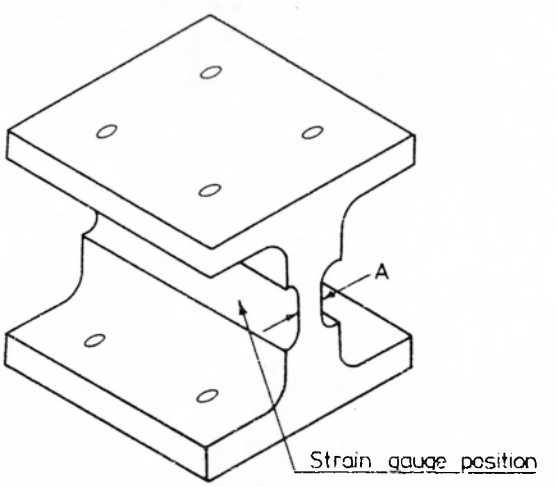

Diagram of moment block

Fig. 37 Schematic diagrams of a force block and a moment block

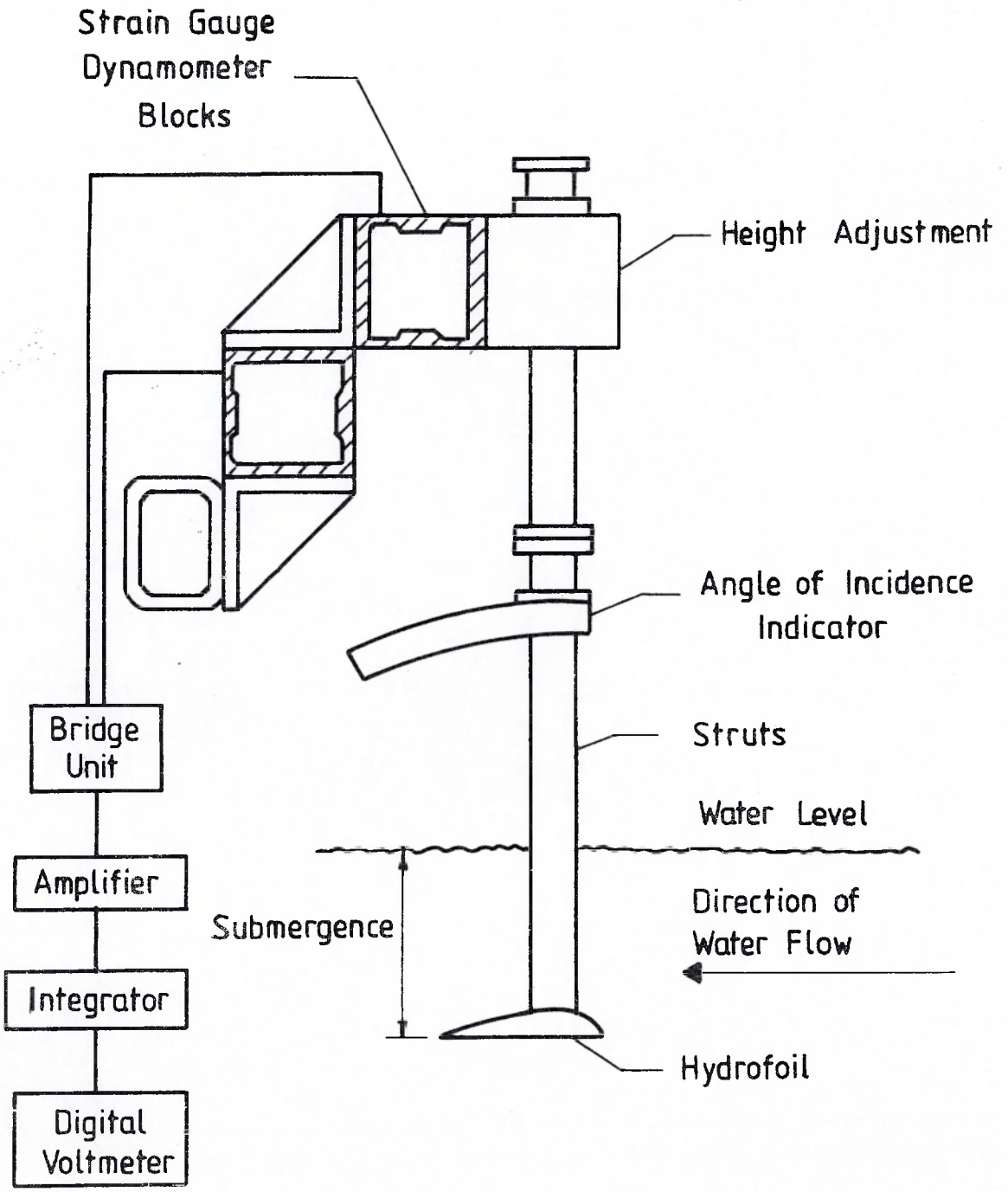

Fig. 38 Schematic diagram of the hydrofoil dynamometer

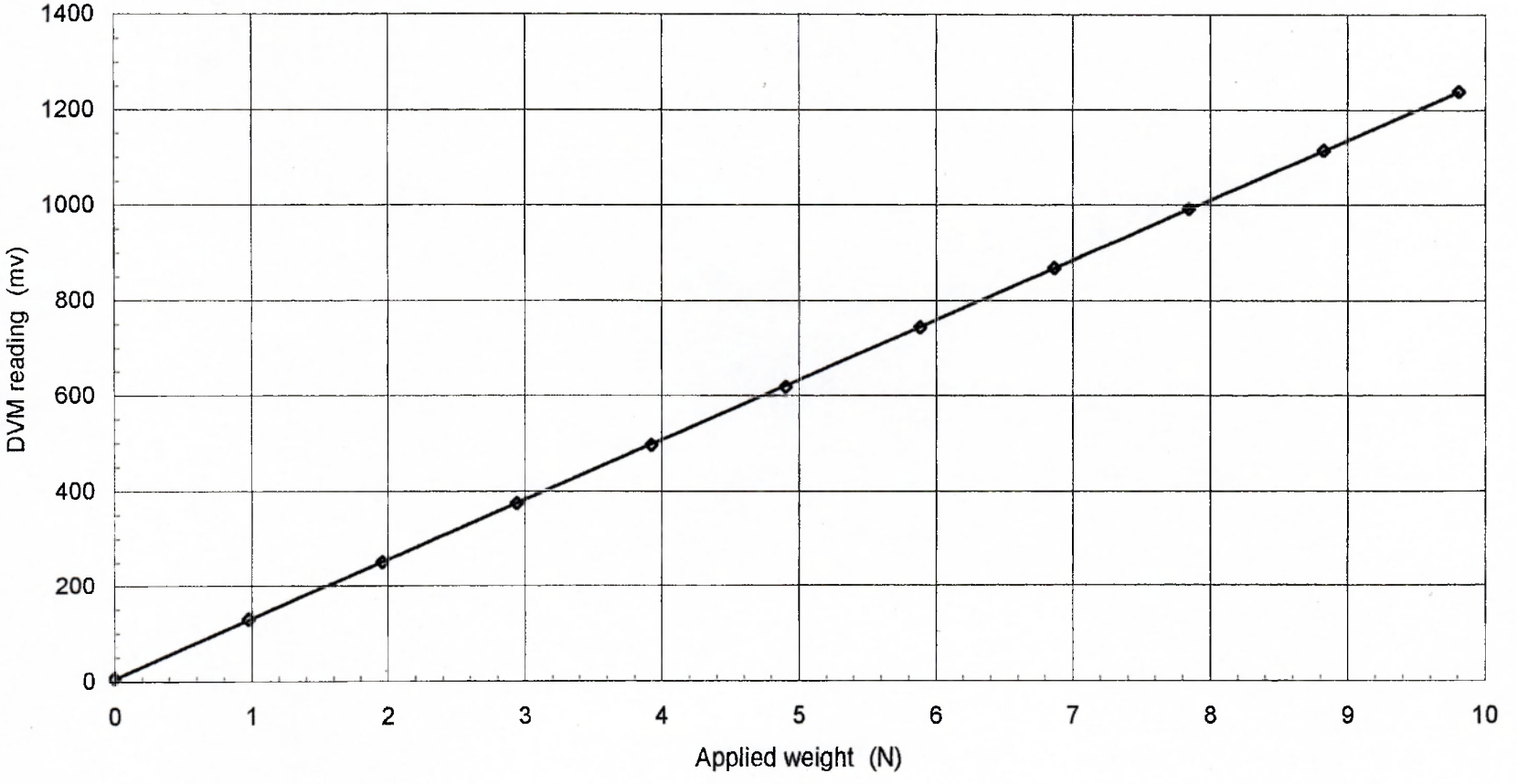

Fig. 39 A typical force block calibration curve

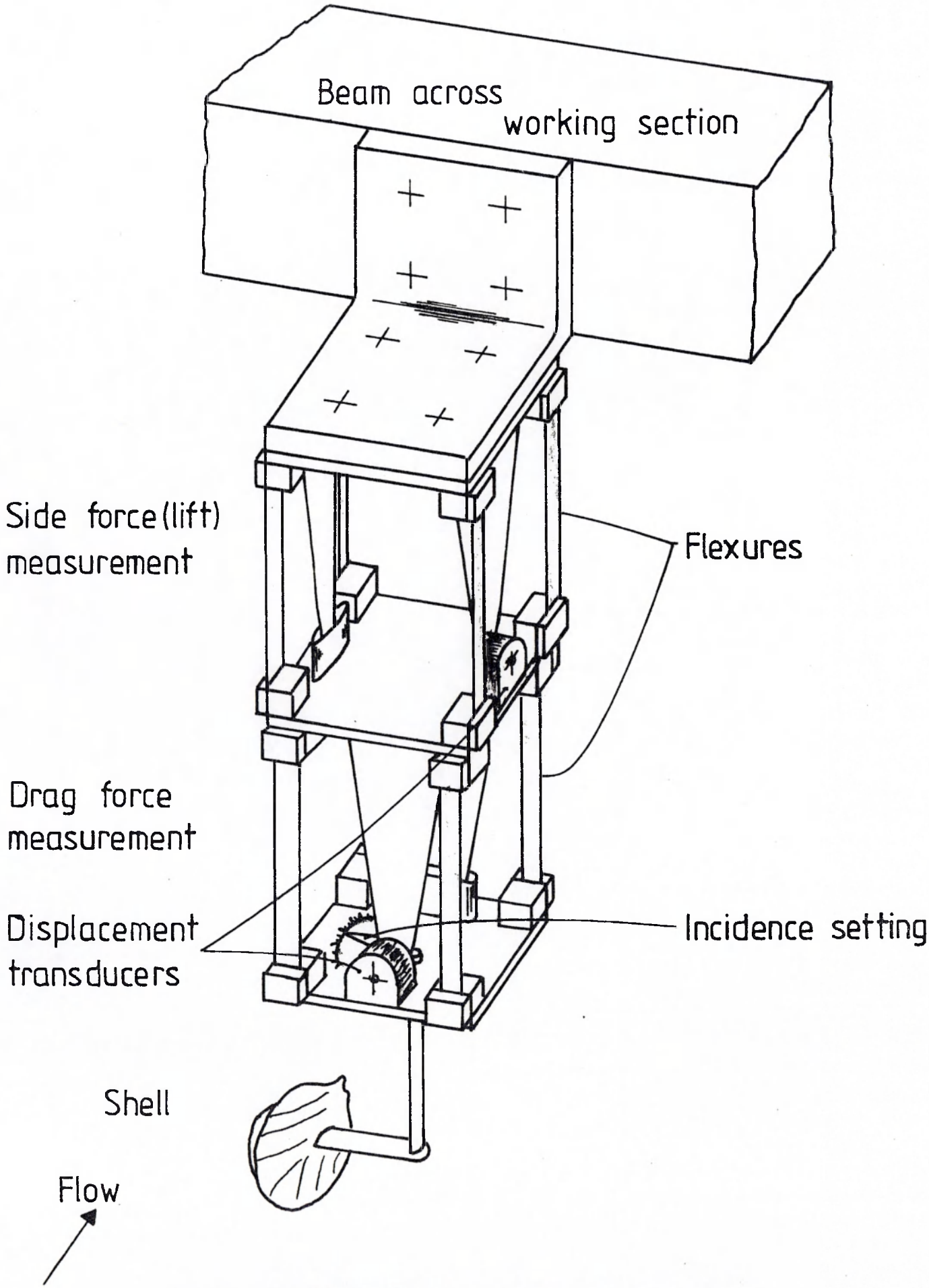

Fig. 40 Schematic diagram of the shell dynamometer

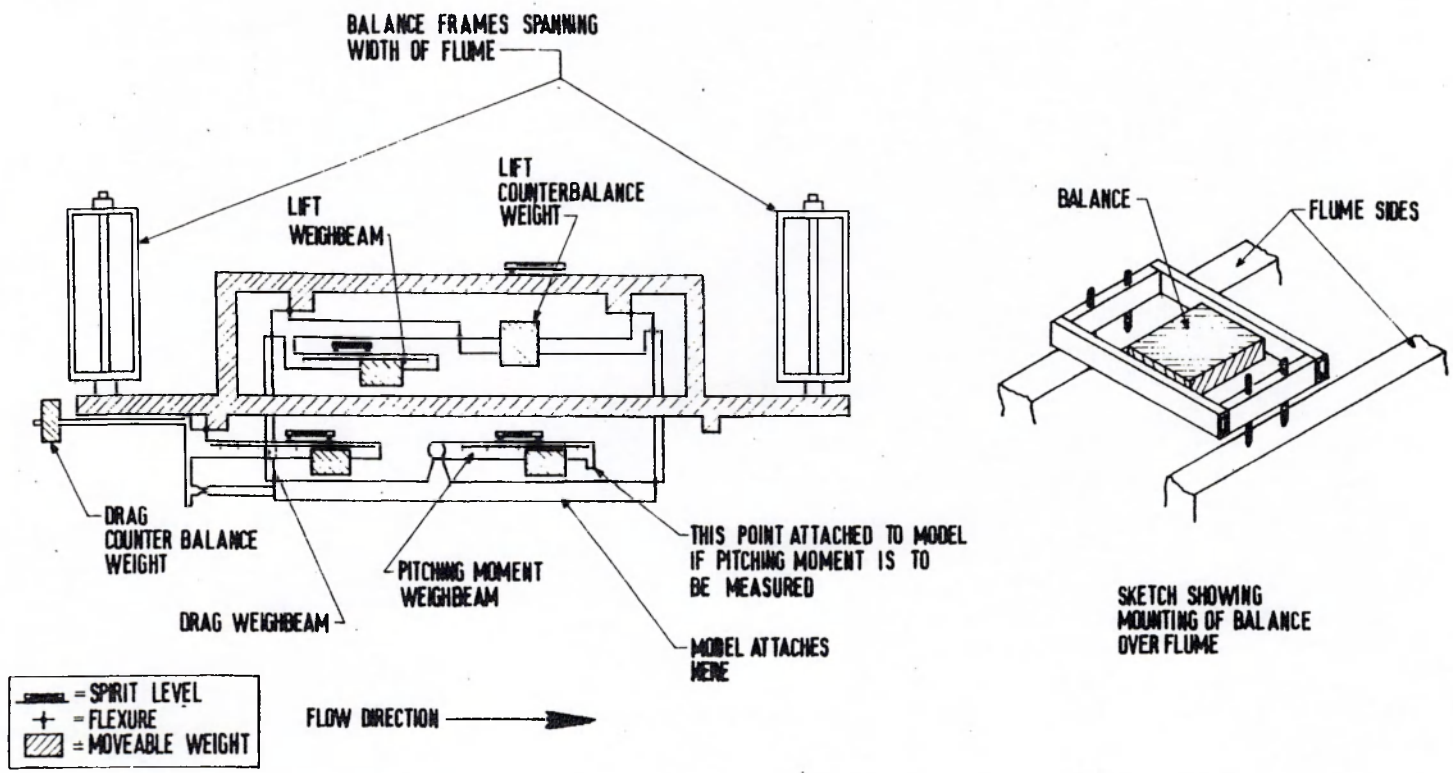

Fig. 41 Schematic diagram of the T.E.M. dynamometer

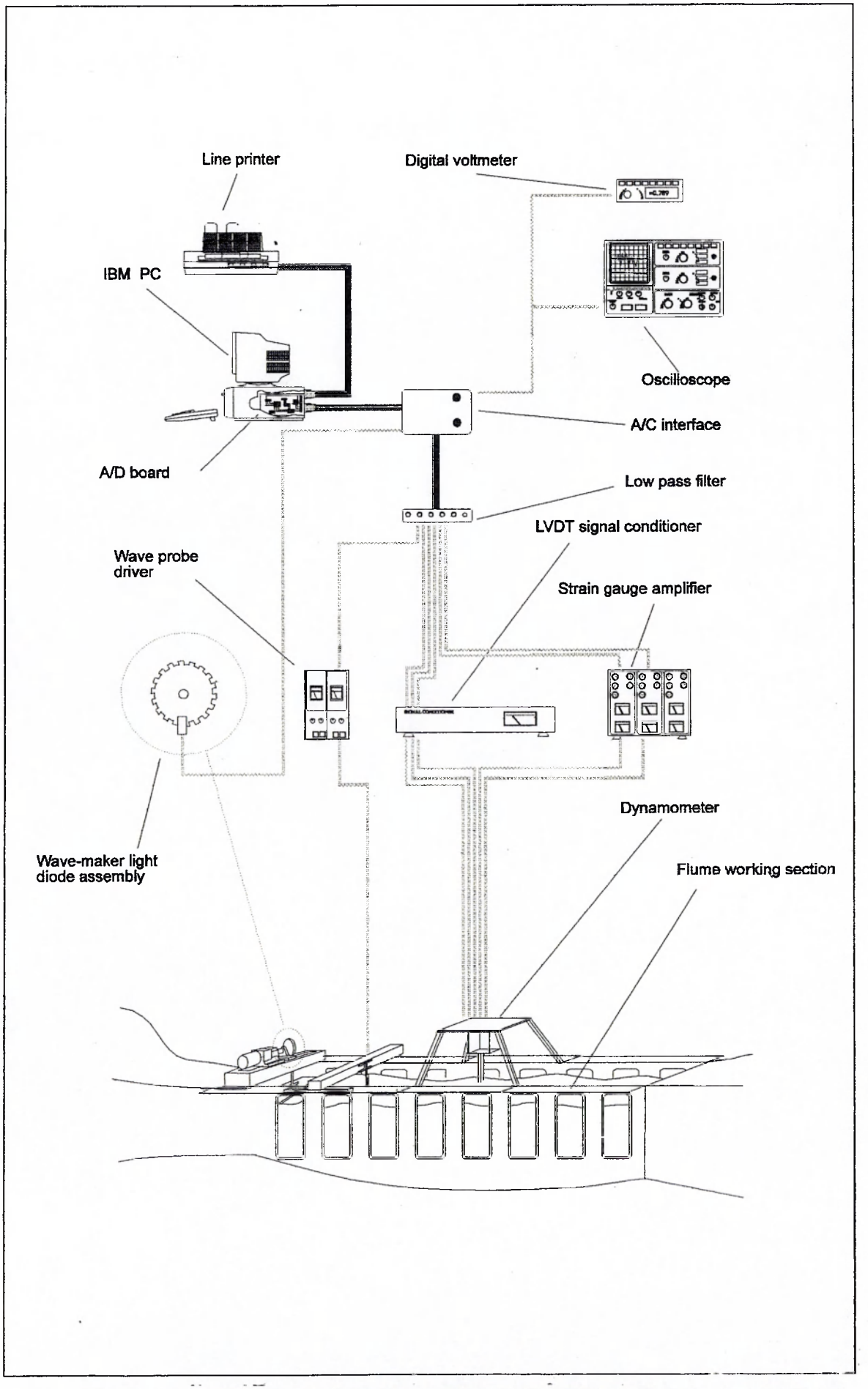

Fig. 42 Schematic diagram of the data collection system for tests of a model in waves

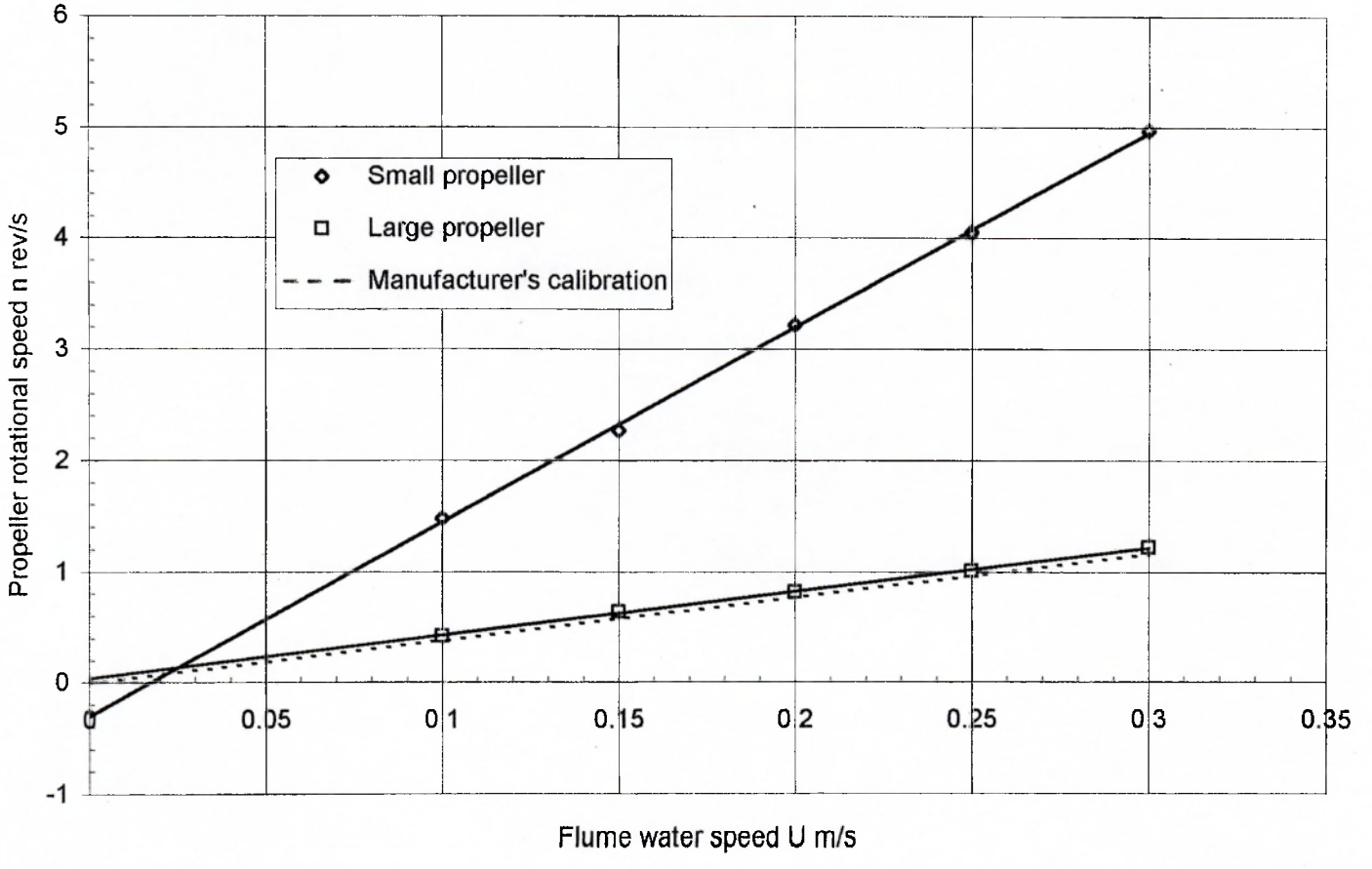

Fig. 43 Calibration curves for the propeller flow meters

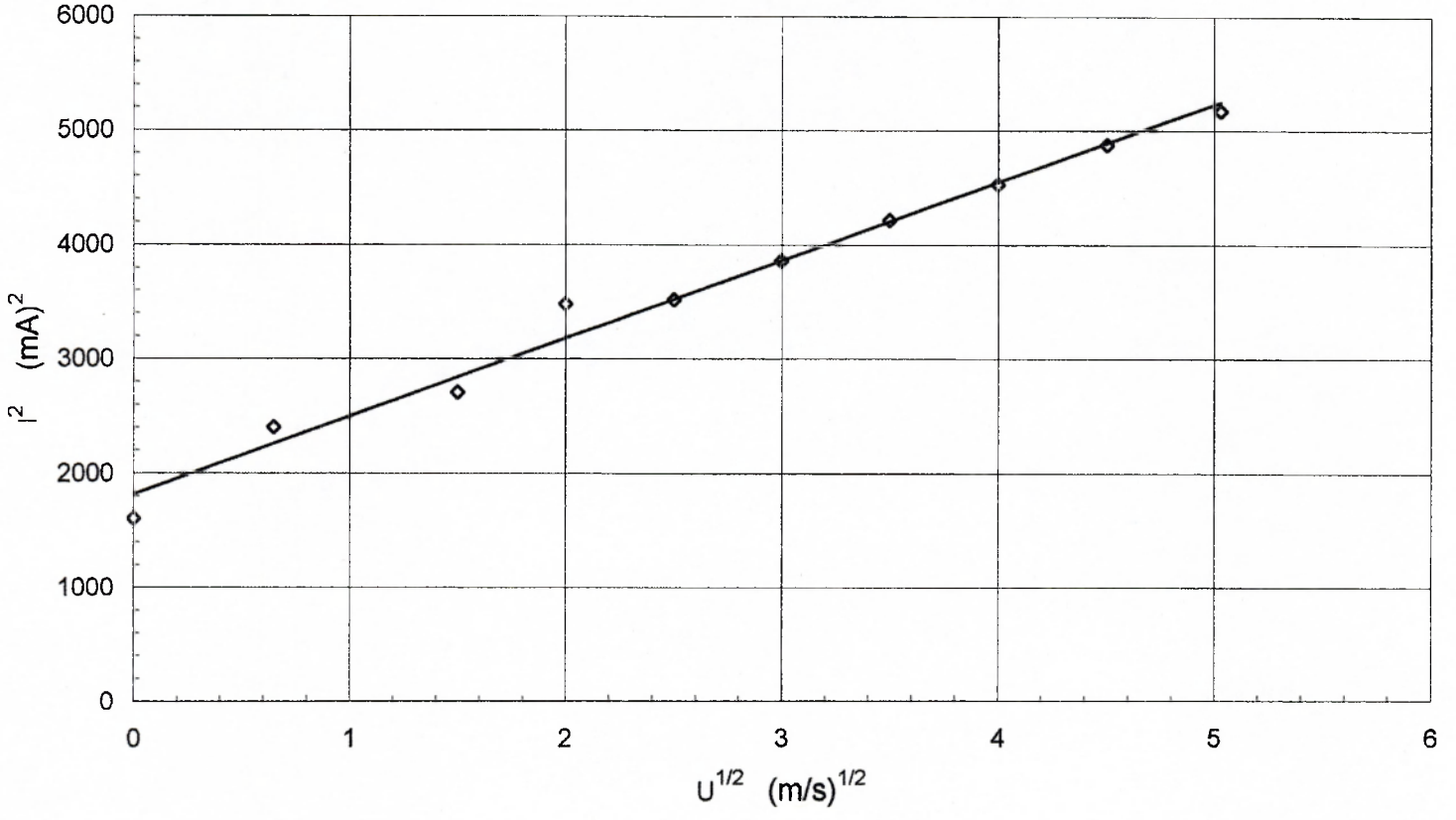

Fig. 44 A calibration curve for a hot wire anemometer in air

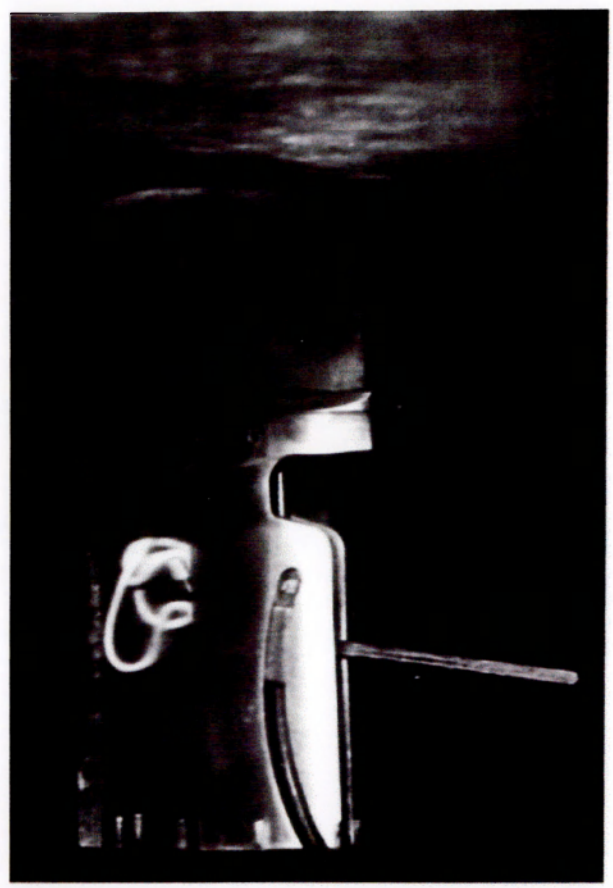

Fig. 45 The flow direction probe (with acrylic cover in place)

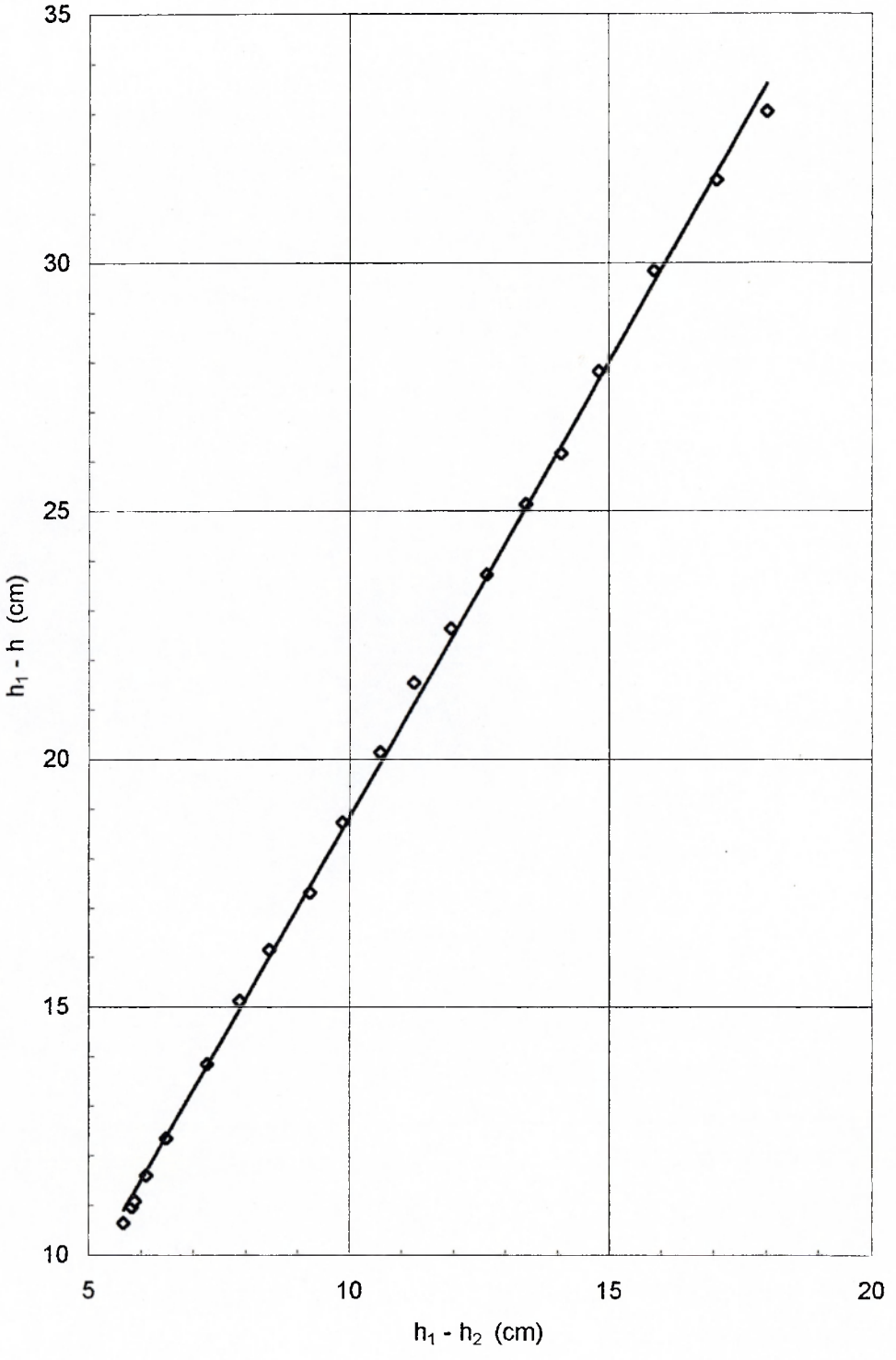

Fig. 46 Calibration curve for the yaw probe

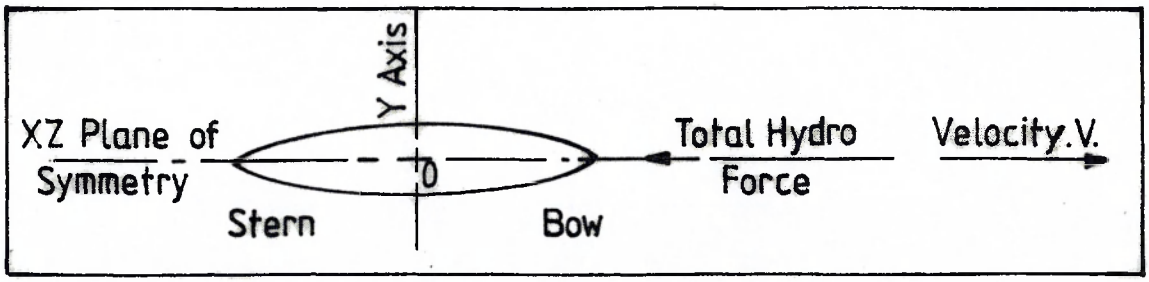

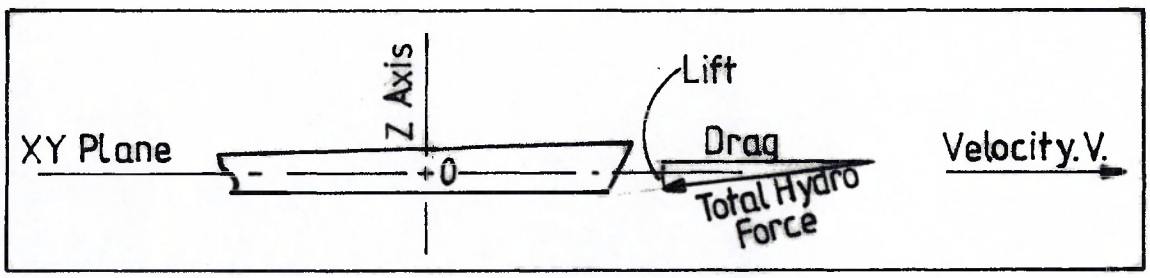

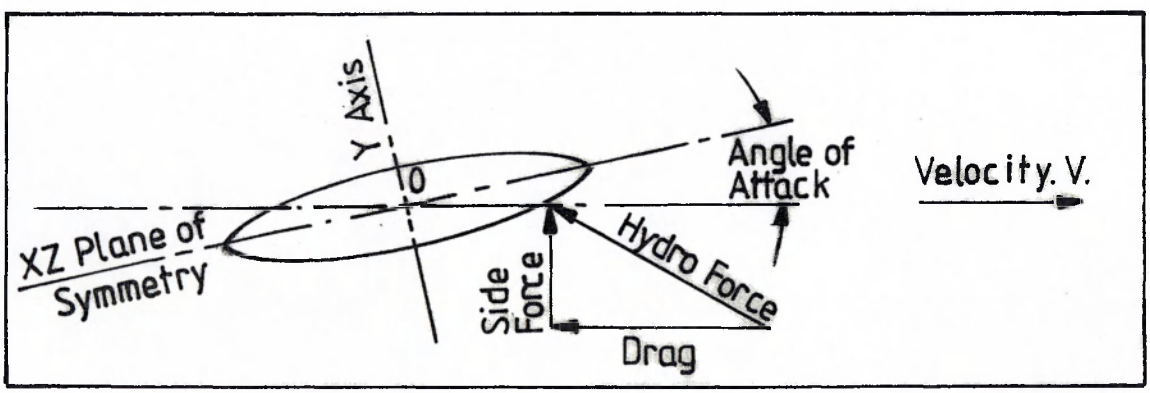

Fig. 47 The hydrodynamic forces on different types of vessel

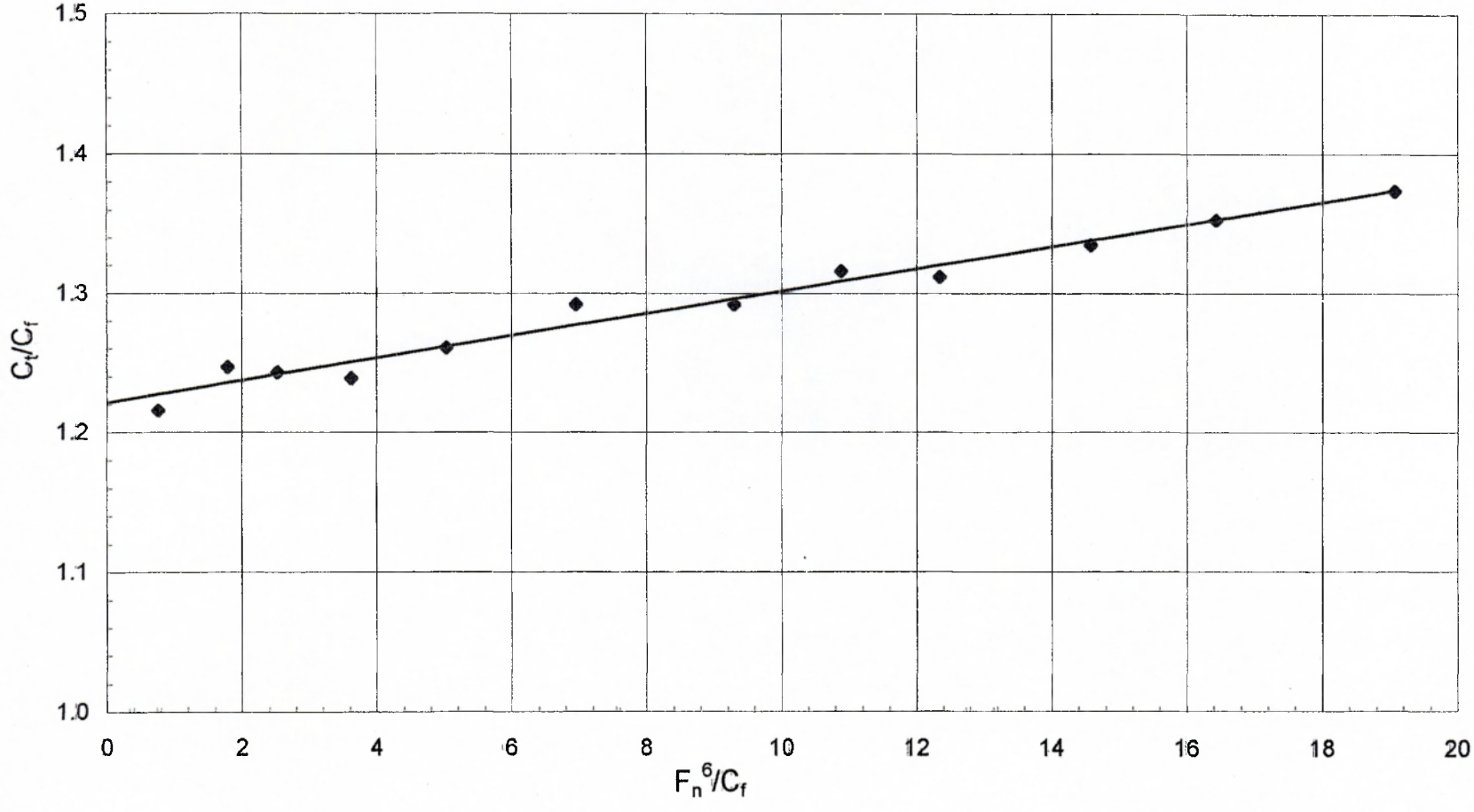

Fig. 48 A graph of resistance data to obtain the form factor using the Prohaska method

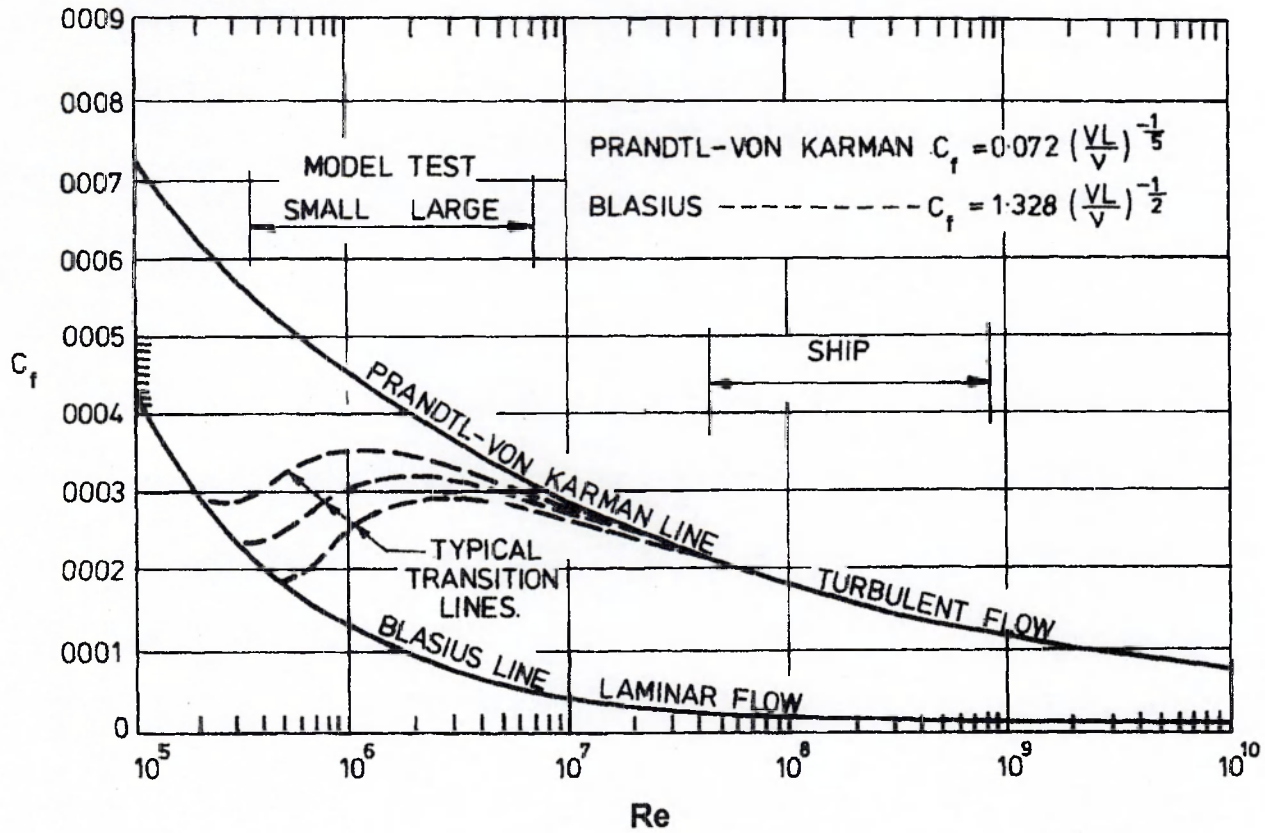

Fig. 49 Laminar and turbulent friction curves

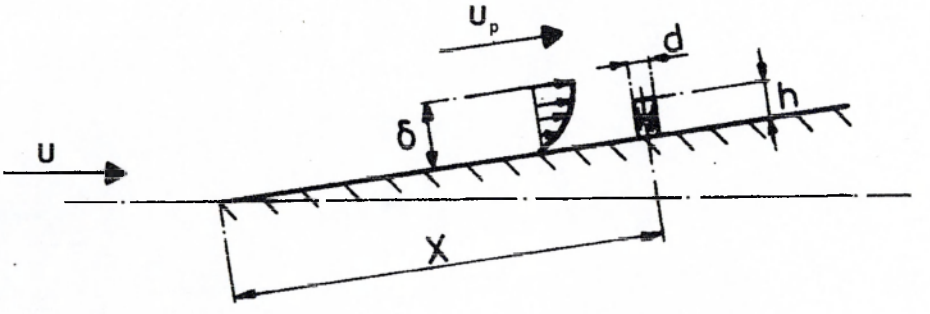

Fig. 50 A turbulence stud in a boundary layer

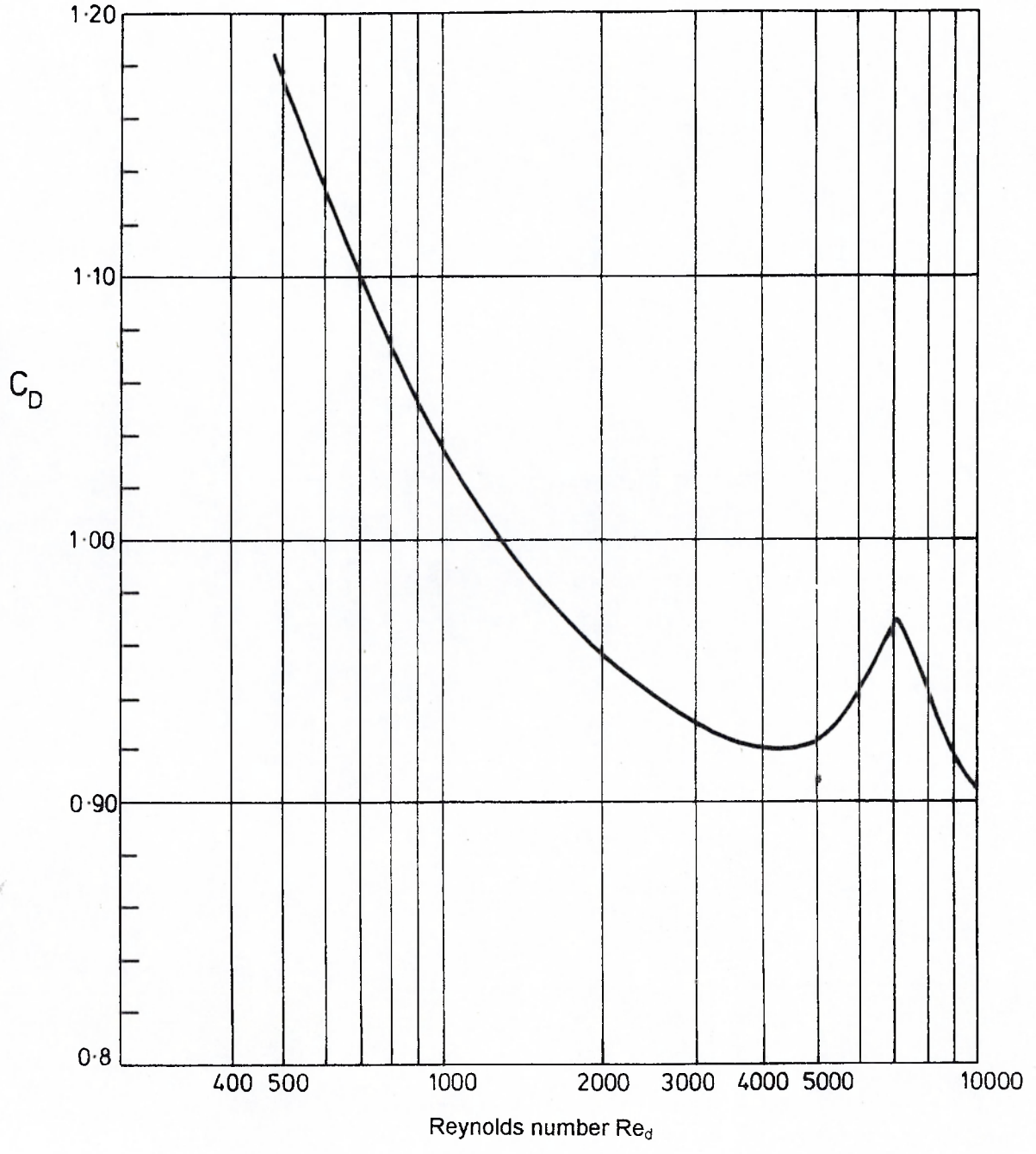

Fig. 51 The variation of stud drag coefficient with Reynolds number

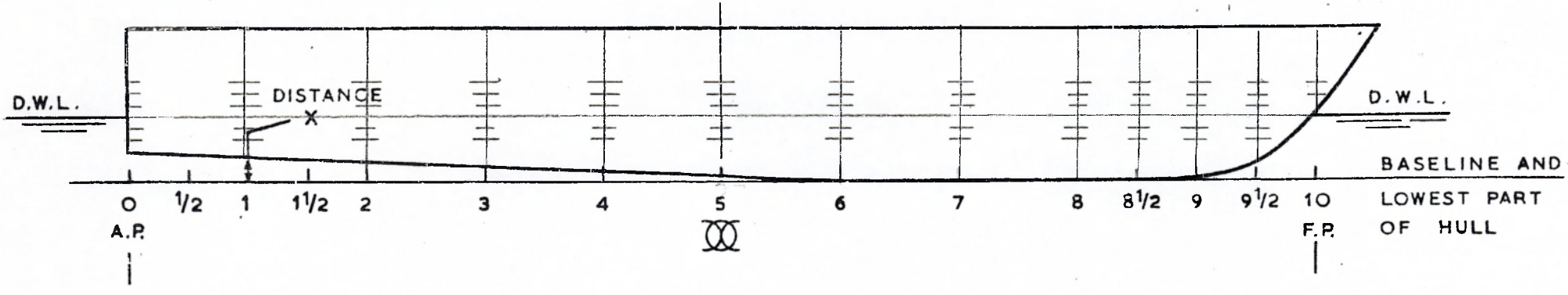

Fig. 52 Diagram of a hull to show the stations and water-lines

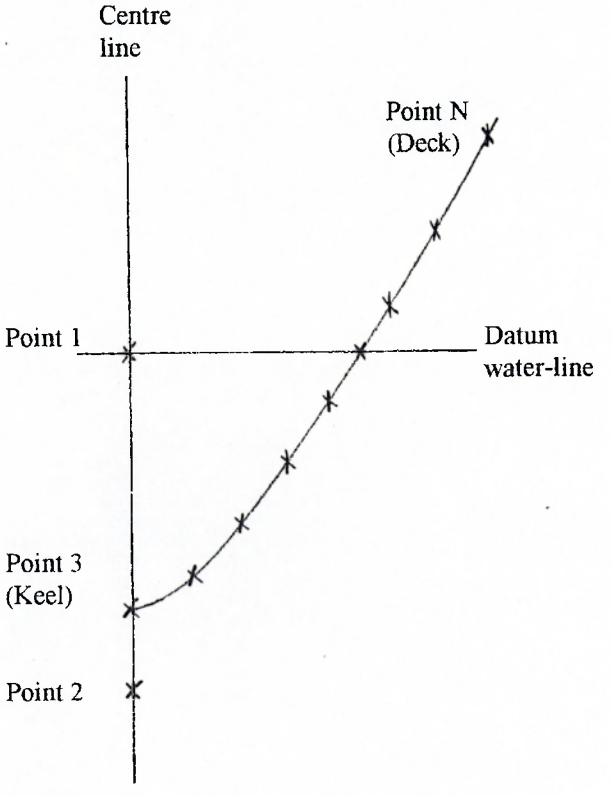

Fig. 53 The sequence for digitising the hull cross-section

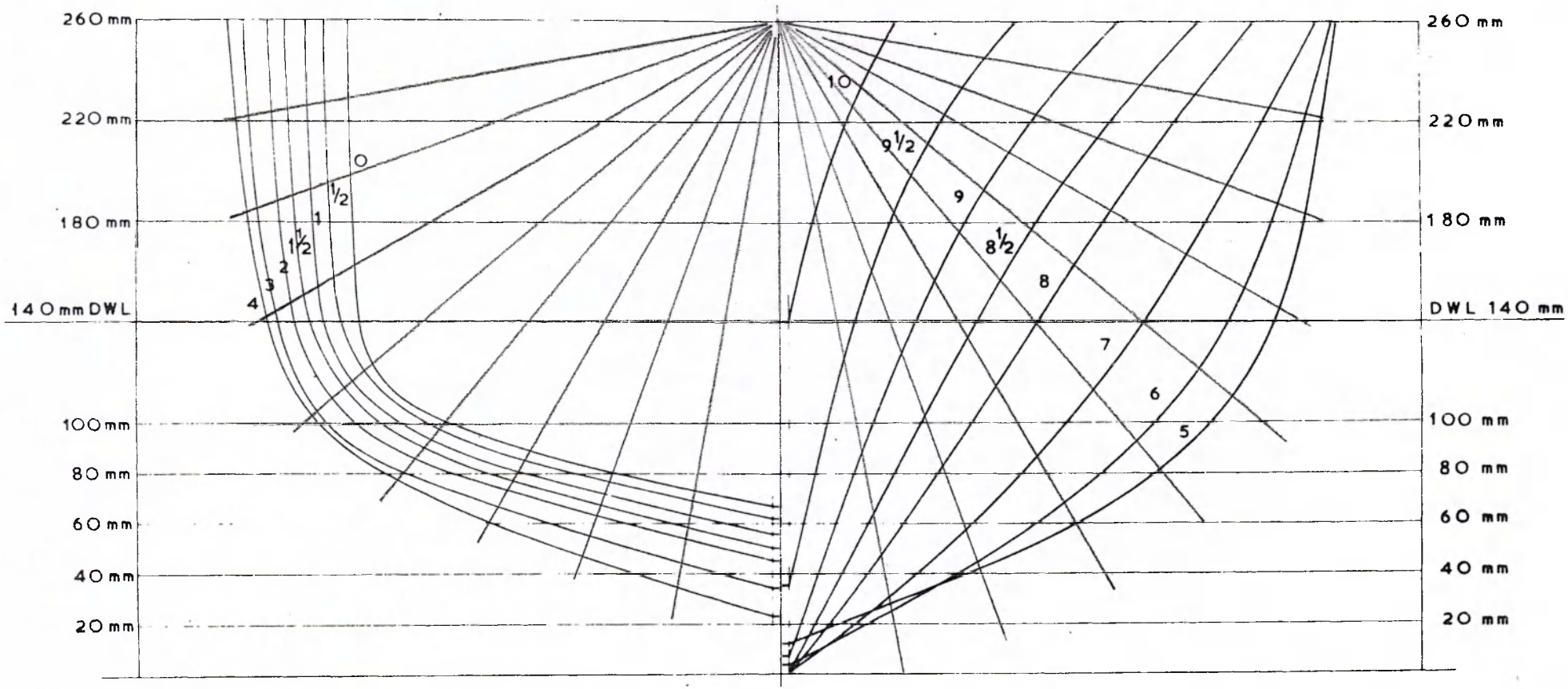

Fig. 54 Diagram of a hull's cross-sections to show the digitisation procedure

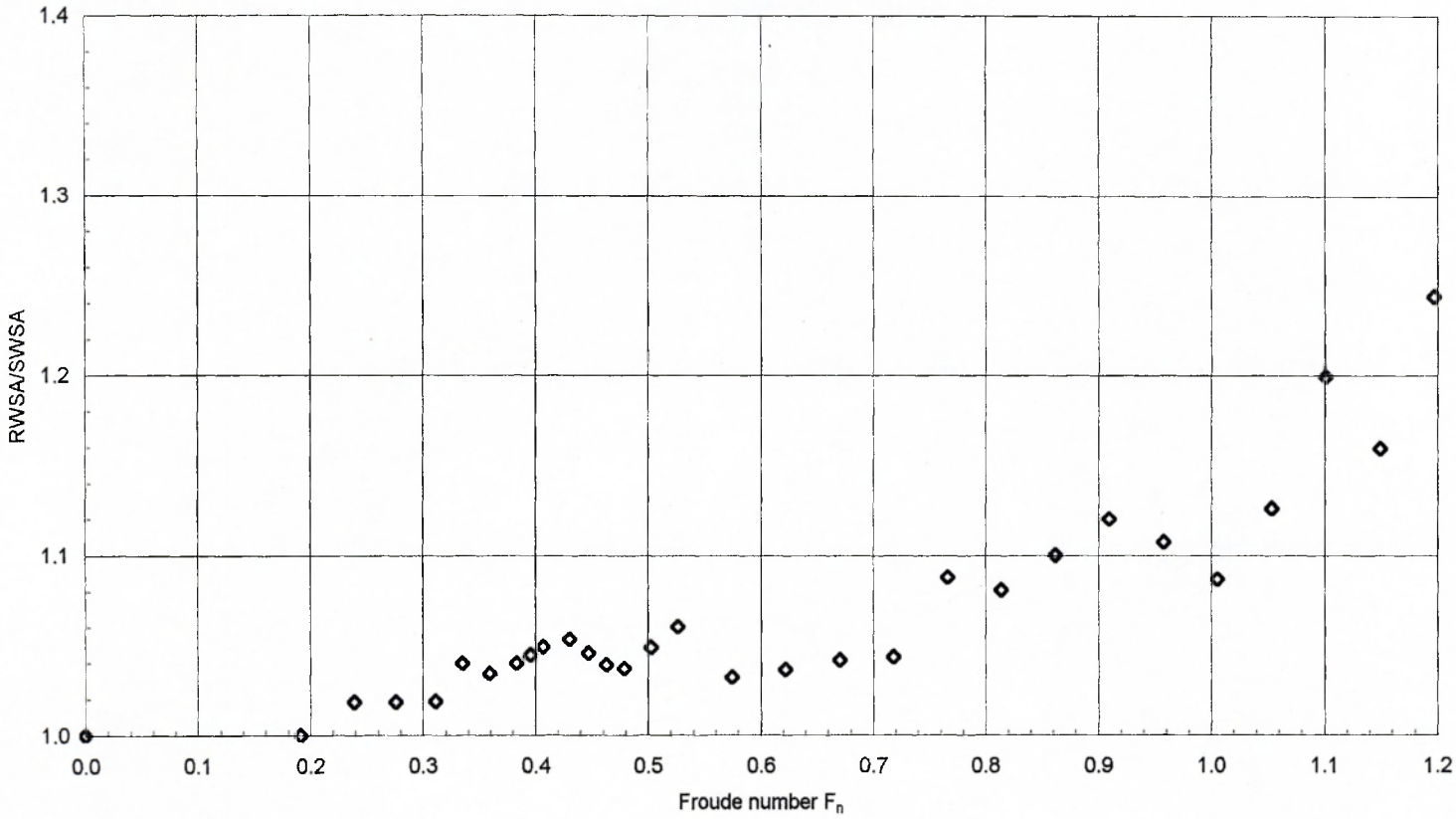

Fig. 55 The variation of actual wetted surface area with speed for an NPL hull

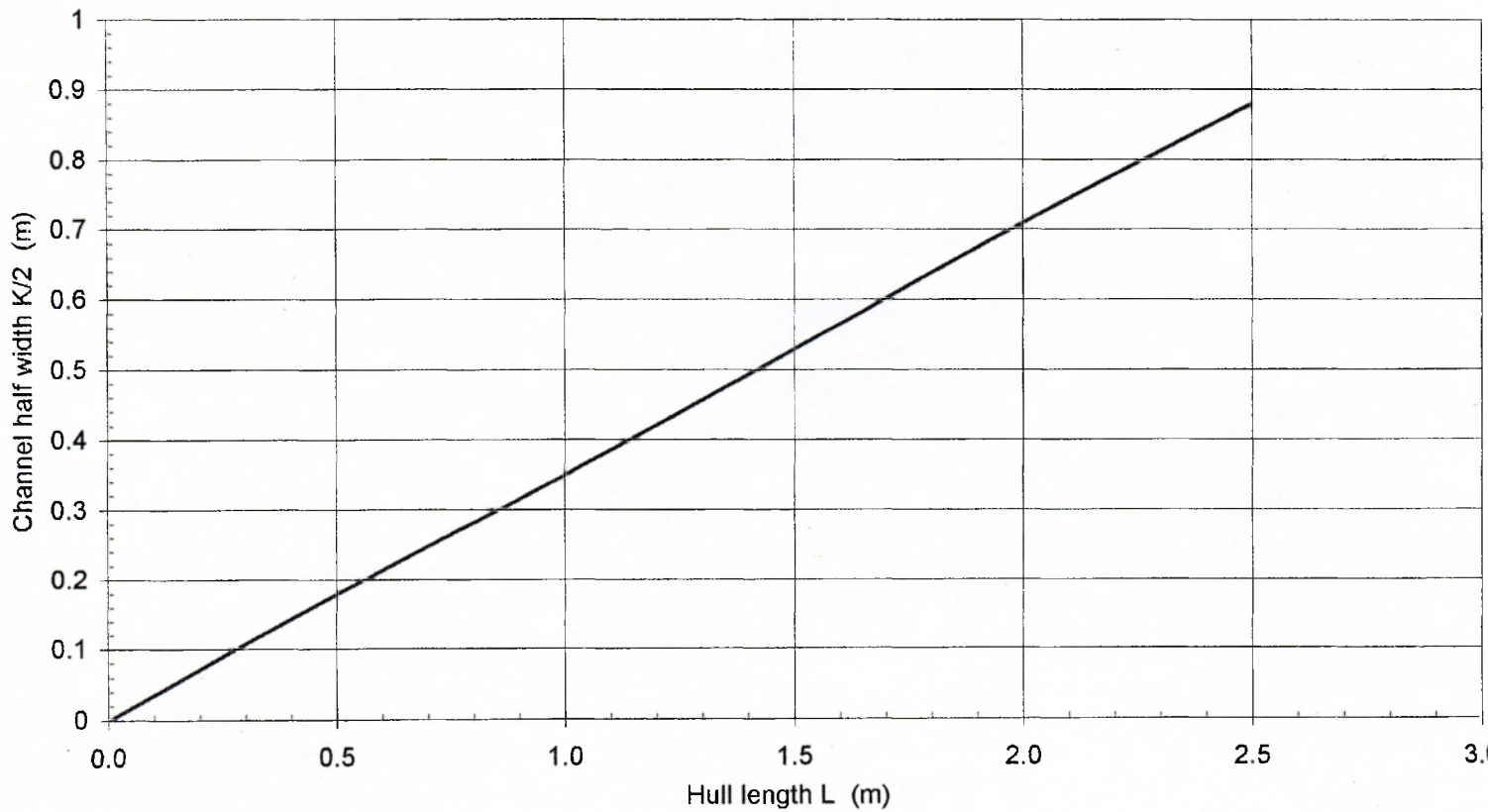

Fig. 56 The variation of channel width to avoid wave reflection onto a hull

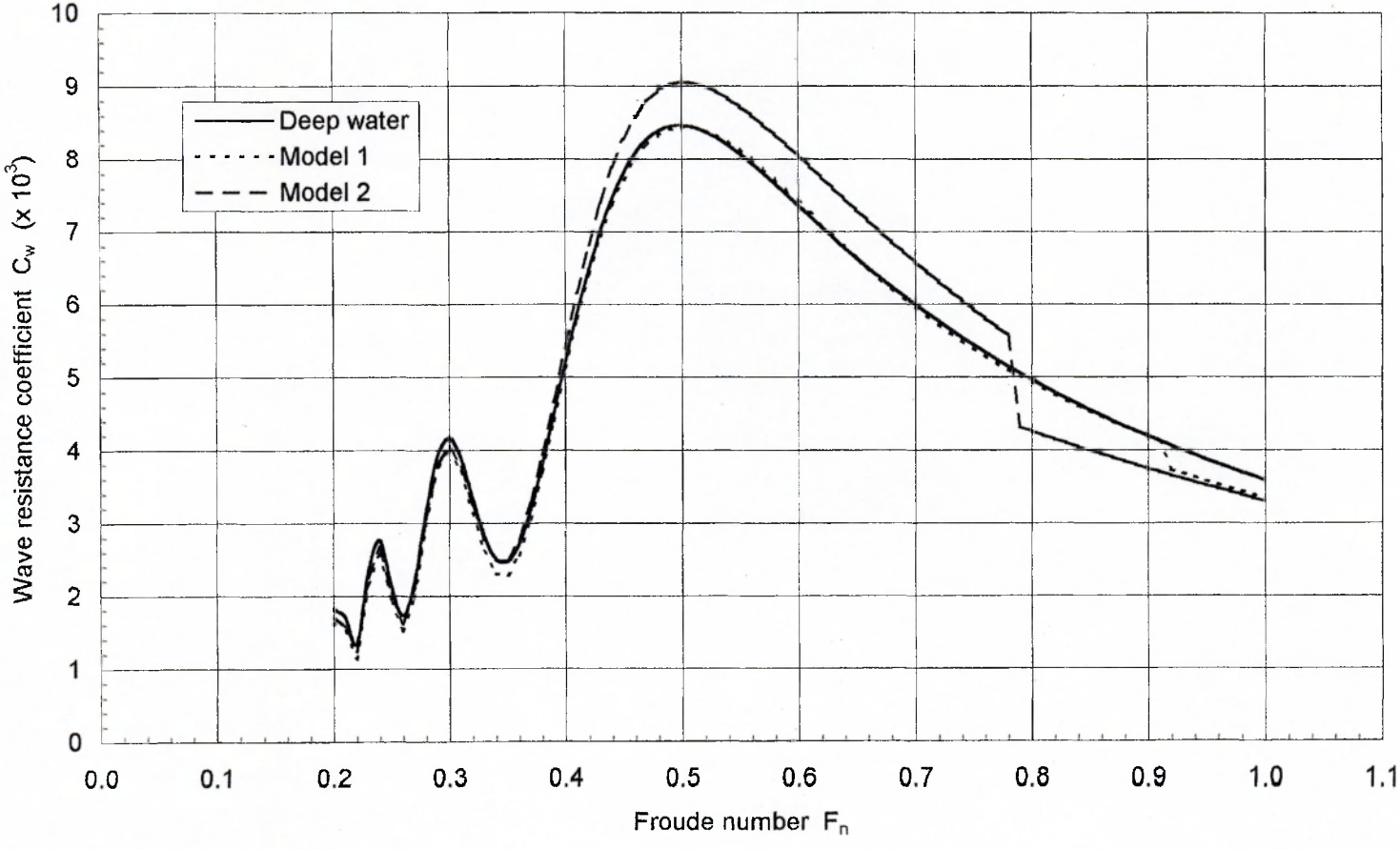

Fig. 57 A comparison of the theoretical wave resistance for two Wigley hulls in a channel

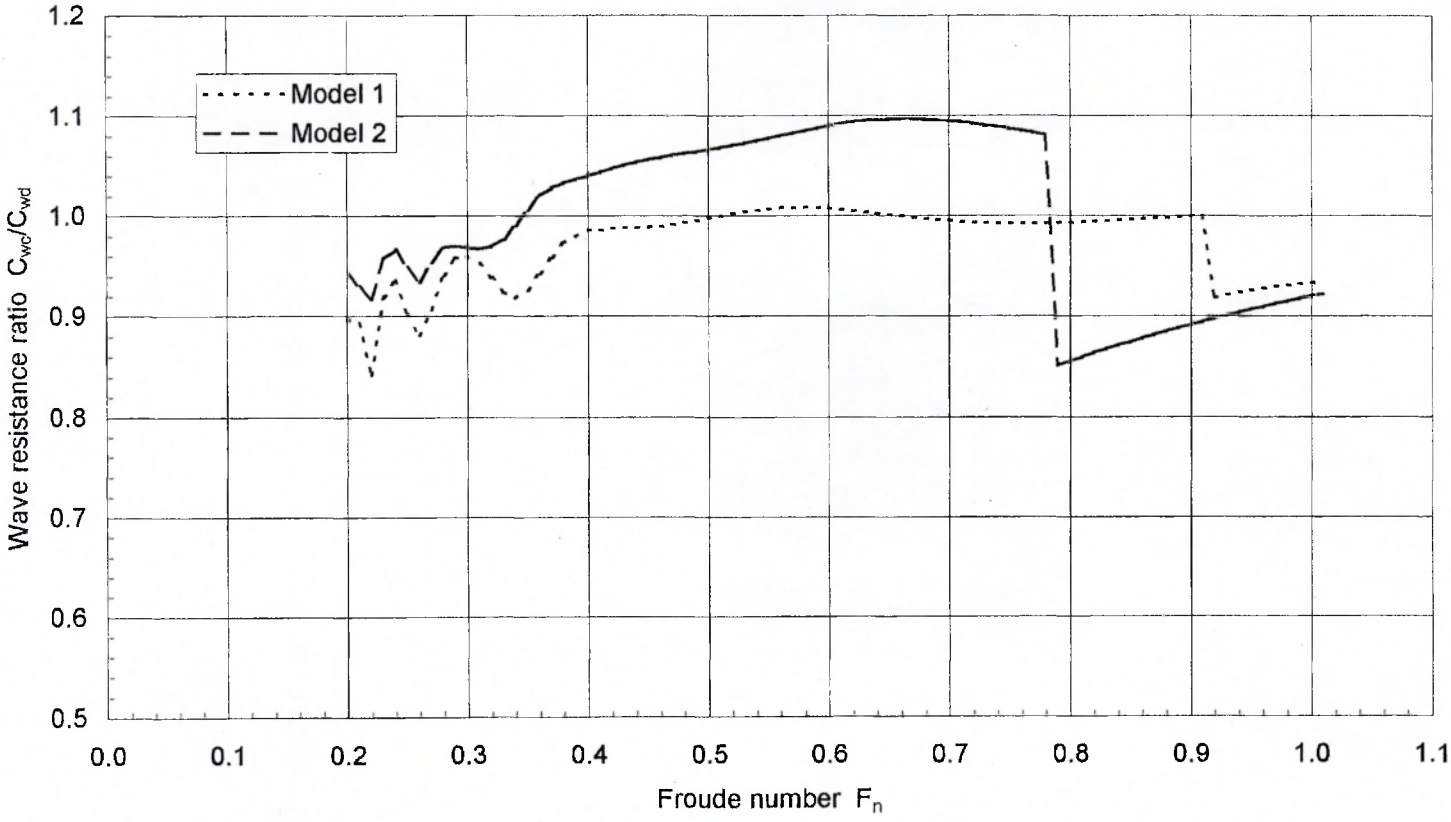

Fig. 58 A comparison of the channel effects on the two different size Wigley hulls

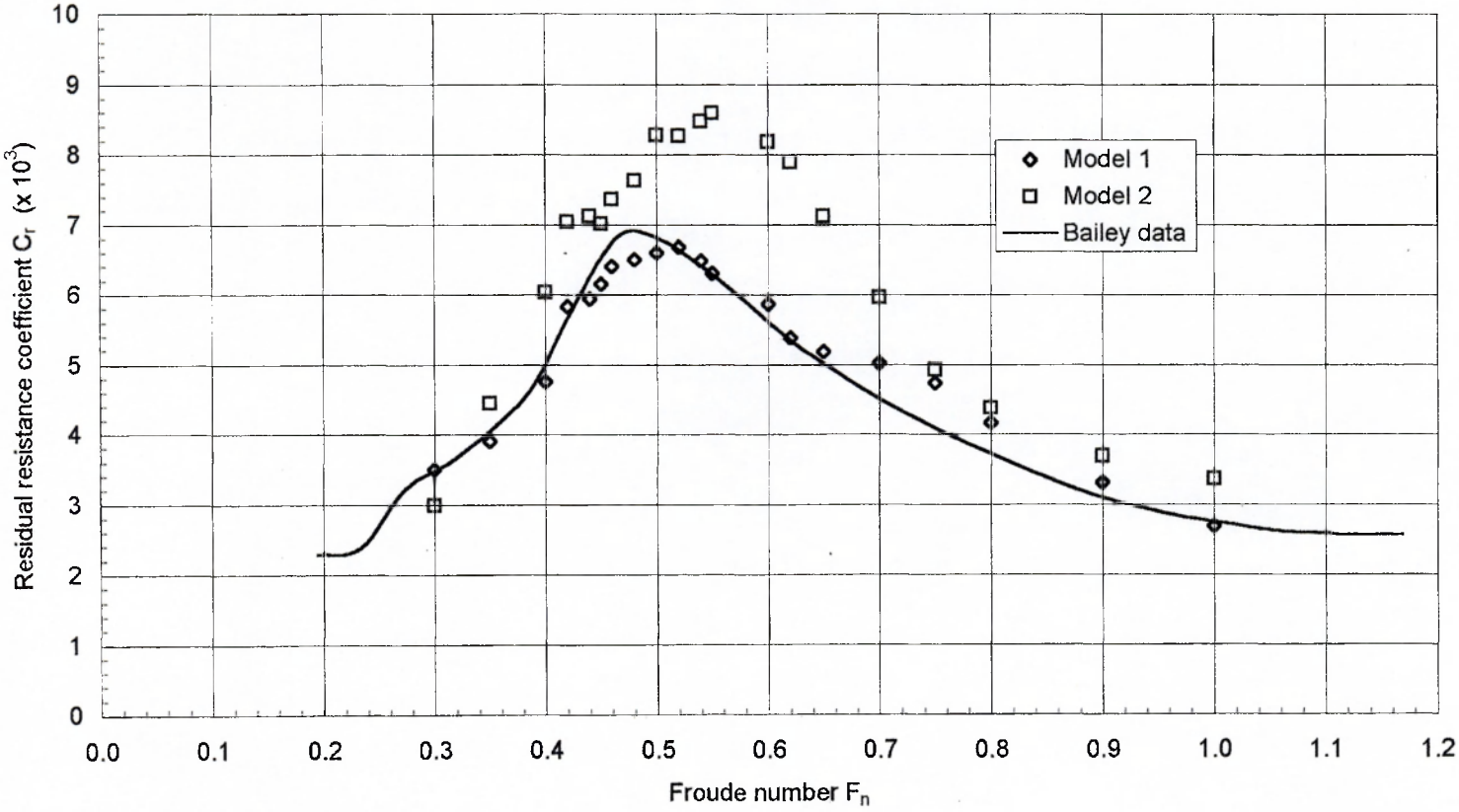

Fig. 59 A comparison of residual resistance for two different sized models of the NPL 100A hull in the water channel

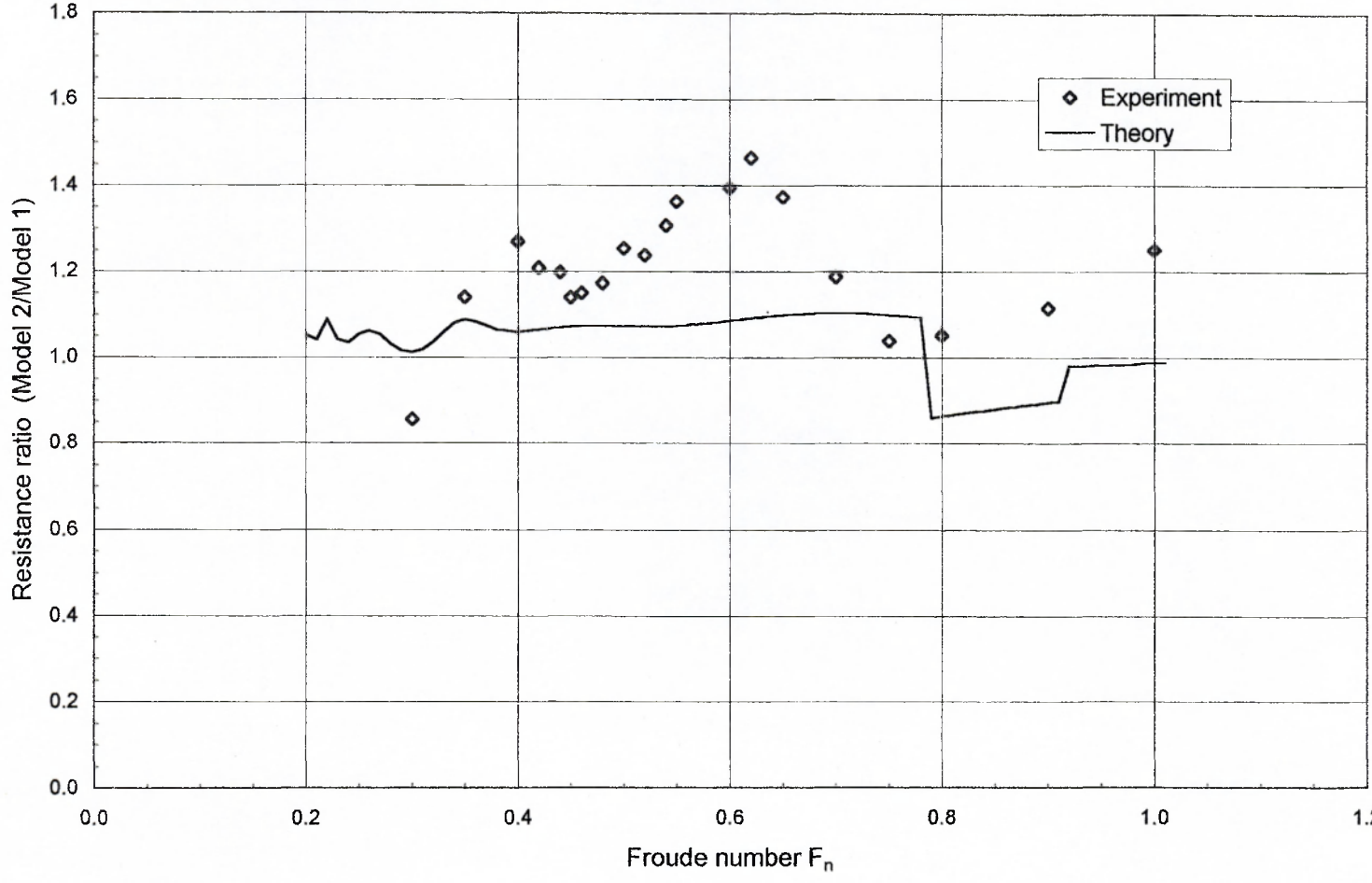

Fig. 60 A comparison of the experimental and theoretical values of the resistance ratio for the effect of channel size

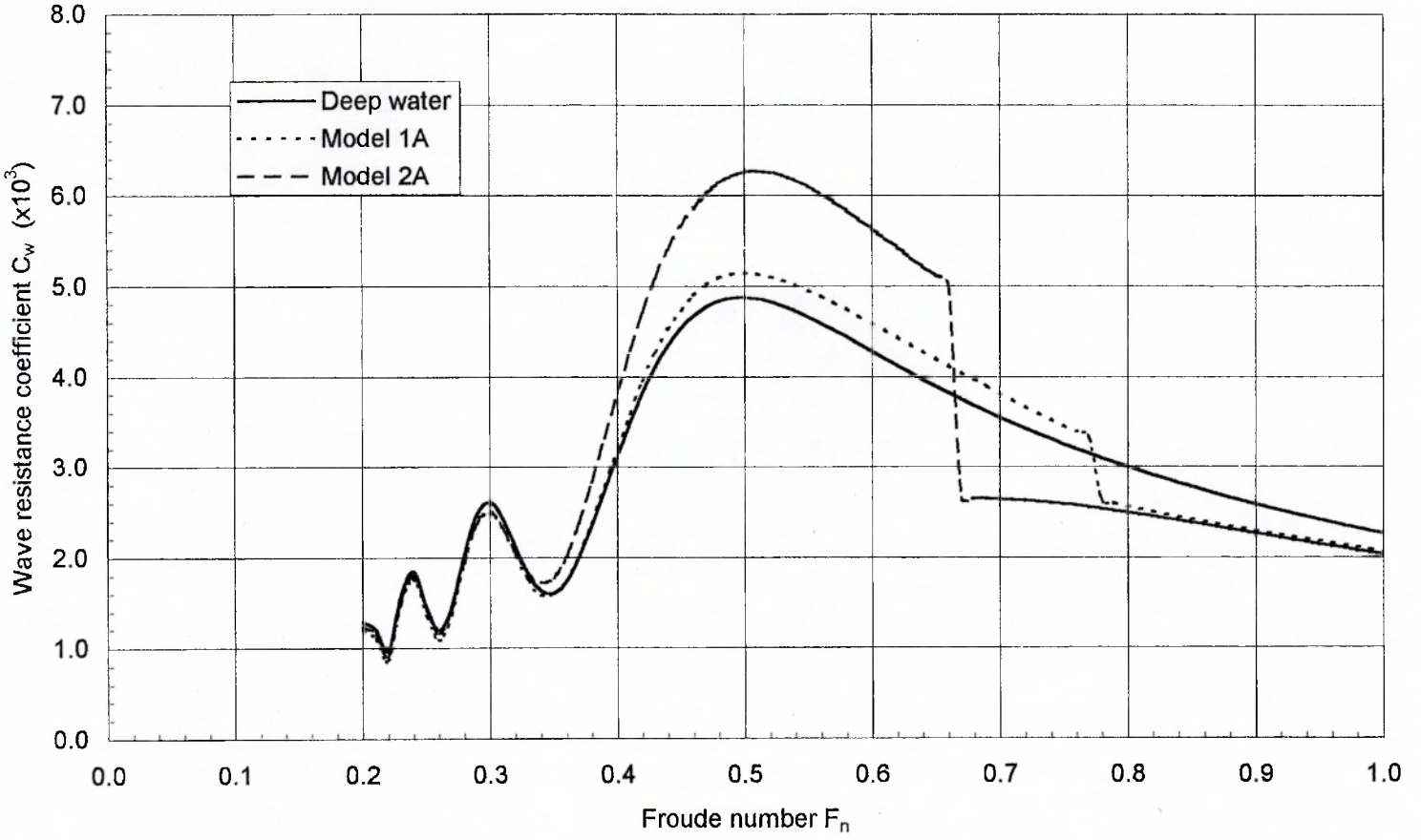

Fig. 61 The resistance of the two modified Wigley hulls (modification A)

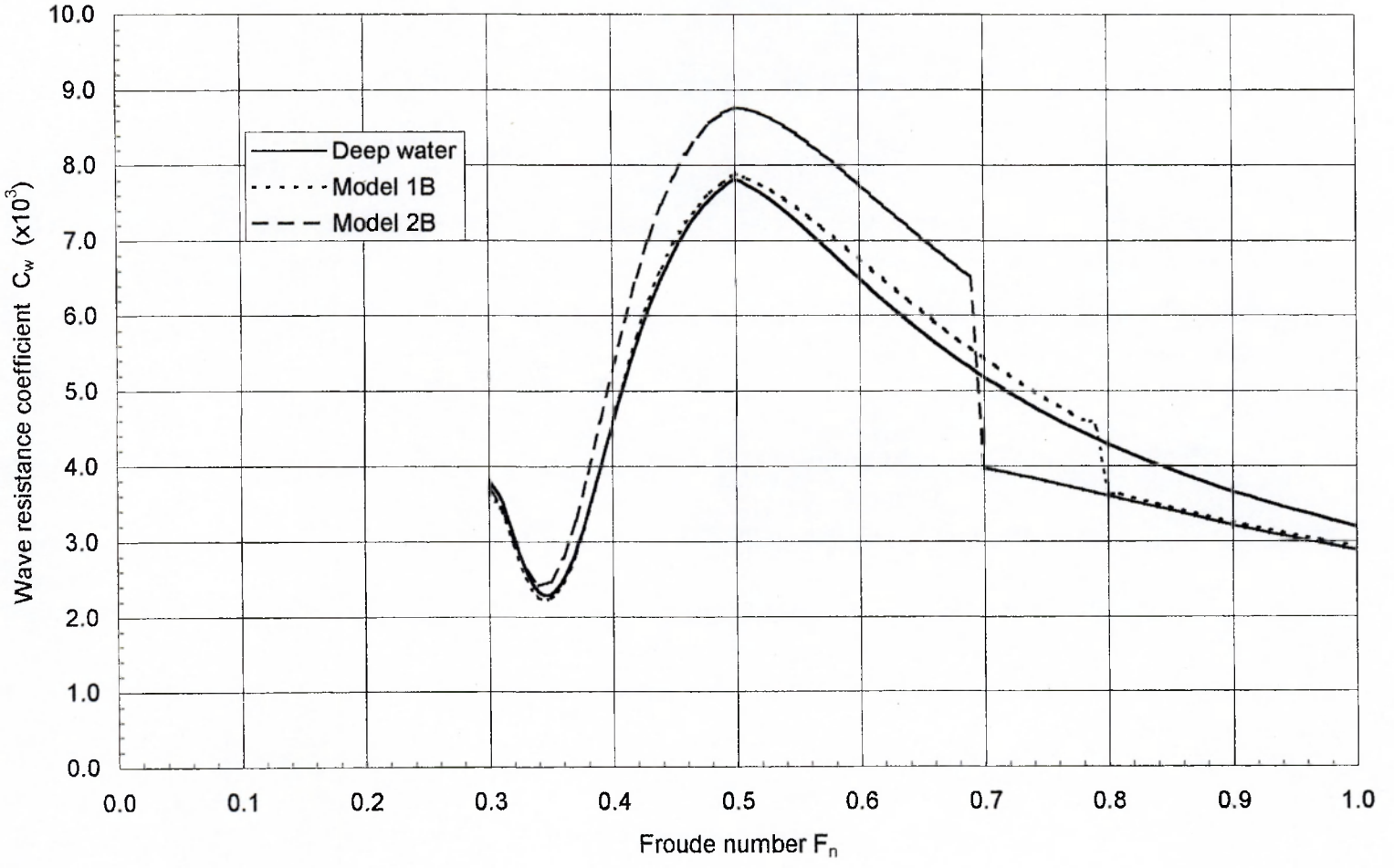

Fig. 62 The resistance of the two modified Wigley hulls (modification B)